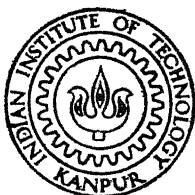


ANALYSIS OF NEW TYPES OF WAVEGUIDE AND MICROSTRIP DISCONTINUITY STRUCTURES AND THEIR PRACTICAL APPLICATIONS

By

R. S. TOMAR

TH
EE/1983/0
T59



**DEPARTMENT OF ELECTRICAL ENGINEERING
INDIAN INSTITUTE OF TECHNOLOGY KANPUR**

AUGUST, 1983

ANALYSIS OF NEW TYPES OF WAVEGUIDE AND MICROSTRIP DISCONTINUITY STRUCTURES AND THEIR PRACTICAL APPLICATIONS

A Thesis Submitted
In Partial Fulfilment of the Requirements
for the Degree of
DOCTOR OF PHILOSOPHY

By

R. S. TOMAR

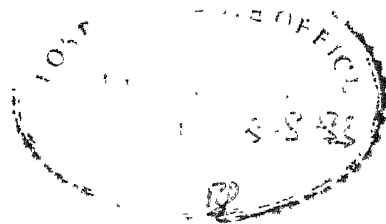
to the

DEPARTMENT OF ELECTRICAL ENGINEERING
INDIAN INSTITUTE OF TECHNOLOGY KANPUR

AUGUST, 1983

14 JUN 1985

11 2 23 20 11
GEN 11 2 23 20 11
87508



ii

CERTIFICATE

This is to certify that the thesis entitled 'ANALYSIS OF NEW TYPES OF WAVEGUIDE AND MICROSTRIP DISCONTINUITY STRUCTURES AND THEIR PRACTICAL APPLICATIONS' submitted by Mr. R.S. TOMAR in partial fulfilment of the requirements for the degree of Doctor of Philosophy is a record of work carried out under my supervision and has not been submitted elsewhere for a degree.

(Dr. Chinmoy Das Gupta)
Assistant Professor
Department of Electrical Engineering
Indian Institute of Technology
KANPUR (India)

A deep sense of gratitude must be expressed to Professor O.G. Vendick, a key person of microwave engineering of Soviet Union, from whose laboratory in the Leningrad Electrical Engineering Institute the idea of this work originated.

Dr. Chinmoy Das Gupta
Thesis Supervisor

ACKNOWLEDGEMENT

The author wishes to record his sincere gratitude to Dr. Chinmoy Das Gupta, author's supervisor, for suggesting the various problems worked out in this thesis and for supervising the work to completion. The author is deeply indebted to him for his constant encouragement and for his constructive criticism and comments throughout the tenure of this work.

The author is sincerely thankful to Dr. P.R.K. Rao and Dr. R.K.S. Rathore for their moral support and encouragement. Sincere thanks are also due to Dr. K.C. Gupta for timely help and for useful suggestions he gave.

A special note of appreciation is due to Mr. V. Kumar and Mr. K.K. Malhotra for the constant help provided by them.

The author also thanks his friends, Mr. Protap Pramanick, Mr. Nirdosh Khosla, Mr. Sanjeev Bhargava, Mr. Inder Krishn Bhatt, Mr. Ashok Dey, Mr. Shailendra Kumar and Mr. Pramod Kumar Srivastava for the timely and invaluable help and for their moral support.

The financial support extended by the Council of Scientific and Industrial Research, New Delhi, is thankfully acknowledged.

Mr. J.S. Rawat deserves a very special note of thanks and appreciation for his careful and efficient typing. Tracing work by Mr. D.K. Mishra, Xeroxing by Mr. Dalip and Cyclostyling by Mr. Ganga Ram and Triveni Tiwari are thankfully appreciated.

TABLE OF CONTENTS

Page

LIST OF FIGURES

LIST OF TABLES

SYNOPSIS

CHAPTER 1	INTRODUCTION	1
CHAPTER 2	MICROWAVE TRANSMISSION LINES AND THEIR DISCONTINUITIES - AN OVERVIEW	5
2.1	General	5
2.2	Coaxial Lines and Their Discontinuities	7
2.3	Waveguides and Their Discontinuities	11
2.3.1	Rectangular waveguide and their discontinuities	13
2.3.1a	Diaphragms and windows	17
2.3.1b	Metallic strips	19
2.3.1c	Posts and mounts	19
2.3.1d	Steps and bifurcations	24
2.4	MIC Lines and Their Discontinuities	26
2.4.1	Methods of analysing a microstrip line	34
2.4.1a	Quasi-static methods	34
2.4.1b	Dispersion models	35
2.4.1c	Fullwave analyses	37
2.4.2	Microstrip discontinuities	40
2.4.2a	Open-ends	41
2.4.2b	Gaps	43
2.4.2c	Steps in width	45
2.4.2d	Bends	45

2.5	Junctions of Similar Lines	47
2.6	Junctions of Dissimilar Lines	47
2.6.1	Coaxial-waveguide junctions	48
2.6.1a	Broadwall coaxial-waveguide junction	50
2.6.2	Coaxial-stripline junction	55
2.6.3	Coaxial-microstrip junctions	57
2.6.4	Waveguide-microstrip junctions	59
2.6.5	Microstrip-slotline junctions	60
2.7	Experimental Characterization of Discontinuities in Microwave Transmission Lines	60
2.7.1	Evaluation of coaxial/waveguide discontinuities	63
2.7.2	Evaluation of microstrip discontinuities	68
2.7.3	Evaluation of junctions of similar lines	69
2.7.4	Evaluation of junctions of dissimilar lines	71
2.8	Conclusions	72
CHAPTER 3	JUNCTION OF RECTANGULAR WAVEGUIDE AND TUNABLE COAXIAL LINE - APPLICATION TO MICROWAVE FILTERING	73
3.1	Analysis of the short-circuited case	76
3.1.1	A simpler condition of resonance	89
3.1.2	An expression for the peak insertion loss	90
3.1.3	The near-resonance equivalent circuit	99

3.2	Analysis of the Air-Gap Case	99
3.2.1	A simpler condition of resonance	106
3.2.2	Expression for the peak insertion loss	107
3.2.3	Near-resonance equivalent circuit	107
3.3	Experimental Results and Discussion	109
3.4	Resonant Contour of the Short-circuited Version: Some Theoretical Results	121
3.4.1	Effects of varying the characteristic impedance of the coaxial line	124
3.4.2	Effects of varying the loss resistance	124
3.4.3	Effects of varying the radius of the probe	124
3.4.4	Effects of varying the height of the waveguide	135
3.5	Analysis of the Short-Circuited Version Including Higher-Order Waveguide Modes	141
3.5.1	Calculation of resonant length	155
3.5.2	Results and discussion	159
3.6	Conclusions	159
CHAPTER 4	JUNCTION OF RECTANGULAR WAVEGUIDE AND TUNABLE COAXIAL LINE - APPLICATION TO EXPERIMENTAL CHARACTERIZATION OF WAVEGUIDE MOUNTS	161
4.1	Analysis of the Rectangular Waveguide-Tunable Coaxial Line Junction by using Lewin's Formulation	165

4.2	Experimental characterization of Singly-Loaded Posts in a Rectangular Waveguide	182
4.2.1	Measurement errors	183
4.2.2	Results and discussion	184
4.3	Experimental Characterization of Doubly-Loaded Posts in a Rectangular Waveguide: a Discussion	188
4.3.1	Use of post loaded at both ends with tunable coaxial lines	193
4.3.2	Use of post loaded at one end with the tunable coaxial line and at the other end with a known reactance	199
4.4	Experimental Determination of the Admittance Seen by the Coaxial Line in a Broad-wall Coaxial-Waveguide Junction: a Discussion	201
4.4.1	Use of tunable coaxial line to determine X and B	206
4.5	Conclusions	208
CHAPTER 5	INPUT IMPEDANCE SEEN BY THE COAXIAL LINE IN A BROAD-WALL COAXIAL-MICROSTRIP LAUNCHER	210
5.1	Analysis of the Proposed Configuration	212
5.2	Results and Discussion	220
5.3	Conclusions	230

CHAPTER 6	CHARACTERIZATION OF A MICROSTRIP TRANS- VERSELY LOADED WITH THIN CONDUCTING POST	231
6.1	Theoretical Analysis of the Confi- guration	232
6.2	Theoretical Results and Discussion	240
6.3	Experimental Results and Discussion	244
6.4	Conclusions	249
CHAPTER 7	CONCLUSIONS	251
APPENDIX I		258
APPENDIX II		267
REFERENCES		272

LIST OF FIGURES

Fig. No.	Title	Page
2.1	An air-filled coaxial line with circular cross-section.	9
2.2	Step discontinuities in a circular coaxial line and their equivalent circuits.	10
2.3	A rectangular waveguide.	14
2.4	Typical equivalent circuit for a discontinuity in a rectangular waveguide.	16
2.5	Diaphragm in a rectangular waveguide and its equivalent circuits.	18
2.6	Metallic strips in a rectangular waveguide.	20
2.7	Inductive metallic posts and their thin-post equivalent circuits.	22
2.8	Thick-post equivalent circuit of a non-resonant inductive post.	23
2.9	A capacitive post and its equivalent circuit.	25
2.10	Cross-sections of various planar structures	29
2.11	A planar waveguide.	38
2.12	Microstrip open-end and its equivalent circuits.	42
2.13	Microstrip gap and its equivalent circuits.	44
2.14	Microstrip step discontinuity and its equivalent circuit	46

Fig. No.	Title	Page
2.15	Microstrip bend and its equivalent circuit	46
2.16	The general broad-wall coaxial-waveguide junction	49
2.17	Common broad-wall coaxial line - rectangular waveguide launcher	52
2.18	The broad-wall junction analysed by Harrington	53
2.19	The broad-wall junction analysed by Lewin	54
2.20	Broadwall junction considered by Williamson	56
2.21	End-fed coaxial-stripline launcher	58
2.22	Broad-wall coaxial-stripline launcher	58
2.23	Some typical microstrip-slotline transitions	61
2.24	Network Analyzer-sweep generator test setup	66
3.1	Common broad-wall coaxial-waveguide junction	75
3.2	Rectangular waveguide-tunable coaxial line junction (short-circuited case)	75
3.3a	Variation of f_5 with frequency	91
3.3b	Variation of f_6 with frequency	92
3.3c	Variation of f_7 with frequency	93
3.3d	Variation of f_8 with frequency	94
3.4	Near-resonance equivalent circuit for the short-circuited version	100
3.5	Rectangular waveguide-tunable coaxial line junction (air-gap case)	101

Fig. No.	Title	Page
3.6	Near-resonance equivalent circuit for the air-gap case	110
3.7	A typical single-stage response for short-circuited case	111
3.8	A typical single-stage response for air-gap case	112
3.9	The photograph showing the X-band configuration employing extremely thin probe	114
3.10	Photograph showing the X-band measurement setup for waveguide components	116
3.11a	Attenuation characteristic of a short - circuited version using an extremely thin probe ($f_0 = 8$ GHz)	117
3.11b	Attenuation characteristic of a short - circuited version using an extremely thin probe ($f_0 = 10$ GHz)	118
3.11c	Attenuation characteristic of a short - circuited version using an extremely thin probe ($f_0 = 12$ GHz)	119
3.12	Definition of various characterizing parameters of a notch response	123
3.13a	Variation of IL_{\max} with f_0 for different values of Z_0	125
3.13b	Variation of Q_1 with f_0 for different values of Z_0	126
3.13c	Variation of Q_2 with f_0 for different values of Z_0	127

Fig. No.	Title	Page
3.13d	Variation of S_1 with f_o for different values of Z_o	128
3.13e	Variation of S_2 with f_o for different values of Z_o	129
3.14a	Variation of IL_{max} with f_o for different values of R_a	130
3.14b	Variation of Q_1 with f_o for different values of R_a	131
3.14c	Variation of Q_2 with f_o for different values of R_a	132
3.14d	Variation of S_1 with f_o for different values of R_a	133
3.14e	Variation of S_2 with f_o for different values of R_a	134
3.15a	Variation of IL_{max} with f_o for different values of r_p	136
3.15b	Variation of Q_1 with f_o for different values of r_p	137
3.15c	Variation of Q_2 with f_o for different values of r_p	138
3.15d	Variation of S_1 with f_o for different values of r_p	139
3.15e	Variation of S_2 with f_o for different values of r_p	140
3.16a	Variation of IL_{max} with f_o with different values of b	142

Fig. No.	Title	Page
3.16b	Variation of Q_1 with f_o for different values of b	143
3.16c	Variation of Q_2 with f_o for different values of b	144
3.16d	Variation of S_1 with f_o for different values of b	145
3.16e	Variation of S_2 with f_o for different values of b	146
3.17	A typical comparison between the results given by eq. (3.5.30) and experimental results	157
4.1	Some typical waveguide mounting structures employing E-plane metallic posts	162
4.2a	E-plane post in a rectangular waveguide (one end terminated into an active device)	166
4.2b	Electromagnetic equivalence of Fig. 4.2a (for small device dimensions)	166
4.3a	Rectangular waveguide-tunable coaxial line junction	169
4.3b	Electromagnetic equivalence of Fig. 4.3a	169
4.4	Lumped-circuit equivalence	171
4.5	Theoretical (Lewin) and experimental attenuation characteristic for $f_o = 10$ GHz and $r_p = 0.115$ mm	178
4.6	Theoretical (Lewin) and experimental attenuation characteristic for $f_o = 10$ GHz and $r_p = 0.435$	179

Fig. No.	Title	Page
4.7	Variation of insertion loss with the resonant length	171
4.8	Variation of percentage errors with frequency	185
4.9	Variation of percentage errors with post diameter	186
4.10	Variation of percentage errors with the characteristic impedance of the coaxial line	187
4.11	Configuration used for fine measurement of resonant lengths	189
4.12	Variation of X_0 with frequency (for $r_p = 0.435, 0.635$ and 0.800 mm)	191
4.13	Variation of $\Sigma(1/X_n)$ with frequency (for $r_p = 0.435$ mm, 0.635 mm, and 0.800 mm)	192
4.14	Arrangement of a doubly-loaded metallic post in a rectangular waveguide	194
4.15	Equivalent circuit of the doubly-loaded post	194
4.16	Simplified equivalent circuit for a centered post	198
4.17	Broadwall coaxial-waveguide junction considered by Williamson	198
4.18	Equivalence for the admittance seen at the coaxial port of the junction shown in Fig. 4.17	205

Fig. No.	Title	Page
4.19	Equivalent circuit of the junction shown in Fig. 4.17, looking from waveguide terminals	205
4.20	Equivalent circuit of the rectangular waveguide-tunable coaxial line junction by using Williamson's analysis	207
5.1	Broadwall coaxial-microstrip launcher	211
5.2	Proposed resonant structure	213
5.3	Planar waveguide equivalence of the proposed structure	215
5.4	Variation of insertion loss with the position of the movable short	221
5.5	Near-resonance equivalent circuit	221
5.6	Photograph showing one fabricated unit	222
5.7	Photograph showing the measurement setup for coaxial components	222
5.8a	Attenuation characteristic of the proposed coaxial-microstrip junction ($f_0 = 2$ GHz)	224
5.8b	Attenuation characteristic of the proposed coaxial-microstrip junction ($f_0 = 3$ GHz)	225
5.8c	Attenuation characteristic of the proposed coaxial-microstrip junction ($f_0 = 4$ GHz)	226
6.1	A microstrip line loaded with thin metallic post	233

Fig. No.	Title	Page
6.2	Planar waveguide equivalence of the configuration shown in Fig. 6.1	233
6.3	Lumped-circuit equivalence	238
6.4	Variation of post reactance and post inductance with r_p/w	214
6.5	Variation of post reactance and post inductance with w/h	242
6.6	Variation of post reactance and post inductance with ϵ_r	243
6.7	Resonant structure involving a gap and the unknown post	246
6.8	Resonant structure involving an open-end and the unknown post.	246

LIST OF TABLES

Table No.	Title	Page
3.1	Comparison between exact and approximate values of the resonant length (short-circuited case, $r_p = 0.115$ mm)	95
3.2	Comparison between exact and approximate values of the resonant length (short - circuited case, $r_p = 0.435$ mm)	96
3.3	Comparison between exact and approximate values of the resonant length (short - circuited case, $r_p = 0.635$ mm)	97
3.4	Comparison between exact and approximate values of the resonant length (air-gap case)	108
3.5	Comparison between theoretical and experimental values of the resonant length	120
3.6	Comparison between values of resonant length obtained with and without the first higher-order mode	158
4.1	Comparison between resonance condition given by eq. (4.1.16) and those given in Chapter 3 ($r_p = 0.115$ mm)	173
4.2	Comparison between resonance condition given by eq. (4.1.16) and those given in Chapter 3 ($r_p = 0.435$ mm)	174

Table No.	Title	Page
4.3	Comparison between resonance condition given by eq. (4.1.16) and those given in Chapter 3 ($r_p = 0.635$ mm)	175
4.4	Comparison between resonance condition given by eq. (4.1.16) and those given in Chapter 3 ($r_p = 0.800$ mm)	176
4.5	Comparison of CPU time required to calculate a full-band resonant contour by the various theoretical models	181
4.6	Experimental values of l_{r1} and l_{r2}	190
5.1	Comparison between theoretical and experimental values of resonant length ($r_p = 0.41$ mm, $Z_{om} = 50$ ohms)	227
5.2	Comparison between theoretical and experimental values of resonant length ($r_p = 0.755$ mm, $Z_{om} = 40$ ohms)	228

SYNOPSIS
ANALYSIS OF NEW TYPES OF WAVEGUIDE AND MICROSTRIP DISCONTINUITY
STRUCTURES AND THEIR PRACTICAL APPLICATIONS

A Thesis Submitted
In Partial Fulfilment of Requirements
for the Degree of
DOCTOR OF PHILOSOPHY
by
R.S. TOMAR
to the
Department of Electrical Engineering
Indian Institute of Technology
Kanpur 208016
August, 1983

Coaxial lines, rectangular waveguides and microstrip lines are the most widely used microwave transmission lines. While coaxial lines and waveguides have been in use since long, and still continue to be an integral part of a typical microwave set up, the emergence of microstrip line (and other MIC's) is a comparatively recent phenomenon. The MIC's offer advantages like reduction in volume and weight, an improved reliability and low cost of production when produced in mass. The interest in waveguides and coaxial lines is being sustained by factors like their higher power handling capability, comparatively low power loss, etc.

An abrupt change in the configuration of a transmission line is termed 'discontinuity'. The discontinuities are either deliberately created or are necessitated by some other considerations. In the first category one can mention examples like stubs, diaphragms and posts used as reactance elements in the line, changes in one or more dimensions, or in the medium, of the line so as to match it to a given load or termination, etc. In the second category fall discontinuities like beads needed to support the inner conductor in a coaxial line, metallic posts needed to mount an active device across a waveguide, microstrip gap used for d.c. blocking, etc.

Besides the above mentioned discontinuities, the junctions of similar/dissimilar lines constitute another very important class of microwave transmission line discontinuity problems. The junctions of similar lines are used primarily for the production of non-reciprocal components like isolators, circulators, tees, directional couplers, etc. The junction of dissimilar lines are needed to serve as a means of launching the electromagnetic energy from one line into the other.

The objectives of this thesis are:

- i) to present the electromagnetic analyses of some new types of discontinuity problems involving coaxial-waveguide and coaxial-microstrip junctions, and to investigate their practical applications, and

- ii) to investigate, both theoretically and experimentally, the case of a microstrip line loaded in the transverse plane with a thin cylindrical metallic post, and suggest areas of application of this new configuration.

A brief chapterwise description of the work reported in this thesis is given below:

1. The first chapter briefly traces the origin and growth of the field of microwave transmission lines and their discontinuities. This chapter also highlights the salient features, from the point of view of practical application, of the work reported in the thesis.
2. The second chapter, besides introducing in brief the basic concepts and definitions used in the thesis, gives an overview on microwave transmission lines and their discontinuities. Various discontinuities in coaxial, waveguide and microstrip forms are discussed. The junctions of similar/dissimilar lines are also discussed. Particular attention is paid to problems that are relevant to the work reported in this thesis. A section on methods of experimental evaluation of microwave transmission line discontinuities is also included.
3. The junction formed by a coaxial line entering the broad wall of a rectangular waveguide has been, and continues to be, a subject of study (see, e.g., [1]-[3]). This

junction is used mainly for coupling the electromagnetic energy from the coaxial line into the waveguide, or vice versa. A useful modification of this junction results if we let a movable short-circuit be present in the coaxial line, i.e. if we let the coaxial line be tunable. The junction of a tunable coaxial line and a rectangular waveguide has some well-known uses, e.g. for matching the coaxial line to the waveguide and thereby maximising the power coupled [4], as a power combining element [5], etc. The utility of this junction was significantly enhanced when it was successfully used for experimental evaluation of complex permittivity of dielectric samples [6]. The third chapter of the thesis examines this junction from one more different angle, i.e. from the viewpoint of its applicability to microwave filtering. Two different versions of the junction are analysed. The first, called the 'short-circuited case', is the case when the tip of the probe is allowed to touch the bottom inner wall of the waveguide. The second, called the 'air-gap case', is the case when an air-gap is allowed to exist between the tip of the probe and the waveguide wall. The analysis of these configurations is complicated by the additional boundary condition that the movable short imposes at the junction plane. The analysis is done under some suitable

simplifying assumptions which help in obtaining a closed - form expression for the transmission coefficient between the waveguide ports [7]-[10].

Both the short-circuited and air-gap cases exhibit a sharp transmission minimum which can be tuned all over the operating band of the waveguide by varying the position of the movable short. Consequently, these structures will find application as new types of prototypes for developing waveguide notch filters and will be especially useful when one is interested in achieving a large continuous mechanical tunability.

The third chapter also presents the results of the experimentation that was taken up on the filtering behavior of the above mentioned configurations. It is seen that the undesirable passband ripples that these configurations exhibit can be brought down to an acceptable level through the use of an extremely thin (electrically) probe. Detailed theoretical results describing the dependence of the filtering parameters (i.e. the peak insertion loss, Q 's, and the skirt selectivities) on the physical parameters (e.g. waveguide dimensions, probe radius, characteristic impedance of the coaxial line, etc.) are presented graphically.

One of the crucial assumptions made in the above mentioned analysis was the neglect of higher-order waveguide modes while writing the total excitation field along the length of the probe. In the last section of the third chapter, an attempt is made to incorporate the effects of the first higher-order mode in the analysis. Only the short-circuited case is considered. It is seen that although, in principle, it is possible to go on refining the analysis for more and more higher-order modes, the tremendous increase in the amount of algebra involved with the inclusion of each new mode (and still more heavy work for the air-gap case) makes this effort rather impractical. Also, it should be noted that for obtaining a practically acceptable performance of the above mentioned configurations, use of extremely thin probes is in any case mandatory, in which case the analysis presented in the earlier sections is sufficiently accurate. The analysis reported in the last section may thus be viewed as a rather revealing academic exercise.

4. The junction of a tunable coaxial line and a rectangular waveguide, which was examined in the third chapter for its filtering aspects, has been re-examined in the fourth chapter. The emphasis now is on its applicability as a method of experimental evaluation of waveguide mounts.

Lewin's formulation for a singly-loaded E-plane waveguide metallic post [11] has been extended to the configuration under consideration. The advantage of this formulation is that, unlike the analysis presented in the third chapter, the effects of all higher-order waveguide modes excited in the vicinity of the post can easily be incorporated in the analysis. A comparison between this formulation and the one presented in the third chapter is made. As expected, the results given by these two different approaches tally for thinner posts.

Analysis reveals that the positions of the movable short for minimum and maximum transmission between the waveguide ports can be correlated to the parameters of the post by means of simple explicit equations. As a result, a very useful method for experimental characterization of waveguide posts results. In comparison with the existing methods of this kind, the present method is superior in the following respects:

- i) No electrical measurements are needed, thus the errors encountered in electrical measurements, e.g. unwanted reflections at various junctions, poor instrument sensitivity, etc., are completely eliminated.
- ii) An explicit measurement of the unknown parameters is possible.

- iii) The configuration used is simple and easy to implement.
- iv) The working equations are quite simple, thus obviating the need of graphical/semigraphical/computer-aided analysis of the measured data.

The above mentioned method is applied to three different posts [12]. Agreement with the theory is good. An extension of the method for characterizing doubly-loaded posts is formulated. Application of the method for characterizing broadwall coaxial-waveguide junctions is discussed.

5. In the fifth chapter, the junction formed by a tunable coaxial line entering a microstrip line through the ground plane is analysed. The planar waveguide dispersion model [13] is used for the analysis, as this model suits the geometry of the problem involved. The analysis runs along lines similar to those followed in the third chapter. This configuration also exhibits a continuously tunable sharp transmission minimum which can be exploited for developing microstrip notch filters with large continuous mechanical tunabilities.

Of the various methods that are used to feed a microstrip line from a coaxial input, the broad-wall launching is an important method. This method becomes especially useful if small ground-plane spacings are involved, and if frequencies above S-band are not used. In this method

the coaxial line is mounted on the ground plane of the microstrip line, and the inner conductor of the coaxial line penetrates the substrate through a cylindrical hole to feed the strip. Although some discussion on this type of launchers is available in the literature [14], no directly usable results on the input impedance seen by the coaxial line (which is a very important parameter in the design/analysis of any coaxial-microstrip launcher) in such a launcher seem to have been reported so far. The fifth chapter of the thesis reports an investigation on this impedance. The aforementioned analysis of the broad-wall junction of a tunable coaxial line and a microstrip line is used for this investigation. The theoretical resonance condition (which is also experimentally verified, for two different sets of parameter values) obtained by the analysis establishes, after proper interpretation, that the feed-wire in a broad-wall coaxial-microstrip launcher can be assumed, for the purpose of writing its input impedance, to act as a thin wire antenna radiating in an unbounded homogeneous dielectric-filled space [15].

6. The sixth chapter analyses the case of a microstrip line loaded in the transverse plane with a thin cylindrical conducting post. Once again, the planar waveguide model [13] is used for the analysis. As expected, it is found that the post offers an inductive reactance across the

microstrip line. The mathematical expression for this reactance is worked out. Theoretical results describing the dependence of this reactance on the various parameters (i.e. aspect ratio of the microstrip, post diameter and dielectric constant of the substrate) of the configuration are presented graphically. The experimental verification of the theory is done by forming a resonant structure consisting of a microstrip open-end/gap (which can be characterized by available methods) and the unknown post and noting the frequency of resonance of the resulting configuration [16].

The configuration analysed in the sixth chapter provides one with an easy means of simulating parallel reactances in a microstrip/stripline, and will find an extensive application in the design of microstrip/stripline filters, impedance-matching sections, etc. where parallel reactances are required. The analysis reported in this chapter will also help in the design of some microstrip-slot line transitions which involve the use of a transversely placed metallic wire [17]).

7. The seventh chapter of the thesis concludes the work by highlighting the various important results obtained and their potential for practical applications.

REFERENCES

- [1] M.M. Braly, 'Rectangular waveguide-to-coax line transitions: 1968', IEEE Transact. on MTT, vol. 17, No. 3, p. 170, March 1969.
- [2] R.L. Eisenhart, P.T. Greiling, L.K. Roberts, and R.S. Robertson, 'A useful equivalence for a coaxial-waveguide junction', IEEE Transact. on MTT, vol. 26, No. 3, pp. 172-174, March 1978.
- [3] A.G. Williamson, 'Analysis and modelling of a coaxial - line/rectangular-waveguide junction', Proc. IEE, Pt. H, MOA, vol. 129, No. 5, pp. 262-270, October 1982.
- [4] T. Moreno, Microwave Transmission Design Data, New York: Dover Publications, 1958, Chapter 10.
- [5] K. Chang and R.L. Ebert, 'W-band power combiner design', IEEE Transact. on MTT, vol. 28, No. 4, pp. 295-305, April 1980.
- [6] C. Das Gupta, 'Microwave measurement of a complex dielectric constant over a wide range of values by means of a waveguide resonator method', IEEE Transact. on MTT, vol. 22, No. 4, pp. 365-372, April, 1974.
- [7] R.S. Tomar and C. Das Gupta, 'A new type of narrow-band-rejection microwave filter with full-band tunability' in Proceedings, International Symposium on Microwaves and Communication, Indian Institute of Technology, Kharagpur, India, December, 1981.
- [8] R.S. Tomar and C. Das Gupta, 'Filtering aspects of some modified versions of the conventional rectangular waveguide-coaxial line junction', in Proceedings, 7th Colloquium on Microwaves Communication, Budapest, Hungary, September 1982.
- [9] R.S. Tomar and C. Das Gupta, 'Analysis of a new type of narrow-band-rejection filter in waveguide form', Arch. Elek. Ubertragung, vol. 37, No. 1/2, pp. 47-50, February 1983.
- [10] R.S. Tomar and C. Das Gupta, 'Analysis and filtering applications of two newly proposed waveguide-coaxial line junctions', to appear in the Journal of Applied Physics.

- [11] L. Lewin, Theory of Waveguides. London: Newnes-Butterworths 1975, Chapter 5.
- [12] R.S. Tomar and C. Das Gupta, 'Experimental characterization of a singly-loaded E-plane waveguide post by using a tunable coaxial line', accepted for publication in the IEEE Transact. on Inst. and Meas.
- [13] G. Kompa and R. Mehran, 'Planar waveguide model for calculating microstrip components', Electronics Letters, vol. 11, No. 19, pp. 459-460, 18th September 1975.
- [14] H. Howe, Stripline circuit design. Dedham: Artech House, 1974, Chapter 2.
- [15] R.S. Tomar and C. Das Gupta, 'Input impedance seen by the coaxial line in a broad-wall coaxial-microstrip launcher', to be sent for publication.
- [16] R.S. Tomar and C. Das Gupta, 'Characterization of a microstrip line transversely loaded with a thin metallic post', to be sent for publication.
- [17] K.C. Gupta, R. Garg, and I.J. Bahl, Microstrip Lines and Slotlines. Dedham: Artech House, 1979, Chapter 6.

CHAPTER 1

INTRODUCTION

The types of transmission lines that are used to carry electromagnetic energy from one place to another vary with the frequency ranges involved. At microwave frequencies, coaxial lines, waveguides and Microwave Integrated Circuits (MIC's) are the most commonly employed lines. The coaxial lines and waveguides have been in use since long, and still continue to enjoy popularity, especially for applications where large powers are involved. The MIC lines, on the other hand, have evolved mainly in the last two decades or so. Their evolution was assisted by factors like the development of semiconductor devices for use at microwave frequencies and the rapid strides made by IC technology at lower frequencies.

The first major recorded research activity which galvanised the status of microwave theory and practice and set many future trends was the one involved in the development of radar and related techniques during world war II. The tremendous amount of information, which was of both theoretical and experimental nature, generated during this activity on microwave transmission lines, their discontinuities and their junctions subsequently appeared in the form of

several books like those by Huxley [1], Ragan [2], Montgomery et.al. [3], Moreno [4], Marcuvitz [5], Lewin [6], King et.al. [7], Schwinger and Saxon [8], etc.

Further progress in the area was recorded by authors like Collin [9], [59], Harrington [10], Young [11], Mittra and Lee [12], Lewin [13], etc., whose works were either fully or partially devoted to this field.

Besides these books, a tremendous amount of information on microwave transmission lines and their discontinuities is also scattered in the form of hundreds of research papers that have been, and are still being, published in this area. Earlier, the accent was mainly on coaxial lines and waveguides. The last two decades have, however, witnessed a phenomenal growth in the literature on MIC lines and their discontinuity structures (including their junctions). The coaxial lines and waveguides have also continued to occupy a major place, especially because of their indispensability for large-power applications. The discontinuities in these lines have been receiving a constant attention of researchers, primarily as regards their analysis. Many new types of structures have been analysed. Most of these structures have come up as a direct consequence of some other physical considerations. For instance, the mounting of an active device in a waveguide inevitably requires use

of metallic posts. An accurate characterization of metallic posts thus becomes a practical necessity, arising out of need to design high-power amplifiers, oscillators, detectors, etc.

Besides the discontinuities in a line, the junctions of similar/dissimilar lines are also a very important subject of study. The junctions of similar lines are used mainly to produce nonreciprocal components like directional couplers, tees, and circulators. The junctions of dissimilar lines are necessitated primarily by the need to feed electromagnetic energy from one line into the other. Sometimes, one line, in a stub form, can also be used as a reactance element in the other line.

The work reported in this thesis concerns with the electromagnetic analyses of the following configurations:

- i) The broadwall junction involving a rectangular waveguide and a tunable coaxial line.
- ii) The broadwall junction involving a microstrip line and a tunable coaxial line.
- iii) The microstrip line loaded in the transverse plane with a thin cylindrical metallic post.

A sufficient amount of experimental results to verify the various theories developed are also given. From the

viewpoint of practical application, the work reported can be highlighted in terms of the following contributions:

- i) New prototypes for developing waveguide/microstrip notch filters with large continuous mechanical tunabilities.
- ii) A new simple method of experimental evaluation of waveguide mounting structures and coaxial - waveguide junctions.
- iii) A new model for the input reactance seen by the coaxial line in a broadwall coaxial-microstrip launcher.
- iv) A very simple method of simulating parallel inductances in a microstrip/stripline. This part of the work assumes a special significance when one keeps in mind the fact that methods of simulating parallel inductance in MIC lines seem not to have received much attention so far.

CHAPTER 2

MICROWAVE TRANSMISSION LINES AND THEIR DISCONTINUITIES - AN OVERVIEW

2.1 GENERAL

A transmission line is a system of material boundaries forming a continuous path from one place to another and capable of directing the flow of electromagnetic energy along this path. If the geometrical dimensions and constants of materials are identical in all transverse sections, the line is said to be uniform; otherwise it is called a nonuniform line. An abrupt change in the physical configuration of a transmission line is called 'discontinuity'.

At microwave frequencies, the most widely used lines are the coaxial lines, the waveguides, and the Microwave Integrated Circuits (MIC's). While coaxial lines and waveguides have been in use since long, and are still indispensable for high power applications, the emergence of MIC's is a comparatively recent phenomenon.

Theoretically speaking, a given transmission line can support an infinite number of distinct field configurations, or 'modes', each of them satisfying Maxwell's equations and the boundary conditions involved. A mode is said to be

'propagating' when the net power flow contributed by it is real, and is termed 'evanescent' when its contribution to the net power flow is imaginary. All modes have a definite 'cut-off' frequency. A mode propagates at frequencies above its cut-off and is evanescent at frequencies below its cut-off. The mode with the lowest cut-off frequency is called the 'dominant' or 'fundamental' mode of propagation in the line.

Most of the practically used microwave transmission lines can be analysed in terms of TE, TM and TEM modes. The transverse electric (TE) modes are characterized by the absence of the component of electric field (E) along the direction of propagation of electromagnetic energy. The transverse magnetic (TM) modes have no component of the magnetic field (H) in the direction of propagation. The transverse electromagnetic (TEM) modes are marked by the absence of the component of both E and H fields in the direction of propagation.

The presence of a discontinuity in a transmission line gives rise to a reflected wave and a storage of reactive energy in the vicinity of the discontinuity because of excitation of higher-order modes. The effects of a discontinuity can be generally described, provided the discontinuity is symmetric and reciprocal, by means of

one reflection coefficient (say τ) and one transmission coefficient (say T). Both τ and T are, in general, complex quantities. For a nonsymmetric and/or nonreciprocal discontinuity, the complete characterization requires knowledge of two reflection coefficients (say τ_1 and τ_2) and two transmission coefficients (say T_1 and T_2).

An alternative representation which is commonly used is to describe the behavior of the discontinuity by an equivalent transmission line circuit which would give rise to reflected and transmitted waves of magnitude proportional to τ and T , respectively.

From the point of view of the lines involved, the various microwave transmission line discontinuities can be divided into the following:

- i) Coaxial line discontinuities
- ii) Waveguide discontinuities
- iii) MIC discontinuities
- iv) Junctions of similar lines
- v) Junctions of dissimilar lines

The following sections discuss, in brief, these various types of discontinuities.

2.2 COAXIAL LINES AND THEIR DISCONTINUITIES

Coaxial lines are the transmission systems in which the electromagnetic waves are transmitted through a

dielectric medium bounded by two coaxial conducting cylinders. The fundamental mode of propagation in these lines is a TEM mode. At relatively higher-frequencies, these lines can support TE and TM modes also.

The most commonly employed coaxial line is the air-filled circular line shown in Fig. 2.1. In this line, the medium is air and both the inner and outer conductors have a circular cross-section. The fundamental (TEM) mode of propagation in this line has a zero cutoff frequency.

The step discontinuities shown, alongwith their equivalent circuits, in Fig. 2.2 are the most commonly encountered coaxial discontinuities. Numerous results, comprising both computer-aided calculations and empirical/semiempirical formulas, on the equivalent shunt capacitances C_d and C_d' are available in literature (see, e.g., [3]-[5], [11], [14]-[18]). The results on coplanar steps in both conductors have been reported by Jurkus [19] and, quite recently, by Sreenivasiah and Chang [20]. Various other coaxial discontinuities, e.g. windows and apertures, infinitely thin disk attached to the inner/outer conductor, abrupt changes in the medium, bifurcations, metallic posts, shunt/series branches, etc. have been discussed by Montgomery, Dicke and Purcell [3], Moreno [4], Marcuvitz [5], Whinnery, Jamieson and Robbins [14]-[15], etc. It is

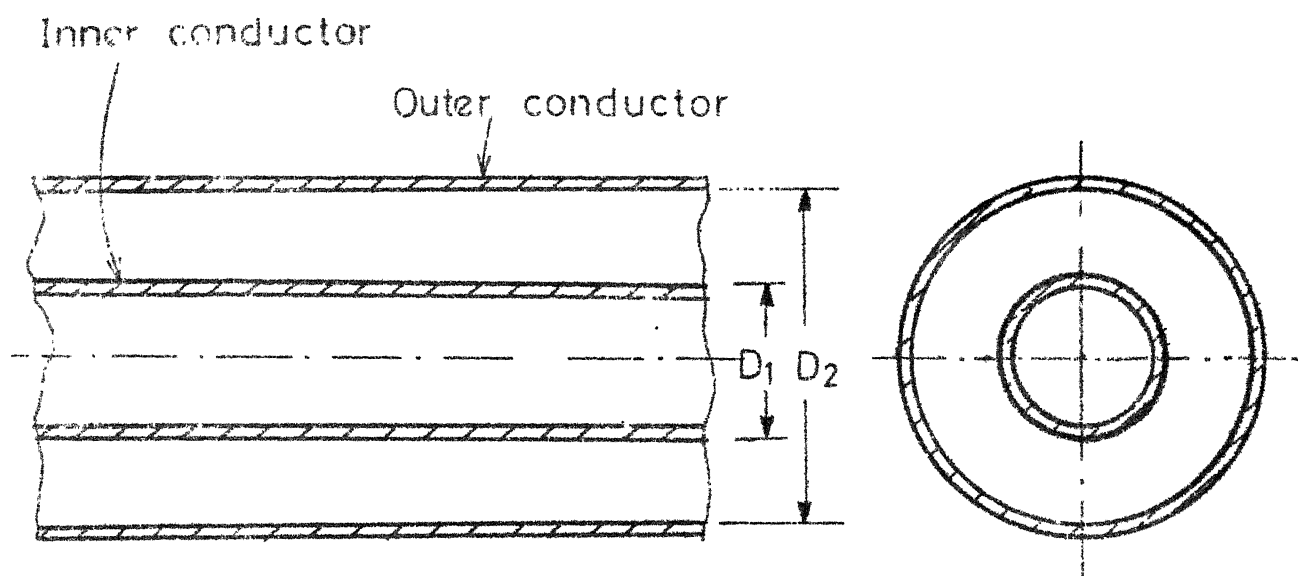
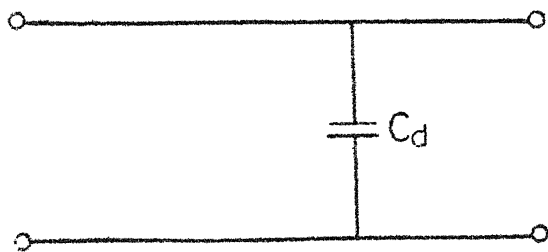
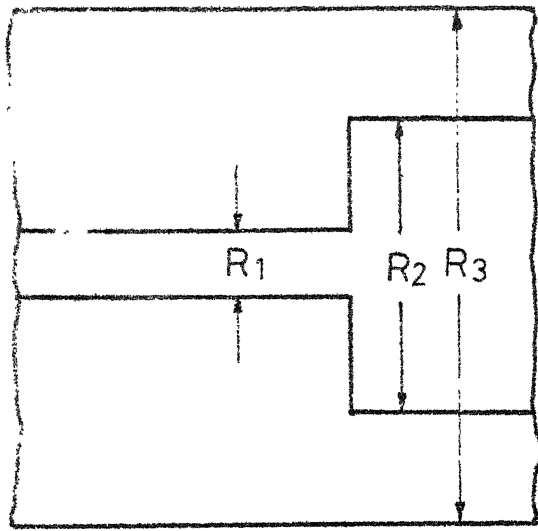
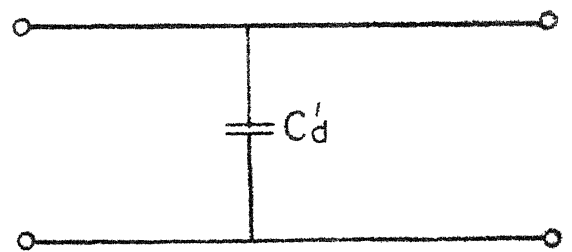
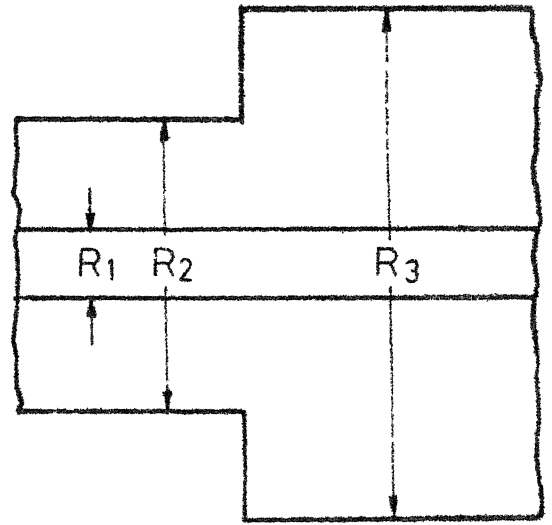


Fig. 2-1 An air-filled coaxial line with circular cross-section



(a) Step in the inner conductor



(b) Step in the outer conductor

Fig. 2-2 Step discontinuities in a circular coaxial line and their equivalent circuits

generally possible to write the equivalent circuits of these more complicated discontinuities as superimposition of those of more than one elementary discontinuities. For instance, the discontinuity capacitance associated with an infinitely thin disk on the inner conductor is twice that associated with a step upto the disk diameter.

In the context of this section, it is also worthwhile to mention that, of late, a large number of new types of coaxial configurations (and/or discontinuities therein), evolved for various specific applications, have started attracting the attention of researchers. Of notable significance are the coaxial cables with non-circular geometry (see, e.g., [21]-[34]), the leaky coaxial cables (see, e.g., [35]-[46]), the nonuniform coaxial lines (see, e.g., [47] - [53]), the coaxial cables with gap in the inner/outer conductor (see, e.g., [54]-[56]), etc.

2.3 WAVEGUIDES AND THEIR DISCONTINUITIES

Any transmission line is a waveguide in the sense that it guides electromagnetic waves. In practice, however, it has been customary to reserve the term 'waveguide' for lines in which the wave propagation is not in the form of a TEM mode. However, with the advent of new types of guiding structures, especially those in MIC form, even this classification has started losing relevance.

Broadly speaking, two types of waveguides have been, and are, in use. They are i) the closed cylindrical conducting tubes and ii) the open boundary structures. In the former, generally known as 'cylindrical waveguides', the hollow walls of the tube serve to confine the electromagnetic fields and thereby guide the electromagnetic energy. In the latter, which are generally termed 'surface waveguides', the electromagnetic energy is guided along the interface between two different media by means of 'surface waves'. The cylindrical waveguides can be subdivided, depending on the geometry of the cross-section, into rectangular waveguides, circular waveguides, elliptic waveguides, guides with arbitrary cross-section, etc. The surface waveguides, which are especially useful at millimeter wave and optical wave frequencies, comprise structures like dielectric slabs, dielectric coated conductors, corrugated structures, etc.

A detailed discussion on surface waveguides and associated discontinuities is beyond the scope of the present study. The interested reader may, however, find a lot of literature on them (see, e.g., [9]-[10], [57]-[65]). Similarly, cylindrical waveguides with nonrectangular cross-section do not constitute a direction of work in this thesis, and will not be discussed here. The interested reader is again referred to the literature (see, e.g., [3] - [5], [9], [13], [66]-[89]).

The following subsection briefly discusses the rectangular waveguide and associated discontinuities.

2.3.1 Rectangular Waveguides and their Discontinuities:

Rectangular waveguide is the most popular waveguide used nowadays. The main reasons behind its popularity are its large bandwidth for single-mode operation, reasonably low attenuation, and good mode-stability for fundamental -mode operation.

The rectangular waveguide consists of a hollow conducting tube of rectangular cross-section, as illustrated in Fig. 2.3. The width of the rectangle is generally denoted by 'a' and height by 'b', as shown. The coordinate axes are generally chosen as marked. This line can not support a TEM mode, but is capable of guiding TE and TM modes. The modes are generally written as $TE_{m,n}$ and $TM_{m,n}$, where the subscripts 'm' and 'n' are integers describing the variation of field components in x and y directions, respectively.

The fundamental mode of propagation in a rectangular waveguide is the TE_{10} mode. For this mode, E_y , H_x and H_z are the only non-zero field components. In view of this, it has become customary to designate discontinuities symmetrical about the y-axis as E-plane discontinuities. The

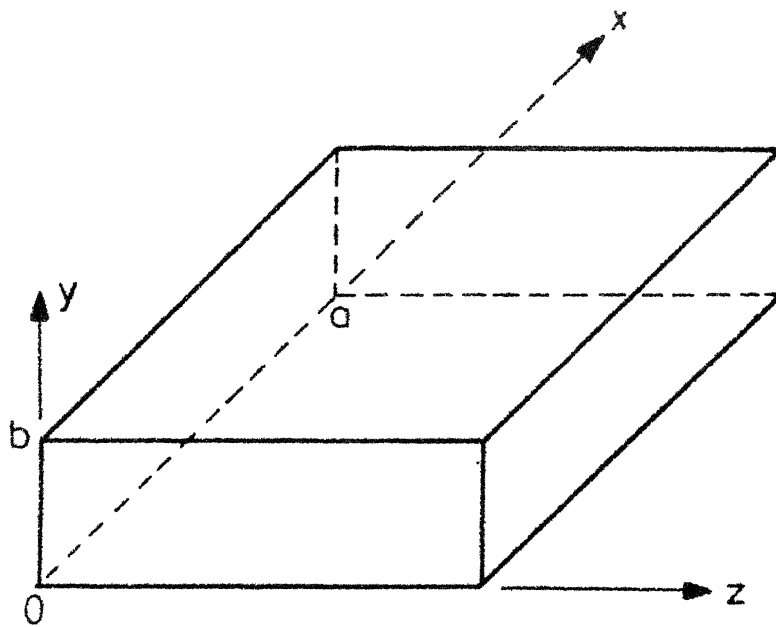


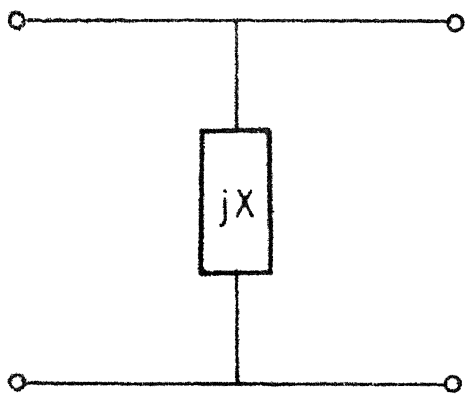
Fig. 2-3 A rectangular waveguide

discontinuities that are symmetrical about the x -axis are called the H-plane discontinuities. The E-plane discontinuities are also referred to as 'inductive' discontinuities because the predominant element in their equivalent circuits is an inductive reactance. The H-plane discontinuities can be regarded as 'capacitive' discontinuities as their equivalent circuits are dominated by capacitive reactances.

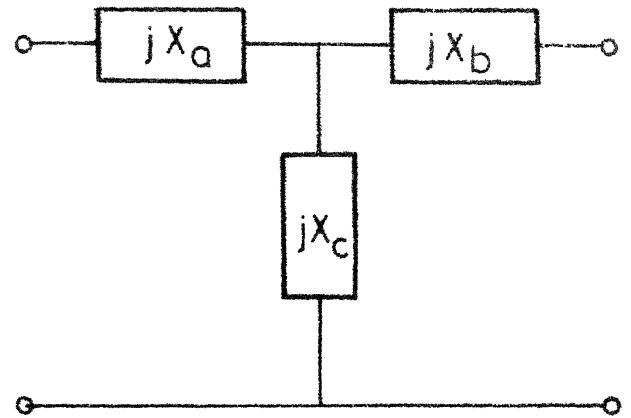
The discontinuities whose dimensions along the z -axis are negligible compared to the wavelength involved are termed 'thin' discontinuities. In most of the cases, the effects of a thin discontinuity can be represented by a shunt element across the guide, as shown in Fig. 2.4a. For 'thick' discontinuities, a more general representation like the one shown in Fig. 2.4b is necessitated⁺.

Of the various techniques available for analysing waveguide discontinuities, the mode-matching techniques, the Wiener-Hopf techniques, the variational techniques, and the quasi-static techniques are most commonly known. A unified account of mode-matching and Wiener-Hopf techniques has been given by Mittra and Lee in their book [12].

⁺A notable exception to this is the case of a H-plane metallic post where the equivalent circuit shown in Fig. 2.4b needs to be used for both thin and thick posts.



(a) Thin discontinuity



(b) Thick discontinuity

Fig.2-4 Typical equivalent circuit for a discontinuity in a rectangular waveguide

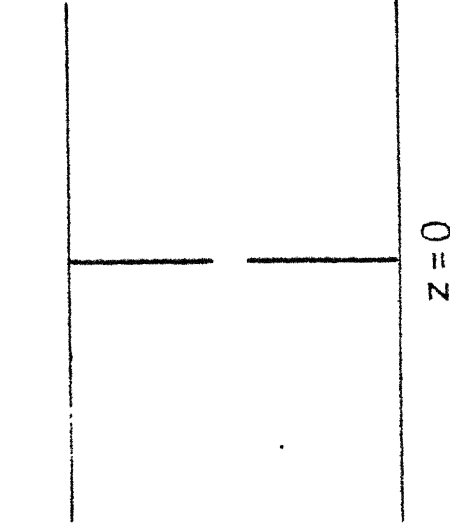
For details on other techniques, one can refer, for example, books by Schwinger and Saxon [8], Collin [9], Harrington [10], Lewin [13], Young [11], [60], etc.

A brief discussion on the various rectangular waveguide discontinuities follows.

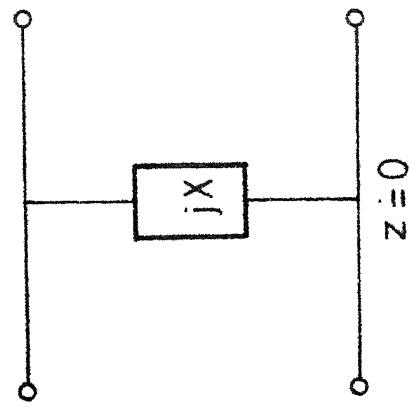
2.3.1a Diaphragms and windows:

One of the most common forms of discontinuity used in waveguide circuits is a metallic partition extending partially across the guide in a plane perpendicular to the direction of propagation, as shown in Fig. 2.5(a). The thickness of the partition is usually small compared with the wavelength involved, but the effects of the thickness can not always be neglected. The opening in the partition may be of any shape. Such a partition is called a diaphragm or an iris. The opening created by the partition is called a window. For thin partitions, the equivalent circuit is just a shunt element, as shown in Fig. 2.5(b). For thick partitions, the equivalent circuit consists of both series and shunt elements, as shown in Fig. 2.5(c).

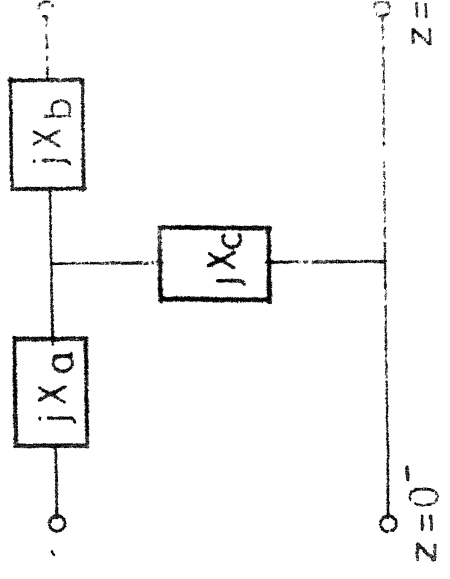
Details on various types of diaphragms and their equivalent circuits are available in several books (see, e.g., [3]-[5], [8]-[10], [13]) and research papers (see, e.g., [90]-[98]). Detailed analysis of the multiple diaphragms is also available [13].



(a) Physical configuration



(b) Thin conductor equivalent circuit



(c) Thick conductor equivalent circuit

Fig.2.5 Diaphragm in a rectangular waveguide and its equivalent circuits

2.3.1b Metallic strips:

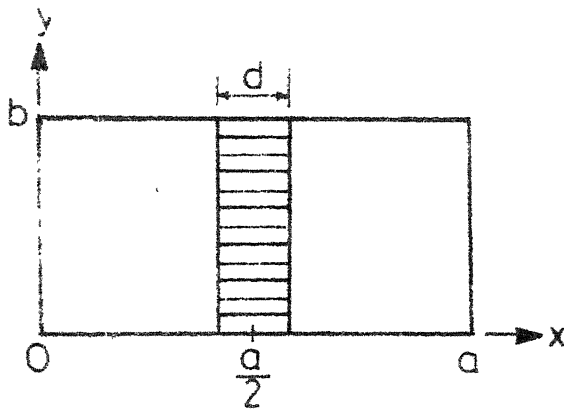
A strip is a thin rectangular conducting sheet placed in a plane across the cross-section of the waveguide. The strips may be placed either in E-plane (inductive strips) or in H-plane (capacitive strips) and may be symmetrical or nonsymmetrical, as shown in Fig. 2.6.

Detailed results on the metallic strips shown in Fig. 2.6 are available in literature (see, e.g., [9], [13]). Several more involved variations like strip and diaphragm combined, more than one strips combined, strip not extending across the entire height of the waveguide, axial strip, etc., have also been analysed (see, e.g., [13], [99]–[101]).

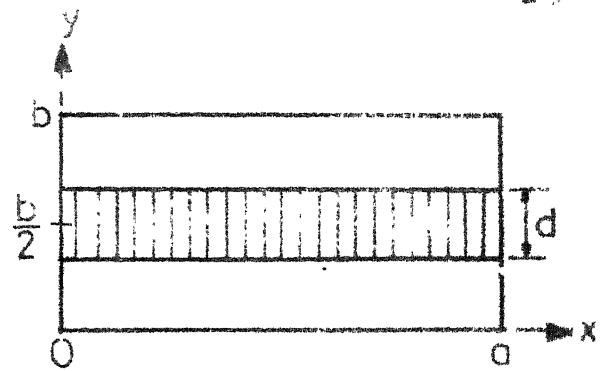
2.3.1c Posts and mounts:

A cylindrical rod (metallic, dielectric, or of any other material) loading the guide in a plane transverse to the direction of propagation is generally referred to as a 'post'. In principle, the cross-section of the post may be circular or noncircular. In practice, however, the posts having circular cross-section are the ones used almost exclusively. The posts may be placed either in E-plane or in H-plane, and may be symmetric or nonsymmetric.

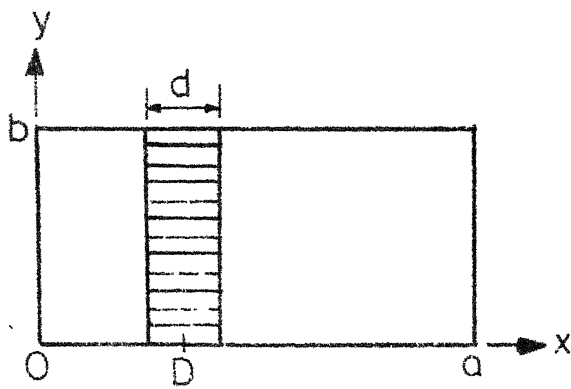
Metallic posts: Metallic posts with circular cross-section are frequently encountered in rectangular waveguides. They



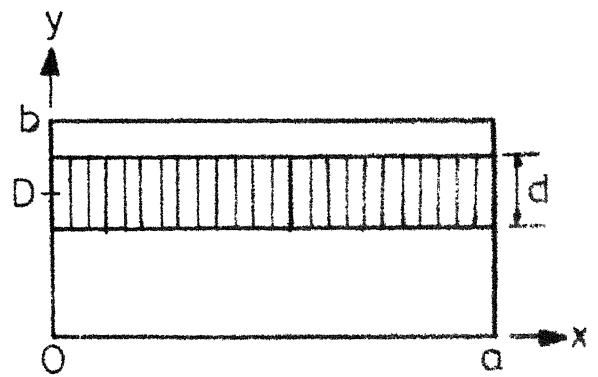
(a) Symmetrical inductive strip



(b) Symmetrical capacitive strip



(c) Unsymmetrical inductive strip



(d) Unsymmetrical capacitive strip

Fig. 2.6 Metallic strips in a rectangular waveguide

are used mainly as reactance elements and for mounting active devices across the guide. In the latter case, the configurations involved are generally known as 'waveguide mounts'.

The metallic posts may be placed in E, H, or any other plane. The E-plane (inductive) posts are illustrated, alongwith the equivalent circuits, in Fig. 2.7. The post which extends only partially along the height of the waveguide has an L-C equivalent circuit and is thus termed a 'resonant' post. On the other hand, the post which spans the full height of the waveguide has an L equivalent circuit, and is called a 'nonresonant' post.

The nonresonant inductive post, a general equivalent circuit for which is shown in Fig. 2.8, is a commonly employed configuration. Of the various results available for this kind of configuration, those given by Marcuvitz [5], Schwinger and Saxon [8] and Lewin [13] are the most well-known ones. The results given by Lewin seem to be more accurate, as Lewin has analysed the problem by taking into account the effects of the finite diameter of the post. In other words, the fine variations of the incident field across the guide in the vicinity of the post, and the variations in the incident field in the direction of

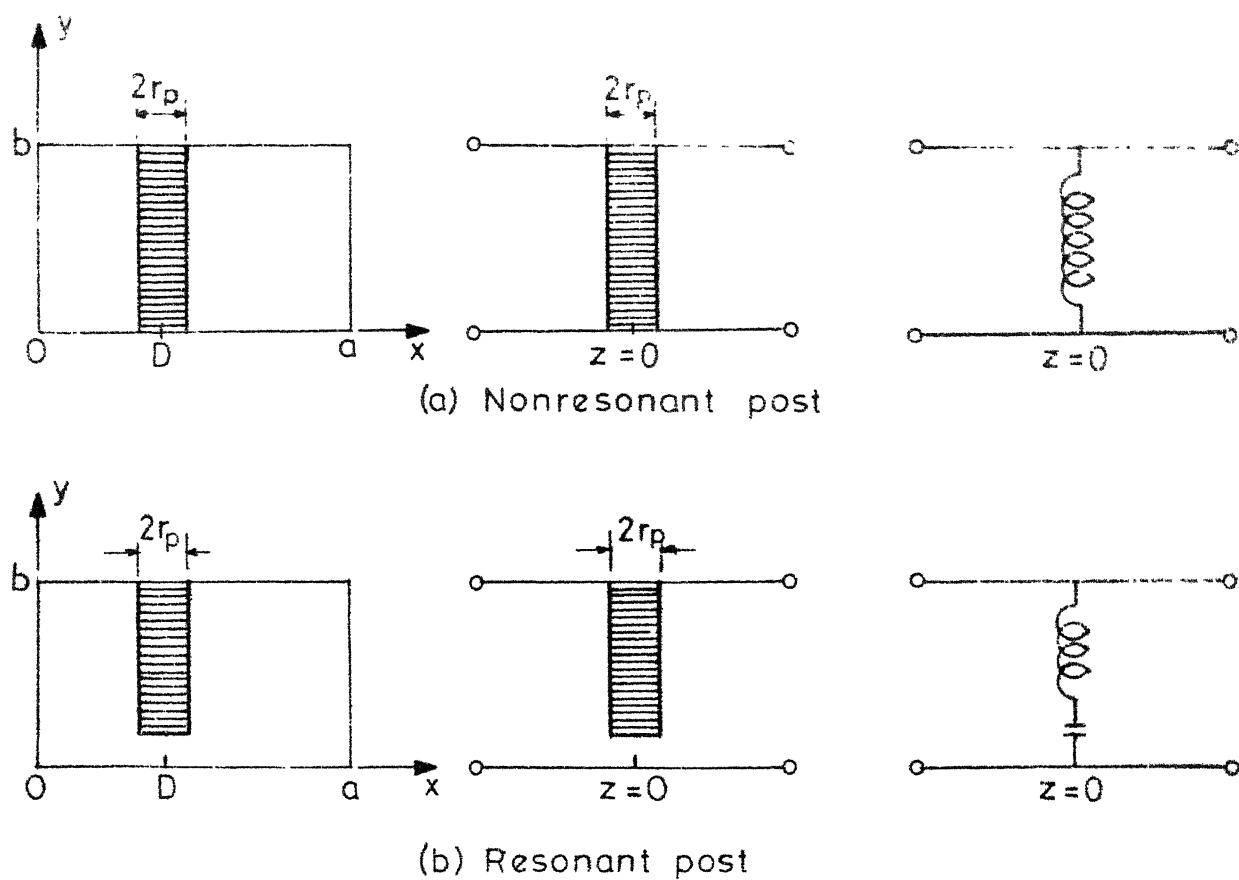


Fig. 2-7 Inductive metallic posts and their thin-post equivalent circuits

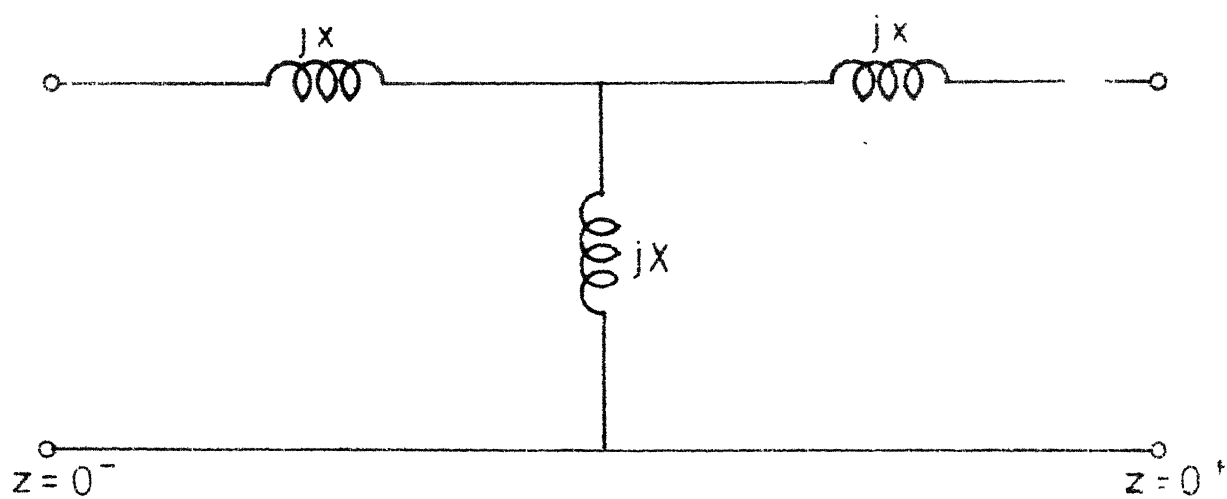


Fig. 2-8 Thick post equivalent circuit of a nonresonant inductive post

propagation across the post, have not been neglected by Lewin as was done by other authors.

Detailed results on various other types of metallic post configurations, e.g., resonant inductive posts, capacitive posts, (see Fig. 2.9), tilted posts, posts loaded at one or both ends, array of posts having one or more gaps, noncircular posts, posts in a ridged waveguide, etc., are also available in literature (see, e.g., [3]-[10], [13], [59], [102]-[123]).

Nonmetallic posts: Nonmetallic posts include dielectric posts, ferrite posts, posts with arbitrary complex permittivity (such as plasma columns, semiconductor rods and biological samples), etc. Detailed information on such posts in a rectangular waveguide can be had from the literature (see, e.g., [3]-[8], [10]-[13], [124]-[130]).

2.3.1d Steps and bifurcations:

An abrupt change in one or both dimensions of the cross-section of a rectangular waveguide is called a 'step'. Besides, any abrupt changes in the medium filling the guide can also be categorised as waveguide steps.

When a waveguide is divided into two guides by means of a thin conducting sheet, the configuration involved is known as a 'bifurcation'.

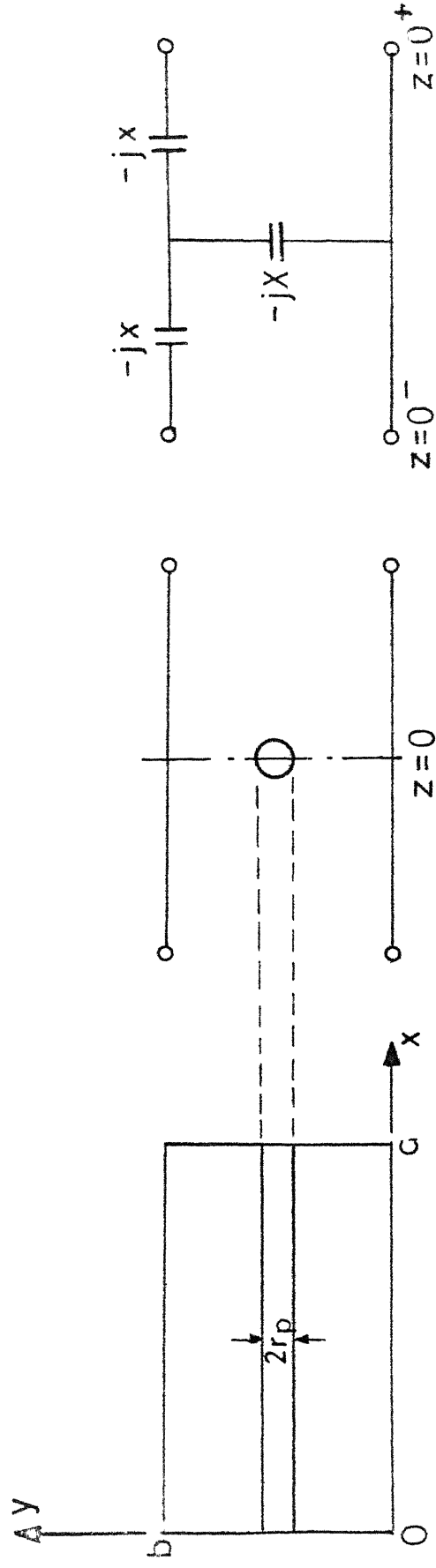


Fig. 2.9 A capacitive post and its equivalent circuit

Steps are frequently encountered in the design of impedance-matching sections, filters, etc. Bifurcations are encountered in components like power dividers and directional couplers.

Generally speaking, steps and bifurcations may be in one or both planes of the cross-section, and may be located symmetrically or asymmetrically.

A detailed discussion on waveguide steps and bifurcations will not be taken up here. The interested reader is referred to the literature (see, e.g., [3]-[10], [12]-[13], [59], [131]-[135]).

Detailed results on various other rectangular waveguide discontinuities such as periodically-loaded guides, holes, slits and apertures in the guide, waveguide bends and corners, conducting sphere in the guide, guide mounted with planar circuit, etc. are available in literature (see, e.g., [1]-[13], [59], [136]-[151]). Various nonuniformities, e.g. corrugated guides, axially-loaded guides, inhomogeneously-filled guides, guides filled with anisotropic medium, curves, twists and tapers in the guide, guides with reactive surface(s), etc. have also been considered (see, e.g., [3]-[7], [9]-[10], [12]-[13], [59], [152]-[157]).

2.4 MIC LINES AND THEIR DISCONTINUITIES

In the earlier days, the microwave circuitry consisted

essentially of coaxial lines and waveguides. The situation is even now the same where high powers are involved. At the low power end, the look of microwave systems is however getting transformed with the arrival of Microwave Integrated Circuits (MIC's). The advantages of MIC's over conventional lines are mainly the reduction in volume and weight, increased reliability, and low cost of production when produced in large numbers.

As in the case of conventional IC's, the MIC's can also be broadly divided into hybrid and monolithic circuits. In monolithic technology, various active devices and their interconnection patterns are formed simultaneously in single crystal substrates. In hybrid technology, the active devices are in the form of chips which are added externally.

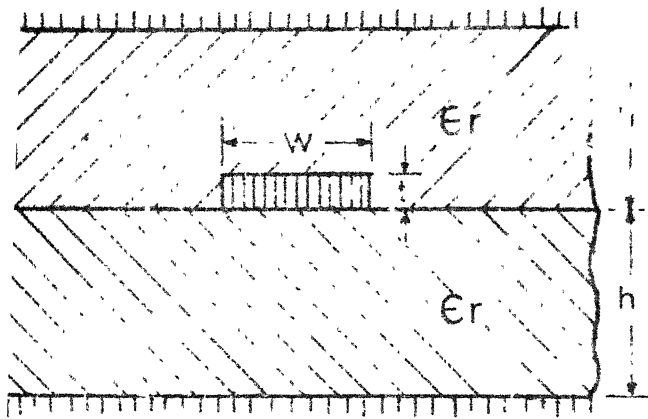
The major thrust in the development of MIC's so far has been in hybrid technology for several reasons. One of these reasons is that the microwave active devices are of a large variety, such as transistors, mixer diodes, varactors, PIN diodes, IMPATT diodes, TED's, etc. To standardise the process specifications so that these several kinds of devices can be simultaneously produced in an optimum way is not easy. Further, in MIC's the interconnections between the active components have relatively large dimensions,

especially where distributed elements are involved. This necessitates large areas of substrates which in the case of monolithic technology turn out to be quite expensive.

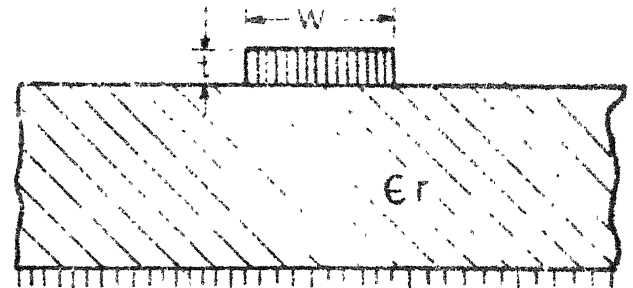
Hybrid technology itself can be divided into two parts, namely thin-film and thick-film technologies. Thick films are usually deposited as conductive, resistive, or insulating layers, through a screen printing process. Thin films are generally deposited in vacuum by evaporation or sputtering. The thickness can be further augmented by electro-plating.

Monolithic IC's become more attractive in the millimeter wave region, where dimensions and size of substrate required become smaller. Two types of substrates are normally used, namely silicon (Si) and gallium arsenide (GaAs). The latter, although more expensive, has the advantage that some of the newer active devices such as TED's can be grown right into the substrate.

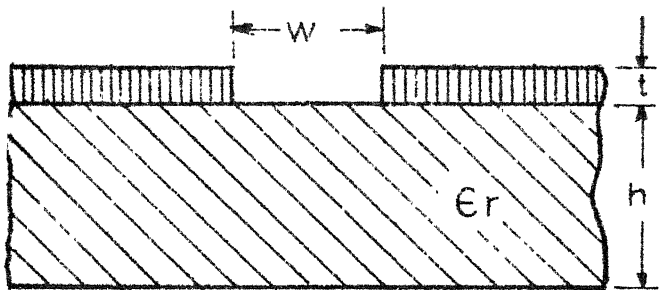
For transmission lines to be used in MIC's, it is desirable that the characteristics of the line (impedance, etc.) should depend on the dimensions in one plane only. This facilitates their fabrication by photoetching of metallised substrates. A few commonly known geometries that meet this requirement are shown in Fig. 2.10. These are the stripline, the microstrip, the slot line, the coplanar



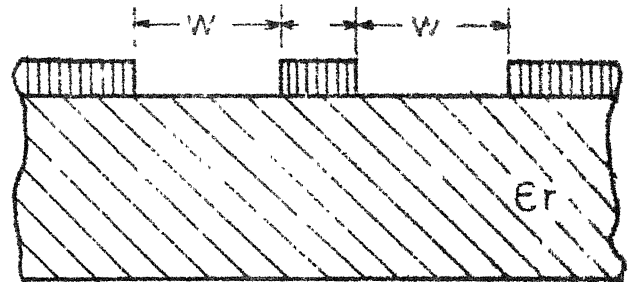
(a) Stripline



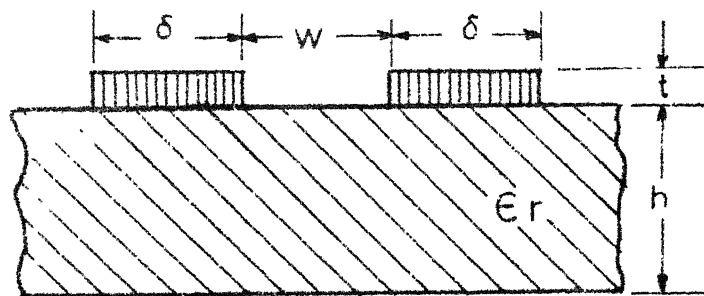
(b) Microstrip line



(c) Slotline



(d) Coplanar waveguide



(e) Coplanar strips

g. 2-10 Cross-sections of various planar structures

waveguide, and the coplanar strips. The stripline supports an exact-TEM mode. The microstrip, which is preferred over the stripline for reasons like ease of mounting components, facility for small on-the-spot adjustments, etc., supports a quasi-TEM mode⁺.

In the stripline, a thin conducting strip is sandwiched between two dielectric laminates metallised on the outer sides (see Fig. 2.10(a)). The mode of propagation is a TEM-mode and the characteristic impedance is evaluated by finding the electrostatic capacitance. The most widely used method of calculation is a set of equations reported by Cohn [158] in 1955. Detailed formulas for the characteristic impedance and propagation constant of a stripline are available in literature (see, e.g., [158]-[160]).

A microstrip line (see Fig. 2.10(b)) consists of a thin conducting strip on one side of a dielectric substrate. The other side of the substrate is completely metallised so as to serve as a ground plane. The microstrip structure may be derived from the stripline configuration by removing the

⁺By quasi-TEM mode is meant the mode in which the axial components of E and H fields are quite small and can be neglected as a first-order approximation. The error introduced by the neglect of axial field-components becomes more pronounced as the frequency is increased.

top ground plane and the upper laminate. In the microstrip line, the electromagnetic energy propagates both in the dielectric substrate below the strip and in the air region above. The fraction of power flowing outside the substrate is a function of strip width and therefore the 'effective' dielectric constant depends on the microstrip width. Thus the guided wavelength becomes a function of the characteristic impedance of the line. Also, the mixed dielectric nature of the microstrip line does not allow propagation of a pure-TEM mode. Moreover, the open dielectric surface of the substrate can support surface-wave modes which could couple to the microstrip propagation unless substrate dimensions are properly chosen so as to avoid this interaction. An exact analysis of the microstrip line requires computer based numerical methods. For most of the practical designs, the propagation mode can, however, be taken as pure TEM and Wheeler's results based on electrostatic analysis [161]-[163] can be used.

The slotline (see Fig. 2.10(c)) consists of a slot or gap in a conductive coating on a dielectric substrate, the other side of the substrate being bare. This line was first proposed by Cohn [164] in 1969. This line differs from the other two lines described above mainly in that the mode of propagation in this line is non-TEM. The main

advantage of this line is that it can be accommodated in microstrip circuits by effecting the desired etching in the ground plane of the substrate. This type of hybrid construction allows a new kind of flexibility in the design, saves the substrate area, and has led to some new types of circuits, e.g. hybrid branch-line directional couplers. Also, some of the circuit elements, which can not be easily achieved in microstrip configuration, can be easily incorporated in the slotline part of the circuit. These, for example, could be short-circuits, high impedance lines, etc.

For more information on slotline and associated structures, the reader is referred to the literature (see, e.g., [164]-[169]).

The coplanar waveguide (CPW) consists of a strip of thin metallic film deposited on the surface of dielectric slab, with two ground planes running adjacent and parallel to the strip on the same surface (see Fig. 2.10(d)). This line was proposed by Wen [170] in 1969. The mode of propagation along a CPW is essentially non-TEM. The electric field between the central conducting strip and ground planes is tangential to the air-dielectric boundary and produces a discontinuity in displacement current density at the interface. This field configuration gives rise to an axial as well as transverse component of the magnetic field. These

components provide the elliptical polarization needed for nonreciprocal ferrite circuits. Also, discrete components may be shunt mounted between the central strip and either of the ground planes and drilling of holes or slots through the substrate is not needed. Thus, CPW's exhibit the two major advantages of the slotline, namely application to ferrite circuits and shunt mounting of components.

The configuration of coplanar strips (CPS) is complementary to that of CPW. It consists of two strips (generally of equal widths) running parallel on the same surface of the dielectric slab (see Fig. 2.10(e)). At lower microwave frequencies, the CPS is useful for carrying signals for high-speed computer circuits.

The CPW and CPS, taken together, are generally termed the 'coplanar lines'. The reader interested in obtaining more information on the coplanar lines is referred to the literature (see, e.g., [165]-[166], [170]-[173]).

Of the various planar transmission structures discussed above, microstrip line is the one which is most commonly used. The main reason for this is the fact that the mode of propagation on a microstrip is almost TEM, which permits an easy approximate analysis and simple transitions to coaxial circuits. Also, as mentioned earlier, the microstrip line

is superior to the stripline (which is the only other planar structure which supports a TEM mode) in respects like ease of mounting components, facility for minor on-the-spot adjustments, etc.

The following subsections briefly survey the various aspects of microstrip transmission line and its discontinuities.

2.4.1 Methods of Analysing a Microstrip Line:

The various methods available for analysing a microstrip line fall in the following main categories.

- i) Quasi-static methods
- ii) Dispersion models
- iii) Full-wave analyses

2.4.1a Quasi-static methods:

In these methods, the nature of mode is considered to be pure TEM and the properties of the line are calculated from its electrostatic capacitance. Two types of capacitances are defined, one (C_a) for a unit length of microstrip configuration with the dielectric substrate replaced by air, and the other (C) for a unit length of microstrip with the dielectric substrate present. The values of the characteristics impedance (Z_{om}) and phase constant (β) can be calculated from C and C_a by means of well-known expressions (see, e.g., [165]-[166]).

The various approaches available for calculating C and C_a are the conformal transformation techniques [161]-[163], [174], the finite-difference method [175], the integral equation approach [176]-[179], and the variational method in FTD [180]-[183]. Detailed discussions on these approaches are available in reviews by Mittra and Itoh [184], Gupta, Garg and Bahl [166], etc.

Of the various quasi-static analyses, the method of modified conformal transformation used by Wheeler [161]-[163] seems to be the only one which gives easy-to-use accurate closed-form solutions. The latest results given by Wheeler are those published in 1977 [163]. The main advantage of these results over those reported earlier [161]-[162] is that only one set of formulas is required for all values of the aspect ratio. This is in contrast with the different sets of formulas given earlier for aspect ratio less than and greater than two. Also, in these new formulas, the effects of finite strip thickness have been incorporated more accurately.

2.4.1b Dispersion models:

The quasi-static methods of microstrip analysis mentioned above do not take into account the non-TEM nature of the microstrip mode. The non-TEM behavior causes the

The various approaches available for calculating C and C_a are the conformal transformation techniques [161]-[163], [174], the finite-difference method [175], the integral equation approach [176]-[179], and the variational method in FTD [180]-[183]. Detailed discussions on these approaches are available in reviews by Mittra and Itoh [184], Gupta, Garg and Bahl [166], etc.

Of the various quasi-static analyses, the method of modified conformal transformation used by Wheeler [161]-[163] seems to be the only one which gives easy-to-use accurate closed-form solutions. The latest results given by Wheeler are those published in 1977 [163]. The main advantage of these results over those reported earlier [161]-[162] is that only one set of formulas is required for all values of the aspect ratio. This is in contrast with the different sets of formulas given earlier for aspect ratio less than and greater than two. Also, in these new formulas, the effects of finite strip thickness have been incorporated more accurately.

2.4.1b Dispersion models:

The quasi-static methods of microstrip analysis mentioned above do not take into account the non-TEM nature of the microstrip mode. The non-TEM behavior causes the

effective dielectric constant (ϵ_{re}) and the characteristic impedance (Z_{om}) of the microstrip to be functions of frequency. Variations in ϵ_{re} are more significant than those in Z_{om} .

There are several semiempirical techniques through which the variations of Z_{om} and ϵ_{re} with frequency (or, as they are popularly known, the dispersion effects) can be modelled. These techniques have been categorised as 'dispersion models'. The various dispersion models such as coupled TEM and TM modes model [185], empirical relation for frequency-dependent phase velocity [186], ridged-waveguide model [187], coupled TEM and TE modes model [188], planar waveguide model [189] and modification of Getsinger's formula [190] have been discussed by Gupta, Garg and Bahl in their book [166]. The central theme in all these models is that the deviation from TEM nature is accounted for quasi-empirically, i.e., some parameters of the model are determined such that the final expression agrees with the known experimental (or exact theoretical) dispersion behavior of the microstrip.

Of the various dispersion models mentioned above, the planar waveguide model [189] is a very powerful tool because this model has some unique features like i) its ability to easily predict the higher-order microstrip modes and ii) the

ease with which many microstrip discontinuity problems can be solved by an application of principles similar to those used for analysing waveguide discontinuities. In this model, the microstrip is approximated by a parallel-plate waveguide of frequency-dependent width and constant height as shown in Fig. 2.11. The top and bottom plates are assumed to be of an infinite electrical conductivity and the side-walls are assumed to be magnetically perfect. The guide is assumed to be filled with a dielectric medium having frequency-dependent permittivity. The expressions for frequency-dependent parameters of the planar waveguide will be presented in Chapter 5, where this model will be applied to analyse a coaxial-microstrip junction problem. The reader is also referred to Appendix I where the field expressions for TEM, TE and TM modes in a planar waveguide are derived.

Recently, one more empirical formula to account for the dispersion effects in a microstrip line has been reported [191]-[192].

2.4.1c Fullwave analyses:

Strictly speaking, a microstrip line can not support a TEM mode. In fact, one can easily show that not even pure TE or TM modes can exist on this line, and that it can support only a hybrid mode (i.e., one in which the longitudinal components of both the electric and magnetic fields are

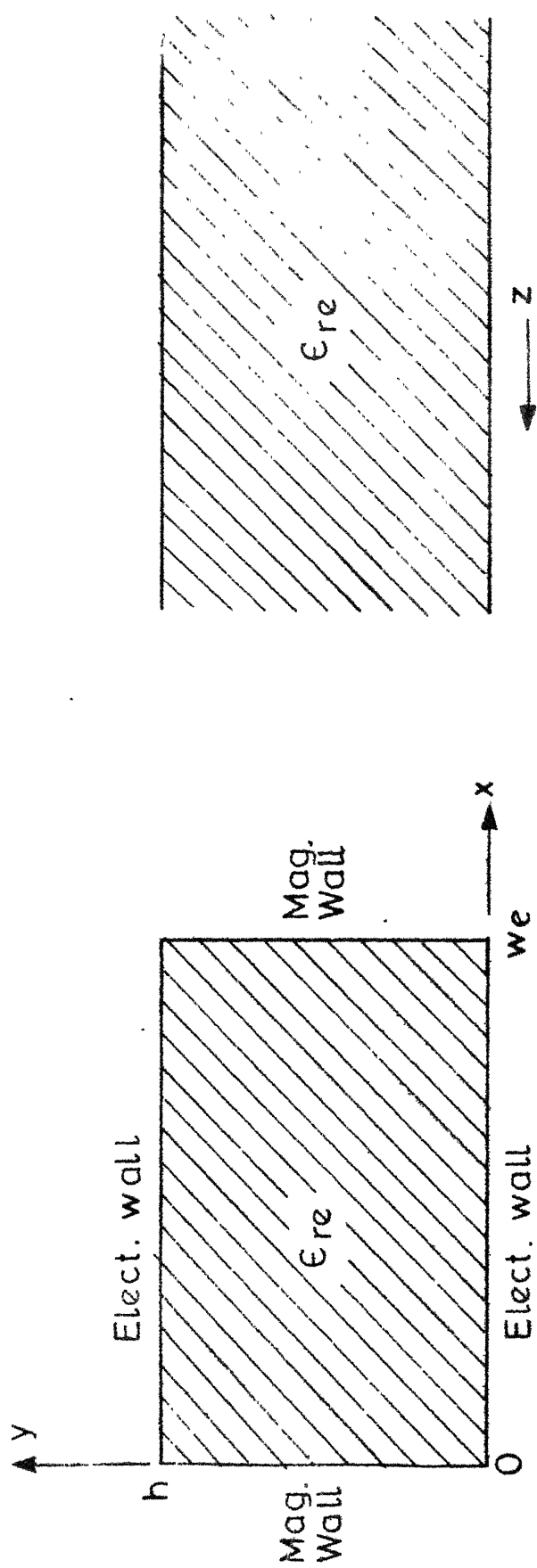


Fig. 2-11 A planar waveguide

nonzero). The methods that opt for an hybrid-mode analysis of the microstrip line are termed 'fullwave analyses'. These methods may be divided into two groups. In one group, the microstrip is analysed alongwith a rectangular enclosure⁺ and the other group deals with the open microstrip. Such a grouping is convenient because different types of mathematical tools are needed for handling closed and open geometries. For instance, a Fourier series representation can be used to express the fields in a closed rectangular structure whereas a Fourier integral representation is suitable for an open structure.

Two orthogonal sets of hybrid modes can be shown to exist on an open/enclosed microstrip line. One of these modes has a symmetric E_z and antisymmetric H_z (E_z even - H_z odd) whereas the other mode is characterized by antisymmetric E_z and symmetric H_z (E_z odd - H_z even). The dominant mode is the lowest-order E_z even - H_z odd mode which, at low frequencies, approaches the quasi-TEM solution.

A number of methods for fullwave analysis of the microstrip line have been suggested. The most commonly known ones are the integral equation method [193]-[194],

⁺The metallic rectangular enclosure is generally used with a microstrip for hermetic sealing, mechanical strength, electromagnetic shielding, mounting the connectors and ease of handling.

the finite difference method [195], and Galerkin's method in FTD [196]-[197]. Detailed discussions on fullwave analyses of the microstrip line are also available in contributions by Mittra and Itoh [184], Gupta and Singh [165], Gupta, Garg and Bahl [166], Kuester and Chang [198], etc.

2.4.2 Microstrip Discontinuities:

Microstrip circuits are invariably accompanied by discontinuities of one type or another. Some of the most common forms of microstrip discontinuities are open ends, gaps, steps in width, bends, etc. Since the dimensions of the discontinuities are generally much smaller than the wavelength in microstrip, lumped-circuit equivalents can be used to approximate the effects of discontinuities. A more complete characterization, however, requires determination of frequency-dependent scattering-matrix coefficients associated with the discontinuity.

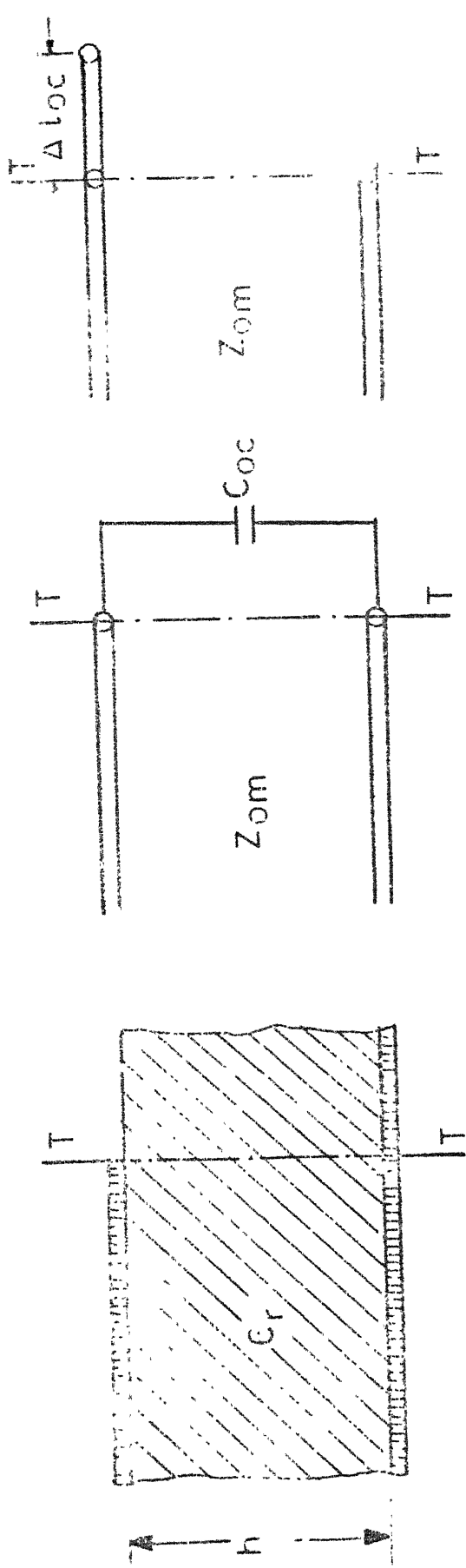
The analysis of a microstrip discontinuity can be based on any of the previously mentioned methods of microstrip analysis. In other words, a given microstrip discontinuity problem can be handled either through quasi-static analyses, or through dispersion models, or through fullwave analyses. In the subsections to follow, a brief survey of the various commonly used microstrip discontinuities and their analyses is presented.

2.4.2a Open-ends:

An abruptly ended microstrip constitutes an open-end in the microstrip, as shown in Fig. 2.12(a). The open-end discontinuity occurs in components like resonators, matching stubs, parallel-coupled filters, etc. The effects of an open-end are represented by means of an excess capacitance C_{oc} in parallel with the line, as shown in Fig. 2.12(b). Alternatively, the open-end can be represented by adding an extra length ΔL_{oc} in line, as shown in Fig. 2.12(c).

The various quasi-static methods that have been applied for analysing an open-ended microstrip line are the matrix inversion method [178], [199], the variational method [200], Galerkin's method in FTD [201], and the use of line sources with charge reversal [202]. Of these, the results reported by Silvester and Benedek [202] are more accurate, as their computations do not involve subtraction of two almost equal large numbers, an ailment from which all other quasi-static methods of analysing an open-ended microstrip suffer.

The quasi-static analyses mentioned above have also been discussed in detail by Gupta, Garg and Bahl [166]. These analyses do not account for dispersion effects. Recently, Bedair and Sobhy [203]-[204] have given frequency-dependent closed-form expressions for the open-end discontinuity in a shielded microstrip line.



(a) The open-end (b) Equivalent circuit I (c) Equivalent circuit II

Fig. 2.12 Microstrip open-end and its equivalent circuits

Detailed easy-to-use formulas for the open-ended microstrip are given in Appendix II.

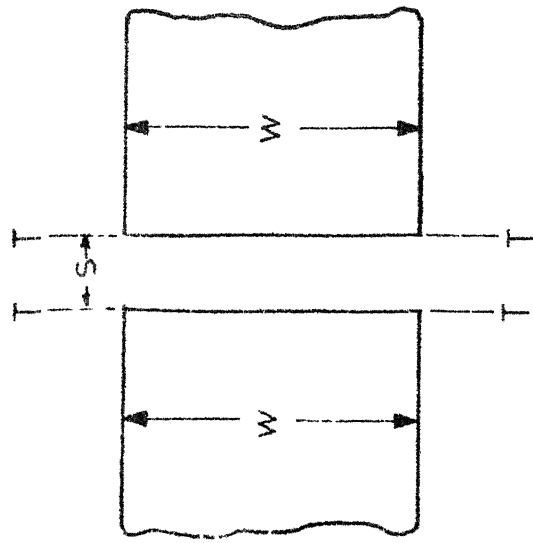
2.4.2b. Gaps:

The gap in microstrip, shown in Fig. 2.13(a), is encountered in components like d.c. blocks, end-coupled filters, coupling elements to resonators, etc.

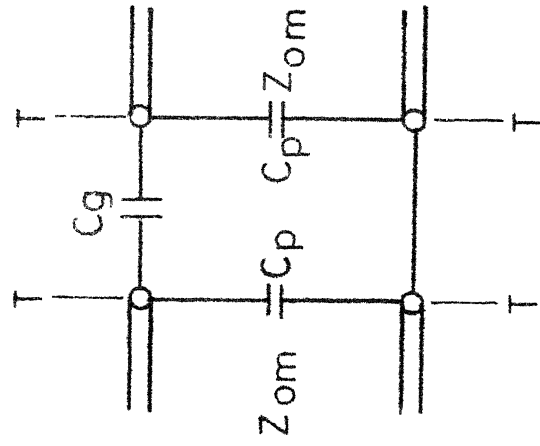
Two types of equivalent circuits of a microstrip gap are used. One of them, as shown in Fig. 2.13b, is a π -network consisting of a series capacitance C_g and two parallel capacitances C_p . The series capacitance C_g arises from the coupling between the strip conductors constituting the gap. The shunt capacitance C_p is the result of the disorder in electric-field distribution at the edge of the strip. The capacitance C_g decreases with increase in gap spacing s . For infinite spacing, C_g should approach zero and C_p should equal the capacitance C_{oc} of an open-ended strip.

Another equivalence which can be used to represent a microstrip gap is by using an extra line length Δl_g , as shown in Fig. 2.13c.

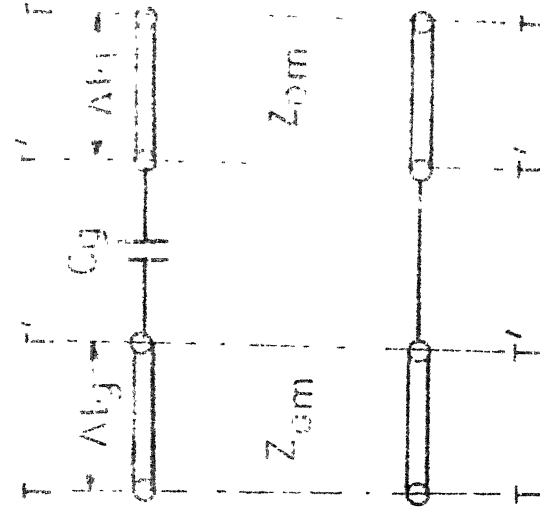
Of the four sets of quasi-static results reported for a microstrip gap configuration [199]-[200], [205]-[206], the results given by Benedek and Silvester [205] are the



(a) The gap



(b) Equivalent circuit I



(c) Equivalent circuit II

Fig. 2.13 Microstrip gap and its equivalent circuits

most accurate ones as the other three results involve subtraction of two almost equal large numbers.

By curve-fitting the available numerical results [205], Garg and Bahl [207] have derived reasonably accurate easy-to-use empirical expressions for C_p and C_g . These results are reproduced in Appendix II.

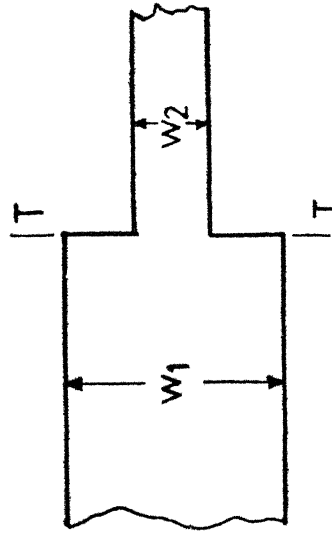
2.4.2c Steps in width:

This type of discontinuity is formed by the junction of two lines of different widths, as shown in Fig. 2.14a. The discontinuity is said to be symmetrical if the axes of the lines are coincident and asymmetric otherwise.

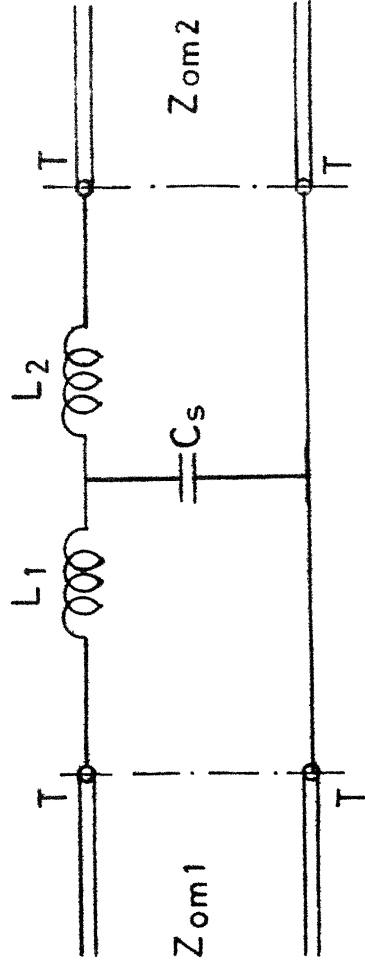
The step discontinuity is often encountered when designing matching transformers, couplers, filters and transitions. The equivalent circuit of a step discontinuity comprises two series inductances and a shunt capacitance, as shown in Fig. 2.14b. Detailed results on steps in microstrip are available in literature (see, e.g., [166], [199], [205], [207], [208]-[212]).

2.4.2d Bends:

A microstrip bend may be formed by two lines of equal or unequal impedances. The bend is normally used for introducing flexibility in the layout of the circuit design.

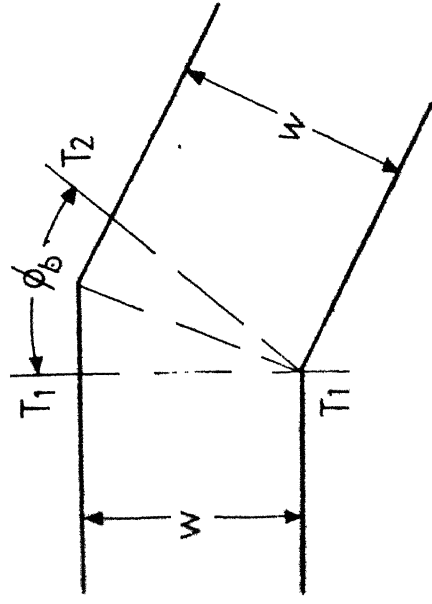


(a) The step in width

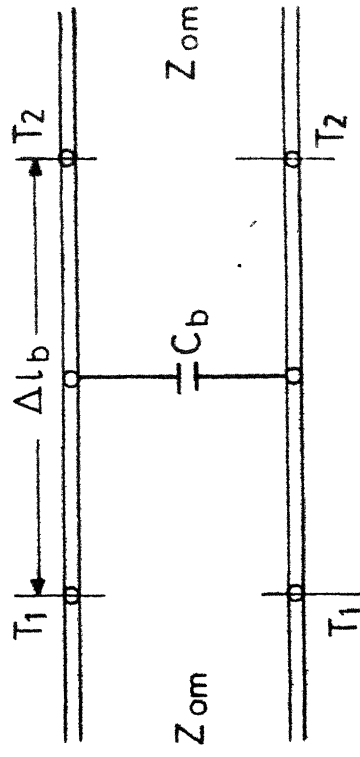


(b) Equivalent circuit

Fig. 2-14 Microstrip step discontinuity and its equivalent circuit



(a) The bend



(b) Equivalent circuit

Fig.2-15 Microstrip bend and its equivalent circuit

A microstrip bend with lines of equal impedances is shown, along with the equivalent circuit, in Fig. 2.15. For detailed results on various types of bends, the reader is referred to the literature (see, e.g., [166], [207], [212]-[216], [219]).

2.5 JUNCTIONS OF SIMILAR LINES

The junctions of two similar lines constitute 'steps' and 'bends' in the line and have been adequately discussed in the previous sections. The junctions of more than two similar lines are used to produce non-reciprocal components like Tees, Directional Couplers, Circulators, power dividers, etc. A detailed discussion on these configurations is beyond the scope of the present study. The interested reader is, however, referred to the literature (see, e.g., [1]-[7], [59], [69], [160], [166], [210], [214]-[224]).

2.6 JUNCTIONS OF DISSIMILAR LINES

The junctions of dissimilar lines are used mainly to serve as a means of launching the electromagnetic energy from one line into the other. Many times, one line, in the form of a stub, may also be employed as reactance element in the other line.

The junctions of dissimilar lines can be categorised, on the basis of the types of lines involved, into coaxial -

waveguide junctions, coaxial-stripline junctions, coaxial-microstrip junctions, coaxial-slotline junctions, waveguide-microstrip junctions, slotline-microstrip junctions, etc. In the subsections to follow, a brief discussion on various commonly known junctions of dissimilar lines is presented.

2.6.1 Coaxial-waveguide Junctions:

As coaxial lines and waveguides have been in use since long, the junctions involving them have also been a constant subject of study. These junctions can be subdivided into two main categories: coaxial line - rectangular waveguide junctions and coaxial line - circular waveguide junctions. Although some analyses of the junctions belonging to the latter category have been reported [5], [225]-[227], the junctions in the former category have clearly received a much wider attention. The reason behind this trend is presumably the fact that, in actual practice, the rectangular waveguide is used more often than its circular counterpart.

Coming to the coaxial line-rectangular waveguide junctions, one again notices a clearcut emphasis on the broadwall configuration (shown in Fig. 2.16) although, admittedly, many other configurations like the coaxially - driven loop (see, e.g., pp. 271-285 of [9]), the coaxially - driven capacitive posts (see, e.g., p. 195 of [10]) and

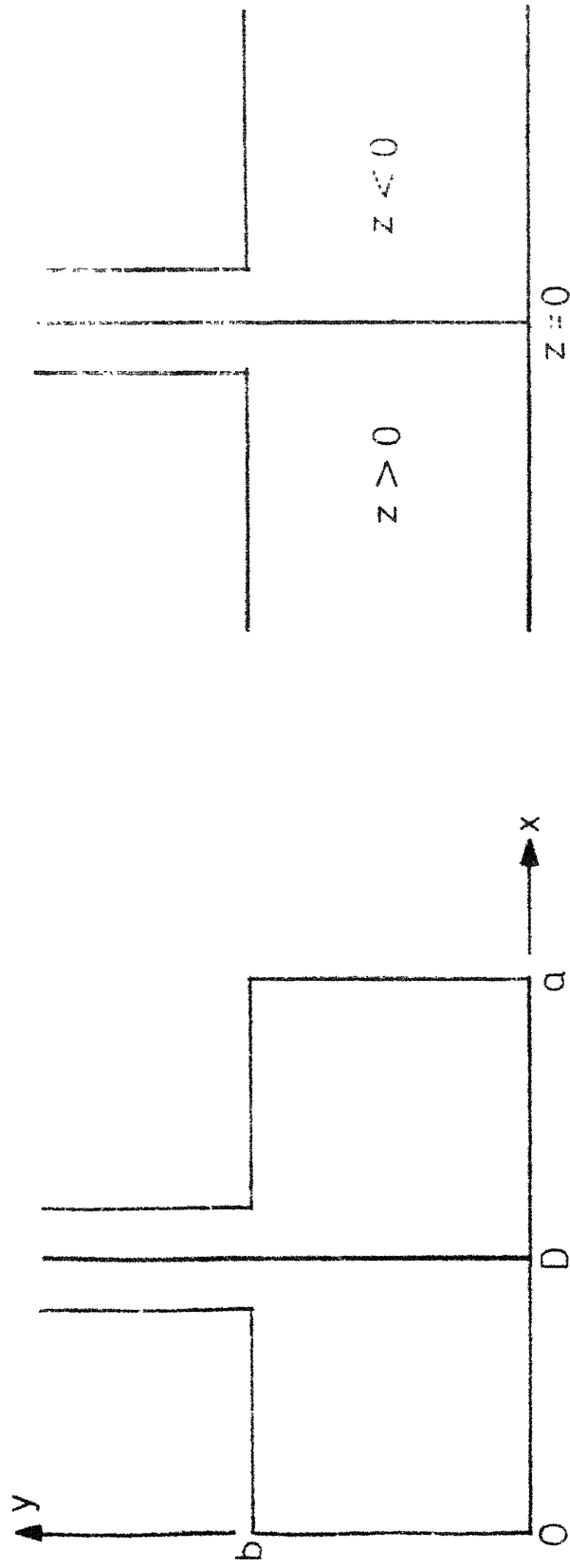


Fig. 2.16 The general broad-wall coaxial-waveguide junction

the end-launcher [228] have also been suggested and analysed. The broadwall configuration and its variations will be discussed in the following subsections.

2.6.1a Broadwall coaxial-waveguide junction:

The junction formed by a coaxial line entering the broadwall of a rectangular waveguide and driving a E-plane probe therein (Fig. 2.16) is a frequently encountered component in microwave circuitry. Over other coaxial line - rectangular waveguide junctions, this junction enjoys unique advantages like large bandwidth, low VSWR, maximum power transfer, etc. Moreover, in many cases, this junction provides the only solution to a designer's coupling or mounting problem.

A concise account of literature on the broadwall junction till 1968 was given by Braly [229] in 1969. In 1978, Eisenhart et.al. [230] established, through extensive experimentation, a very useful equivalence between the properties of this junction and those of another well-known configuration (namely, a gap-loaded E-plane waveguide post). Besides these authors, several other authors like Collin (pp. 256-271 of [9] and pp. 183-187 of [59]), Harrington (pp. 178-179, pp. 425-428 and p. 444 of [10]) and Lewin (p. 158-163 of [13]) have also analysed this and similar

problems. The case considered by Collin, which is a very commonly known method of ensuring broad-band coupling between coaxial line and waveguide, is shown in Fig. 2.17. In this configuration, the coaxial line drives a resonant E-plane waveguide post and one end of the waveguide is terminated in a short-circuit. The values of l and l_r to ensure full coupling may be found graphically, as suggested by Collin.

The case considered by Harrington, alongwith the equivalent circuit as derived by him, is shown in Fig. 2.18. In this case, the waveguide is assumed to be matched at both ends. The infinite series involved in the expression for X diverges because of the assumption taken by Harrington that the probe is infinitesimally thin. As a result, no meaningful results can be obtained for X by using Harrington's formulation.

The case considered by Lewin is shown, alongwith the equivalent circuit as proposed by him, in Fig. 2.19. This case is identical to the one considered by Harrington, with the only exception*that the waveguide ports have been assumed to be terminated arbitrarily. The formulation given by Lewin will be discussed in detail in Chapter 4, where this formulation will be applied for analysing a coaxial-waveguide junction problem.

87508

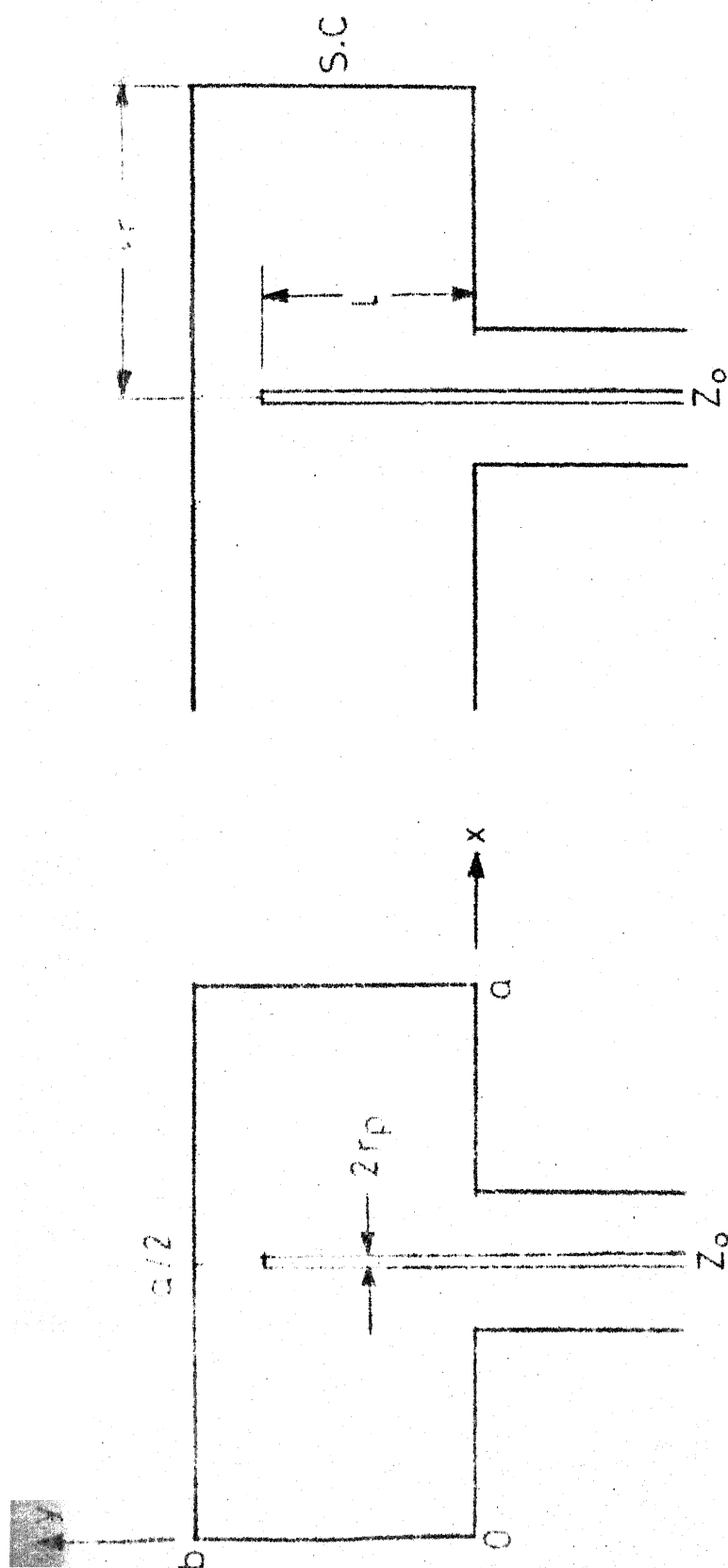
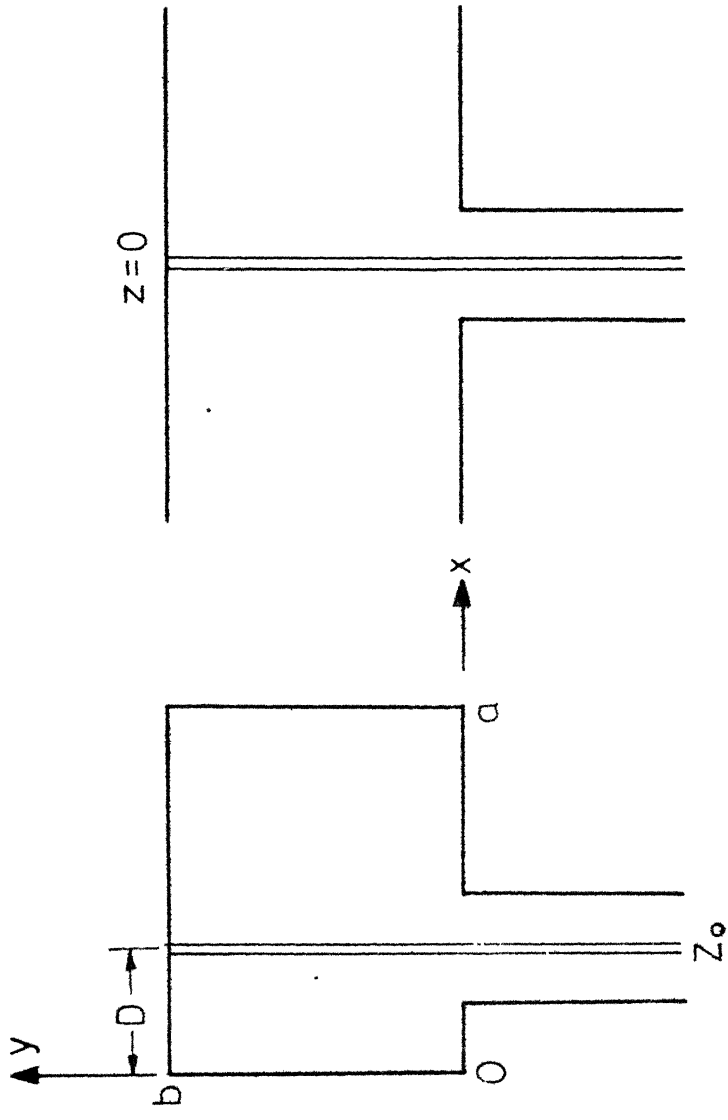
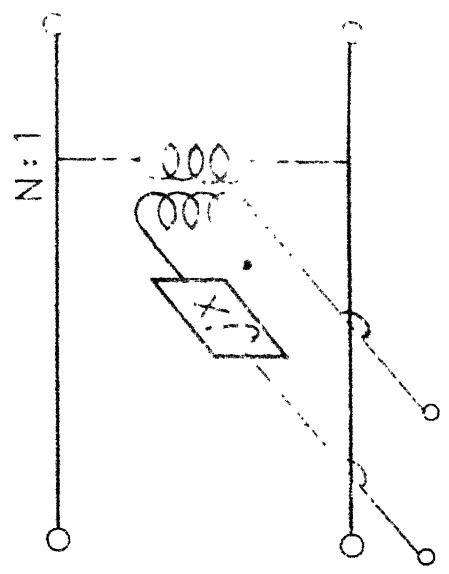


Fig. 2-17 Common broad-wall coaxial line - rectangular waveguide launcher

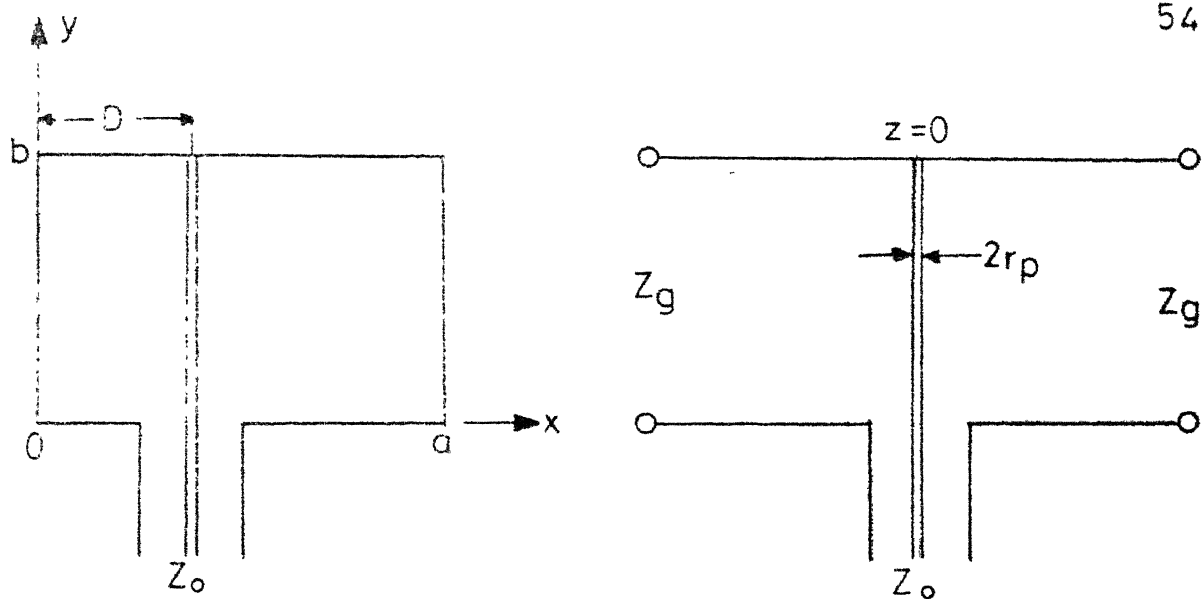


(a) The junction

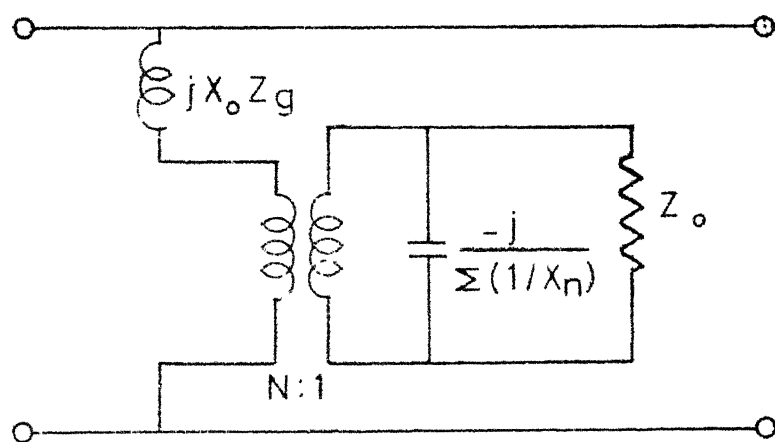


(b) Equivalent circuit

Fig. 2.18 The broad-wall junction analysed by Harrington



(a) The junction



(b) Equivalent circuit

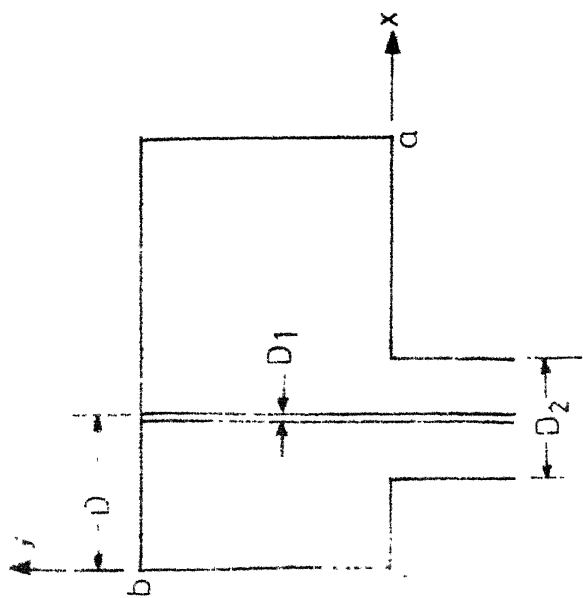
Fig.2.16 The broad-wall junction analysed by Lewin

Recently, Williamson [231] has reviewed the latest status of the broadwall coaxial-waveguide junction especially as regards its analysis. He has also refined the equivalent-circuit of the junction by incorporating effects of dimensions of the coaxial aperture in the analysis. The case considered by him is shown, alongwith the equivalent-circuit proposed him, in Fig. 2.20. The formulation given by Williamson will also be considered in Chapter 4.

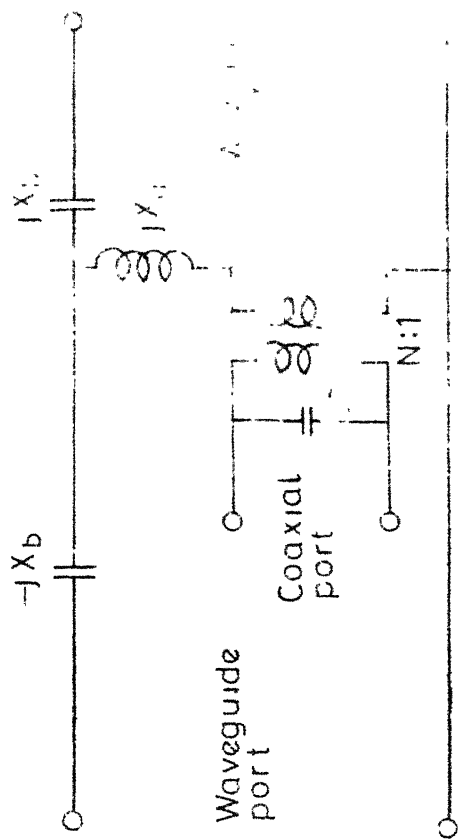
2.6.2 Coaxial-Stripline Junction:

Coaxial-to-stripline junctions constitute the largest variety of stripline feeds. One of the main reasons for this is the fact that striplines are mostly used for broadband systems where the bandwidth of the conventional waveguides is not adequate.

The most commonly employed coaxial-stripline junction is the end-fed launcher shown in Fig. 2.21. In this method, the contact between two lines is effected by a tab extending from the inner conductor of the coaxial line. The tab is held in contact with the strip by the pressure between the two pieces of the triplate construction. The best results are obtained ($V_{SWR} < 1.1$) when the chosen ground-plane spacing is close to the outside dimensions of the coaxial line. A broad-band model for a typical junction of this



(a) Sectional view of the junction



(b) Equivalent circuit

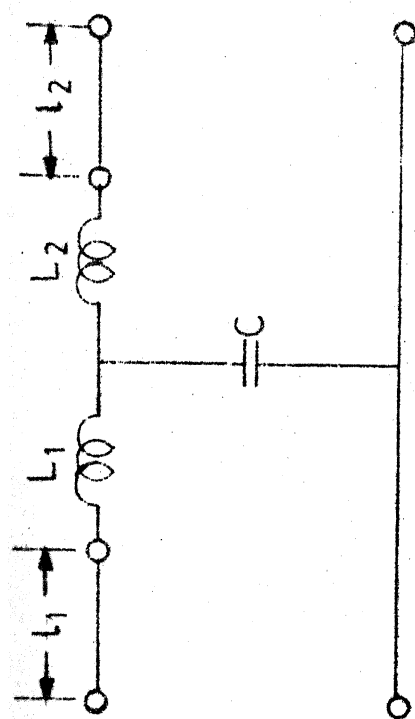
Fig.2-20 Broadwall junction considered by Williamson

type has recently been proposed by Chapman and Aitchison [232]. Several other variations of this junction, e.g. use of an interface (or of several transitions) in case of narrow ground-plane spacings, have been discussed by Howe [160]. Howe has also recommended the use of broadwall launching (Fig. 2.22) for cases in which i) ground-plane spacings are small and ii) frequencies involved are not above S-band. In the broadwall launching, the coaxial line is mounted on one of the ground planes and the central conductor of the coaxial line penetrates the substrate through a cylindrical hole to feed the strip.

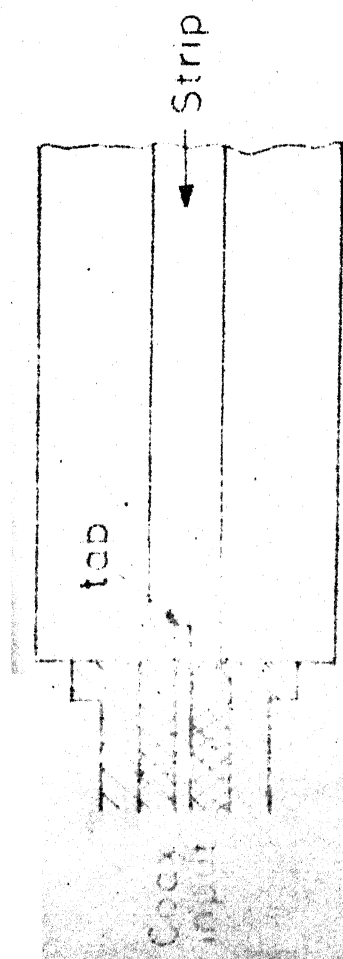
2.6.3 Coaxial-Microstrip Junction:

Coaxial-to-microstrip junctions are very much similar to the corresponding stripline versions. Sometimes, an intermediate section of stripline is used between the coaxial line and the microstrip.

The end-fed coaxial-microstrip launcher has been studied thoroughly (see, e.g., [233]-[236]). The broadwall launcher seems, however, not to have received much attention. In Chapter 5 of this thesis, a model for the input reactance seen by the coaxial line in such a launcher will be developed.



(b) An equivalent circuit



(a) Cross-section of the configuration

Fig. 2.21 End-fed coaxial-stripline launcher

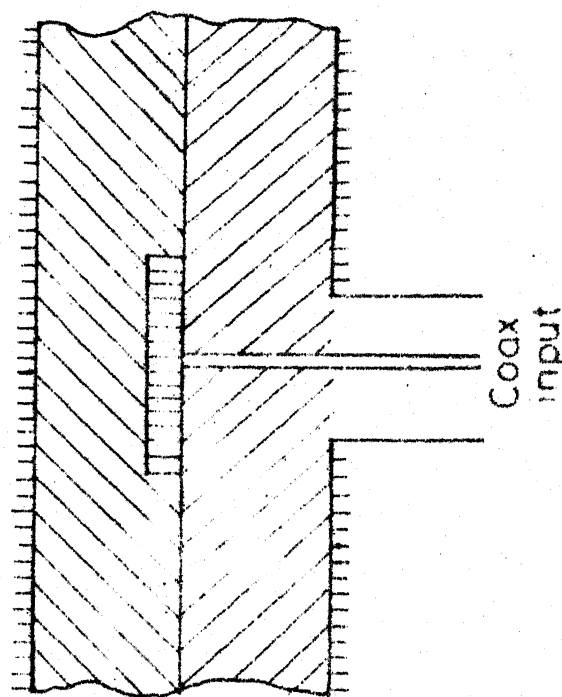


Fig. 2.22 Broad-wall coaxial-stripline launcher

2.6.4 Waveguide-Microstrip Junctions:

A very common method of realising waveguide-to-microstrip junctions is to combine waveguide-coaxial and coaxial-microstrip transitions in a single unit. Similar technique can be used for realising waveguide-stripline junctions also. Details on various junctions using this principle can be found in literature [160].

A waveguide-microstrip transition for operation near 30 GHz was described by Schneider [237] in 1969. This transition involves transformation from a rectangular waveguide using a four-stepped ridge. A tab connected to the top of the last step of the ridge is pressed against the microstrip using an insulated screw. The microstrip ground-plane is in continuation with the other broadwall of the waveguide. This transition was reported to have a return loss of more than 30 dB, an insertion loss of less than 0.1 dB, and a bandwidth of 17 percent.

A simpler waveguide-to-microstrip transition was suggested by Knerr [238] in 1968. In his version, waveguide and microstrip are perpendicular to each other and the substrate is perpendicular to the axis of the waveguide. In other words, the transition suggested by Knerr is very much similar to the broadwall coaxial-waveguide junction discussed earlier.

Further details on the above mentioned waveguide-microstrip junctions can be found in literature (see, e.g., [160], [237]-[238]).

2.6.5 Microstrip-Slotline Junctions:

Some commonly known microstrip-slotline transitions are shown in Fig. 2.23. Of particular relevance to this thesis are the configurations shown in Fig. 2.23c, 2.23d and 2.23e where thin transversely placed metallic wires short-circuit the microstrip with the ground plane. The characterization of such a wire in microstrip line will be the subject of study in Chapter 6 of this thesis.

Details on various microstrip-slotline junctions, including those shown in Fig. 2.23, can be found in literature (see, e.g., [166]).

Details on various other types of junctions of dissimilar lines, e.g., coaxial-slotline junctions, coaxial-coplanar line junctions, etc., can also be found in literature (see, e.g., [166]).

2.7 EXPERIMENTAL CHARACTERIZATION OF DISCONTINUITIES IN MICROWAVE TRANSMISSION LINES

The experimental characterization of microwave transmission line discontinuities has been, and continues to be, a very important aspect of microwave engineering.

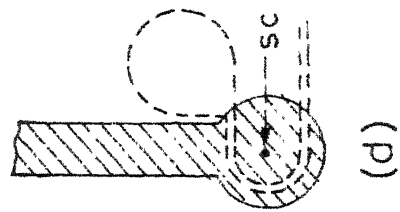
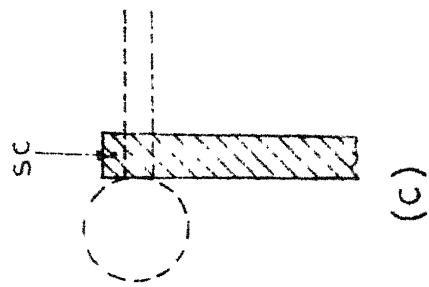
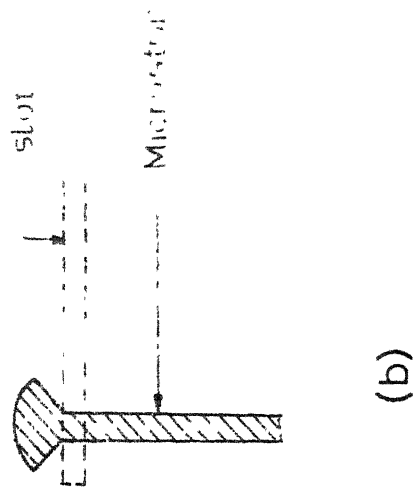
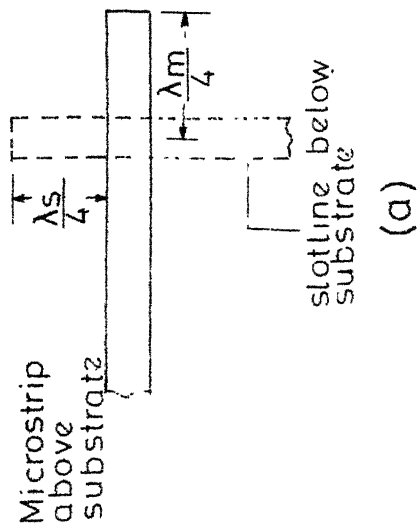


Fig.2.23 Some typical microstrip-slotline transitions

It helps in checking the theoretical models developed for various discontinuities. Sometimes, an extensive amount of experimentation is also taken up so as to empirically determine one or more of the parameters involved in the theoretical formulation.

The refinement of the well-established techniques of experimental evaluation of discontinuities is a constant subject of research. The refinements are generally necessitated by new demands on accuracy, ease of implementation and reliability, advent of new technology, etc. Moreover, the emergence of a new type of guiding structure and associated discontinuities may also require new methods of experimental characterization.

The most commonly used approach for experimental evaluation of discontinuities in microwave transmission lines (especially in coaxial lines and waveguides) is to treat the unknown discontinuity as a network having two (or more, if necessary) ports. The characterization can then be done by measuring either the impedance/admittance matrix or the scattering matrix which describe the inter-relationship between the ports. The measurement of the scattering matrix is more accurate and easy to implement, and is thus preferred.

The following subsections briefly discuss the experimental evaluation of various microwave transmission line discontinuities.

2.7.1 Evaluation of Coaxial/Waveguide Discontinuities:

The classically available methods of experimental characterization of two-port coaxial (or waveguide) discontinuities are the slotted-line techniques, the nodal-shift techniques, the sliding-termination techniques, the resonance curve techniques, the bridge techniques, etc. These methods measure the impedance of the unknown discontinuity through graphical/semigraphical interpretation of the measured data. The measured data may be electrical and/or mechanical. The electrical measurements include measurements of quantities like the voltage standing-wave ratio (VSWR), the complex reflection coefficient, the phase angle, etc. The mechanical quantities to be measured are generally the lengths.

A well-known classical method for the measurement of scattering matrix of a given two-port coaxial (or waveguide) discontinuity is the three-point method. In this method, one of the ports is terminated into a movable short-circuit. The complex reflection coefficient at the other port is measured for three different positions of the movable

short. The values of the reflection coefficient thus measured are interpreted graphically so as to yield the information of interest. One particular advantage of this method is that its accuracy can be increased by merely taking more laboratory data, i.e. by using smaller intervals between consecutive positions of the movable short. The graphical procedure employed to interpret the data indicates the presence of systematic or random errors and averages the accumulated information directly.

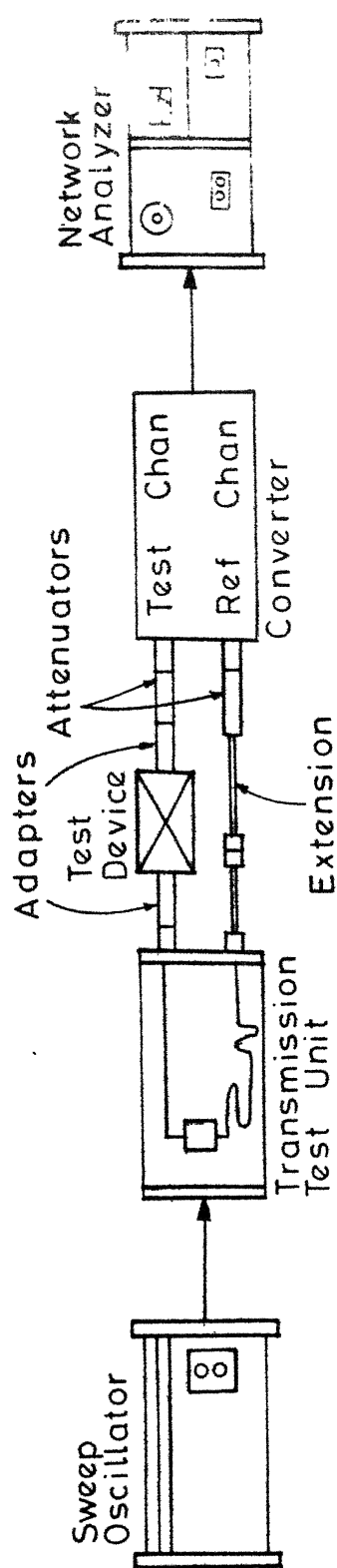
Details on the various above mentioned techniques can be found in literature (see, e.g., [239]-[241]).

Generally speaking, the scattering matrix characterization of a two-port discontinuity requires the measurement of four scattering parameters, namely the two reflection coefficients (S_{11} and S_{22}) and the two transmission coefficients (S_{12} and S_{21}). However, for a symmetrical discontinuity, $S_{11} = S_{22} = \tau$ (say) and $S_{12} = S_{21} = T$ (say). Thus the characterization of a symmetrical discontinuity requires measurement of only one reflection coefficient (τ) and only one transmission coefficient (T).

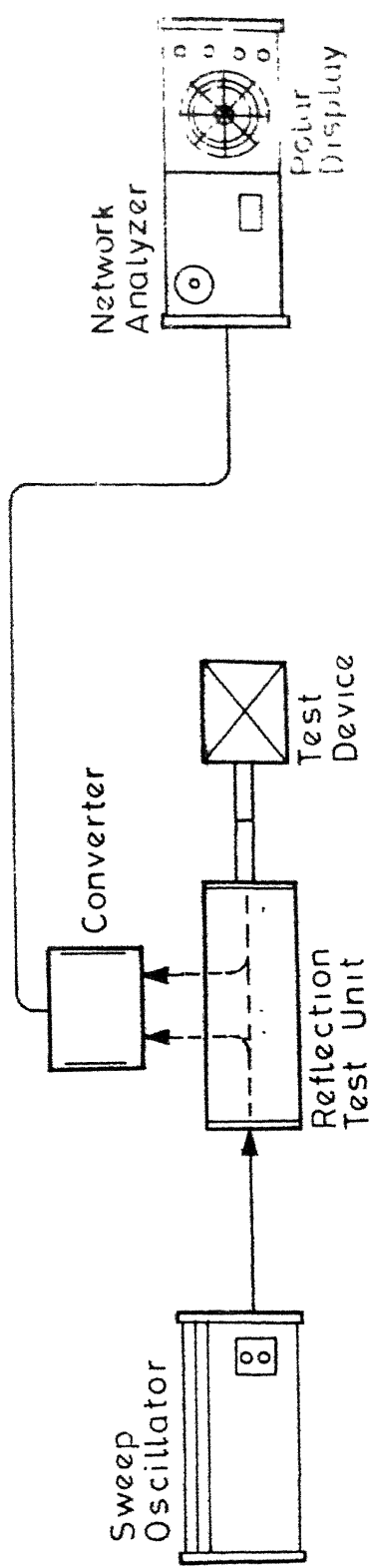
Nowadays, the most widely used method of measuring the transmission and reflection coefficients is the sweep generator-network analyzer combination developed by the

Hewlett-Packard [240]-[241]. In this system, the transmission coefficients are measured by using a 'transmission test', the basic diagram of which is shown in Fig. 2.24(a). In this arrangement, the sweep generator drives a unit called the 'transmission test unit' which divides the incoming power equally between a 'test channel' and a 'reference channel'. These 'channels' then feed a 'harmonic converter' which converts the signal to a lower frequency called the intermediate frequency (i.f.), alongwith preserving the original information of interest contained in the signal. The i.f. is then fed to the network analyzer which displays the information in a form suitable for taking measurements. The difference in magnitude and phase readings on the network analyzer before and after the unknown component is placed in the test channel gives the magnitude and phase of the transmission coefficient of the component.

The basic diagram of the setup used to measure the reflection coefficients is shown in Fig. 2.24b. In this arrangement, the sweep generator drives a 'reflection test unit' which, in turn, drives the network analyzer through a harmonic converter. The component whose reflection coefficient is to be measured can be connected to a third port (generally labeled 'unknown') in the reflection test



(a) Transmission measuring system



(b) Measuring reflection or impedance

Fig. 2.24 Network Analyzer-Sweep Generator test setup

unit. Initially the network analyzer is calibrated against a short-circuit load as the reflection coefficient of this load is known. The reflection coefficient of the unknown component can then be directly read after replacing the short-circuit by the component.

The various methods outlined above are difficult to apply when one deals with situations in which the reflection is composed of many discontinuities at different distances in the line. In such situations, the principle of time-domain reflectometry (TDR) proves to be very useful. The TDR employs a step generator and an oscilloscope in a system that is best described as a closed-loop radar [240]. A voltage step is propagated down the transmission line under investigation, and the incident and reflected voltage waves are monitored by an oscilloscope at a particular point on the line. Discontinuities separated by more than a minimum prescribed distance will produce distinctly separated echoes that write their own response on the oscilloscope face. Thus the discontinuities can be located accurately and one can also have a sound (qualitative) idea of the equivalent circuits of various discontinuities. Another feature of the TDR is that small reflections can be easily analysed in the presence of large reflections at another plane on the line, since these reflections are

separated from each other on the display. This allows one to clean up the design of a component by eliminating these different discontinuities one at a time.

Of late, many new developments, both in theory and technology, as regards the experimental evaluation of coaxial (or waveguide) components have been taking place. Numerous methods have come up, some based on new theoretical ideas, some based on the latest available technology, and some based on both. For instance, one can refer to methods like the automatic network analyzer (see, e.g., [240]-[250]) the combination of automatic network analyzer and TDR principle (see, e.g., [251]-[252]), the six-port reflectometer (see, e.g., [253]-[258]), the homodyne detection system [259], the numerical processing of a large measured data [260], the use of voltage-wave scattering parameters [261]-[263], the eigen-value approach [264], the delay-line based techniques [265], etc.

2.7.2 Evaluation of Microstrip Discontinuities:

The mode of propagation in a microstrip line is an almost-TEM mode. Consequently, it is natural to expect that the various methods of experimental evaluation of coaxial discontinuities may be extended to the microstrip discontinuities. In other words, a microstrip discontinuity can also be regarded as a two-port network and the characterization

can be done by measuring the scattering matrix. In actual practice, however, the uncertainty in the behavior of the coaxial-microstrip transitions that are inevitably present seriously affects the accuracy of any such measurements. As a result, the most commonly employed methods of experimental characterization of microstrip discontinuities are generally based on incorporating the unknown discontinuity in a resonating structure and measuring the change in resonance frequency. The resonators are kept loosely coupled to the test equipment so that the measurement is not affected by the uncertain characteristics of the coaxial - microstrip transitions. Both the linear and ring resonators have been used, each having its own distinct advantages and range of applicability.

Further details on the resonance methods of experimental evaluation of two-port microstrip discontinuities can be found in literature (see, e.g., [166], [266]). The characterization of multiport circuits has also been discussed [267].

2.7.3 Evaluation of Junctions of Similar Lines:

The most obvious way of characterizing a junction of more than two similar lines would be to carry out a separate 2-port transmission/reflection measurement for each

different pair of ports. Such a method has two main disadvantages:

- i) The number of measurements is large, thereby making the method a little cumbersome.
- ii) The finite reflections from the (generally) imperfect auxillary loads terminating the unused ports affect the accuracy of the method seriously.

To overcome the first disadvantage, Speciale [268] has suggested a new technique of determining the complex scattering matrix of a multiport component through a single measurement. The shortcoming of Speciale's method is, however, that it requires use of a special type of multiport network analyzer.

Recently, Tippet and Speciale [269] have exploited Woods' voltage-wave scattering matrix formulation [261] - [263], [270] for measuring the scattering matrix of multiport components with only a 2-port network analyzer. They have shown that a complete elimination of the errors induced due to imperfect auxillary loads can be achieved if Woods' formulation is used.

Further details on the above mentioned methods of experimental characterization of junctions of similar lines can be found in literature [268]-[269].

2.7.4 Evaluation of Junctions of Dissimilar Lines:

The impedance seen by the main line in a junction of two dissimilar lines is a parameter which is of great practical interest. The knowledge of this impedance helps in accurate analysis/synthesis of such junctions. A direct measurement of this impedance is made difficult by the fact that the exact plane of transition is generally inaccessible.

In the case of coaxial-waveguide junctions, the input impedance seen by the coaxial line is generally measured by using subminiature coaxial cables and connectors which can isolate the terminals of interest electrically without affecting the surrounding field conditions. Authors like Eisenhart et.al. [230] and Shetty and Rao [271] have reported results obtained by using this method. An alternative and simpler method of measuring the impedance seen by the coaxial line in a broad-wall coaxial-waveguide junction will be suggested in Chapter 4 of this thesis.

The experimental characterization of coaxial-microstrip junctions also requires special techniques like those suggested by Bianco et.al. [272], Majewski et.al. [235], Souza and Talboys [236], etc. These techniques are generally aimed at characterizing an end-fed coaxial-microstrip

launcher and no results on the broad-wall version seem to have been reported so far. A model for the input reactance seen by the coaxial line in a broad-wall coaxial-microstrip launcher will be formulated in Chapter 5 of this thesis.

2.8 CONCLUSIONS

A brief uptodate survey of various microwave transmission lines and their discontinuities is presented. The junctions of similar/dissimilar lines are discussed. The various methods of experimental evaluation of microwave transmission-line discontinuities are reviewed and put in perspective.

CHAPTER 3

JUNCTION OF RECTANGULAR WAVEGUIDE AND TUNABLE COAXIAL LINE - APPLICATION TO MICROWAVE FILTERING

The junction formed by a coaxial line entering the broad-wall of a rectangular waveguide and driving a E-plane probe therein (Fig. 3.1) has been, and continues to be, a very important subject of study (see, e.g., [9], [10], [13], [59], [229]-[231]). This junction is a component which is often taken for granted. But the hard fact, as remarked by Eisenhart et.al. [230] in 1978, is that most of the successful applications of this junction depend upon empirically determined knowledge rather than on theoretical analysis. The most recent remarks on the status of research on this junction have been made by Williamson [231] who, in 1982, wrote the following:-

Coaxial-line/rectangular waveguide junctions have application in a wide variety of microwave devices, including transitions from coaxial line to rectangular waveguide, power combiners, microwave electronics, etc. Despite their applications, however, relatively little research has been devoted to their analysis and modelling, and most designs have been based on empirical knowledge.

A useful modification of the junction shown in Fig. 3.1 results if we let the far end of the coaxial line be terminated into a movable short-circuit, i.e. if we let the coaxial line be tunable. The junction of a tunable coaxial line and a rectangular waveguide has some well-known uses, e.g. for matching the coaxial line to the waveguide and thereby maximising the power coupled [4], as a power combining element [273], etc. The utility of this junction was significantly enhanced when it was successfully used by Das Gupta for experimental evaluation of complex permittivity of dielectric samples [274].

The objective of this chapter is to analyse the rectangular waveguide-tunable coaxial line junction from the viewpoint of its applicability in microwave filtering. Two different versions of the junction will be considered. The first, named as the short-circuited case, is the case when the tip of the probe is allowed to touch the bottom inner face of the waveguide. The second, named as the air-gap case, is the case when an air-gap is allowed to exist between the tip of the probe and the waveguide wall.

As we shall see, both the short-circuited and air-gap cases exhibit a sharp minimum in the transmission coefficient between the waveguide ports. The frequency at which the minimum transmission takes place can be varied all over

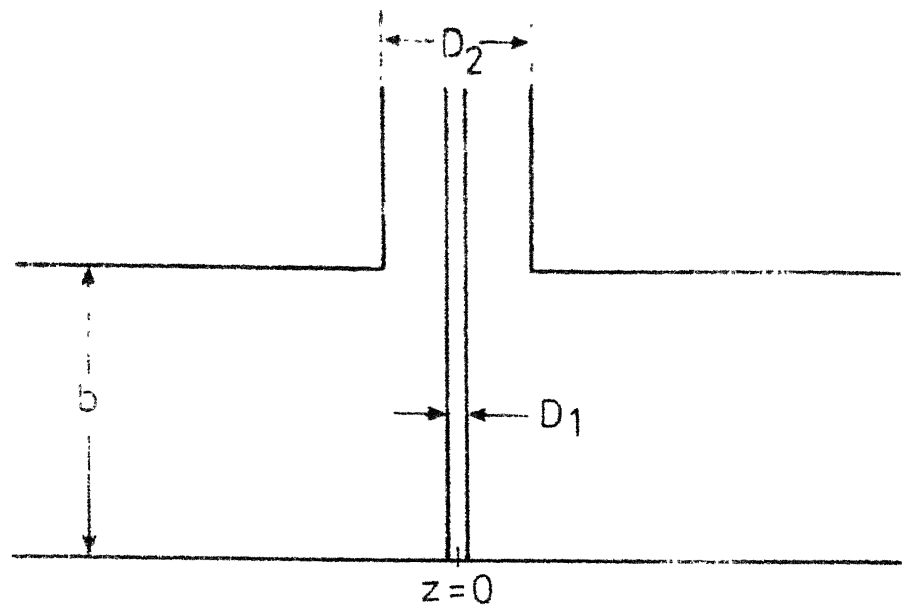


Fig 3.1 Common broad-wall coaxial-waveguide junction

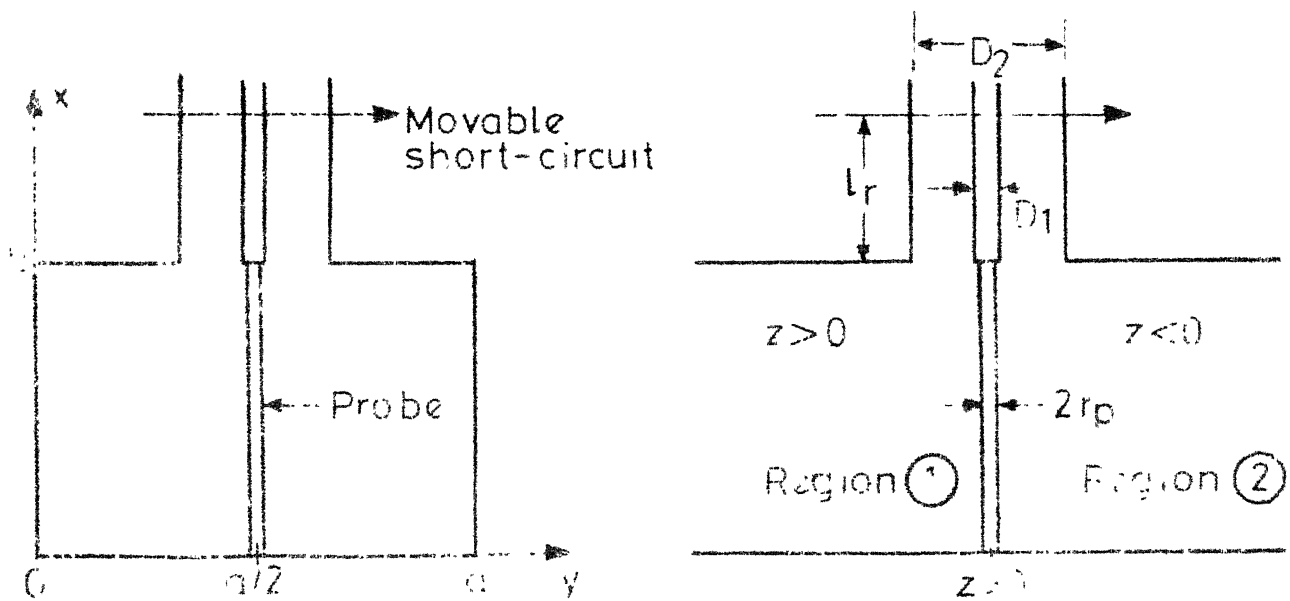


Fig 3.2 Rectangular waveguide-tunable coaxial line junction(short-circuited case)

the operating band of the waveguide by varying the position of the movable short. Consequently, these structures will find application as new types of prototypes for developing waveguide notch filters with large continuous mechanical tunability.

The following subsection presents the analysis of the short-circuited version.

3.1 ANALYSIS OF THE SHORT-CIRCUITED CASE:

The configuration of the short-circuited version is shown in Fig. 3.2. Various dimensions and the coordinate axes are chosen as shown. The analysis of this configuration will be carried out under some suitable simplifying assumptions which help in arriving at a reasonably accurate closed-form solution for the transmission coefficient between the waveguide ports. The simplifying assumptions to be made follow

- i) The probe radius $r_p \ll \lambda$, λ being the free-space wavelength involved, so that the probe can be simulated by a y -directed filamental current $I(y) \delta(x-a/2) \delta(z)$ situated at $x = a/2$, $z=0$.
- ii) Because the probe is thin, the scalar potential and current at any point y along the length of the probe can be represented by means of transmission-line equations.

This assumption follows from Das Gupta's work [274] wherein the validity of this assumption was demonstrated in the case of a closely similar configuration.

- iii) The system losses (including that due to the contact between the tip of the probe and the waveguide wall) can be described in terms of an effective loss resistance R_a assumed to be lumped at the tip of the probe, i.e. at $y=0$.
- iv) The higher-order coaxial-line modes excited at the junction plane $y=b$ are negligible.
- v) Higher-order waveguide modes excited around the E-plane probe have a negligible contribution to the resultant electric field along the length of the probe.
- vi) The frequencies involved are such that the TE_{10} mode is the only propagating waveguide mode.

Assuming a unity amplitude incident electric field, the general E-field expressions in regions 1 and 2 can be constructed as

$$E_{y1} = \underbrace{\sin \frac{\pi x}{a} e^{jk_{z1,0} z}}_{\text{incident field}} + \underbrace{\sum_{m=1}^{\infty} \sum_{n=0}^{\infty} R_{m,n} \sin \frac{m\pi x}{a} \cos \frac{n\pi y}{b} e^{-jk_{z_{m,n}} z}}_{\text{reflected field}}$$

(3.1.1a)

and

$$E_{y2} = \underbrace{\sum_{m=1}^{\infty} \sum_{n=0}^{\infty} T_{m,n} \sin \frac{m\pi x}{a} \cos \frac{n\pi y}{b} e^{jk_{z_{m,n}} z}}_{\text{transmitted field}} \quad (3.1.1b)$$

where E_{y1} is the y-component of the total electric field in the region 1 and E_{y2} is that in region 2. R's are the various reflection coefficients, and T's the various transmission coefficients. The propagation constant in the z-direction is given by

$$k_{z_{m,n}} = \sqrt{[k_0^2 - (m\pi/a)^2 - (n\pi/b)^2]} \quad (3.1.2)$$

and

$$k_0 = 2\pi/\lambda \quad (3.1.3)$$

The x-components of the total magnetic field are given as

$$\begin{aligned} H_{x1} &= \frac{1}{j\omega\mu_0} \frac{\partial E_{y1}}{\partial z} \\ &= \frac{1}{\omega\mu_0} \left[k_{z_{1,0}} \sin \frac{\pi x}{a} e^{jk_{z_{1,0}} z} - \sum_{m=1}^{\infty} \sum_{n=0}^{\infty} k_{z_{m,n}} R_{m,n} \right. \\ &\quad \left. \sin \frac{m\pi x}{a} \cos \frac{n\pi y}{b} e^{-jk_{z_{m,n}} z} \right] \end{aligned} \quad (3.1.4a)$$

and

$$\begin{aligned}
 H_{x2} &= \frac{1}{j\omega\mu_0} \frac{\partial E_{y2}}{\partial z} \\
 &= \frac{1}{\omega\mu_0} \sum_{m=1}^{\infty} \sum_{n=0}^{\infty} k_{z_{m,n}} T_{m,n} \sin \frac{m\pi y}{a} \cos \frac{n\pi y}{b} e^{jk_{z_{m,n}} z}
 \end{aligned}
 \quad (3.1.4b)$$

Since the probe is simulated by a filamental current at $x=a/2$, $z=0$, the fields in eq. (3.1.1) must satisfy

$$\begin{aligned}
 E_{y1}(z=0^+) &= E_{y2}(z=0^-) & 0 \leq x \leq a \\
 \text{and } 0 &\leq y \leq b
 \end{aligned}
 \quad (3.1.5)$$

which yields

$$\begin{aligned}
 1 + R_{1,0} &= T_{1,0} & \text{for } m=1, n=0 \\
 \text{and } R_{m,n} &= T_{m,n} & \text{for } m > 1, n > 0
 \end{aligned}
 \quad (3.1.6)$$

The boundary condition that the fields in eq. (3.1.4) must satisfy is

$$H_{x1}(z=0^+) - H_{x2}(z=0^-) = I(y) \delta(x-a/2) \delta(z) \quad (3.1.7)$$

which can easily be shown to yield [13]

$$R_{m,n} = - \frac{\hat{\epsilon}_n \sin(m\pi/2)}{\omega \epsilon_0 a b k_{z_{m,n}}} \left(k_0^2 - \frac{n^2 \pi^2}{b^2} \right) \int_0^b I(y') \cos \frac{n\pi y'}{b} dy'
 \quad (3.1.8)$$

where,

$$\begin{aligned} \epsilon_n &= 1 \quad \text{for } n = 0 \\ &= 2 \quad \text{for } n > 0 \end{aligned} \quad (3.1.9)$$

Picking $m=1$, $n=0$ term in eq. (3.1.8) and using the notation τ for $R_{1,0}$, we write

$$\tau = \frac{1}{N_0} \int_0^b I(y') dy' \quad (3.1.10)$$

where the normalising factor is

$$N_0 = - \frac{ab}{120\pi} \sqrt{1 - (\lambda/2a)^2} \quad (3.1.11)$$

Eq. (3.1.10) reflects the relationship between the fundamental mode reflection coefficient τ and the probe current $I(y)$.

Now, in order to calculate the probe current, we assume that the scalar potential $V(y)$ and current $I(y)$ at any point y along the length of the probe can be represented by means of the transmission-line equations:

$$\frac{d^2 V}{dy^2} = -\beta^2 V \quad (3.1.12a)$$

and

$$\frac{d^2 I}{dy^2} = -\beta^2 I - j \frac{E_R \beta}{Z_{op}} \quad (3.1.12b)$$

where,

$$\beta = 2\pi / \lambda \quad (3.1.13)$$

and the probe characteristic impedance is given by

$$Z_{op} = 60 \left[\ln \frac{2}{\beta r_p} + \gamma + Ci(\beta b) - \frac{\sin \beta b}{\beta b} \right] \quad (3.1.14a)$$

where $\gamma = 0.5772\dots$ is the Euler's constant and Ci is the well-known integral defined by

$$Ci(x) = - \int_x^\infty \frac{\cos u}{u} du \quad (3.1.15)$$

For all practical purposes, one can use

$$Z_{op} = 60 \left[\ln(\lambda/2\pi r_p) + 0.116 \right] \quad (3.1.14b)$$

instead of eq. (3.1.14a) without introducing too much error.

In eq. (3.1.12b), E_R is the resultant excitation along the probe length.

At this juncture, it is to be noted that the above formulation of probe is equivalent to representing the probe by a thin-wire excited antenna situated in an homogeneous unbounded medium. The latter is the case for which Schelkunoff and Friis [275] have given a complete formulation. The eqs. (3.1.12) - (3.1.14) follow from that formulation.

The total excitation along the length of the probe can be written in regions 1 and 2 as

$$E_{R1} = 1 + \tau + \sum_{m=2}^{\infty} \sum_{n=1}^{\infty} R_{m,n} \sin \frac{m\pi}{2} \cos \frac{n\pi y}{b} \quad (3.1.16a)$$

and

$$E_{R2} = T + \sum_{m=2}^{\infty} \sum_{n=1}^{\infty} T_{m,n} \sin \frac{m\pi}{2} \cos \frac{n\pi y}{b} \quad (3.1.16b)$$

where the notation T has been employed for the fundamental - mode transmission coefficient T_{10} .

Eqs. (3.1.16) and (3.1.6), taken together, establish that

$$E_{R1} = E_{R2} = E_R \text{ (say)} \quad (3.1.17)$$

Now, in view of the simplifying assumption v), we can write

$$E_R = 1 + \tau \quad (3.1.18)$$

The validity of neglecting the higher-order terms while writing eq. (3.1.18) will be discussed later while comparing the theoretical and experimental results.

Eq. (3.1.12) leads to the following solution:

$$V(y) = Z_{op} (I^+ e^{-j\beta y} - I^- e^{j\beta y}) \quad (3.1.19a)$$

and

$$I(y) = I^+ e^{-j\beta y} + I^- e^{j\beta y} - \frac{jE_R}{\beta Z_{op}} \quad (3.1.19b)$$

where I^+ and I^- are the two arbitrary constants involved. To determine I^+ and I^- , we use the following boundary conditions:

$$a) \quad (V/I)_{y=0} = R_a \quad (3.1.20)$$

Where R_a is the effective loss resistance, assumed to be lumped at the tip of the probe, as mentioned earlier.

$$b) \quad (V/I)_{y=b} = jX_k \quad (3.1.21)$$

Where the TEM-mode reactance of the tunable coaxial line is

$$X_k = Z_0 \tan \beta l_r \quad (3.1.22)$$

Z_0 being the characteristic impedance of the coaxial line given by the well known formula

$$Z_0 = 60 \ln (D_2/D_1) \quad (3.1.23)$$

where D_1 and D_2 are respectively the inner and outer conductor diameters.

Application of the boundary conditions (3.1.20) and (3.1.21) to the eq. (3.1.19) leads to the following equations in I^+ and I^- :

$$Z_1 I^+ - Z_2 I^- = V_1 \quad (3.1.24)$$

$$\text{and } Z_3 I^+ - Z_4 I^- = V_2 \quad (3.1.25)$$

$$\text{where } Z_1 = Z_{op} - R_a \quad (3.1.26a)$$

$$Z_2 = Z_{op} + R_a \quad (3.1.26b)$$

$$Z_3 = (Z_{op} - jX_k) e^{-j\beta b} \quad (3.1.26c)$$

$$Z_4 = (Z_{op} + jX_k) e^{j\beta b} \quad (3.1.26d)$$

and

$$V_1 = - \frac{jR_a(1+\tau)}{\beta Z_{op}} \quad (3.1.27a)$$

$$V_2 = \frac{X_k(1+\tau)}{\beta Z_{op}} \quad (3.1.27b)$$

The solution of eqs. (3.1.24) and (3.1.25) is

$$I^+ = \frac{Z_4 V_1 - Z_2 V_2}{Z_1 Z_4 - Z_2 Z_3} \quad (3.1.28a)$$

and

$$I^- = \frac{Z_3 V_1 - Z_1 V_2}{Z_1 Z_4 - Z_2 Z_3} \quad (3.1.28b)$$

Now, it can easily be shown that

$$Z_4 V_1 - Z_2 V_2 = \frac{1+\tau}{\beta Z_{op}} (f_1 + jf_2) \quad (3.1.29a)$$

and

$$Z_3 V_1 - Z_1 V_2 = \frac{1+\tau}{\beta Z_{op}} (f_3 + jf_4) \quad (3.1.29b)$$

where,

$$f_1 = -X_k(Z_{op} + R_a) + R_a(Z_{op} \sin \beta b + X_k \cos \beta b) \quad (3.1.30a)$$

$$f_2 = R_a(X_k \sin \beta b - Z_{op} \cos \beta b) \quad (3.1.30b)$$

$$f_3 = -X_k(Z_{op} - R_a) - R_a(Z_{op} \sin \beta b + X_k \cos \beta b) \quad (3.1.30c)$$

and

$$f_4 = R_a(X_k \sin \beta b - Z_{op} \cos \beta b) \quad (3.1.30d)$$

Similarly, one can also see that

$$Z_1 Z_4 - Z_2 Z_3 = f_5 + jf_6 \quad (3.1.31)$$

where,

$$f_5 = 2R_a (X_k \sin \beta b - Z_{op} \cos \beta b) \quad (3.1.32a)$$

and

$$f_6 = 2Z_{op} (X_k \cos \beta b + Z_{op} \sin \beta b) \quad (3.1.32b)$$

Consequently, eq. (3.1.28) may be rewritten as

$$I^+ = \frac{1+\tau}{\beta Z_{op}} \frac{f_1+jf_2}{f_5+jf_6} \quad (3.1.33a)$$

and

$$I^- = \frac{1+\tau}{\beta Z_{op}} \frac{f_3+jf_4}{f_5+jf_6} \quad (3.1.33b)$$

Using eqs. (3.1.19b) and (3.1.33) in the eq. (3.1.10), and solving, we arrive at the following:

$$\beta^2 Z_{op} N_o \frac{\tau}{1+\tau} = j \frac{f_7+jf_8}{f_5+jf_6} - j\beta b \quad (3.1.34)$$

where,

$$f_7 = (f_3 - f_1) (1 - \cos \beta b) + (f_4 + f_2) \sin \beta b \quad (3.1.35a)$$

and

$$f_8 = (f_4 - f_2) (1 - \cos \beta b) - (f_3 + f_1) \sin \beta b \quad (3.1.35b)$$

Eq. (3.1.35) can be simplified to give

$$f_7 = 2R_a [2X_k (1 - \cos \beta b) - Z_{op} \sin \beta b] \quad (3.1.36a)$$

and,

$$f_8 = 2Z_{op} X_k \sin \beta b \quad (3.1.36b)$$

Eq. (3.1.34) can be further manipulated to yield

$$\tau = - \frac{\eta_1 + j\eta_2}{\eta_3 + j\eta_4} \quad (3.1.37)$$

where,

$$\eta_1 = f_7 - \beta b f_5 \quad (3.1.38a)$$

$$\eta_2 = f_8 - \beta b f_6 \quad (3.1.38b)$$

$$\eta_3 = \eta_1 - \beta^2 Z_{op} N_o f_6 \quad (3.1.38c)$$

$$\text{and } \eta_4 = \eta_2 + \beta^2 Z_{op} N_o f_5 \quad (3.1.38d)$$

The fundamental mode transmission coefficient is then given by

$$T = 1 + \tau = \beta^2 Z_{op} N_o \frac{-f_6 + jf_5}{\eta_3 + j\eta_4} \quad (3.1.39)$$

The corresponding insertion loss is

$$IL = 20 \log \frac{1}{|T|} \quad (3.1.40)$$

The insertion loss will be minimum or maximum when

$$\frac{d}{dx_k} |T|^2 = 0 \quad (3.1.41)$$

In order to solve the resonance condition (3.1.41), we use eq. (3.1.39) to write

$$|T|^2 = \beta^4 Z_{op}^2 N_o^2 \frac{F_2}{F_1} \quad (3.1.42)$$

where

$$\begin{aligned} F_1 = & f_7^2 + f_8^2 + (\beta^2 b^2 + \beta^4 Z_{op}^2 N_o^2)(f_5^2 + f_6^2) \\ & - 2\beta b(f_5 f_7 + f_6 f_8) + 2\beta^2 Z_{op} N_o(f_5 f_8 - f_6 f_7) \end{aligned} \quad (3.1.43)$$

and

$$F_2 = f_5^2 + f_6^2 \quad (3.1.44)$$

Now, it is easy to show that

$$f_7^2 + f_8^2 = h_{12} X_k^2 + h_{11} + h_{10} \quad (3.1.45a)$$

$$f_5 f_7 + f_6 f_8 = h_{22} X_k^2 + h_{21} X_k + h_{20} \quad (3.1.45b)$$

$$f_5 f_8 - f_6 f_7 = h_{32} X_k^2 + h_{31} X_k + h_{30} \quad (3.1.45c)$$

$$\text{and } f_5^2 + f_6^2 = h_{42} X_k^2 + h_{41} X_k + h_{40} \quad (3.1.45d)$$

where,

$$h_{12} = 16R_a^2 (1 - \cos \beta b)^2 + 4Z_{op}^2 \sin^2 \beta b \quad (3.1.46a)$$

$$h_{11} = -16 Z_{op} R_a^2 \sin \beta b (1 - \cos \beta b) \quad (3.1.46b)$$

$$h_{10} = 4 Z_{op}^2 R_a^2 \sin^2 \beta b \quad (3.1.46c)$$

$$h_{22} = 8R_a^2 \sin \beta b (1 - \cos \beta b) + 4 Z_{op}^2 \sin \beta b \cos \beta b \quad (3.1.46d)$$

$$h_{21} = -4Z_{op} R_a^2 [\sin^2 \beta b + 2 \cos \beta b (1 - \cos \beta b)] \\ + 4 Z_{op}^3 \sin^2 \beta b \quad (3.1.46e)$$

$$h_{20} = 4 Z_{op}^2 R_a^2 \cos \beta b \sin \beta b \quad (3.1.46f)$$

$$h_{32} = 4Z_{op} R_a [\sin^2 \beta b - 2 \cos \beta b (1 - \cos \beta b)] \quad (3.1.46g)$$

$$h_{31} = -8Z_{op}^2 R_a \sin \beta b (1 - \cos \beta b) \quad (3.1.46h)$$

$$h_{30} = 4Z_{op}^3 R_a \sin^2 \beta b \quad (3.1.46i)$$

$$h_{42} = 4(Z_{op}^2 \cos^2 \beta b + R_a^2 \sin^2 \beta b) \quad (3.1.46j)$$

$$h_{41} = 4Z_{op}(Z_{op}^2 - R_a^2) \sin 2\beta b \quad (3.1.46k)$$

$$\text{and } h_{40} = 4Z_{op}^2 (Z_{op}^2 \sin^2 \beta b + R_a^2 \cos^2 \beta b) \quad (3.1.46l)$$

so that

$$F_1 = u_{12} X_k^2 + u_{11} X_k + u_{10} \quad (3.1.47)$$

and

$$F_2 = u_{22} X_k^2 + u_{21} X_k + u_{20} \quad (3.1.48)$$

where,

$$u_{1i} = h_{1i} - 2\beta b h_{2i} + 2\beta^2 Z_{op} N_o h_{3i} + (\beta^2 b^2 + \beta^4 Z_{op}^2 N_o^2) h_{4i} \quad (3.1.49)$$

$$\text{and } u_{2i} = h_{4i} \quad (3.1.50)$$

Eqs. (3.1.49) and (3.1.50) hold good for $i = 0, 1$ and 2 .

The resonance condition (3.1.41) will be satisfied when

$$F_1 \frac{dF_2}{dX_k} = F_2 \frac{dF_1}{dX_k} \quad (3.1.51)$$

which, using eqs. (3.1.47) - (3.1.48), yields

$$U_2 X_k^2 + U_1 X_k + U_0 = 0 \quad (3.1.52)$$

where,

$$U_2 = u_{12} u_{21} - u_{11} u_{22} \quad (3.1.53a)$$

$$U_1 = 2(u_{12} u_{20} - u_{10} u_{22}) \quad (3.1.53b)$$

$$\text{and } U_0 = u_{11}u_{20} - u_{10}u_{21} \quad (3.1.53c)$$

The values of X_k for minimum and maximum insertion loss are thus given by

$$X_k = \frac{-U_1 \pm \sqrt{U_1^2 - 4U_0U_2}}{U_2} \quad (3.1.54)$$

the positive sign to be used for minimum loss and the negative sign for maximum loss.

The position of the movable short for a given value of X_k can be calculated using

$$l_r = (\lambda/2\pi) \tan^{-1} (X_k/Z_0) \quad (3.1.55)$$

The value of l_r needed for maximum insertion loss shall hereinafter be termed the 'resonant length'. Also, the frequency at which the loss is maximum shall be termed the 'resonance frequency' or the 'center frequency'.

The calculation of resonant length by using eq. (3.1.54) is obviously a little cumbersome algebraically. In the following subsection, a simple but accurate approximation for the resonant length of a short-circuited version is presented.

3.1.1 A Simpler Condition of Resonance:

Actual computations reveal that, of all the basic functions involved in the expression for the insertion loss, the function f_6 changes its sign at resonance, whereas the

functions f_5, f_7 and f_8 cross the frequency of resonance in a monotonous manner. The situation is illustrated, for a typical set of parameter values, through the various graphs shown in Fig. 3.3.

Equating f_6 in eq. (3.1.32b) to zero, one gets

$$Z_o \tan \beta l_r + Z_{op} \tan \beta b = 0 \quad (3.1.56)$$

which can serve as a simpler condition of resonance than the eq. (3.1.54). To test the accuracy of this resonance condition, comparisons between the values of the resonant length given by eqs. (3.1.54) and (3.1.56) were made, for various sets of parameter values. The error involved was seen to be barely noticeable as illustrated, for a few typical cases, in Tables 3.1, 3.2 and 3.3.

3.1.2 An Expression for the Peak Insertion Loss:

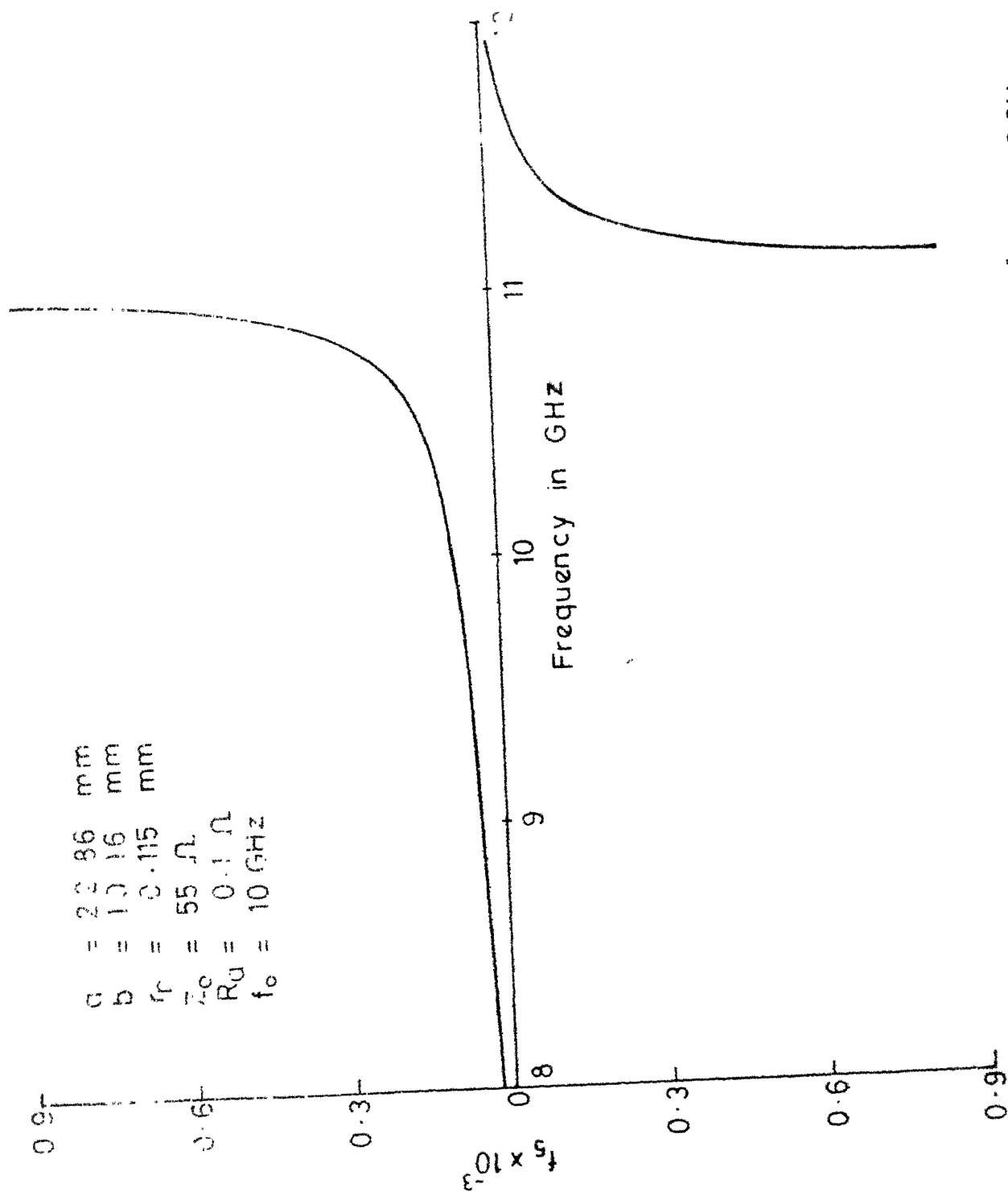
Eq. (3.1.56) dictates that at resonance

$$X_k = -Z_{op} \tan \beta b \quad (3.1.57)$$

Substituting this value of X_k in eqs. (3.1.32) and (3.1.35), we get,

$$f_5|_{\text{resonance}} = -2Z_{op} R_a \sec \beta b \quad (3.1.58a)$$

$$f_6|_{\text{resonance}} = 0 \quad (3.1.58b)$$

Fig. 3-3a Variation of f_s with frequency

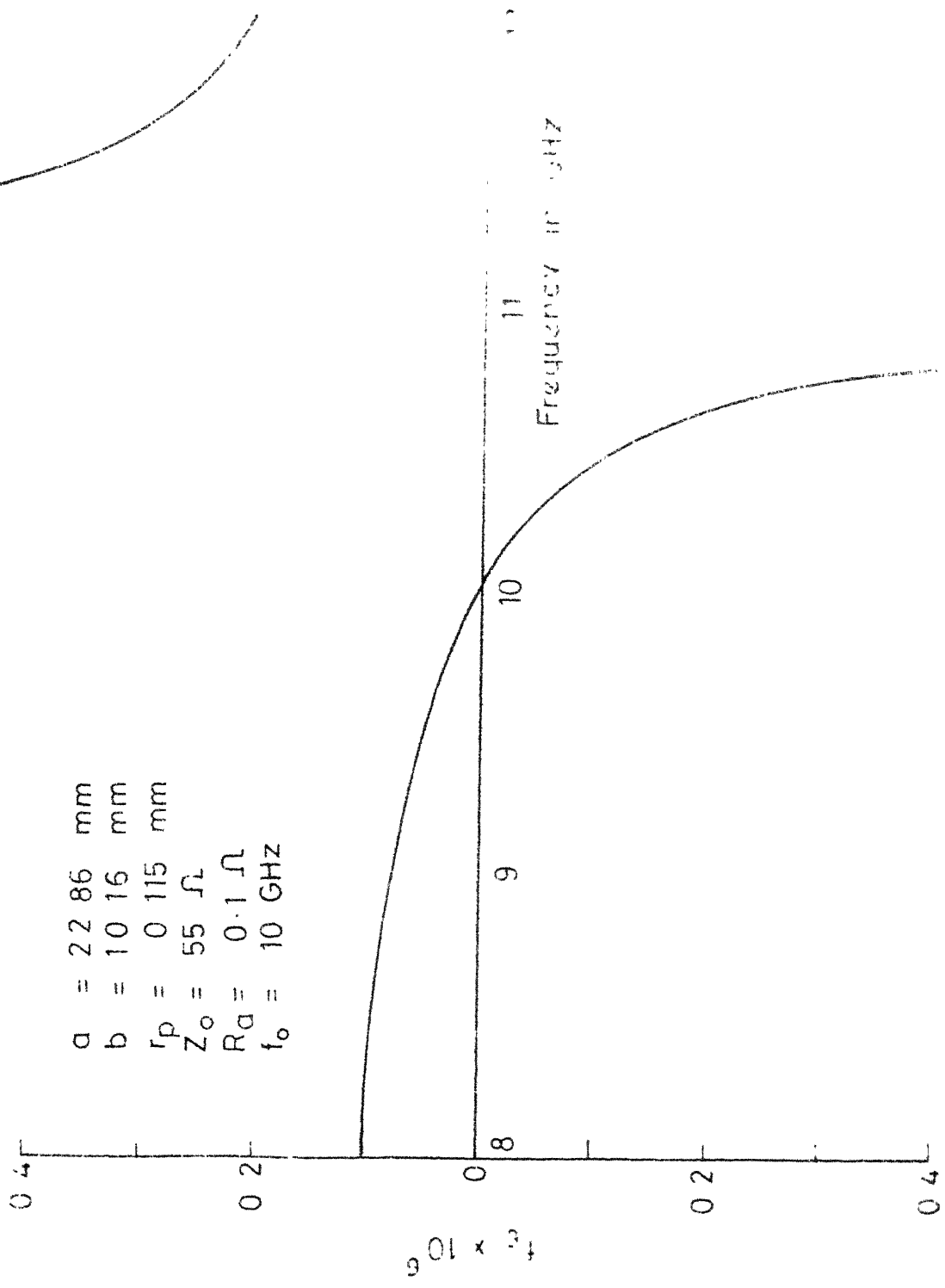


Fig. 3-3b variation of f_6 with frequency

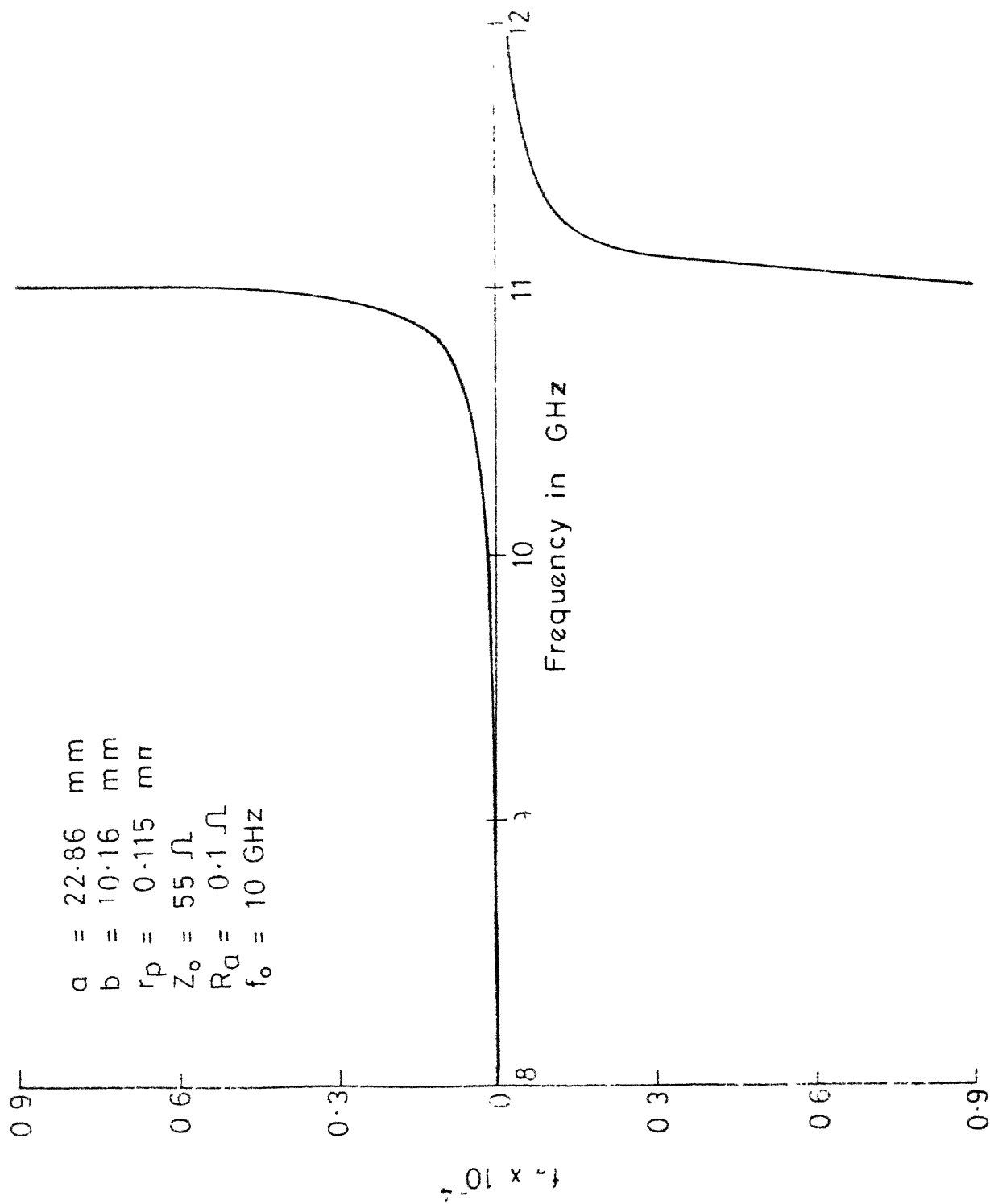


Fig. 3-3c Variation of f_7 with frequency

$a = 22.86 \text{ mm}$
 $b = 10.16 \text{ mm}$
 $r_p = 0.115 \text{ mm}$
 $Z_o = 55 \Omega$
 $R_a = 0.1 \mu\Omega$
 $f_o = 10 \text{ GHz}$

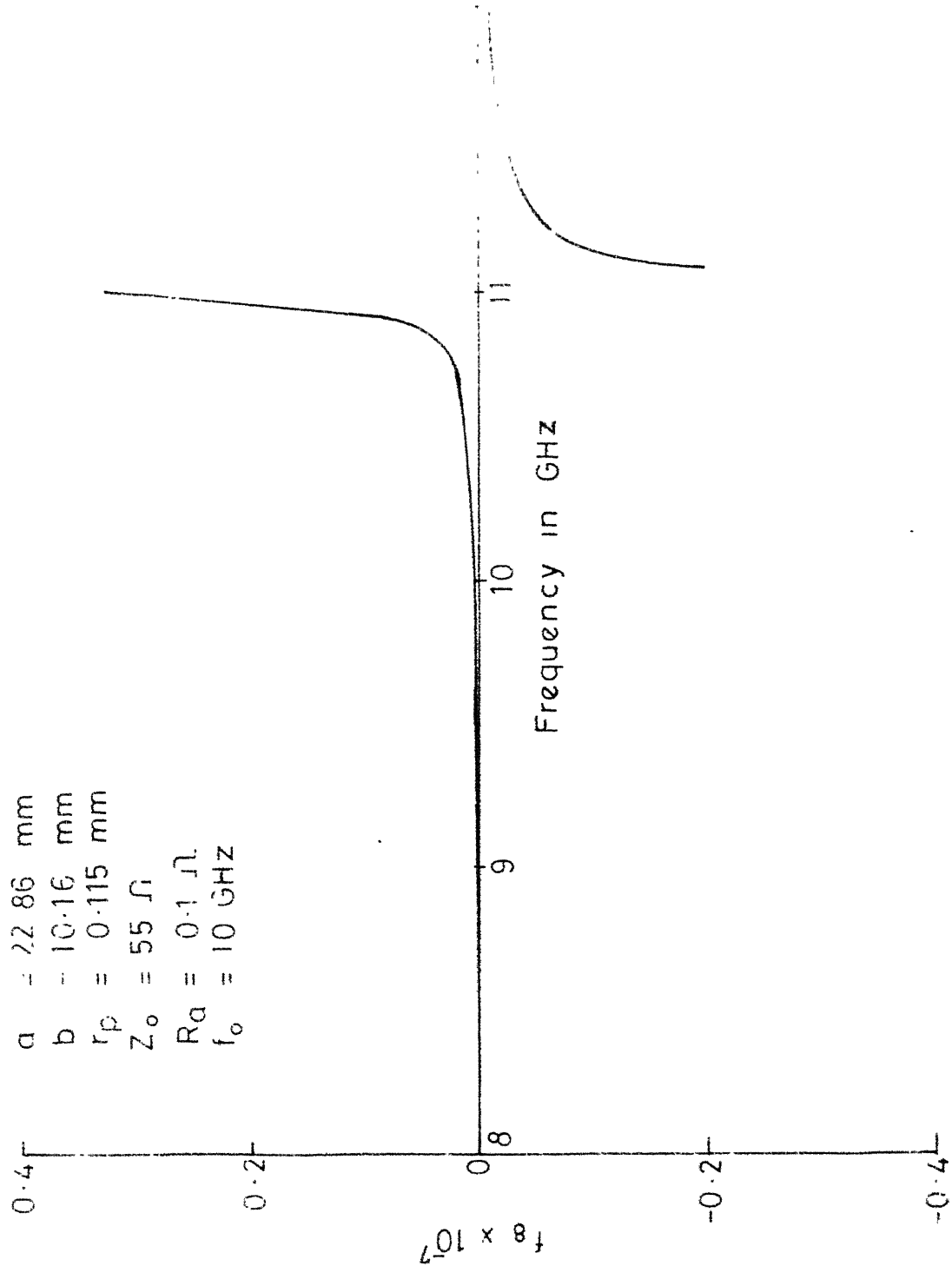


Fig. 3-3d Variation of f_8 with frequency

Table 3.1

Comparison between exact and approximate values of the resonant length
(short-circuited case, $r_p = 0.115$ mm)

$a = 22.86$ mm, $b = 10.16$ mm, $Z_o = 55.00$ ohms

Frequency in GHz	Resonant length (in mm)		
	Exact (using eq. (3.1.54))		
	$R_a = 0.50$ ohm	$R_a = 2.00$ ohms	$R_a = 5.00$ ohms
8.00	9.1918139	9.1918139	9.1918138
9.00	7.8866967	7.8866967	7.8866967
10.00	6.7946093	6.7946093	6.7946093
11.00	5.8147061	5.8147061	5.8147061
12.00	4.8384857	4.8384857	4.8384864

Table 3.2

Comparison between exact and approximate values of the resonant length
(short-circuited case, $r_p = 0.435$ mm)

$a = 22.86$ mm, $b = 10.16$ mm, $Z_0 = 55.00$ ohm

Frequency in GHz	Resonant length (in mm)			Approximate (using eq. 3.1.56)
	Exact (using eq. 3.1.54)	$R_a = 2.00$ ohms	$R_a = 5.00$ ohms	
8.00	9.0988792	9.0988792	9.0988792	9.0988791
9.00	7.6571052	7.6571052	7.6571052	7.6571052
10.00	6.4305300	6.4305300	6.4305300	6.4305300
11.00	5.3048960	5.3048960	5.3048960	5.3048962
12.00	4.1664410	4.1664410	4.1664410	4.1664414

Table 3.3

Comparison between exact and approximate values of the resonant length
(short-circuited case, $r_p = 0.635$ mm)

$a = 22.86$ mm, $b = 10.16$ mm, $Z_o = 55.00$ ohms

Frequency in GHz	Resonant length (in mm)		
	Exact (using eq. 3.1.54)		Approximate (using eq. 3.1.56)
	$R_a = 0.50$ ohm	$R_a = 2.00$ ohms	
8.00	9.0523550	9.0523550	9.0523748
9.00	7.5417234	7.5417234	7.5417234
10.00	6.2484218	6.2484218	6.2484217
11.00	5.0554179	5.0554179	5.0554182
12.00	3.8562612	3.8562612	3.8562606

$$f_7 \Big|_{\text{resonance}} = -2Z_{\text{op}} R_a (2 \tan \beta b - \sin \beta b) \quad (3.1.58c)$$

$$\text{and } f_8 \Big|_{\text{resonance}} = -2Z_{\text{op}}^2 \tan \beta b \sin \beta b \quad (3.1.58d)$$

Substituting these values in eq. (3.1.39), alongwith using eq. (3.1.38), one gets the following expression for the peak insertion loss IL_{max} .

$$IL_{\text{max}} = 20 \log X \quad (3.1.59)$$

where

$$X = \frac{\sqrt{(X_1^2 + X_2^2)}}{|\beta^2 Z_{\text{op}} N_o|} \quad (3.1.60)$$

$$\text{with } X_1 = \beta^2 Z_{\text{op}} N_o + \frac{f_8}{f_5} \Big|_{\text{resonance}}$$

$$= \beta^2 Z_{\text{op}} N_o + (Z_{\text{op}}/R_a) \sin^2 \beta b \quad (3.1.61a)$$

and

$$\begin{aligned} X_2 &= \beta b - \frac{f_7}{f_5} \Big|_{\text{resonance}} \\ &= \beta b - \sin \beta b (2 - \cos \beta b) \end{aligned} \quad (3.1.61b)$$

Actual computations reveal that, for practical cases, $|X_2| \ll |X_1|$ and we can safely write

$$X = \frac{X_1}{|\beta^2 Z_{\text{op}} N_o|} \quad (3.1.62)$$

3.1.3 The Near-resonance Equivalent Circuit:

In view of the resonance condition described by eq. (3.1.56), the near-resonance behavior of the short-circuited case can be represented by means of the lumped equivalent circuit shown in Fig. 3.4. This equivalent circuit helps us in understanding the behavior of the short-circuited configuration physically. Two reactances, X_p and X_k , and a loss resistance, R_a , constitute the equivalent circuit. $X_p = -Z_{op} \tan \beta b$ is the reactance offered by the E-plane waveguide probe, and $X_k = Z_o \tan \beta l_r$ is the reactance of the tunable coaxial line. As X_k can be varied from $-\infty$ to $+\infty$, it can be used to tune out any conceivable values of X_p . In other words, a given frequency can be rejected by setting $X_k = X_p$ at that frequency. The frequency to be rejected (f_o) can be varied all over the operating band of the waveguide by varying the position (l_r) of the movable short, the relationship between f_o and l_r being governed by eqs. (3.1.55) and (3.1.56).

3.2 ANALYSIS OF THE AIR-GAP CASE:

The air-gap case is shown in Fig. 3.5. It differs from the short-circuited case in that there exists a finite air-gap of length ' δ ' between the tip of the probe and the waveguide wall. The analysis of the air-gap case will also be done under the various simplifying assumptions made in analysing the short-circuited case and will run along

3.1.3 The Near-resonance Equivalent Circuit:

In view of the resonance condition described by eq. (3.1.56), the near-resonance behavior of the short-circuited case can be represented by means of the lumped equivalent circuit shown in Fig. 3.4. This equivalent circuit helps us in understanding the behavior of the short-circuited configuration physically. Two reactances, X_p and X_k , and a loss resistance, R_a , constitute the equivalent circuit. $X_p = -Z_{op} \tan \beta b$ is the reactance offered by the E-plane waveguide probe, and $X_k = Z_o \tan \beta l_r$ is the reactance of the tunable coaxial line. As X_k can be varied from $-\infty$ to $+\infty$, it can be used to tune out any conceivable values of X_p . In other words, a given frequency can be rejected by setting $X_k = X_p$ at that frequency. The frequency to be rejected (f_o) can be varied all over the operating band of the waveguide by varying the position (l_r) of the movable short, the relationship between f_o and l_r being governed by eqs. (3.1.55) and (3.1.56).

3.2 ANALYSIS OF THE AIR-GAP CASE:

The air-gap case is shown in Fig. 3.5. It differs from the short-circuited case in that there exists a finite air-gap of length ' δ ' between the tip of the probe and the waveguide wall. The analysis of the air-gap case will also be done under the various simplifying assumptions made in analysing the short-circuited case and will run along

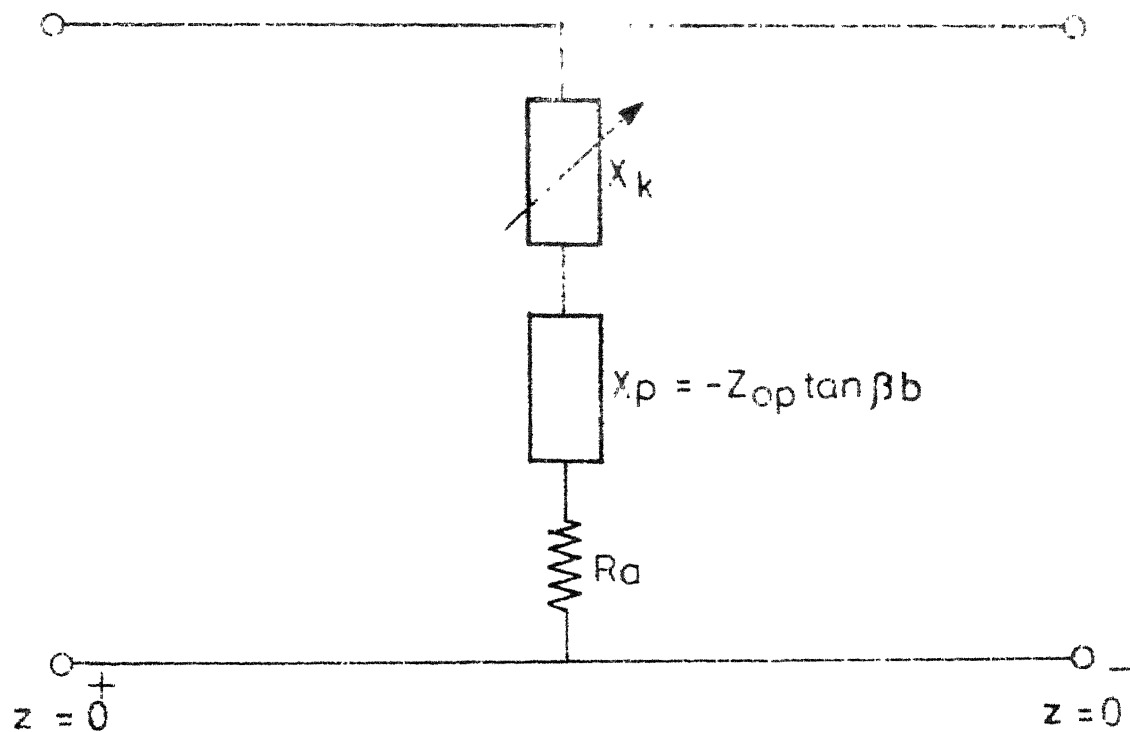


Fig 3-4 Near-resonance equivalent circuit for the short-circuited version

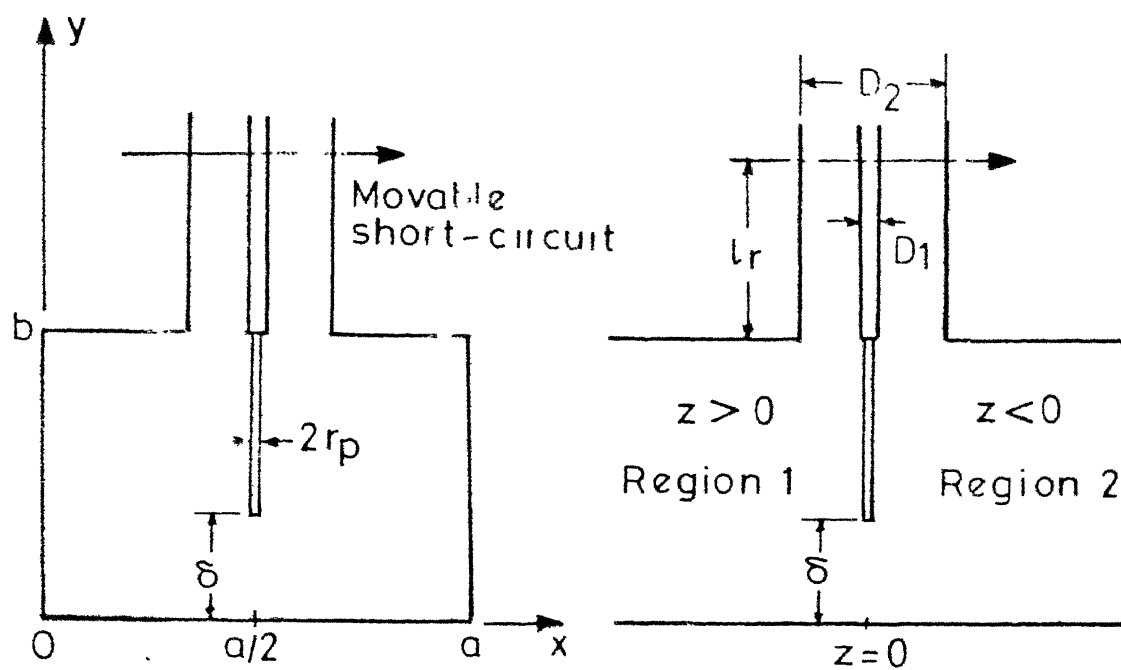


Fig. 3 5 Rectangular waveguide-tunable coaxial line junction (air-gap case)

identical lines. The essential difference will lie in the fact that the relationship between the fundamental-mode reflection coefficient and probe current will be given, instead of eq. (3.1.10), by

$$\tau = -\frac{1}{N_0} \int_{\delta}^b I(y') dy' \quad (3.2.1)$$

Also, the boundary condition depicted by eq. (3.1.20) will be replaced by

$$(V/I)_{y=\delta} = R_a - jX_a \quad (3.2.2)$$

where R_a is the usual loss resistance and X_a is the reactance of the air-gap. The value of X_a is

$$X_a = 1/2\pi f(C_p + C_f) \quad (3.2.3)$$

where f is the frequency involved in c/s, and parallel-plate and fringing capacitances are given by [13]

$$C_p = \epsilon_0 \pi r_p^2 / \delta \quad (3.2.4)$$

and

$$C_f = 4 \epsilon_0 r_p [1 - \gamma + \ln(2r_p / \delta)] \quad (3.2.5)$$

One more difference, although minor, to be noted is that the eq. (3.1.14a) for the probe characteristic impedance will be replaced by

$$Z_{op} = 60 \left[\ln \frac{2}{\beta r_p} + \gamma + \text{Ci } \beta(b - \delta) - \frac{\sin \beta(b - \delta)}{\beta(b - \delta)} \right] \quad (3.2.6)$$

eqs. (3.1.26) and (3.1.27) modify to

$$Z_1 = (Z_{op} - R_a + jX_a) e^{-j\beta\delta} \quad (3.2.7a)$$

$$Z_2 = (Z_{op} + R_a - jX_a) e^{j\beta\delta} \quad (3.2.7b)$$

$$Z_3 = (Z_{op} - jX_k) e^{-j\beta b} \quad (3.2.7c)$$

$$Z_4 = (Z_{op} + jX_k) e^{j\beta b} \quad (3.2.7d)$$

and

$$V_1 = -\frac{1+\tau}{\beta Z_{op}} (X_a + jR_a) \quad (3.2.8a)$$

$$V_2 = \frac{1+\tau}{\beta Z_{op}} X_k \quad (3.2.8b)$$

Eqs. (3.1.30) and (3.1.32) will be replaced by

$$\begin{aligned} f_1 = & X_a X_k (\sin\beta b - \sin\beta\delta) - R_a X_k (\cos\beta\delta - \cos\beta b) \\ & - Z_{op} (X_a \cos\beta b - R_a \sin\beta b + X_k \cos\beta\delta) \end{aligned} \quad (3.2.9a)$$

$$\begin{aligned} f_2 = & X_a X_k (\cos\beta\delta - \cos\beta b) + R_a X_k (\sin\beta b - \sin\beta\delta) \\ & - Z_{op} (X_a \sin\beta b + R_a \cos\beta b + X_k \sin\beta\delta) \end{aligned} \quad (3.2.9b)$$

$$\begin{aligned} f_3 = & X_a X_k (\sin\beta b - \sin\beta\delta) + R_a X_k (\cos\beta\delta - \cos\beta b) \\ & - Z_{op} (X_a \cos\beta b + R_a \sin\beta b + X_k \cos\beta\delta) \end{aligned} \quad (3.2.9c)$$

$$\begin{aligned} f_4 = & -X_a X_k (\cos\beta\delta - \cos\beta b) + R_a X_k (\sin\beta b - \sin\beta\delta) \\ & + Z_{op} (X_a \sin\beta b - R_a \cos\beta b + X_k \sin\beta\delta) \end{aligned} \quad (3.2.9d)$$

and,

$$f_5 = 2R_a[X_k \sin\beta(b-\delta) - Z_{op} \cos\beta(b-\delta)] \quad (3.2.10a)$$

$$f_6 = 2(Z_{op}^2 - X_a X_k) \sin\beta(b-\delta) + 2 Z_{op} (X_a + X_k) \cos\beta(b-\delta) \quad (3.2.10b)$$

Eq. (3.1.36) becomes

$$f_7 = 2R_a[2X_k \{1 - \cos\beta(b-\delta)\} - Z_{op} \sin\beta(b-\delta)] \quad (3.2.11a)$$

and

$$f_8 = 2Z_{op}(X_a + X_k) \sin\beta(b-\delta) + 4X_a X_k [1 - \cos\beta(b-\delta)] \quad (3.2.11b)$$

whereas eq. (3.1.38) changes to

$$\eta_1 = f_7 - \beta(b-\delta)f_5 \quad (3.2.12a)$$

$$\eta_2 = f_8 - \beta(b-\delta)f_6 \quad (3.2.12b)$$

$$\eta_3 = \eta_1 - \beta^2 Z_{op} N_o f_6 \quad (3.2.12c)$$

and

$$\eta_4 = \eta_2 + \beta^2 Z_{op} N_o f_5 \quad (3.2.12d)$$

The reflection and transmission coefficients are given by

$$\tau = - \frac{\eta_1 + j\eta_2}{\eta_3 + j\eta_4} \quad (3.2.13)$$

$$\text{and } T = 1 + \tau = \beta^2 Z_{op} N_o \frac{-f_6 + jf_5}{\eta_3 + j\eta_4} \quad (3.2.14)$$

The condition for resonance modifies to

$$U_2 X_k^2 + U_1 X_k + U_0 = 0 \quad (3.2.15)$$

where

$$U_2 = u_{12} u_{21} - u_{11} u_{22} \quad (3.2.16a)$$

$$U_1 = 2(u_{12} u_{20} - u_{10} u_{22}) \quad (3.2.16b)$$

$$U_0 = u_{11} u_{20} - u_{10} u_{21} \quad (3.2.16c)$$

and the values of u_{1i} and u_{2i} ($i = 0, 1$ and 2) are given by

$$u_{1i} = h_{1i} - 2\beta(b-\delta)h_{2i} + 2\beta^2 Z_{op} N_o h_{3i} + [\beta^2(b-\delta)^2 + \beta^4 Z_{op}^2 N_o^2] h_{4i} \quad (3.2.17a)$$

and

$$u_{2i} = h_{4i} \quad (3.2.17b)$$

The values of various h 's, revised for the air-gap case, follow

$$h_{12} = 4[4R_a^2(1-e_1)^2 + Z_{op}^2 e_2^2 + 4X_a^2(1-e_1)^2 + 4Z_{op} X_a e_2(1-e_1)] \quad (3.2.18a)$$

$$h_{11} = 8Z_{op}[Z_{op} X_a e_2^2 + 2(X_a^2 - R_a^2)e_2(1-e_1)] \quad (3.2.18b)$$

$$h_{10} = 4Z_{op}^2(R_a^2 + X_a^2) e_2^2 \quad (3.2.18c)$$

$$h_{22} = 4[Z_{op}^2 e_1 e_2 - 2(X_a^2 - R_a^2) e_2 (1 - e_1) - Z_{op} X_a (1 - e_1)^2] \quad (3.2.18d)$$

$$h_{21} = 4Z_{op}[-R_a^2 \{e_2^2 + 2e_1(1 - e_1)\} + X_a^2 \{-e_2^3 + 2e_1(1 - e_1)\} + Z_{op}^2 e_2^2 + 2Z_{op} X_a e_2] \quad (3.2.18e)$$

$$h_{20} = 4Z_{op}^2[(R_a^2 + X_a^2)e_1 e_2 + Z_{op} X_a e_2^2] \quad (3.2.18f)$$

$$h_{32} = 4R_a[Z_{op}(1 - e_1)^2 + 4X_a e_2(1 - e_1)] \quad (3.2.18g)$$

$$h_{31} = -8Z_{op} R_a (1 - e_1)(Z_{op} e_2 + 2X_a e_1) \quad (3.2.18h)$$

$$h_{30} = 4Z_{op}^3 R_a e_2^2 \quad (3.2.18i)$$

$$h_{42} = 4(R_a^2 e_2 + Z_{op}^2 e_1^2 + X_a^2 e_2^2 - 2Z_{op} X_a e_1 e_2) \quad (3.2.18j)$$

$$h_{41} = 8Z_{op}[(Z_{op}^2 - R_a^2 - X_a^2)e_1 e_2 + Z_{op} X_a (e_1^2 - e_2^2)] \quad (3.2.18k)$$

$$h_{40} = 4Z_{op}^2[R_a^2 e_1^2 + (X_a e_1 + Z_{op} e_2)^2] \quad (3.2.18l)$$

$$e_1 = \cos\beta(b - \delta) \quad (3.2.18m)$$

$$e_2 = \sin\beta(b - \delta) \quad (3.2.18n)$$

3.2.1 A Simpler Condition of Resonance:

A simpler condition of resonance can be obtained by equating f_6 given by eq. (3.2.10b) to zero, as was done for the short-circuited case. This leads to

$$Z_o \tan\beta l_r = Z_{op} \frac{X_a + Z_{op} \tan\beta(b - \delta)}{X_a \tan\beta(b - \delta) - Z_{op}} \quad (3.2.19)$$

which can serve as a useful alternative to eq. (3.2.15). To test the accuracy of this approximate condition of resonance, a comparison between the values of l_r given by eqn. (3.2.15) and (3.2.19) is given, for a few typical cases, in Table 3.4. The error involved is again seen to be negligible.

3.2.2 Expression for the Peak Insertion Loss:

By using the resonance condition (3.2.19) in eq. (3.2.14) it can easily be shown that

$$IL_{\max} = 20 \log X \quad (3.2.20)$$

where,

$$X = \frac{\sqrt{X_1^2 + X_2^2}}{|\beta^2 Z_{op} N_o|} \quad (3.2.21)$$

with

$$X_1 = \beta^2 Z_{op} N_o + \frac{Z_{op}^2 e_2^2 + 2Z_{op} X_a e_2 (1-e_1) + X_a^2 [e_2^2 + 2e_1(1-e_1)]}{Z_{op} R_a} \quad (3.2.22a)$$

and

$$X_2 = \beta(b - \delta) + \frac{X_a(1-e_1)^2 - Z_{op} e_2(2-e_1)}{Z_{op}} \quad (3.2.22b)$$

where e_1 and e_2 are as given by eqs. (3.2.18m) and (3.2.18n). Again, it is found that for practical cases $|X_2| \ll |X_1|$ and can be safely neglected.

3.2.3 Near-resonance Equivalent Circuit:

In view of eq. (3.2.19), the near-resonance behavior of the air-gap case can be modelled by the lumped equivalence

Table 3.4

Comparison between exact and approximate values of the resonant length
(air-gap case)

$a=22.86$ mm, $b=10.16$ mm, $r_p = 0.435$ mm, $Z_0=55.00$ ohms, $R_a=0.50$ ohm

Frequency in GHz	Resonant length (in mm)			
	$\delta = 1.00$ mm		$\delta = 5.00$ mm	
	Exact	Approximate	Exact	Approximate
8.00	1.7843012	1.7843012	5.8972893	5.8972892
			8.9845052	8.9845062
9.00	15.6043960	15.6043960	4.4995641	4.4995641
			7.9433307	7.9433258
10.00	12.0523780	12.0523780	3.2196127	3.2196127
			7.1105175	7.1105341
11.00	9.7497755	9.7497755	2.0034547	2.0034547
			6.4292613	6.4293124
12.00	8.2054806	8.2054806	0.8511590	0.8511590
			5.8618072	5.8617812

Table 3.4

Comparison between exact and approximate values of the resonant length
(air-gap case)

$a=22.86$ mm, $b=10.16$ mm, $r_p = 0.435$ mm, $Z_0=55.00$ ohms, $R_a=0.50$ ohm

Frequency in GHz	Resonant length (in mm)			
	$\delta = 1.00$ mm		$\delta = 5.00$ mm	
	Exact	Approximate	Exact	Approximate
8.00	1.7843012	1.7843012	5.8972893	5.8972892
			8.9845052	8.9845062
9.00	15.6043960	15.6043960	4.4995641	4.4995641
			7.9433307	7.9433258
10.00	12.0523780	12.0523780	3.2196127	3.2196127
			7.1105175	7.1105341
11.00	9.7497755	9.7497755	2.0034547	2.0034547
			6.4292613	6.4293124
12.00	8.2054806	8.2054806	0.8511590	0.8511590
			5.8618072	5.8617812

shown in Fig. 3.6 . It can easily be visualised that, at least in principle, this configuration can also be used to reject any frequency in the operating band of the waveguide.

3.3 EXPERIMENTAL RESULTS AND DISCUSSION:

In order to test the theory developed in the preceding sections, a single-stage X-band prototype with $a=22.86$ mm, $b=10.16$ mm, $D_1=4.00$ mm and $D_2=10.00$ mm was fabricated. Many values of the probe diameter were used. As expected, a tunable sharp peak in the loss characteristic was observed. The behavior at frequencies away from the resonance frequency, i.e. the pass-band behavior, however, showed unacceptably large ripples. The magnitude of these ripples was seen to be lowered by introducing a small air-gap ' δ '. The situation is illustrated, for $r_p = 0.435$ mm and $f_o = 10$ GHz, through the Figs. 3.7 and 3.8.

The experimental performance of the type shown in Figs. 3.7 and 3.8 is far from satisfactory, especially if one is interested in the full-band behavior of these configurations. For full-band applicability, the ripples need minimising. To achieve this, the following line of thought was pursued.

The undesirable discrepancy between theory and experiment, as manifest in Figs. 3.7 and 3.8, can be

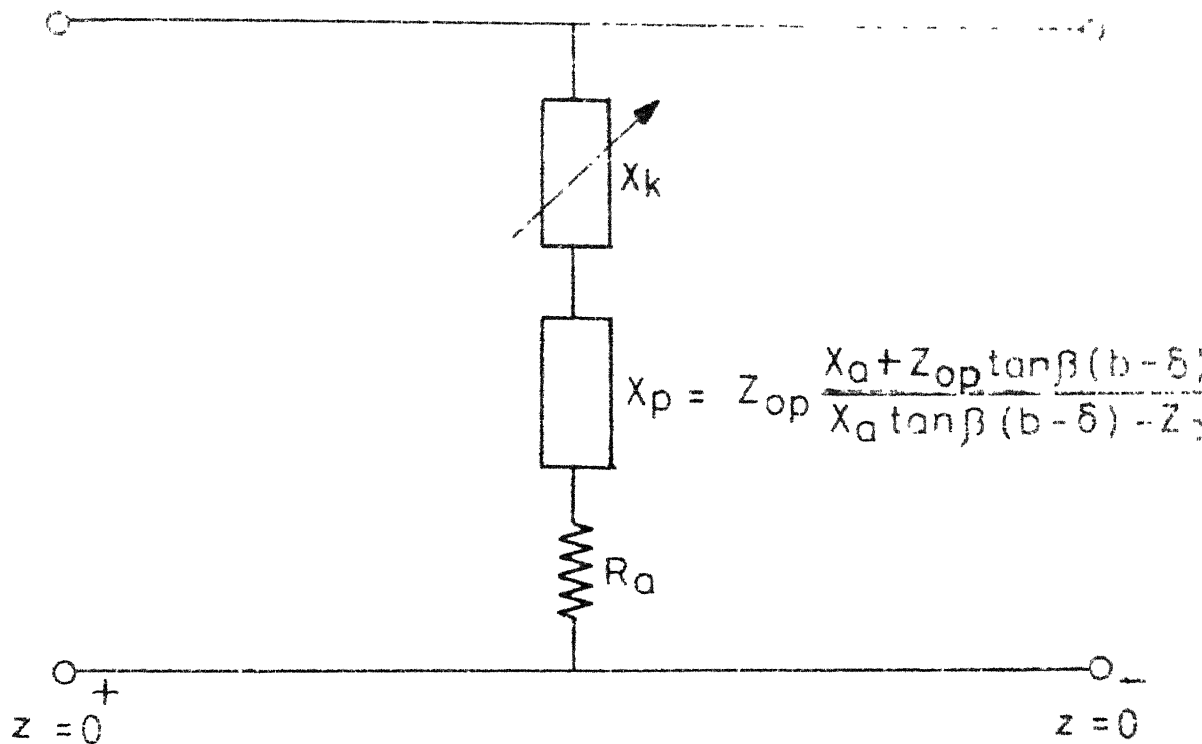


Fig.3-6 Near-resonance equivalent circuit for the air-gap case

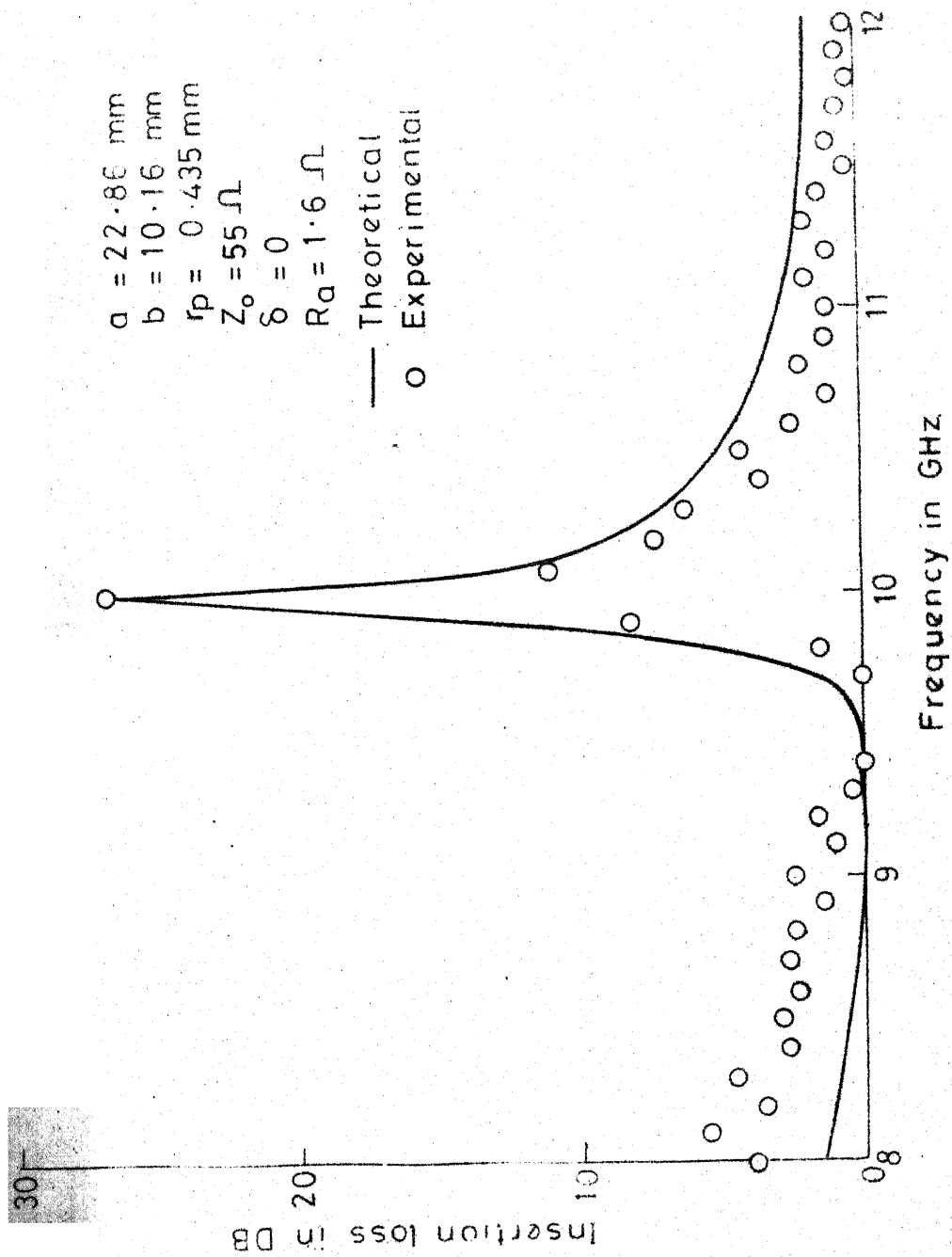


Fig.3.7 A typical single-stage response for short-circuited case

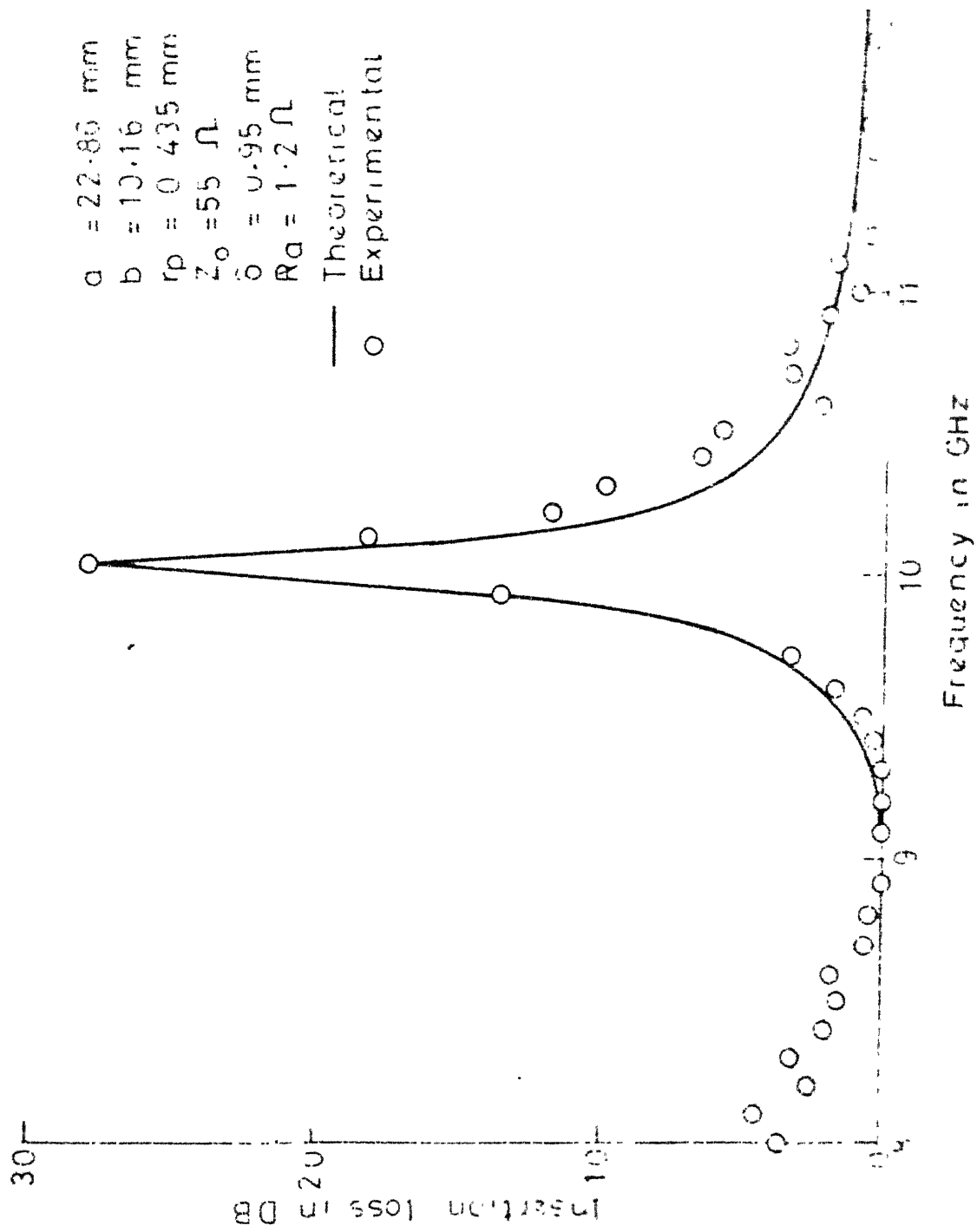


Fig. 3.8 A typical single-stage response for air-gap coupler

attributed to the various simplifying assumptions made in the analysis. Of all these assumptions, the neglect of higher-order terms while writing eq. (3.1.18) and the assumption of a constant R_a throughout the band while making the theoretical computations seem to be of crucial significance. Both of these assumptions can be expected to be more valid if the amount of physical perturbation within the waveguide is small. Hence, in order to reduce the unwanted ripples, we should either increase δ to a significant fraction of b , or should decrease r_p to a minimum value.

Both of the above mentioned options were tried. The larger values of δ resulted in a sharp deterioration in the peak insertion loss with increasing center frequency, and this limited the useful tuning range to only a small lower portion of the band.

The second option was implemented by choosing an extremely thin probe ($r_p = 0.115$ mm). Such a thin probe was mechanically weak and would have buckled under the load of the tuning mechanism. So the experiment was done by keeping the prototype in a horizontal position. The probe was kept in position by passing it through an axially-cut slot in the bottom wall of the waveguide and holding it there through an external pressure, as shown photographically in Fig. 3.9. The measurement setup used was the conventional H.P. sweep

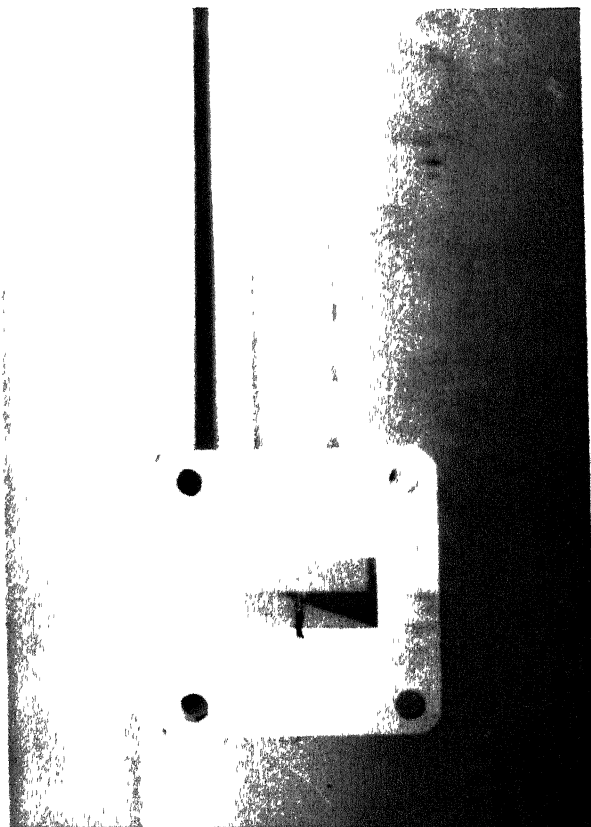


Fig. 3.9: Photograph showing the X-band configuration employing extremely thin probe.

generator-network analyzer combination. A photograph of this setup is shown in Fig. 3.10.

Theoretical and experimental loss characteristics for $r_p = 0.115$ mm are compared in Fig. 3.11. It is seen that the pass-band loss remains mostly within 1 dB which is a practically acceptable value. Also, the deterioration in the peak insertion loss with change in center frequency is moderate and does not seriously limit the tuning range.

Theoretical and experimental values of the resonant length are compared in Table 3.5, for nine different center frequencies.

The discrepancies between theory and experiment, as observed in Fig. 3.11 and Table 3.5, can be attributed to the following factors:

- i) Various simplifying assumptions made in the analysis.
- ii) The measurement conditions were such that a small departure of the probe from its vertical position at $x=a/2$ was always there. The effects of this 'tilting' would also have caused some error.
- iii) While looking at Table 3.5, the experimental uncertainty in the measurement of length (± 0.1 mm in the present instance) must be kept in mind.

The pass-band VSWR of the short-circuited configuration (with $r_p = 0.115$ mm) was found to be generally of the order of 1.10 or less.

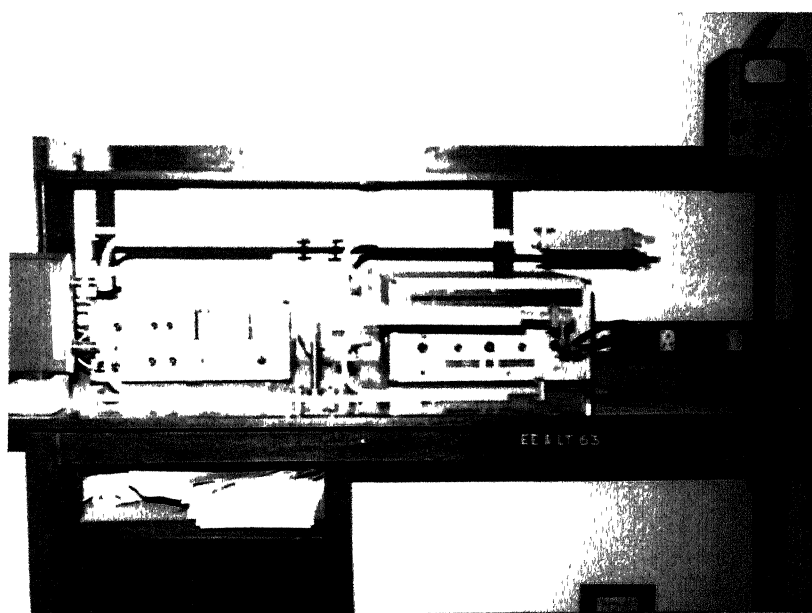


Fig. 3.10: Photograph showing the X-band measurement setup for waveguide components.

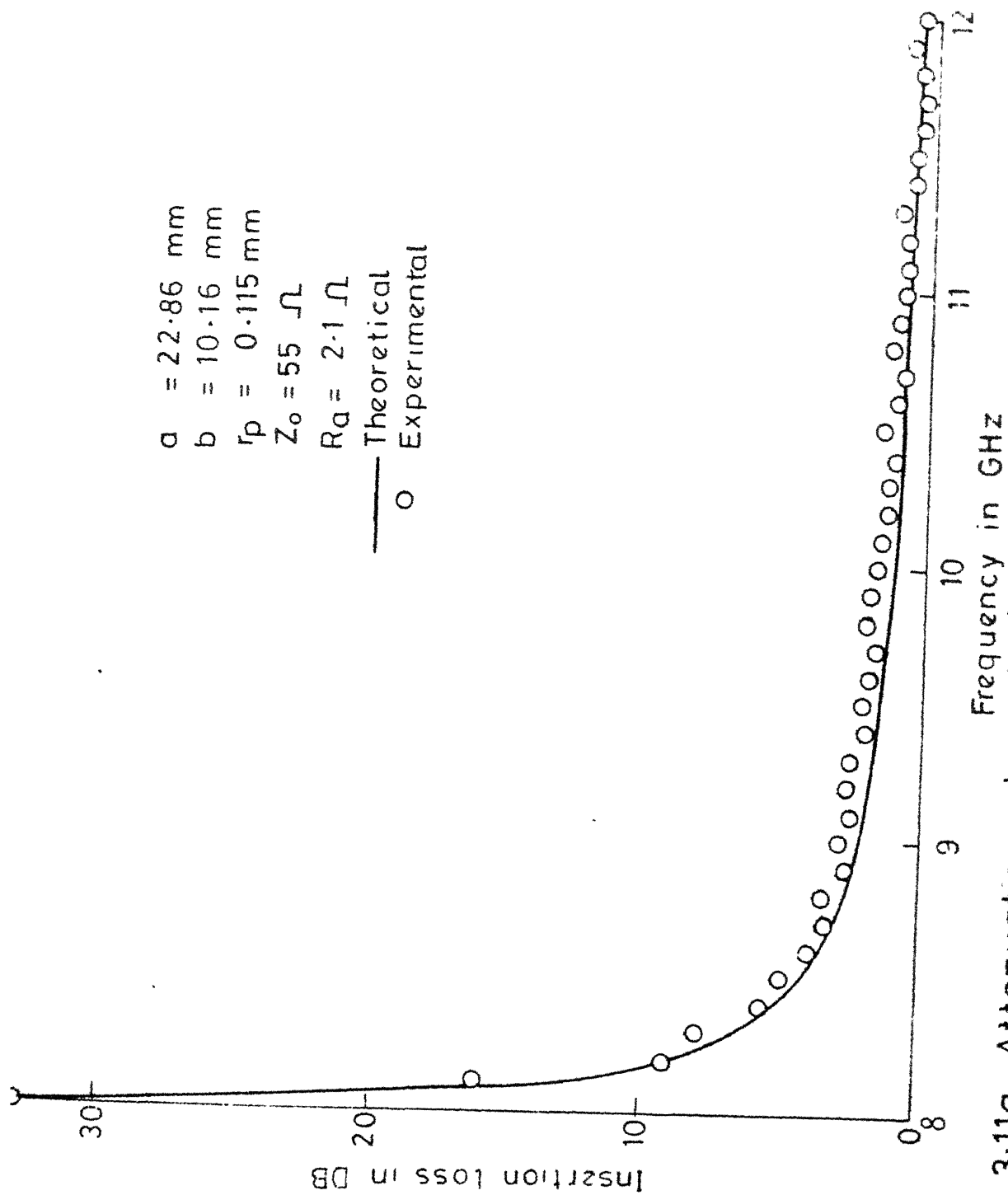


Fig. 3-11a Attenuation characteristic of a short-circuited version using an extremely thin probe ($f_0 = 8 \text{ GHz}$)

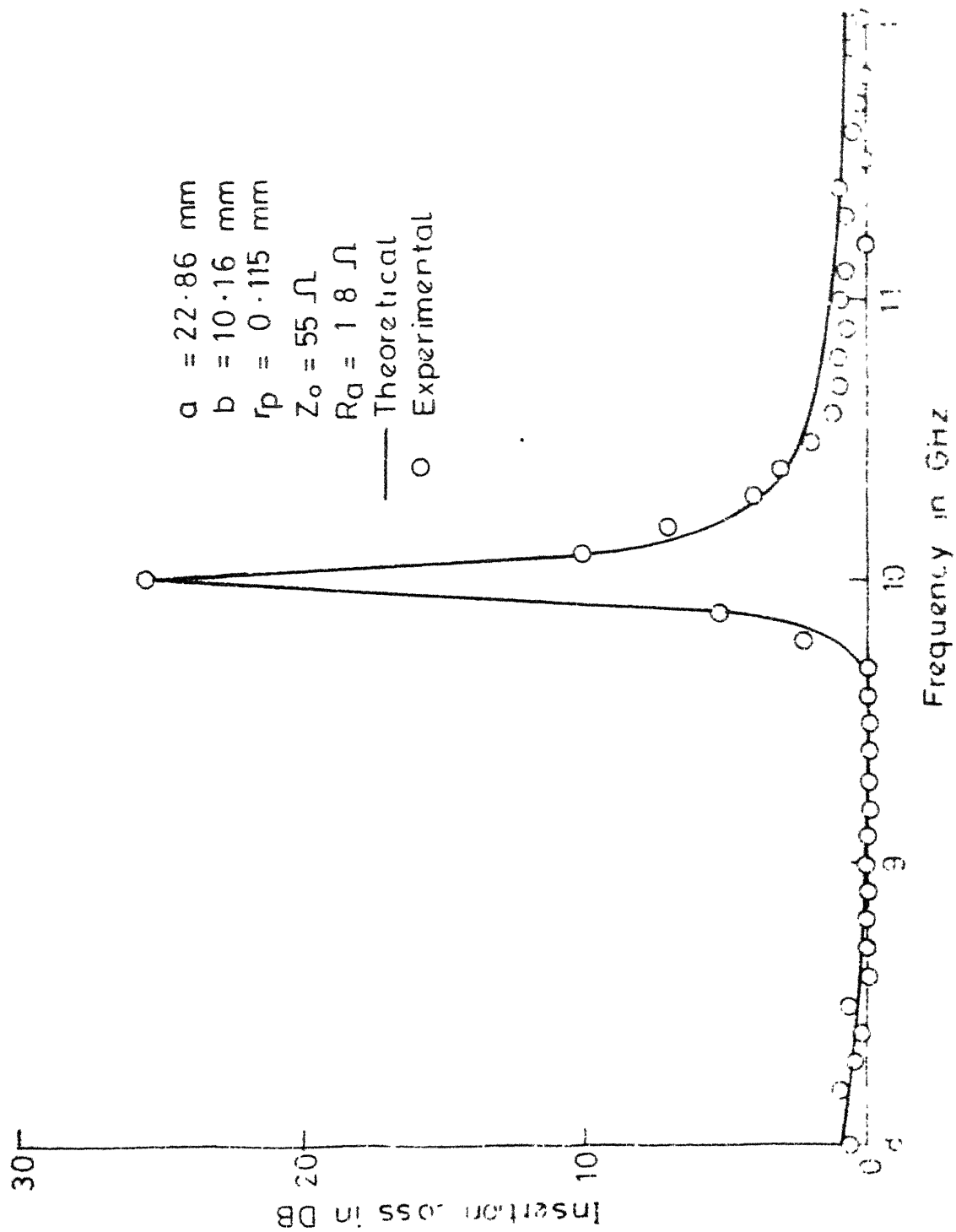


Fig 311b Attenuation characteristic of a short-circuited version using an extremely thin probe ($f_o = 10 \text{ GHz}$)

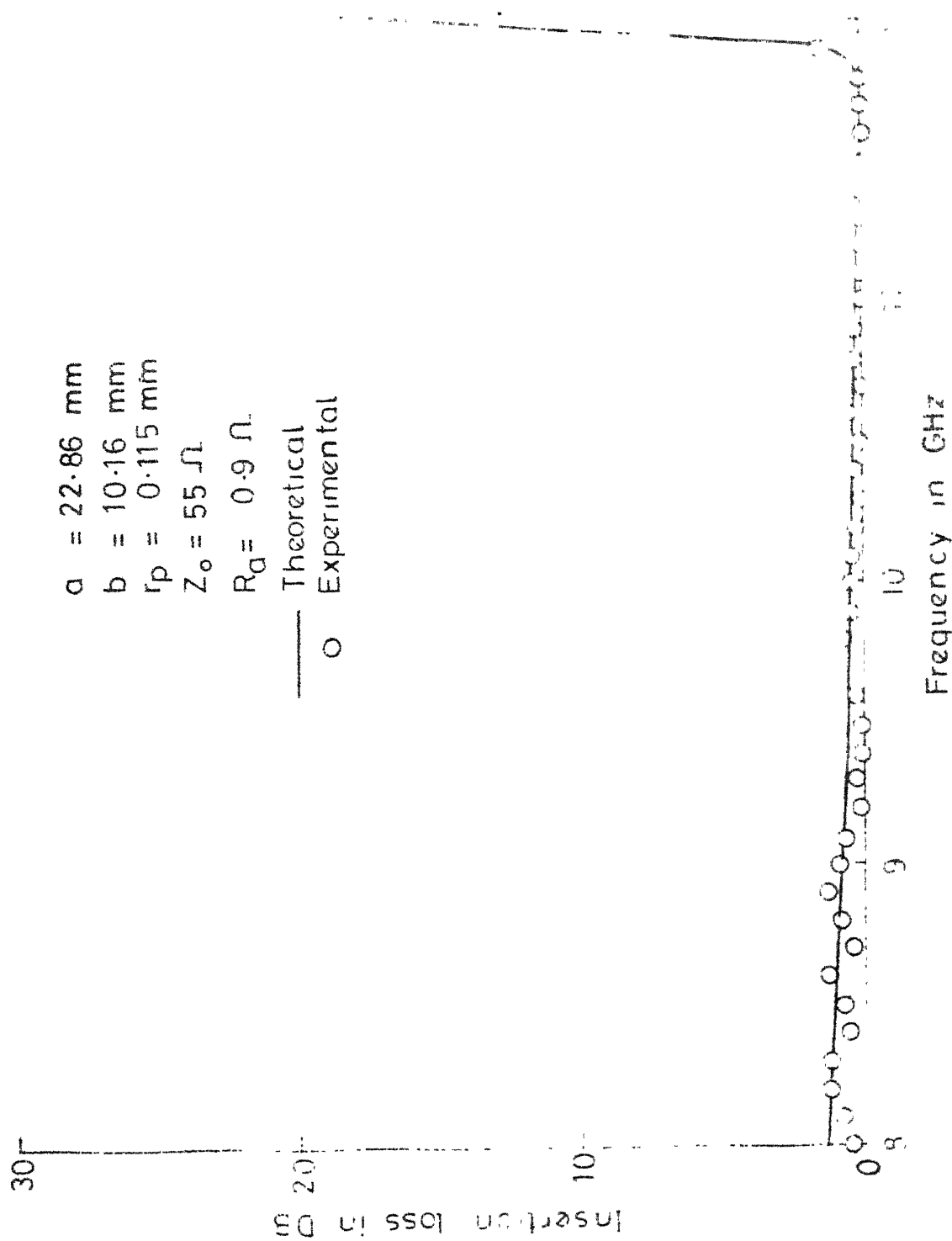


Fig. 3-11c Attenuation characteristic of a short circuited version using an extremely thin probe ($f_o = 12 \text{ GHz}$)

Table 3.5

Comparison between theoretical and experimental values of the resonant length.

$a=22.86$ mm, $b=10.16$ mm, $r_p = 0.115$ mm, $Z_o = 55.00$ ohms, $\delta = 0$

Frequency in GHz	Resonant length (in mm)	
	Theoretical	Experimental
8.00	9.19	9.20
8.50	8.51	8.50
9.00	7.88	7.90
9.50	7.32	7.30
10.00	6.79	6.80
10.50	6.30	6.20
11.00	5.81	5.70
11.50	5.33	5.20
12.00	4.84	4.70

3.4 RESONANT CONTOUR OF THE SHORT-CIRCUITED VERSION: SOME THEORETICAL RESULTS

In the previous sections, electromagnetic analyses of the short-circuited and air-gap cases were presented, under some suitable simplifying assumptions. Through the experimental results, it was demonstrated that the ripples in the pass-band can be brought down to an acceptable level by making use of an extremely thin (electrically) probe. Some improvement in the ripples can also be effected by incorporating an optimally chosen air-gap of length δ_{opt} in the structure. A fresh value of δ_{opt} is necessitated with each change in the center frequency. The values of δ_{opt} that are required are, generally speaking, much lesser than b . The larger values of δ result in a marked deterioration in the values of IL_{max} with increasing f_0 . This limits the useful tuning range of the configuration severely. Hence, in actual practice, larger values of δ are not recommended except when one is willing to sacrifice the tunability.

The aim of this section is to present theoretical results depicting the effects of varying Z_0 , R_a , r_p and b on the performance of a single-stage short-circuited version. The results are checked against experimental evidence, wherever possible and thought necessary.

The results presented in this section will help in gaining an insight into the interdependence of the physical parameters of the configuration and its frequency response. They will serve as a useful guideline to the designer who, before going to the multistage configurations of this type, will prefer to optimize the performance of the single-stage section through a judicious choice of its physical parameters.

A notch (or narrow-band-rejection) response can be characterized by its peak insertion loss (IL_{\max}), the two quality factors (Q_1 and Q_2), and the two skirt selectivities (S_1 and S_2). The definitions of these characterizing parameters are illustrated in Fig. 3.12.

Using the theoretical model developed in the section 3.1, a computer program was written to calculate IL_{\max} , Q_1 , Q_2 , S_1 and S_2 for a given set of values of a, b, r_p, R_a, Z_0 and f_0 . The calculation of the peak insertion loss was performed by using eq. 3.1.59. The calculation of the quality factors and skirt selectivities was done using their basic definitions illustrated in Fig. 3.12. This was necessary because accurate explicit formulas for these parameters were difficult to derive.

The results obtained by the above mentioned procedure are discussed in the following subsections.

↑ Insertion
loss

$$Q_1 = f_0 / f_1$$

$$Q_2 = f_0 / f_2$$

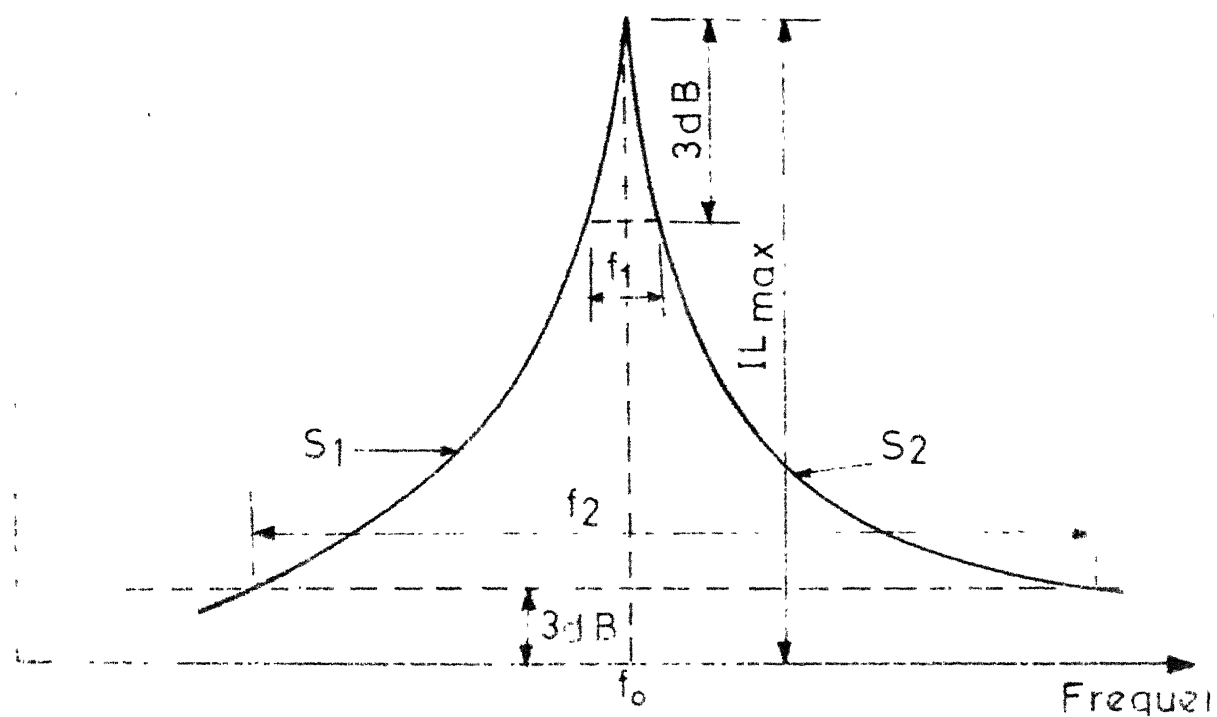


Fig 3-12 Definition of various characterizing parameters of a notch response

3.4.1 Effects of Varying the Characteristic Impedance of the Coaxial Line:

The variations of IL_{\max} , Q_1 , Q_2 , S_1 and S_2 with f_o are shown in Fig. 3.13, for different values of Z_o . The following conclusions can be drawn:

- i) IL_{\max} is independent of variations in Z_o .
- ii) Lower values of Z_o produce larger variations of Q_1 , Q_2 , S_1 and S_2 with f_o .
- iii) Values of the L.H.S. skirt selectivity (S_1) are always a little higher than the corresponding values of the R.H.S. skirt selectivity (S_2).

3.4.2 Effects of Varying the Loss Resistance:

The effects of varying R_a on the variations of IL_{\max} , Q_1, Q_2 , S_1 and S_2 with f_o are depicted in Fig. 3.14. The following conclusions can easily be drawn:

- i) Higher values of R_a result in lower values of IL_{\max} , S_1 , S_2 and Q_1 .
- ii) Q_2 shows somewhat larger variations with f_o for higher values of R_a .
- iii) Values of S_1 are always a little higher than the corresponding values of S_2 .

3.4.3 Effects of Varying the Radius of the Probe:

The effects of varying r_p are shown in Fig. 3.15. These results should be viewed a little cautiously for the theory used is valid only for extremely thin (electrically) probes.

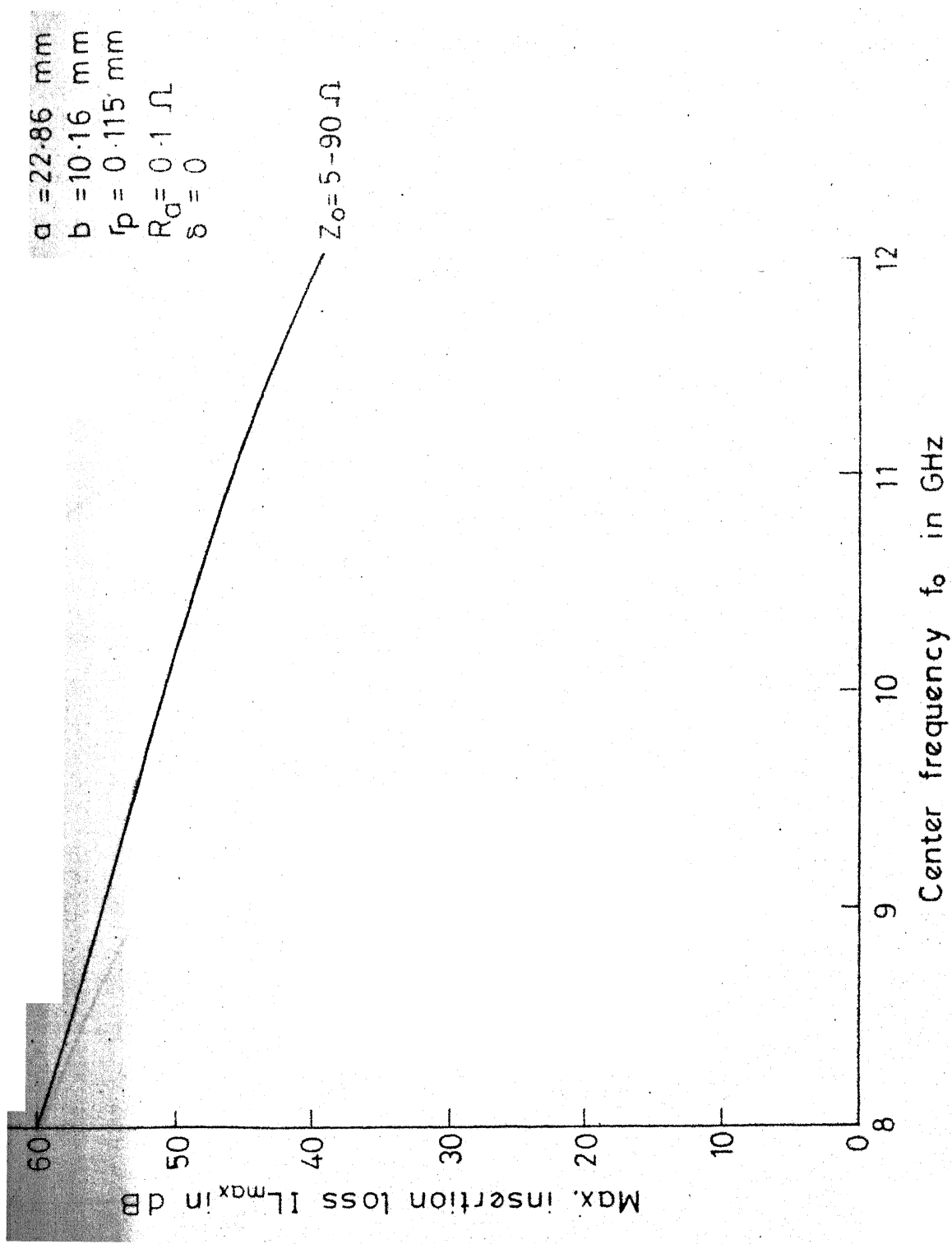


Fig. 3-13a Variation of IL_{\max} with f_0 for different values of Z_0

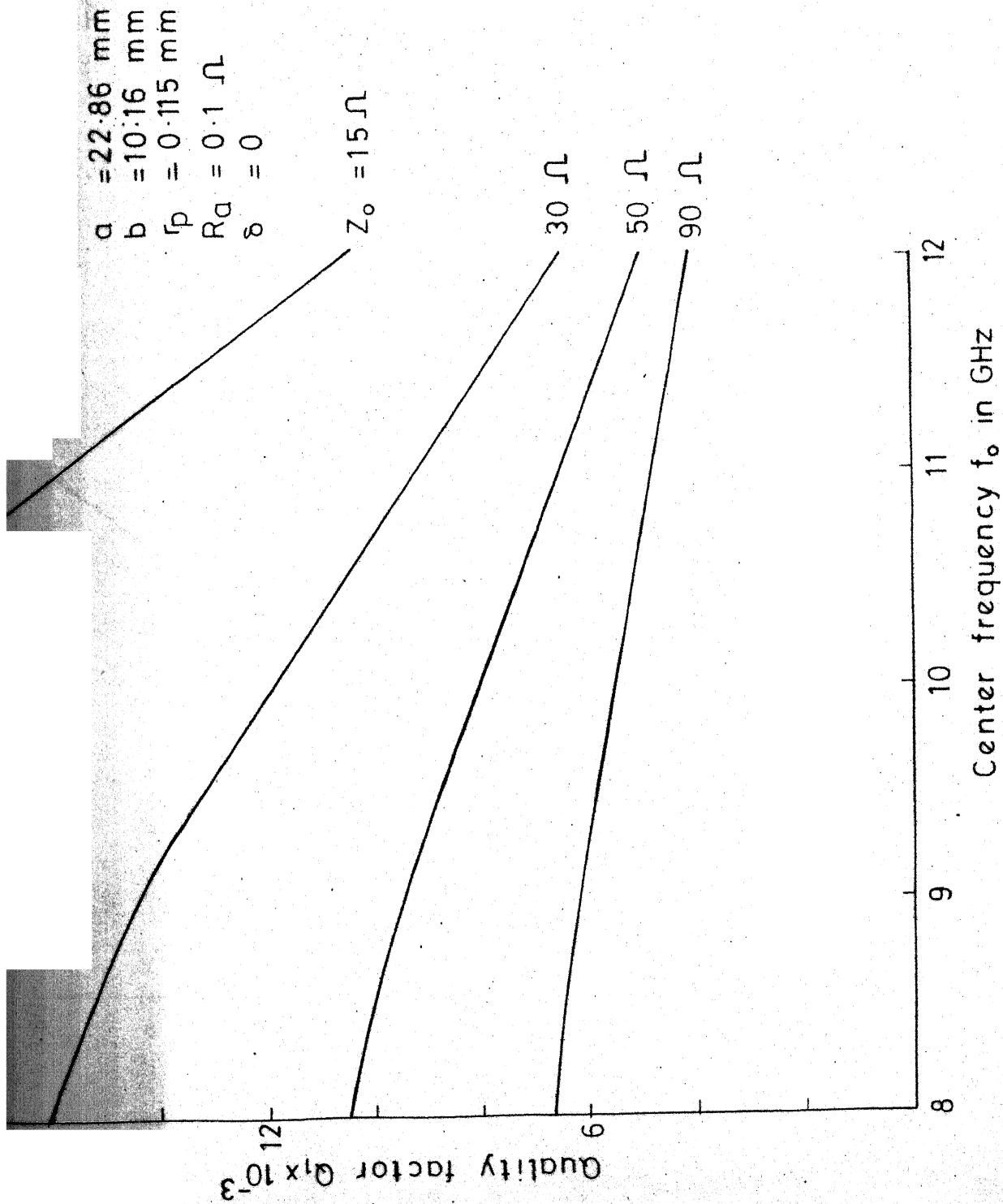


Fig. 3-13b Variation of Q_1 with f_0 for different values of Z_o

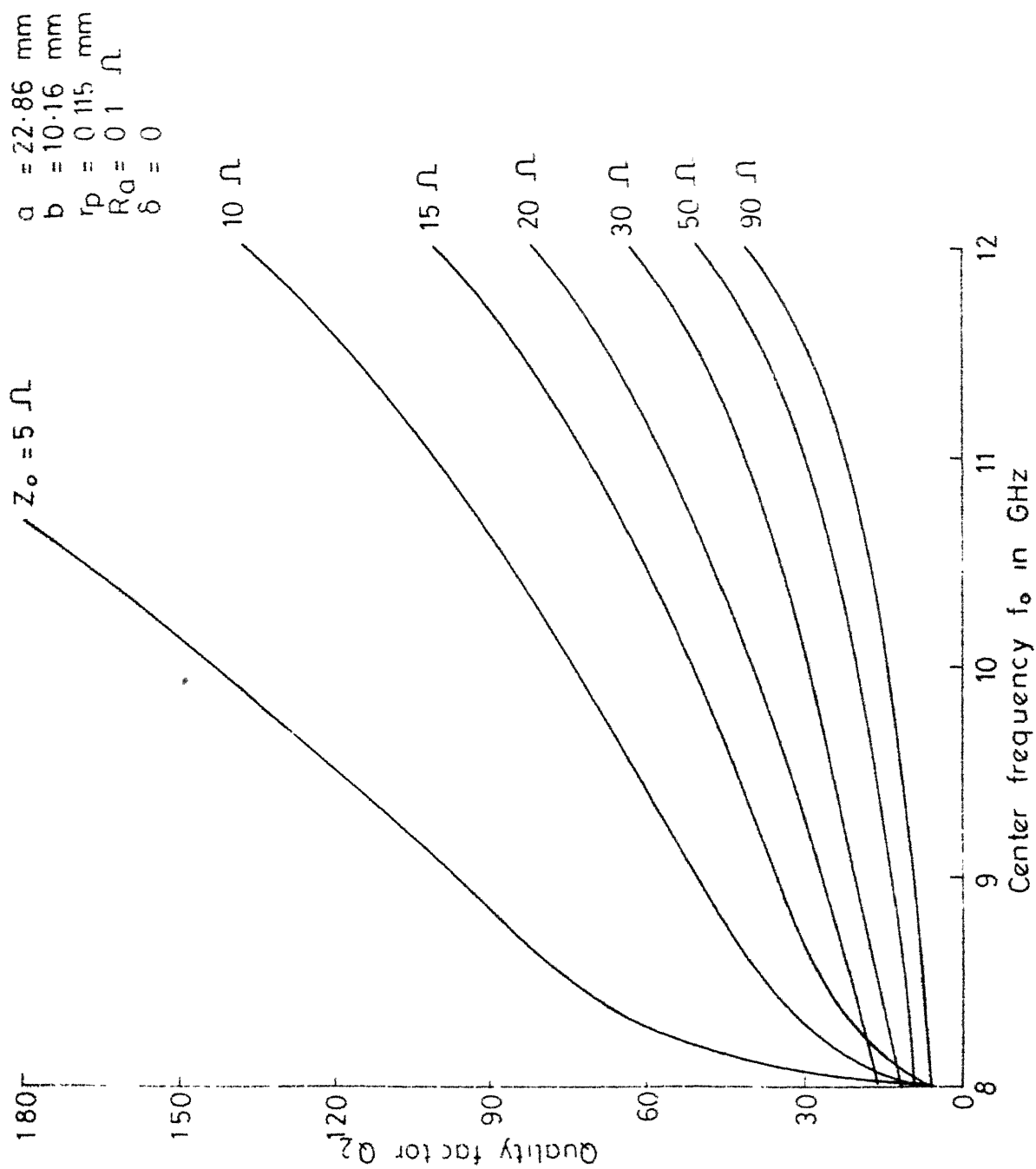


Fig. 3-13c Variation of Q_2 with f_0 for different values of Z_0

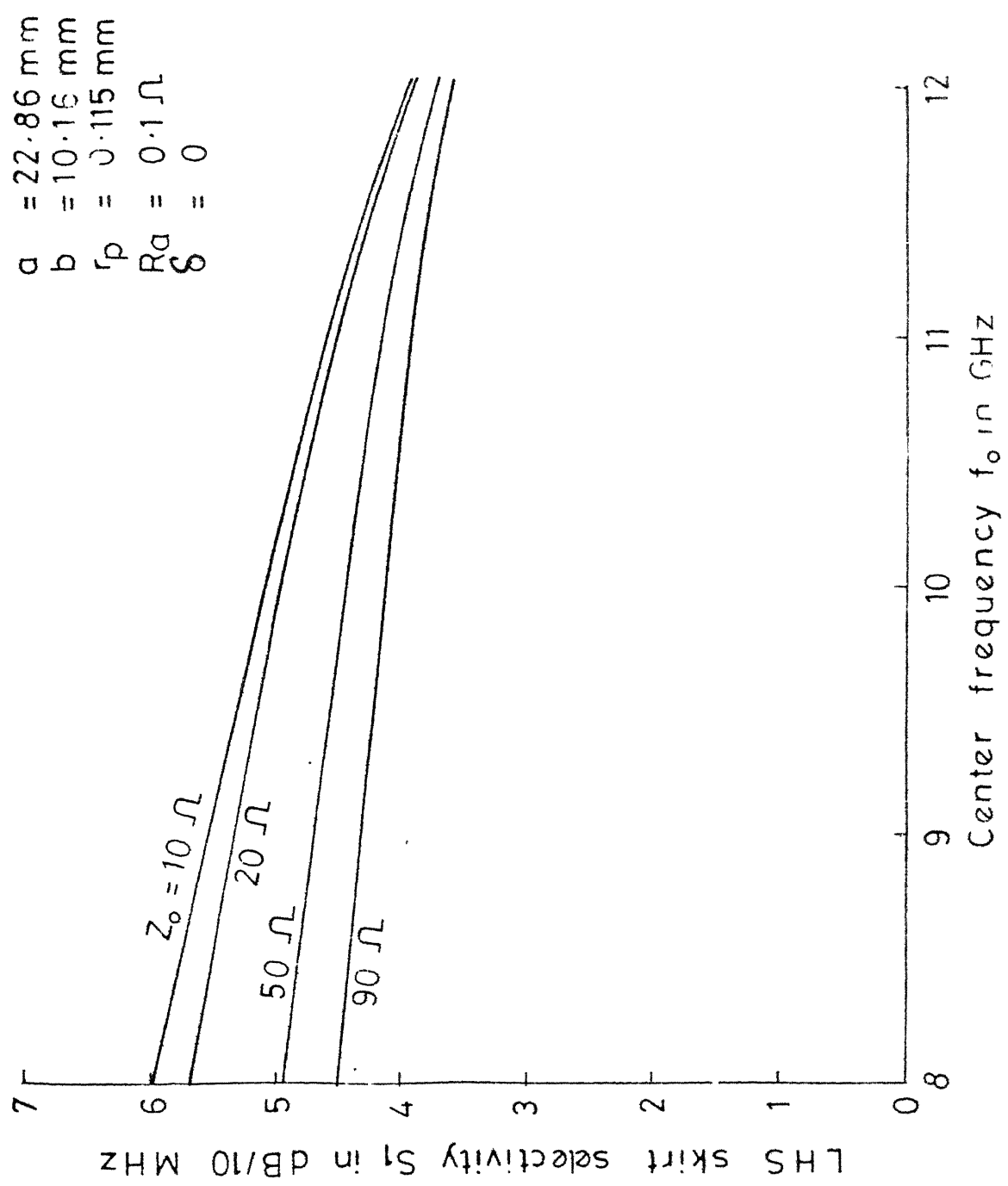


Fig. 3.13d Variation of S_1 with f_0 for different values of Z_0

$a = 22.86 \text{ mm}$
 $b = 10.16 \text{ mm}$
 $r_p = 0.115 \text{ mm}$
 $R_a = 0.1 \Omega$
 $\delta = 0$

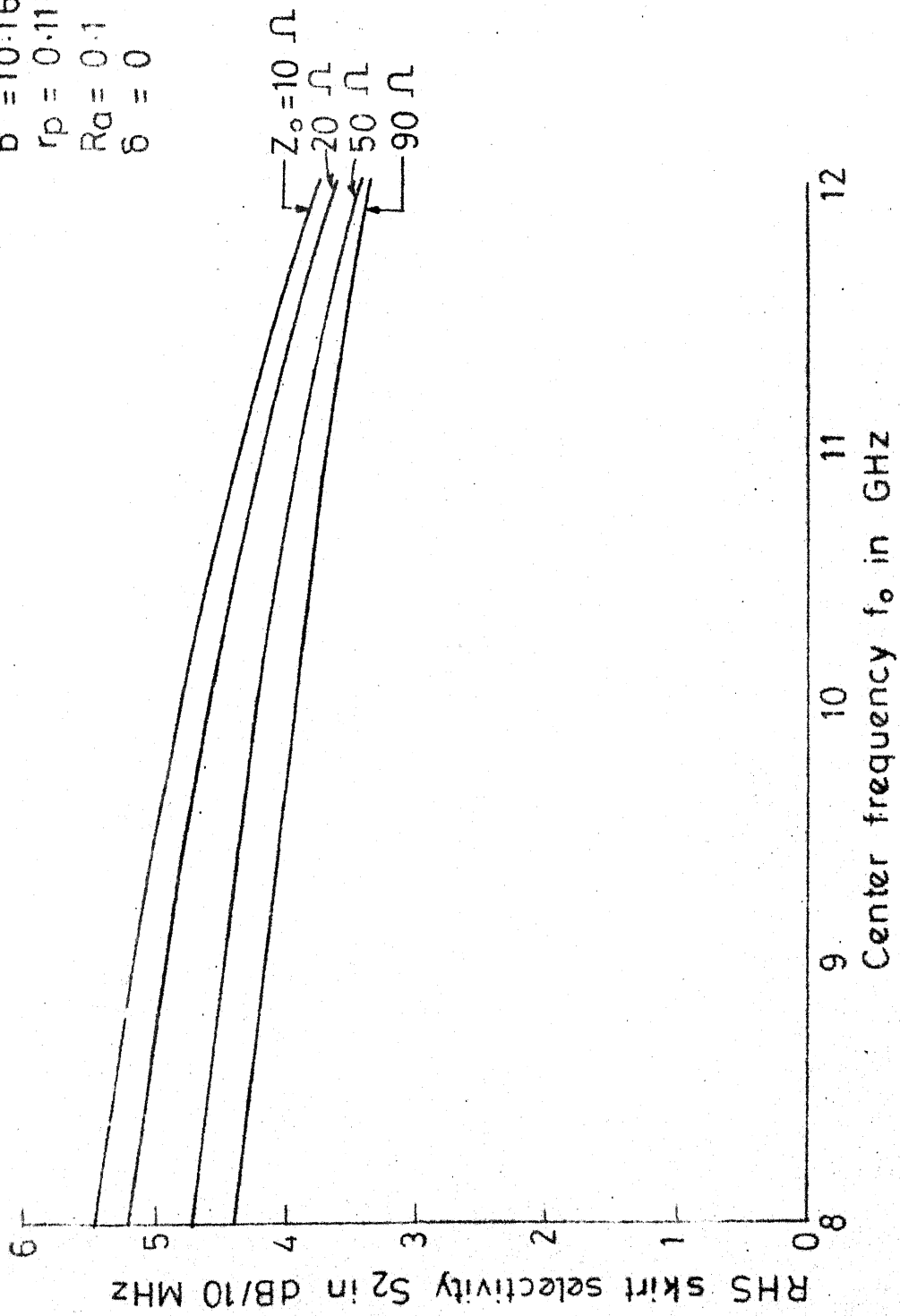


Fig.3.13e Variation of S_2 with f_0 for different values of Z_0 .

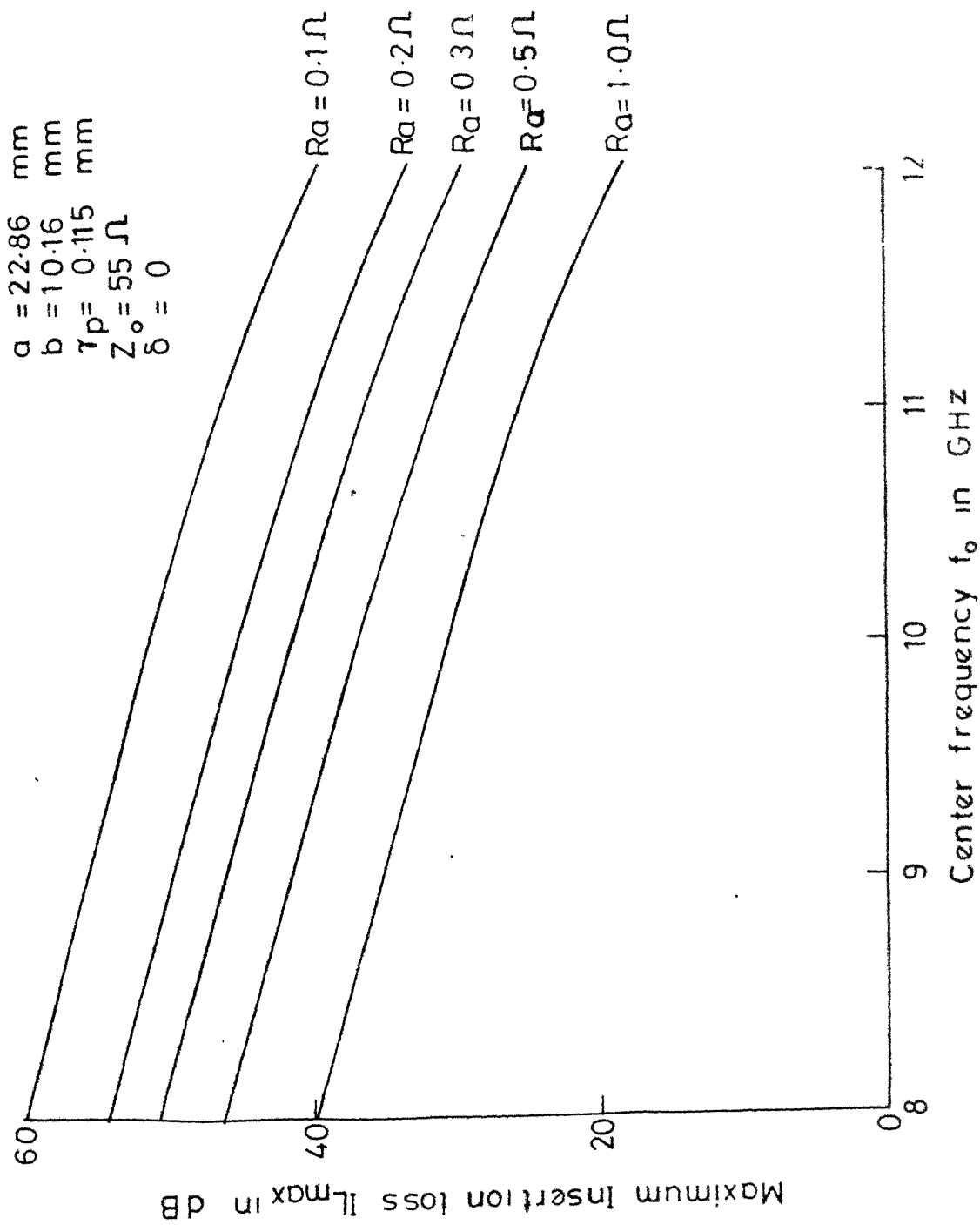


Fig. 3-14a Variaton of IL_{\max} with f_o for different values of R_a

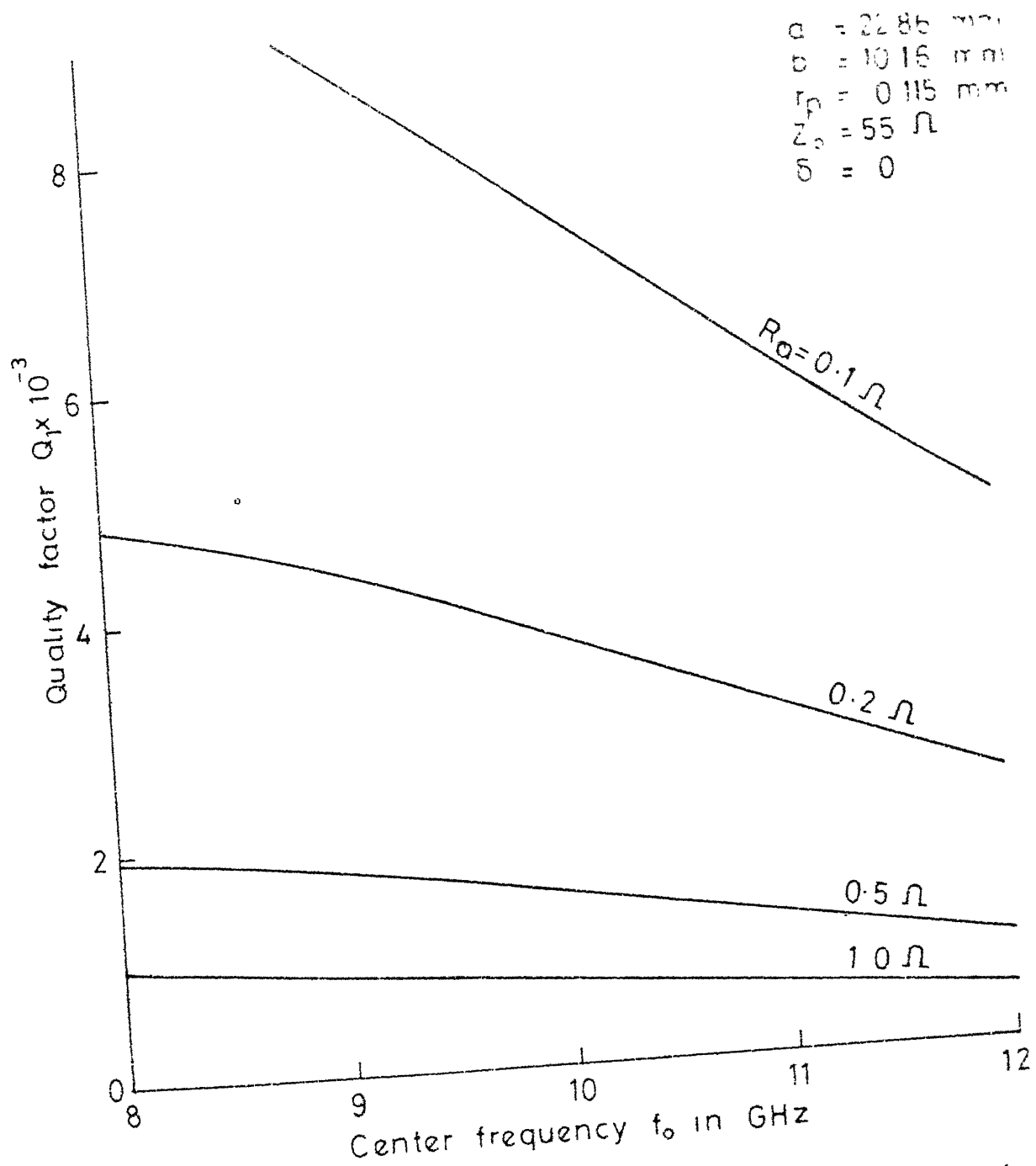


Fig.3-14b Variation of Q_1 with f_0 for different values of R_a

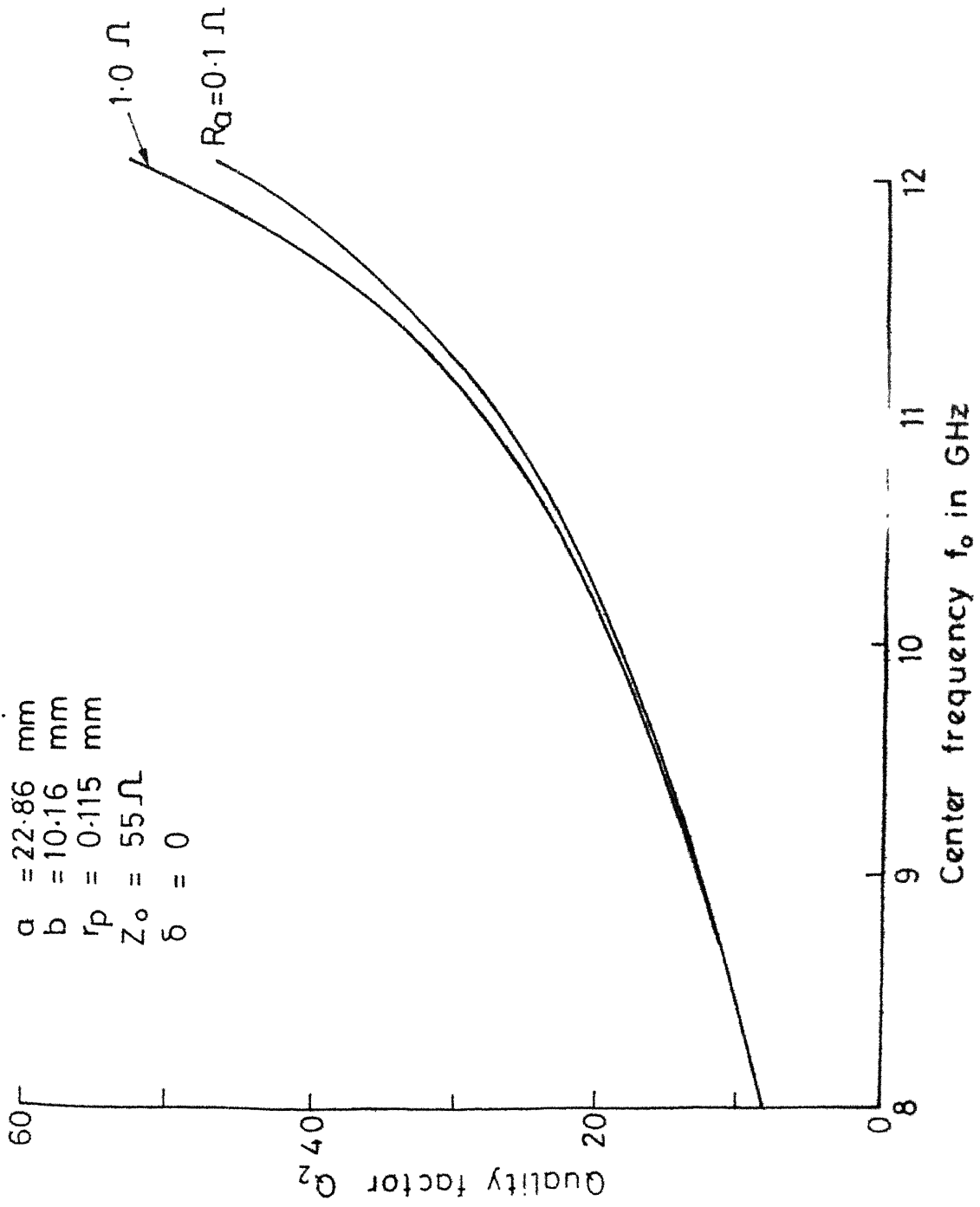


Fig. 3-14c Variation of Q_2 with f_0 for different values of R_a

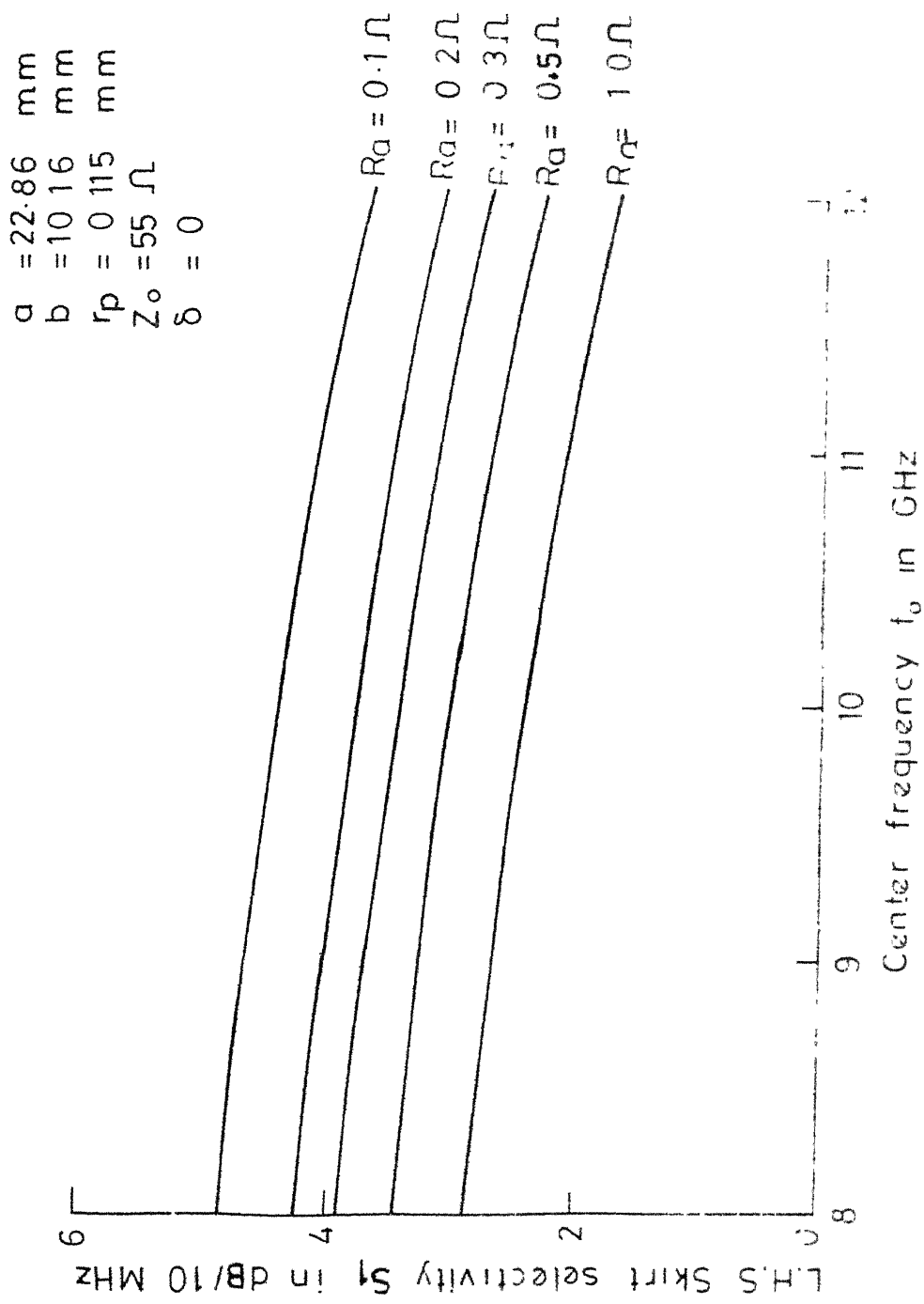


Fig. 3-14d Variation of S_1 with f_0 for different values of R_a

$a = 22.86 \text{ mm}$
 $b = 12.7 \text{ mm}$
 $r_D = 0.15 \text{ mm}$
 $Z_0 = 55 \Omega$
 $\delta = 0$

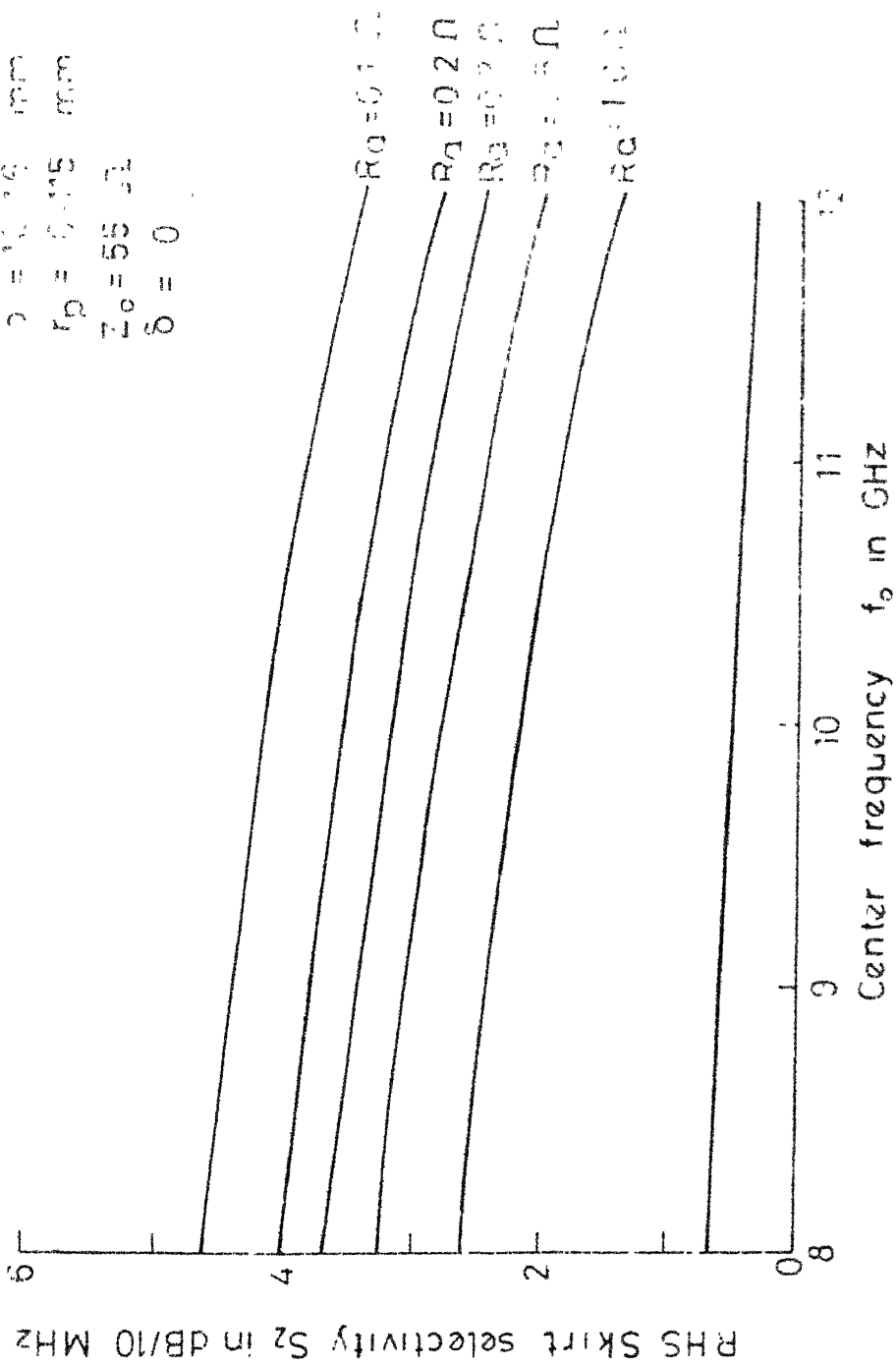


Fig 3-14e Variation of S_2 with f_0 for different values of R_L

The following points need to be observed:

- i) Theoretically, the variation of IL_{\max} with f_o remains unchanged (Fig. 3.15a) for different values of r_p . In practice, however, it was seen that the thick probes produce larger variations of IL_{\max} with f_o . The reason for this discrepancy between theoretical and experimental results lies obviously in the various simplifying assumptions made in the analysis, the assumption of an electrically thin probe and of a constant R_a throughout the band being probably the most crucial of all.
- ii) Higher values of r_p result in lower values of (but improved frequency dependence of) Q_1, Q_2, S_1 and S_2 . This was seen to be true in practice also.
- iii) One very important point which is not within the premises of the theory but needs recalling is the improved pass-band ripples when thinner probes are used.
- iv) Values of S_1 are always a little higher than the corresponding values of S_2 .

3.4.4 Effects of Varying the Height of the Waveguide:

Improvements in the resonant contour can also be sought by reducing the height of the waveguide near and on both sides of the discontinuity. The reduced-height portion of the waveguide can be matched to the standard-height portion by means of suitable impedance-matching transformers.

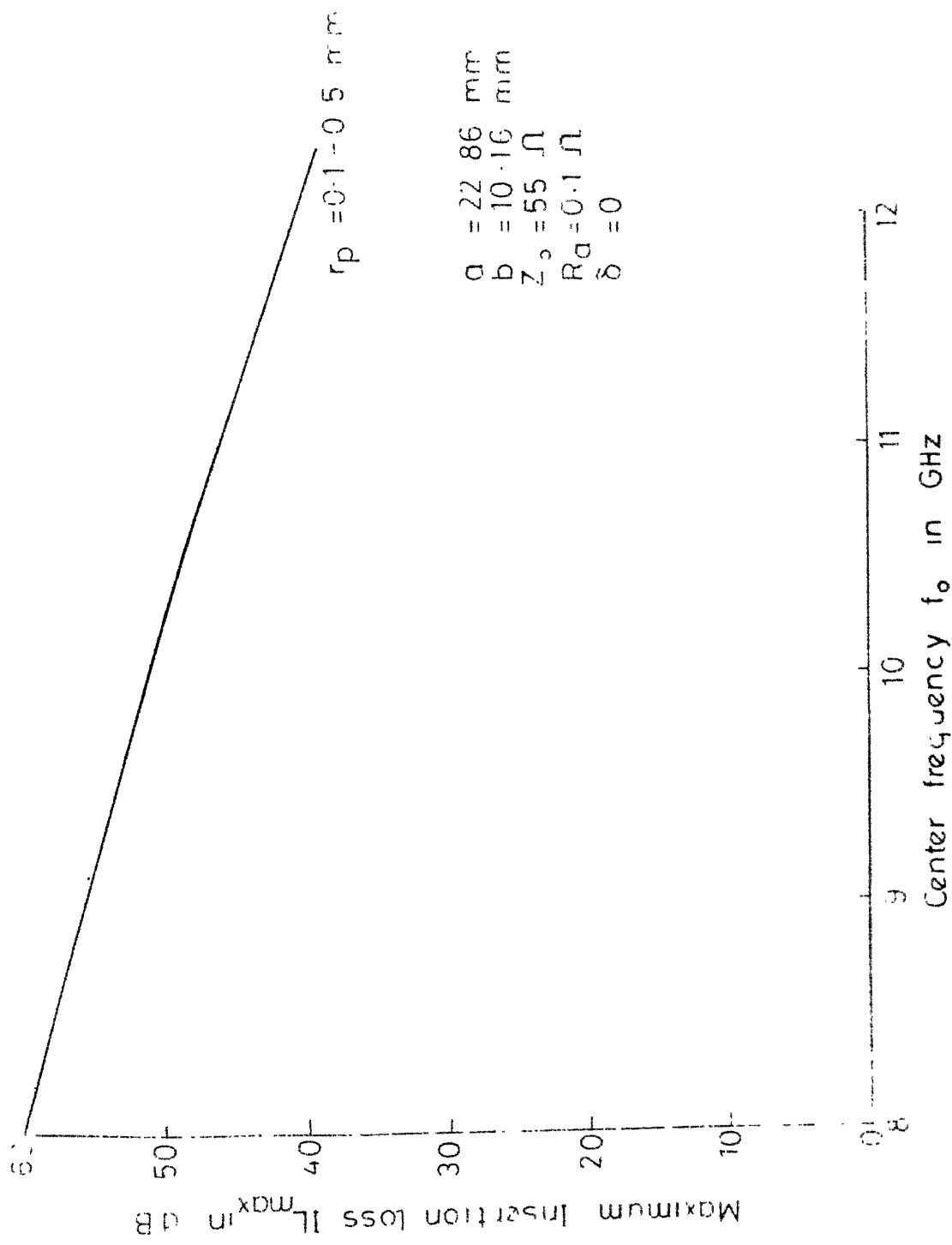


Fig. 3-15a Variation of IL_{max} with f_0 for different values of r_p

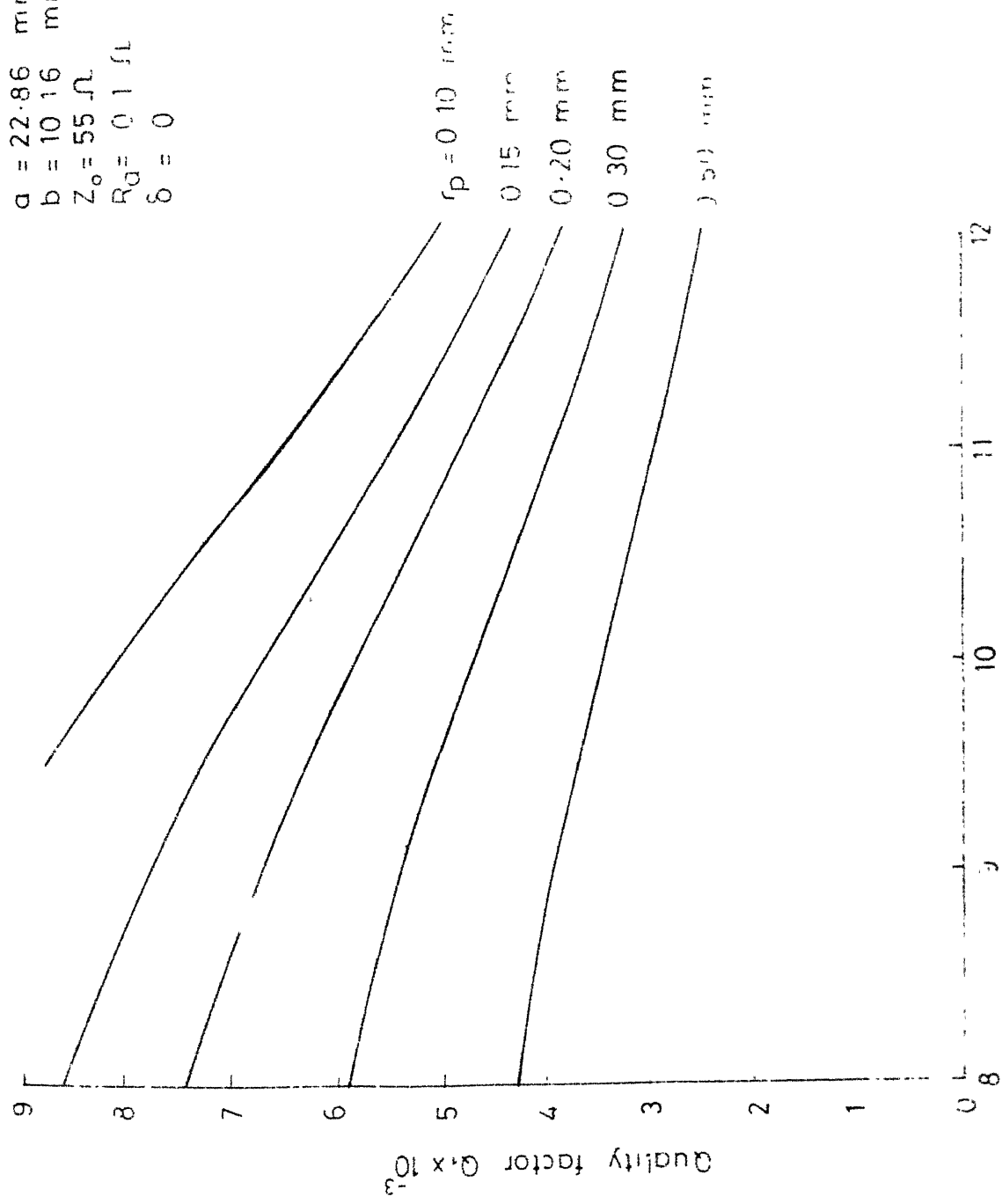


Fig 3-15b Variation of Q_1 with f_0 for different values of r_p

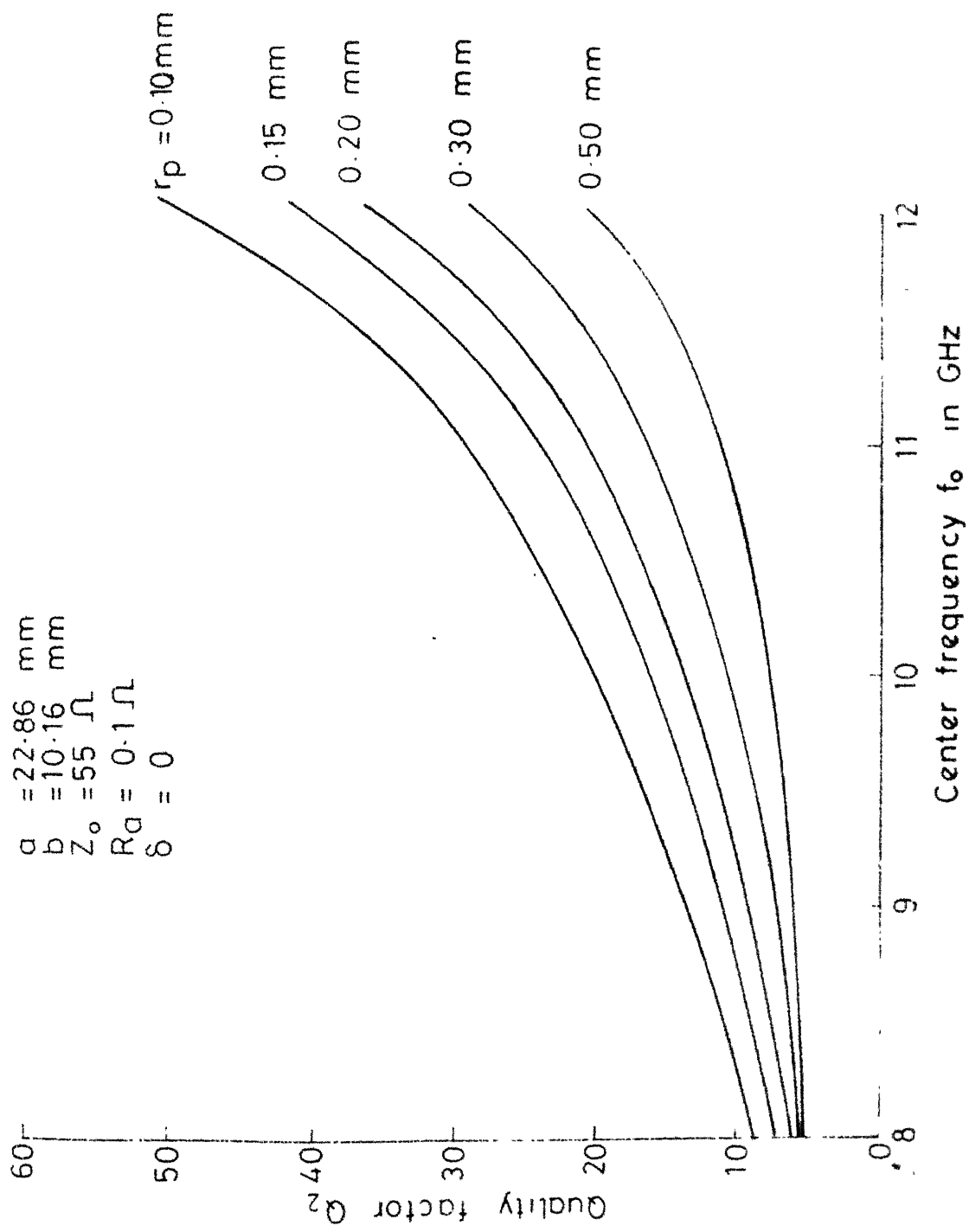


Fig. 3-15c Variation of Q_2 with f_0 for different value of r_p

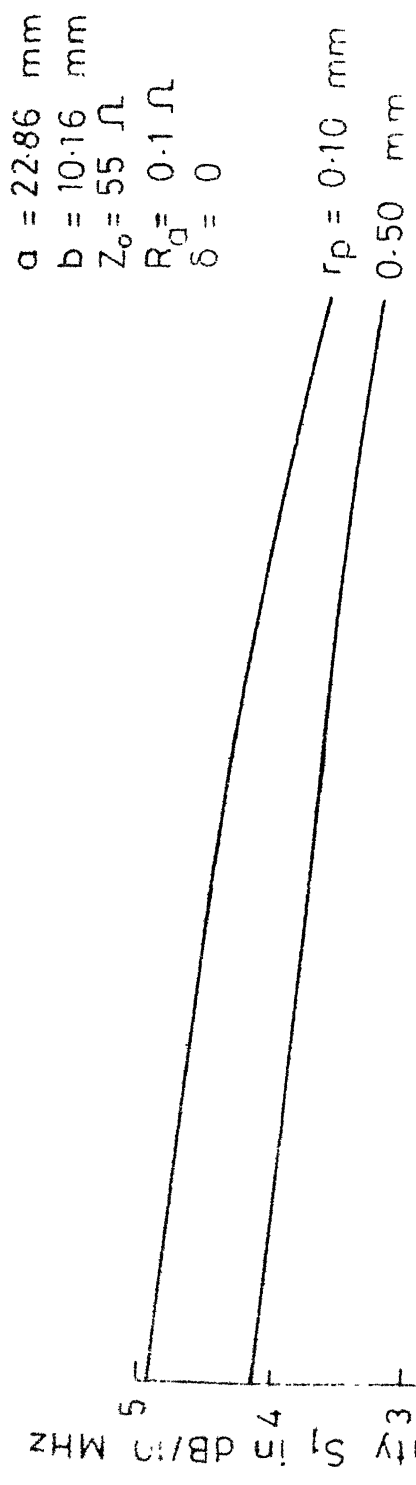


Fig.3.15d Variation of S_1 with f_0 for different values of r_p

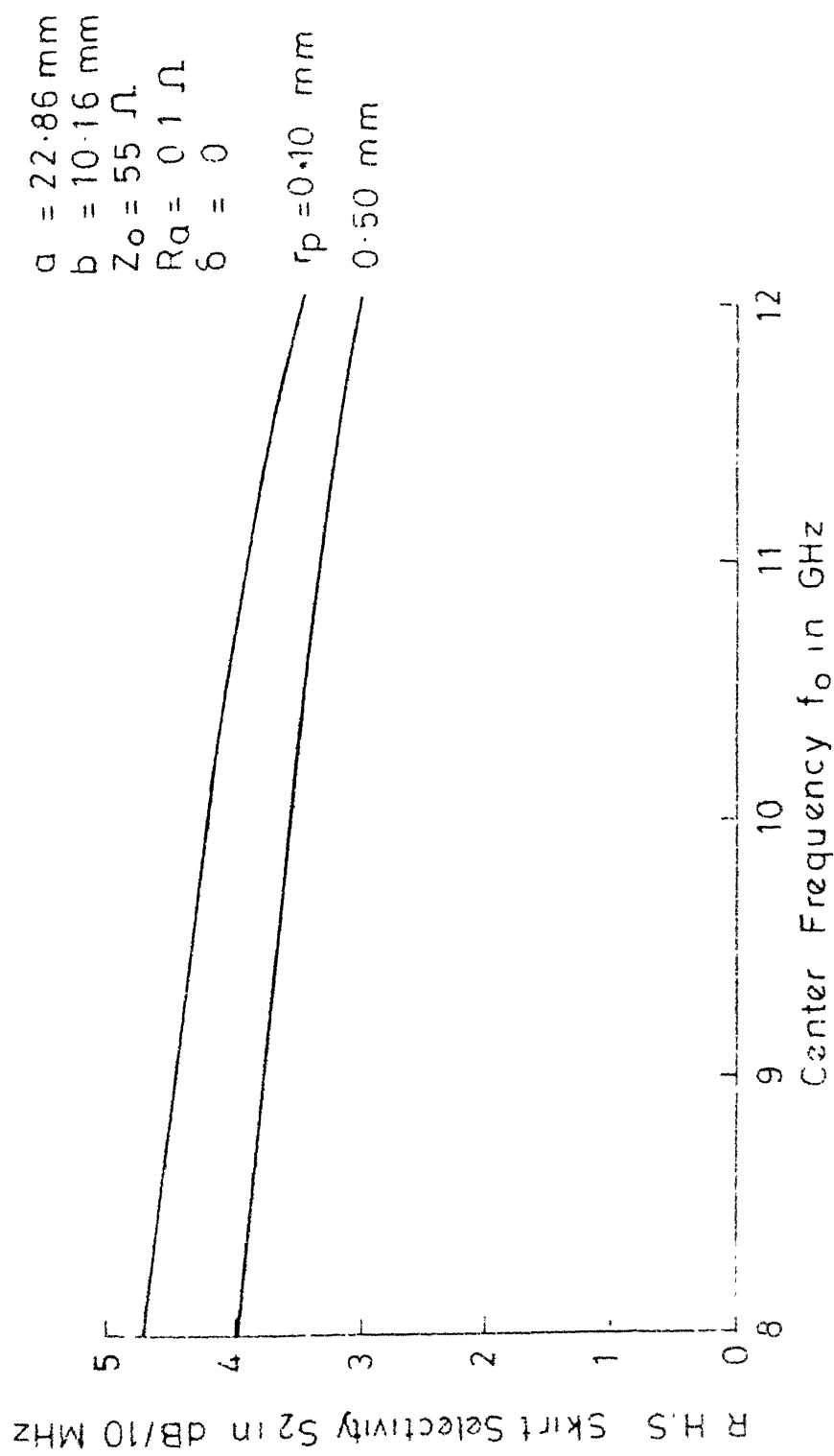


Fig.3.15e Variation of S_2 with f_0 for different values of r_p

The effects of varying b on the dependence of IL_{\max} , Q_1 , Q_2 , S_1 and S_2 on f_0 are depicted in Fig. 3.16. The following conclusions can be drawn:

- i) Smaller values of b improve the dependence of IL_{\max} on f_0 .
- ii) There exists an optimum value (say b_{opt}) of b such that
 - a) with $b = b_{\text{opt}}$, the variations of Q_1 , Q_2 , S_2 and S_2 with f_0 are reduced to minimum and
 - b) for $b < b_{\text{opt}}$, no further improvement in the response is observed.

For the case shown in Fig. 3.16, the value of b_{opt} lies somewhere between 7.5 mm and 6.0 mm.

- iii) Values of S_1 are always a little higher than the corresponding values of S_2 .

3.5 ANALYSIS OF THE SHORT-CIRCUITED VERSION INCLUDING HIGHER-ORDER WAVEGUIDE MODES:

One of the most crucial assumptions made in the analysis presented in Section 3.1 is the neglect of higher-order waveguide modes while writing eq. (3.1.18). An analysis including the effect of the first higher-order mode is presented in this section. It is seen that, in principle, it is possible to go on refining the analysis for higher and higher modes.

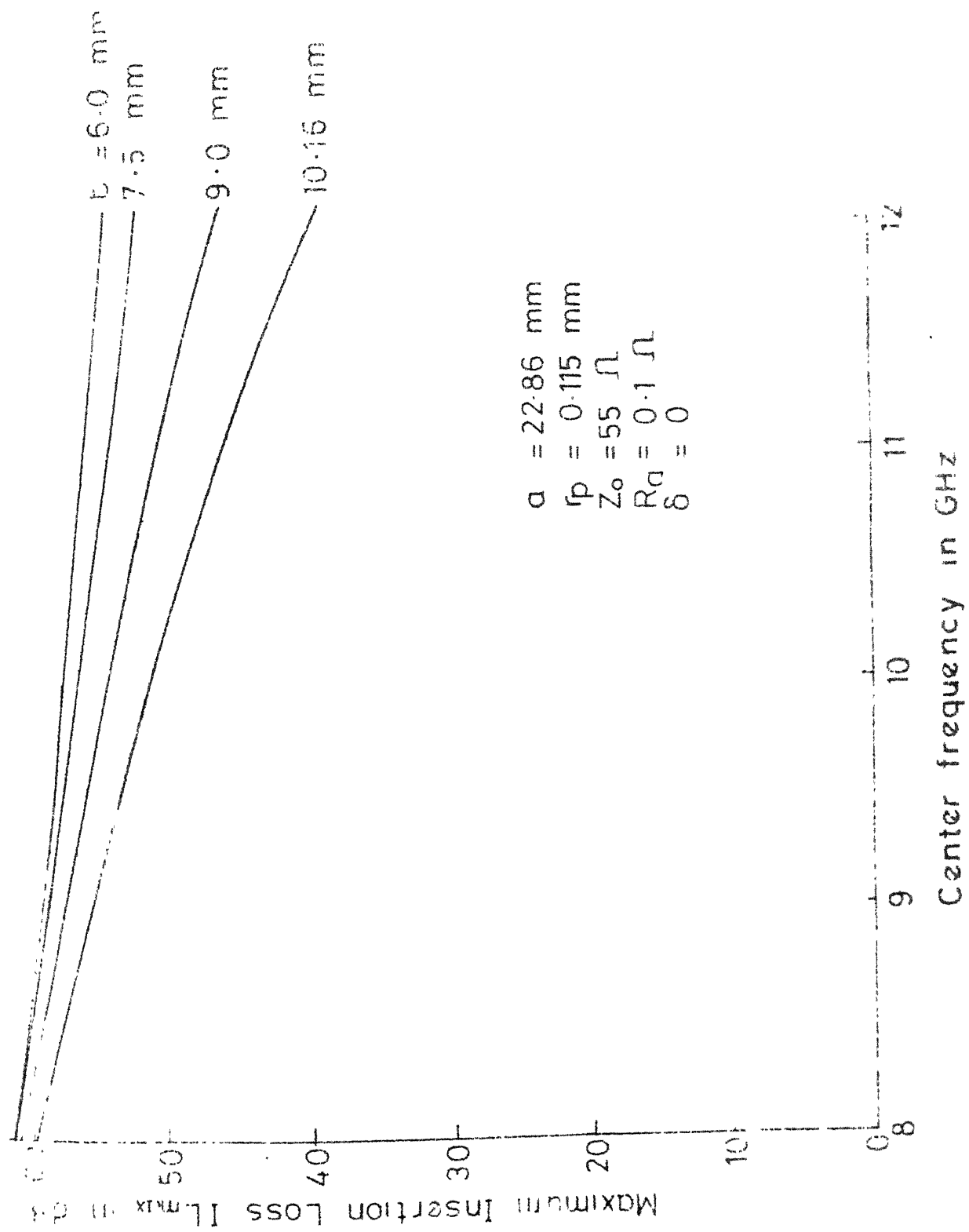


Fig. 3-16a Variation of IL_{max} with f_0 for different values of b

$a = 22.86 \text{ mm}$
 $r_p = 0.115 \text{ mm}$
 $Z_0 = 55 \Omega$
 $R_Q = 0.1 \Omega$
 $\delta = 0$

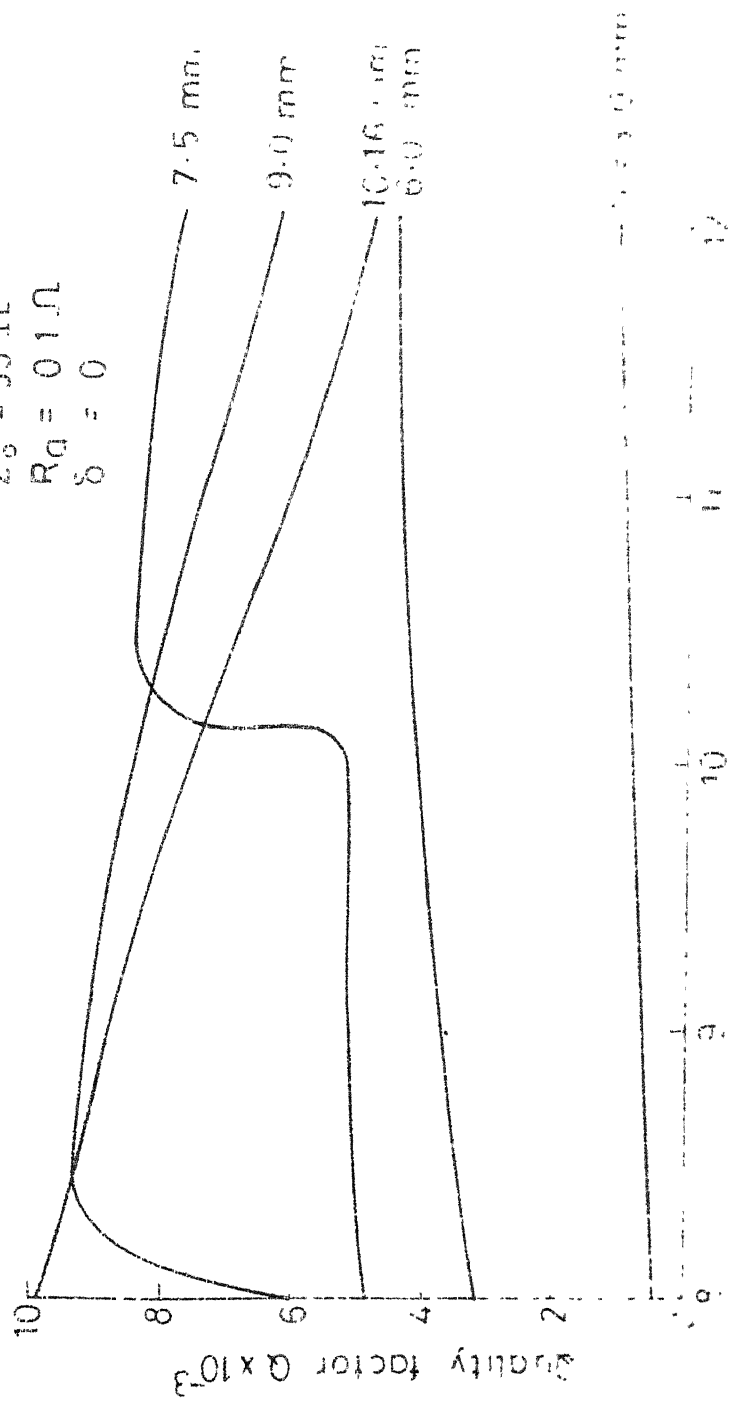


Fig 316b Variation of Q_1 with f_0 for different values of h

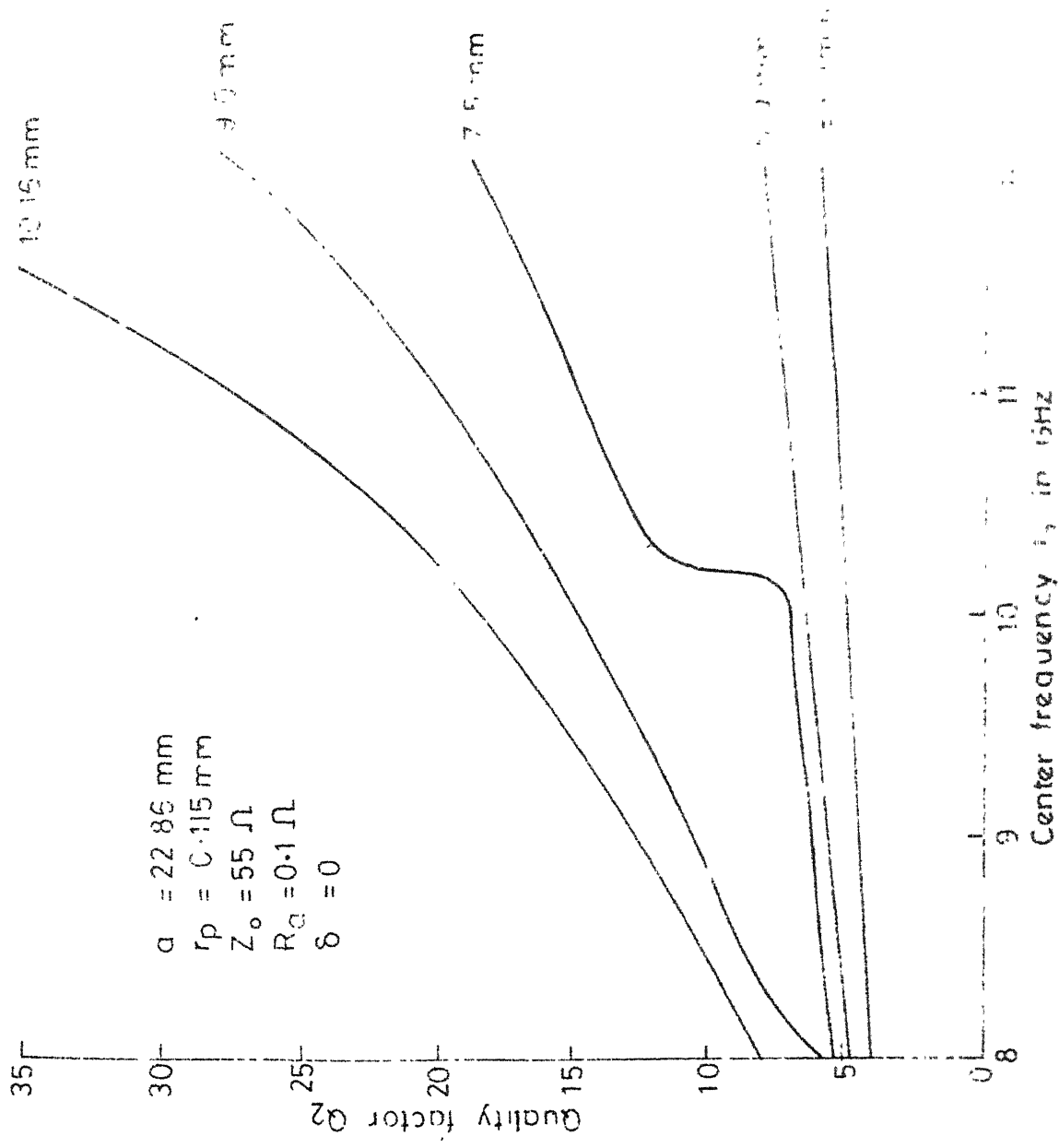


Fig. 3-16c Variation of Q_2 with f_0 for different values of a

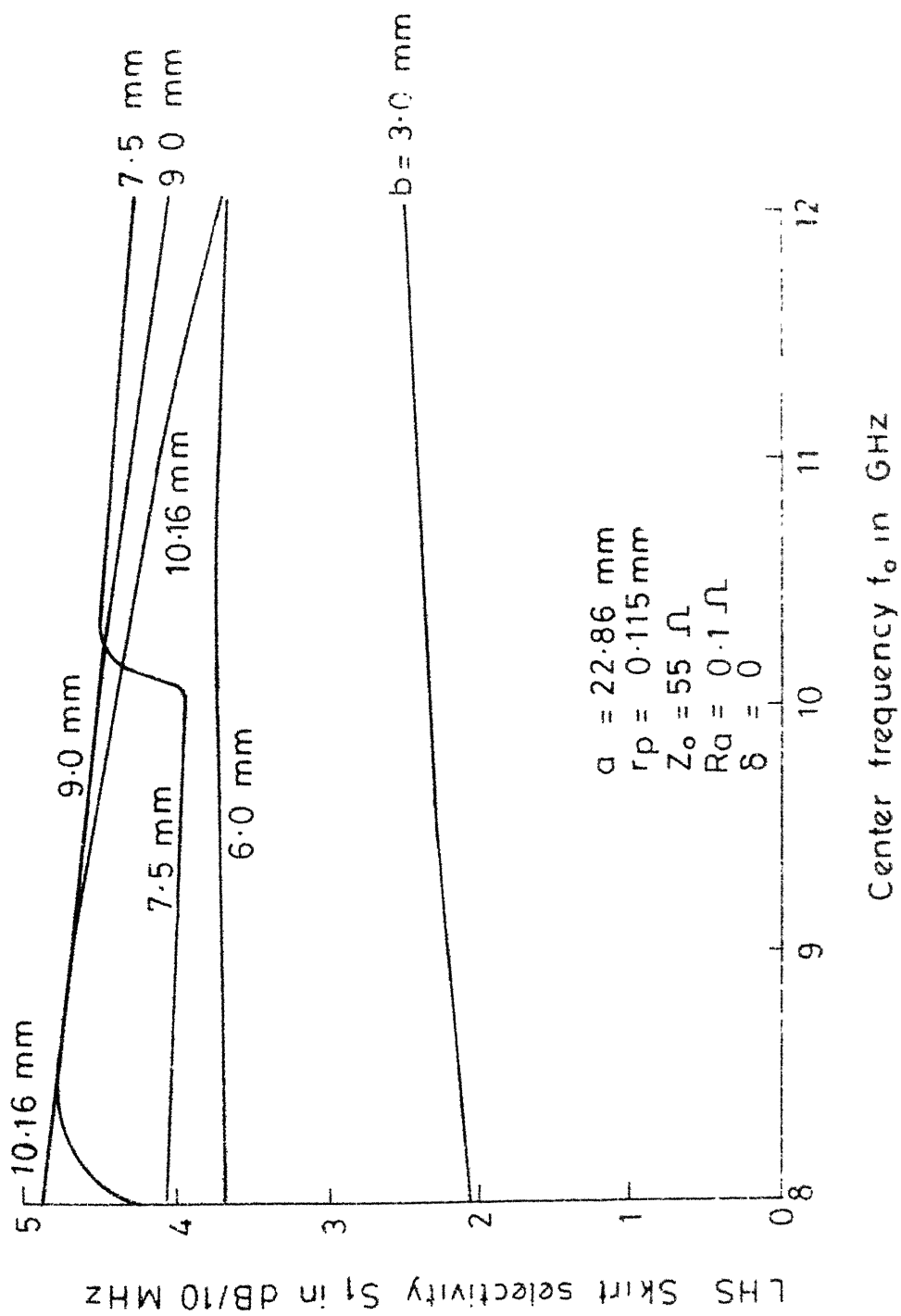


Fig.3.16d Variation of S_1 with f_0 for different values of b

$a = 22.86 \text{ mm}$
 $r_p = 0.115 \text{ mm}$
 $Z_o = 55 \Omega$
 $R_a = 0.1 \Omega$
 $\delta = 0$

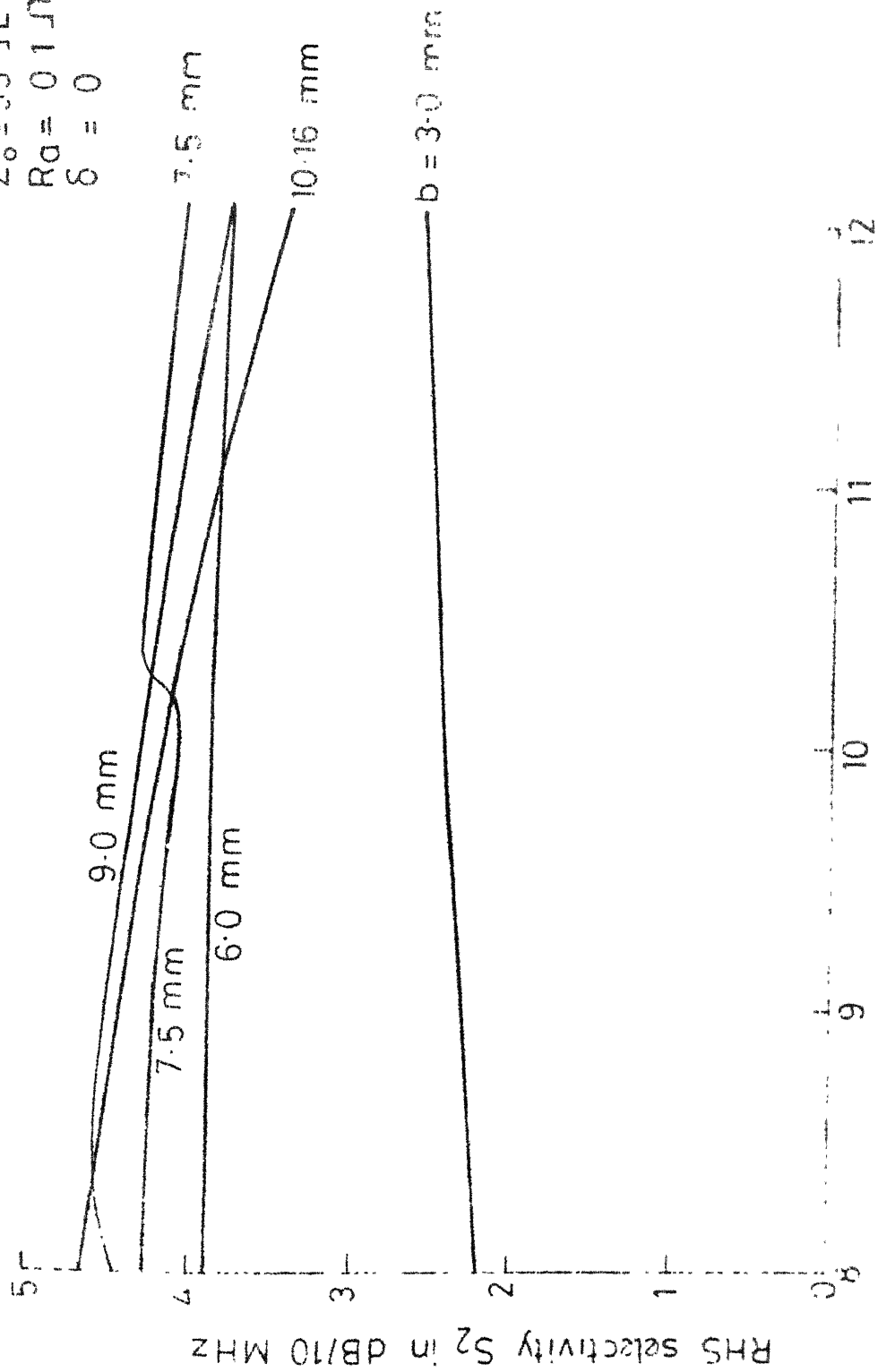


Fig. 3-16e Variation of S_2 with f_0 for different values of b

However, the tremendous increase in the amount of algebra involved with the inclusion of each new mode puts a practical limit on this kind of approach.

The fundamental mode of propagation in a rectangular waveguide is the TE_{10} mode. This mode is followed by higher-order TE modes like TE_{20} , TE_{01} , TE_{11} , TE_{21} , TE_{02} and so on. As TE_{0n} modes will have $E_y = 0$, the contribution of these modes to E_R in eq. (3.1.18) will be zero. Also, for a centered probe, the contribution of the TE_{20} mode to E_R can easily be seen to be zero. Thus, for all practical purposes, the first higher-order mode to be included in E_R is the TE_{11} mode. We should replace eq. (3.1.18) by

$$E_R = 1 + R_{1,1} \cos \frac{\pi y}{b} \quad (3.5.1)$$

where $R_{1,1}$ is the (unknown) reflection coefficient of the TE_{11} mode.

Eq. (3.1.12) can easily be shown to modify to

$$\left(\frac{d^2}{dy^2} + \beta^2\right) V(y) = -\frac{\pi}{b} R_{1,1} \sin \frac{\pi y}{b} \quad (3.5.2a)$$

and

$$\left(\frac{d^2}{dy^2} + \beta^2\right) I(y) = -\frac{j\beta}{Z_{op}} \left(1 + R_{1,1} \cos \frac{\pi y}{b}\right) \quad (3.5.2b)$$

Defining

$$\tau_1 = \frac{R_{1,1}}{1 - \pi^2 / \beta^2 b^2} \quad (3.5.3)$$

the solution to eq. (3.5.2) can be written as

$$V(y) = Z_{op} (I^+ e^{-j\beta y} - I^- e^{j\beta y}) - \frac{\pi \tau_1}{\beta^2 b} \sin \frac{\pi y}{b} \quad (3.5.4a)$$

and

$$I(y) = I^+ e^{-j\beta y} + I^- e^{j\beta y} - \frac{j}{\beta Z_{op}} (1 + \tau + \tau_1 \cos \frac{\pi y}{b}) \quad (3.5.4b)$$

The application of boundary conditions in eqs. (3.1.20) and (3.1.21) yields

$$Z_1 I^+ - Z_2 I^- = V_1 \quad (3.5.5)$$

$$Z_3 I^+ - Z_4 I^- = V_2 \quad (3.5.6)$$

where

$$Z_1 = Z_{op} - R_a \quad (3.5.7a)$$

$$Z_2 = Z_{op} + R_a \quad (3.5.7b)$$

$$Z_3 = (Z_{op} - jX_k) e^{-j\beta b} \quad (3.5.7c)$$

$$Z_4 = (Z_{op} + jX_k) e^{j\beta b} \quad (3.5.7d)$$

and

$$V_1 = - \frac{jR_a}{\beta Z_{op}} (1 + \tau + \tau_1) \quad (3.5.8a)$$

$$V_2 = \frac{X_k}{\beta Z_{op}} (1 + \tau - \tau_1) \quad (3.5.8b)$$

The solution to eqs. (3.5.5) and (3.5.6) is

$$I^+ = \frac{1}{\beta Z_{op}} \frac{f_1 + jf_2}{f_5 + jf_6} \quad (3.5.9a)$$

and

$$I^- = \frac{1}{\beta Z_{op}} \frac{f_3 + jf_4}{f_5 + jf_6} \quad (3.5.9b)$$

where,

$$f_1 = (1 + \tau)g_{11} + \tau_1 g_{12} \quad (3.5.10a)$$

$$f_2 = (1 + \tau) g_{21} + \tau_1 g_{22} \quad (3.5.10b)$$

$$f_3 = (1 + \tau)g_{31} + \tau_1 g_{32} \quad (3.5.10c)$$

$$f_4 = (1 + \tau)g_{41} + \tau_1 g_{42} \quad (3.5.10d)$$

and f_5 and f_6 are given by eq. (3.1.32). The values of various g 's are as follows:

$$g_{11} = -X_k(Z_{op} + R_a) + R_a(Z_{op} \sin \beta b + X_k \cos \beta b) \quad (3.5.11a)$$

$$g_{12} = X_k(Z_{op} + R_a) + R_a(Z_{op} \sin \beta b + X_k \cos \beta b) \quad (3.5.11b)$$

$$g_{21} = R_a(X_k \sin \beta b - Z_{op} \cos \beta b) \quad (3.5.11c)$$

$$g_{22} = g_{21} \quad (3.5.11d)$$

$$g_{31} = -R_a(X_k \cos \beta b + Z_{op} \sin \beta b) - X_k(Z_{op} - R_a) \quad (3.5.11e)$$

$$g_{32} = -R_a(X_k \cos \beta b + Z_{op} \sin \beta b) + X_k(Z_{op} - R_a) \quad (3.5.11f)$$

$$g_{41} = g_{21} \quad (3.5.11g)$$

$$\text{and } g_{42} = g_{41} \quad (3.5.11h)$$

Using eqs. (3.5.4b) and (3.5.9) in eq. (3.1.10), and manipulating, we arrive at

$$\beta^2 Z_{op} N_o \tau = j \frac{(f_3 + jf_4)(1 - e^{j\beta b}) - (f_1 + jf_2)(1 - e^{-j\beta b})}{f_5 + jf_6} - j\beta(1 + \tau) \quad (3.5.12)$$

It turns out that

$$(f_3 + jf_4)(1 - e^{j\beta b}) - (f_1 + jf_2)(1 - e^{-j\beta b}) = f_7 + jf_8 \quad (3.5.13)$$

where

$$f_7 = (f_3 - f_1)(1 - \cos \beta b) + (f_2 + f_4) \sin \beta b \quad (3.5.14a)$$

and

$$f_8 = (f_4 - f_2)(1 - \cos \beta b) - (f_1 + f_3) \sin \beta b \quad (3.5.14b)$$

Using eq. (3.5.10), we write

$$f_3 - f_1 = (1 + \tau)(g_{31} - g_{11}) + \tau_1(g_{32} - g_{12}) \quad (3.5.15a)$$

$$f_3 + f_1 = (1 + \tau)(g_{31} + g_{11}) + \tau_1(g_{32} + g_{12}) \quad (3.5.15b)$$

$$f_4 - f_2 = (1 + \tau)(g_{41} - g_{21}) + \tau_1(g_{42} - g_{22}) \quad (3.5.15c)$$

$$\text{and } f_4 + f_2 = (1 + \tau)(g_{41} + g_{21}) + \tau_1(g_{42} + g_{22}) \quad (3.5.15d)$$

Using eq. (3.5.11), we write

$$g_{31} - g_{11} = h_{11} \quad (3.5.16a)$$

$$g_{32} - g_{12} = h_{12} \quad (3.5.16b)$$

$$g_{31} + g_{11} = h_{21} \quad (3.5.16c)$$

$$g_{32} + g_{12} = h_{22} \quad (3.5.16d)$$

$$g_{41} - g_{21} = h_{31} \quad (3.5.16e)$$

$$g_{42} - g_{22} = h_{32} \quad (3.5.16f)$$

$$g_{41} + g_{21} = h_{41} \quad (3.5.16g)$$

$$\text{and } g_{42} + g_{22} = h_{42} \quad (3.5.16h)$$

where,

$$h_{11} = 2R_a [X_k(1 - \cos \beta b) - Z_{op} \sin \beta b] \quad (3.5.17a)$$

$$h_{12} = -2R_a [X_k(1 + \cos \beta b) + Z_{op} \sin \beta b] \quad (3.5.17b)$$

$$h_{21} = -2Z_{op} X_k \quad (3.5.17c)$$

$$h_{22} = 2Z_{op} X_k \quad (3.5.17d)$$

$$h_{31} = 0 \quad (3.5.17e)$$

$$h_{32} = 0 \quad (3.5.17f)$$

$$h_{41} = 2R_a (X_k \sin \beta b - Z_{op} \cos \beta b) \quad (3.5.17g)$$

$$\text{and } h_{42} = h_{41} \quad (3.5.17h)$$

Thus eq. (3.5.15) becomes

$$f_{3-f_1} = (1 + \tau) h_{11} + h_{12} \tau_1 \quad (3.5.18a)$$

$$f_{3+f_1} = (1 + \tau) h_{21} + h_{22} \tau_1 \quad (3.5.18b)$$

$$f_{4-f_2} = 0 \quad (3.5.18c)$$

$$\text{and } f_{4+f_2} = (1 + \tau) h_{41} + h_{42} \tau_1 \quad (3.5.18d)$$

The eq. (3.5.14) then yields

$$f_7 = (1 + \tau) f_{71} + \tau_1 f_{72} \quad (3.5.19a)$$

$$\text{and } f_8 = (1 + \tau) f_{81} + \tau_1 f_{82} \quad (3.5.19b)$$

where

$$f_{71} = -2R_a [Z_{op} \sin \beta b - 2X_k (1 - \cos \beta b)] \quad (3.5.20a)$$

$$f_{72} = -2Z_{op} R_a \sin \beta b \quad (3.5.20b)$$

$$f_{81} = 2Z_{op} X_k \sin \beta b \quad (3.5.20c)$$

$$\text{and } f_{82} = -2Z_{op} X_k \sin \beta b \quad (3.5.20d)$$

Eq. (3.5.12) transforms to

$$X_1 = X_2 (1 + \tau) + X_3 \tau_1 \quad (3.5.21)$$

where,

$$X_1 = \beta^2 Z_{op} H_0 \quad (3.5.22a)$$

$$X_2 = j \left[\frac{f_{71} + j f_{81}}{f_5 + j f_6} - \beta b \right] \quad (3.5.22b)$$

and,

$$X_3 = j \frac{f_{72} + j f_{82}}{f_5 + j f_6} \quad (3.5.22c)$$

Another equation involving the unknowns τ and τ_1 can be obtained by using eq. (3.1.8) for TE_{11} mode. It can easily be shown from this equation that

$$\tau_1 = \frac{1}{j N_1} \int_0^b I(y') \cos \frac{\pi y'}{b} dy' \quad (3.5.23)$$

where,

$$N_1 = \frac{ab}{2\beta\eta} \sqrt{\left(\frac{\pi}{a}\right)^2 + \left(\frac{\pi}{b}\right)^2 - \beta^2} \quad (3.5.24)$$

Using eqs. (3.5.4b) and (3.5.9) in eq. (3.5.23), and manipulating, we finally arrive at

$$X_4 \tau_1 = X_5 (1+\tau) + X_6 \tau_1 \quad (3.5.25)$$

where,

$$X_4 = \beta^2 Z_{op} N_1 \quad (3.5.26a)$$

$$X_5 = - \frac{1}{1-\pi^2/\beta^2 b^2} \frac{f_{91}+j f_{101}}{f_5+j f_6} \quad (2.5.26b)$$

and,

$$X_6 = - \left[\frac{\beta b}{2} + \frac{1}{1-\pi^2/\beta^2 b^2} \frac{f_{92}+j f_{102}}{f_5+j f_6} \right] \quad (3.5.26c)$$

where f_5 and f_6 are given by eq. (3.1.32) and

$$f_{91} = 2Z_{op} R_a \sin \beta b \quad (3.5.27a)$$

$$f_{92} = 2R_a [Z_{op} \sin \beta b + 2X_k (1 + \cos \beta b)] \quad (3.5.27b)$$

$$f_{101} = 2Z_{op} X_k \sin \beta b \quad (3.5.27c)$$

and

$$f_{102} = -2Z_{op} X_k \sin \beta b \quad (3.5.27d)$$

Proper eliminations between the simultaneous eqs. (3.5.21) and (3.5.25) lead to

$$\tau = \frac{X_2 + \frac{X_3 X_5}{X_4 - X_6}}{X_1 - X_2 - \frac{X_3 X_5}{X_4 - X_6}} \quad (3.5.28)$$

and

$$\tau_1 = \frac{X_5(1 + \tau)}{X_4 - X_6} \quad (3.5.29)$$

The fundamental-mode transimission coefficient is given by

$$T = 1 + \tau = \frac{X_1}{X_1 - X_2 - \frac{X_3 X_5}{X_4 - X_6}} \quad (3.5.30)$$

One can, at least in theory, go on refining this solution to account for further higher-order waveguide modes. For example, if the effect of the TE_{21} mode (which is the next higher-order mode after TE_{11}) is to be incorporated, one will ultimately land up into three simultaneous equations involving τ , τ_1 and τ_2 (the reflection coefficient of TE_{21} mode) the solution of which will yield the information of interest. The procedure will obviously involve much more lengthy algebraic simplifications. In fact, the algebraic rigor involved will keep on increasing with the number of higher-order modes that one wishes to account for.

The analysis discussed above can also be extended to the air-gap case. The amount of algebraic manipulations involved in the analysis of the air-gap case will be much more as compared with that in the short-circuited case.

The disadvantage of the above reported analyses lies in the heavy amount of algebraic work involved. This disadvantage is, however, greatly offset by the fact that the end-product of these analyses is a closed-form solution. No summations of infinite series, as encountered in the formulations to be discussed in Chapter 4, are involved, thereby reducing the CPU time on the computer significantly.

3.5.1 Calculation of Resonant Length:

Although vigorous attempts to derive a closed-form condition of resonance were made, it soon became clear that the complicated structure of eq. (3.5.30) will not permit an easy and accurate explicit expression for the resonant length.

A standard NAG library subroutine (named EO4ABF) available at the I.I.T. Kanpur Computer Centre was used to locate the minimum of $|T|$ using eq. (3.5.30). The results obtained were accurate upto eighth decimal place.

3.5.2 Results and Discussion:

The closed-form solution described by eq. (3.5.30) was applied to the $r_p = 0.115$ mm case depicted in Fig. 3.11. The difference between the results given by eqs. (3.1.39) and (3.5.30) was seen to be generally negligible, the maximum departure (occurring at resonance) not being more than a few percent. As an illustration, the results for $f_0 = 10$ GHz are

presented in Fig. 3.17. An important point to be noted at this juncture is that, like eq. (3.1.39), the eq. (3.5.30) also does not predict the pass-band ripples, thus indicating that the neglect of higher-order modes in writing E_R is not the probable cause of pass-band ripples. This point will be further elaborated upon in the next chapter wherein a theoretical model incorporating effects of all the higher-order waveguide modes will be presented.

The values of the resonant length (for $r_p = 0.115$ mm) computed by the procedure outlined in subsection 3.5.1 and by eq. (3.1.56) are compared in Table 3.6, for nine different center frequencies. The experimental values are also given. It is seen that the method described in subsection 3.5.1 gives values that are on the higher side of those given by eq. (3.1.56). This point will also be elaborated upon in the next chapter.

Before concluding this section, some remarks on the relevance of the analysis reported herein are in order. We have seen earlier that, in order to bring the pass-band ripples down to an acceptable level, the use of an extremely thin probe is mandatory, in which case the analysis reported in Section 3.1 is sufficiently accurate. The analysis reported in this last section may thus not be required for most of the practical purposes. The academic importance of

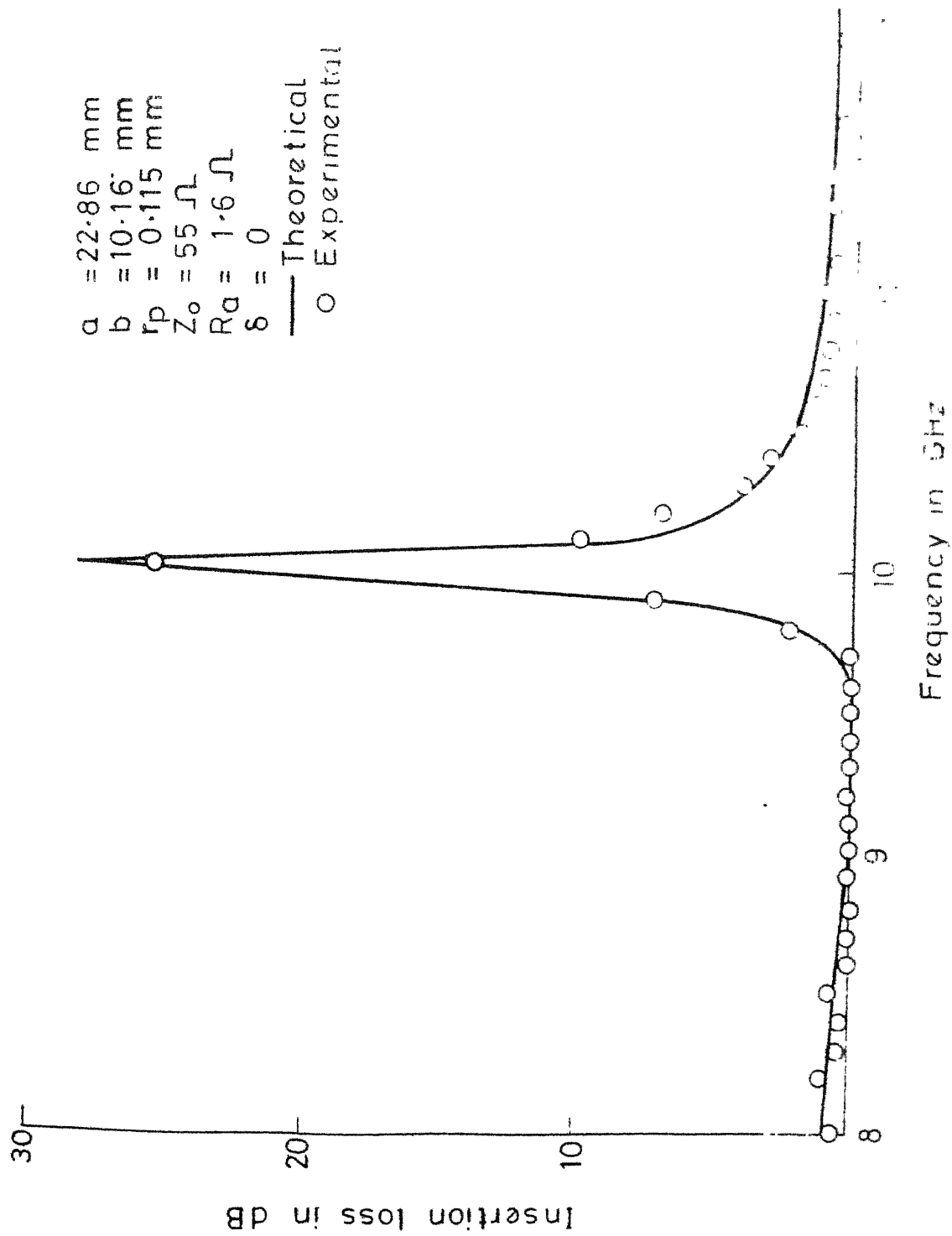


Fig-3-17 A Typical comparison between the results of the theoretical and experimental results

Table 3.6

Comparison between values of resonant length obtained with and without the first higher-order mode.

$a = 22.86$ mm, $b = 10.16$ mm, $r_p = 0.115$ mm, $Z_0 = 55.00$ ohms,
 $\delta = 0$

Frequency in GHz	Resonant length (in mm)		Experimental
	Theoretical		
	With first higher- order mode (subsection 3.5.1)	Without first higher-order mode (eq. 3.1.56)	
8.00	9.32	9.19	9.20
8.50	8.64	8.51	8.50
9.00	8.04	7.88	7.90
9.50	7.49	7.32	7.30
10.00	6.98	6.79	6.80
10.50	6.51	6.30	6.20
11.00	6.06	5.81	5.70
11.50	5.62	5.33	5.20
12.00	5.17	4.84	4.70

this analysis can, however, not be denied as this analysis helps in i) confirming that the higher-order waveguide modes excited around the probe are not the cause of pass-band ripples and ii) establishing a procedure whereby closed-form solution incorporating effects of as many higher-order modes as one likes can be obtained, provided one is willing to undertake the extensive amount of algebraic effort involved.

3.6 CONCLUSIONS:

i) The broad-wall Rectangular Waveguide-Tunable Coaxial Line Junction has been investigated from the viewpoint of its application to microwave filtering, an aspect which has hitherto not been looked into. Two types of cases, namely the short-circuited and air-gap cases, are analysed.

ii) The above mentioned configurations exhibit a sharp mechanically tunable transmission minimum between the waveguide ports. They will thus find application as new types of prototypes for developing waveguide notch filters with large continuous mechanical tunability.

iii) The configurations considered require use of an extremely thin (electrically) probe, so as to minimise the amount of physical perturbation within the waveguide, and thereby reduce the pass-band ripples to a practically acceptable level. At X-band, this leads to requiring a mechanically

weak probe which has to be kept in position through external means. At C and S bands, however, an electrically thin probe will have sufficient mechanical strength also. Thus the configurations suggested will be especially useful for S and C bands.

iv) For lack of facilities to test waveguide components at S and C bands, no experimentation could be taken up at these bands. The various results reported are only at X-band, for which an accurate measurement setup was available.

v) The configurations suggested are simple and easy to fabricate. Their filtering characteristics compare well with those of a corresponding YIG-tuned single-stage section (for detailed information on the YIG-tuned sections, see, e.g., [217], [276]-[278]).

vi) The analyses reported yield closed-form expressions for the transmission coefficient between the waveguide ports. For practical cases, these expressions are sufficiently accurate and can be used to predict the filtering response of the single-stage sections.

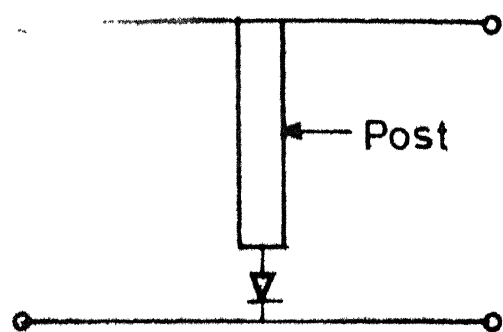
vii) The various resonance conditions obtained in this chapter will serve as a check point for the more general formulation to be presented in the next chapter.

CHAPTER 4

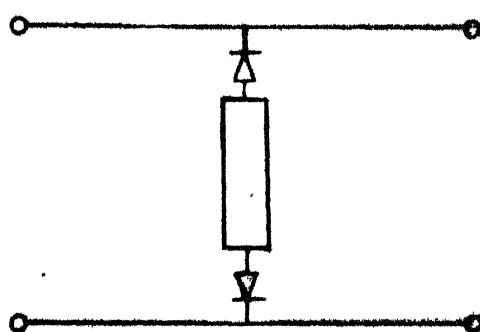
JUNCTION OF RECTANGULAR WAVEGUIDE AND TUNABLE COAXIAL LINE - APPLICATION TO EXPERIMENTAL CHARACTERIZATION OF WAVEGUIDE MOUNTS

The most widely known method of mounting the active devices across a rectangular waveguide is the use of E-plane cylindrical metallic posts. Such structures, besides providing an easy means of supporting the devices physically, make the biasing of the devices quite easy. Various commonly employed configurations of this type are shown in Fig. 4.1. The accurate characterization (both theoretical and experimental) of these configurations is a very important aspect of present-day microwave engineering. Such a characterization helps in the analysis/synthesis of waveguide amplifiers, oscillators, mixers, detectors, filters, etc., where mounting structures of this type are frequently encountered.

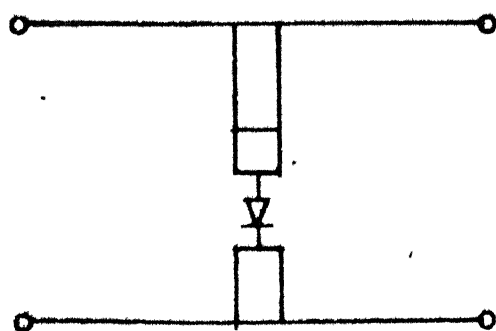
The theoretical characterization of waveguide mounts has been an active subject of study, particularly in the period starting from late sixties till date (see, e.g. [13], [102]-[123]). A corresponding amount of attention has, however, not been paid to evolving new simple methods of experimental characterization of these structures. Most of the reported experimental results are based on either of the following two approaches:



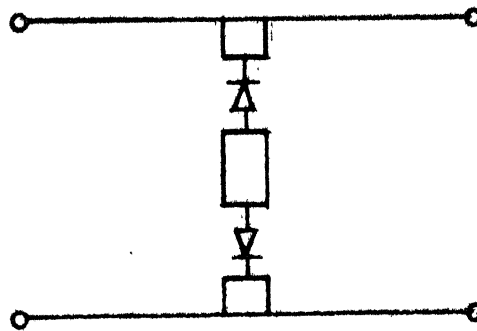
(a) Post loaded at one end



(b) Post loaded at both ends



(c) Single-gap arrangement



(d) Two-gap arrangement

Fig. 4.1 Some typical waveguide mounting structures employing E-plane metallic posts

- i) To treat the mount as a waveguide obstacle and to measure its scattering parameters by any of the well-established techniques of characterizing two-port waveguide components.
- ii) To measure the terminal impedance^{*} of the mount by using special techniques, such as the use of sub-miniature coaxial cables, which enable one to isolate the terminals of interest electrically from the rest of the system.

In the first category lie results reported by Marcuvitz [5], El-Sayed [110], [114], Bauer and Penfield [279], Joshi and Cornick [115], [116], Hangstrom and Kollberg [121], etc. In the second category, one can mention results reported by authors like Eisenhart and Khan [105], Hicks and Khan [123], Shetty and Rao [271], Williamson [122], etc.

The objective of this chapter is to exploit the Rectangular Waveguide - Tunable Coaxial Line Junction, which was considered in Chapter 3 from the viewpoint of its applicability to microwave filtering, for the experimental characterization of waveguide mounts. Lewin's formulation [13]

* Terminal impedance is defined as the impedance offered by the mount across the terminals of the device.

for loaded metallic posts in a rectangular waveguide has been extended to the configuration under consideration. The analysis reveals that the positions of the movable short for minimum and maximum transmission between the waveguide ports can be correlated to the parameters of the post by means of simple explicit equations. Consequently, a very simple method of experimental determination of the post parameters emerges. In comparison with the methods based on approaches mentioned above, the present method is superior in the following respects:

- i) No electrical measurements are needed; thus the errors encountered in electrical measurements, e.g. unwanted reflections at various junctions, poor sensitivity of the instruments, etc., are completely eliminated.
- ii) An explicit measurement of the unknown post parameters is possible.
- iii) The configuration used is simple and easy to implement.
- iv) The working equations are quite simple, thus obviating the need of graphical/semigraphical/computer-aided analysis of the measured data.

Although the method is applied only to the singly-loaded posts, it can easily be extended to doubly-loaded

posts, as shown in Section 4.3. The method can also be extended to measure the parameters involved in the equivalent circuit for the input impedance seen by the coaxial line in a broad-wall coaxial-waveguide junction, as discussed in Section 4.4.

4.1 ANALYSIS OF THE RECTANGULAR WAVEGUIDE - TUNABLE COAXIAL LINE JUNCTION BY USING LEWIN'S FORMULATION

The E-plane cylindrical metallic post in a rectangular waveguide, terminated at one end into an active device, is shown in Fig. 4.2a. If we assume the device dimensions to be small (which is true for most of the practical cases), the device can be simulated by a lumped load Z_1 (generally non-linear) at the end of the post, as shown in Fig. 4.2b.

The configuration shown in Fig. 4.2b was analysed by Lewin [13]. He showed that the singly-loaded E-plane post in a rectangular waveguide can be represented by means of an impedance Z across the guide. The value of this impedance is given by

$$Z = jX_0 Z_g + \frac{\operatorname{cosec}^2 \frac{\pi D}{a}}{\frac{1}{Z_1} - \sum_{n=1}^{\infty} \frac{1}{jX_n}} \quad (4.1.1)$$

where the normalised first-order post reactance is

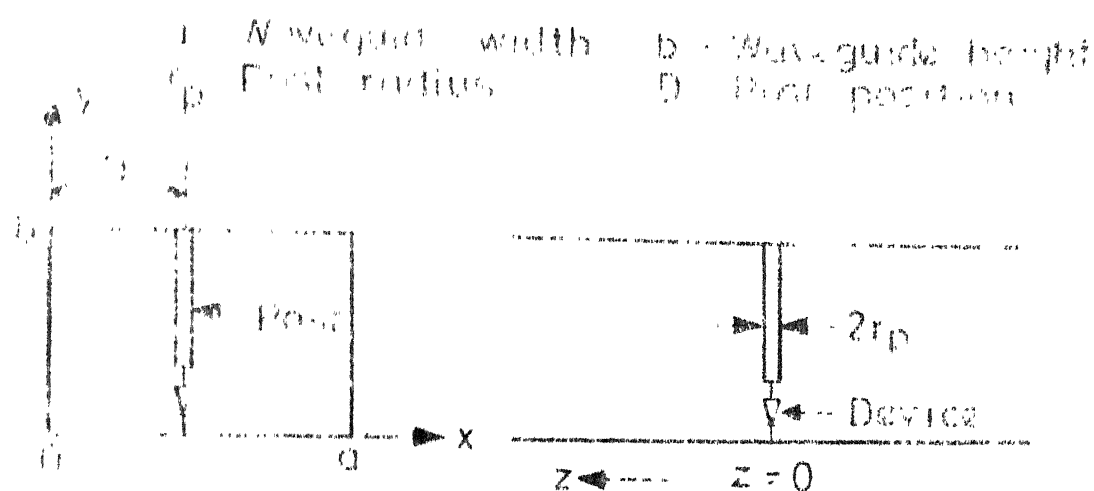


Fig. 4-2a F-plane post in a rectangular waveguide
 (One end terminated into an active device)

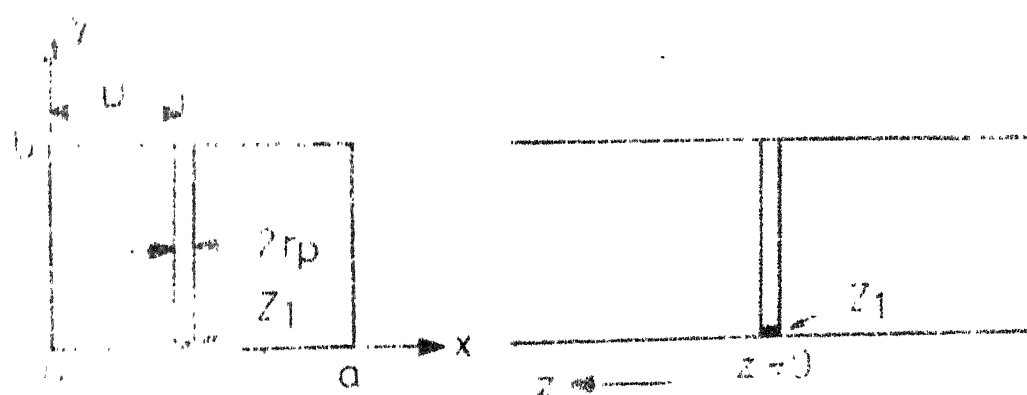


Fig. 4-2b Electromagnetic equivalence of Fig. 4-2a
 (For small device dimensions)

$$\begin{aligned}
X_0 = & (a/2 \lambda_g) \operatorname{cosec}^2(\pi D/a) [\ln \sin(\pi D/a) - \ln \sin(\pi r_p/2a) \\
& + \cos(2\pi D/a) - \cos(\pi r_p/a) + \sum_{m=2}^{\infty} \{ (m^2 - \beta^2 a^2 / \pi^2)^{-1/2} - 1/m \} \\
& \{ \cos(m\pi r_p/a) - \cos(2m\pi D/a) \}] \quad (4.1.2)
\end{aligned}$$

which, for $r_p \rightarrow 0$, simplifies to

$$\begin{aligned}
X_0 = & (a/2 \lambda_g) \operatorname{cosec}^2(\pi D/a) [\ln \{ (2a/\pi r_p) \sin(\pi D/a) \} - 2 \sin^2(\pi D/a) \\
& + 2 \sum_{m=2}^{\infty} \sin^2(m\pi D/a) \{ (m^2 - \beta^2 a^2 / \pi^2)^{-1/2} - 1/m \}] \quad (4.1.3)
\end{aligned}$$

In eqs. (4.1.2) and (4.1.3), the dimensions a, b, r_p and D are as defined in Fig. 4.2. The other parameters are

$$i) \text{ Free-space propagation constant } \beta = 2\pi/\lambda \quad (4.1.4)$$

where λ is the free-space wavelength involved.

$$ii) \text{ Guided wavelength } \lambda_g = \lambda / \sqrt{[1 - (a/2a)^2]} \quad (4.1.5)$$

$$iii) \text{ Guide impedance } Z_g = 2\eta(b/a)(\lambda_g/\lambda) \quad (4.1.6)$$

where $\eta = 120\pi$ approximately.

The parameter X_n in eq. (4.1.1) is a non-normalised reactance defined by Lewin in his formulation of the problem. Lewin has worked out the following expression for $\Sigma(1/X_n)$:

$$\sum_{n=1}^{\infty} \frac{1}{X_n} = \frac{1}{\omega C_{\text{gap}}} + \frac{4\pi\beta}{\eta b} \left[\sum_{n=1}^M \frac{r_p K_1(r_p \gamma_n)}{\gamma_n \{ K_0(r_p \gamma_n) - K_n(r_p \gamma_n) \}} \right] \quad (4.1.7)$$

where,

$$M = \frac{b}{2\pi r_p} \quad (4.1.8)$$

$$\tau_n = \sqrt{(n^2\pi^2/b^2 - \beta^2)} \quad (4.1.9)$$

$$\text{and } \omega = 2\pi f \quad (4.1.10)$$

f being the frequency involved. C_{gap} is the capacitance contributed by the small gap that exists between the tip of the post and bottom inner face of the waveguide.

The small correction term in eq. (4.1.7) is given as

$$S' = \sum_{n=M+1}^{\infty} \left[\frac{r_p K_1(r_p \tau_n)}{\tau_n \{K_0(r_p \tau_n) - K_0(2D \tau_n)\}} - \frac{r_p b}{\pi n} \right] \quad (4.1.11)$$

$K_n(x)$ in eqs. (4.1.7) and (4.1.11) represents the modified Bessel function of second kind, of order n and having an argument x .

Now, the Rectangular Waveguide - Tunable Coaxial Line Junction (Fig. 4.3a) can, for the purposes of analysis, be replaced by a singly-loaded post (Fig. 4.3b), provided that the load Z_1 is interpreted as the reactance of the tunable coaxial line. That is

$$Z_1 = jX_k = jZ_0 \tan \beta l_r \quad (4.1.12)$$

where Z_0 is the characteristic impedance of the coaxial line

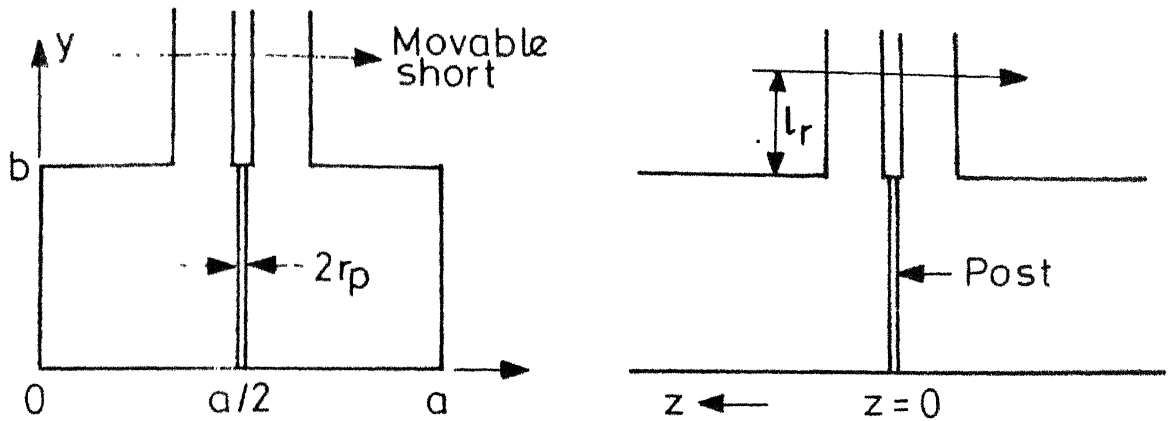


Fig. 4-3a Rectangular waveguide-Tunable coaxial line junction

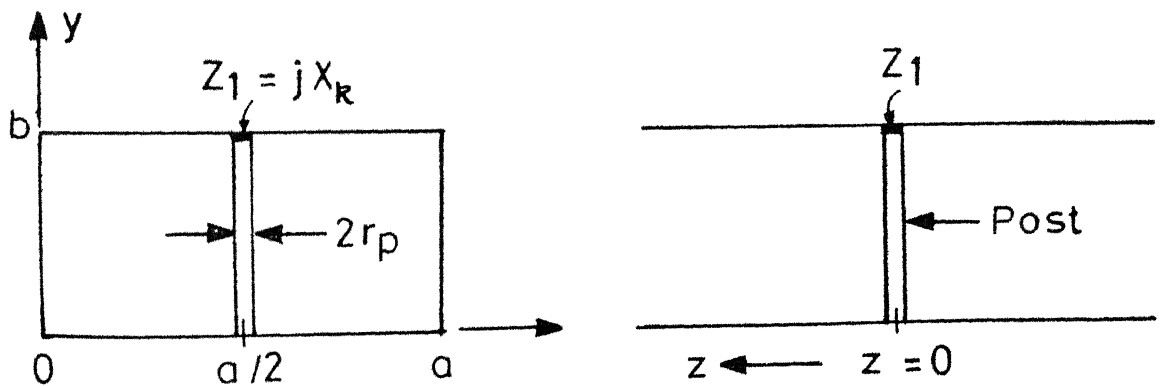


Fig. 4-3b Electromagnetic equivalence of Fig. 4-3a

(given by eqn.(3.1.23)) and l_r is the position of the movable short, or the 'resonant length'.

It can easily be seen that the configuration shown in Fig. 4.3b is electromagnetically identical to that shown in Fig. 4.2b, with, of course, $D=a/2$ and Z_1 as given by eq. (4.1.12). Thus, the lumped-circuit equivalence of the junction shown in Fig. 4.3a will consist of an impedance Z across the guide, as shown in Fig. 4.4. The value of Z can be written as

$$Z = jX_o Z_g + \frac{1}{G_a + j \sum_{n=1}^{\infty} \frac{1}{X_n} - \frac{j}{X_k}} \quad (4.1.13)$$

where a loss conductance G_a has been introduced to empirically take care of the system losses.

The fundamental mode reflection coefficient can then be calculated using the well-known relation

$$\tau = - \frac{Z_g}{Z_g + 2Z} \quad (4.1.14)$$

The fundamental mode transmission coefficient is

$$T = \frac{2Z}{Z_g + 2Z} \quad (4.1.15)$$

The transmission will be minimum when

$$\frac{1}{X_k} = \sum_{n=1}^{\infty} \frac{1}{X_n} - \frac{1}{X_o Z_g} \quad (4.1.16)$$

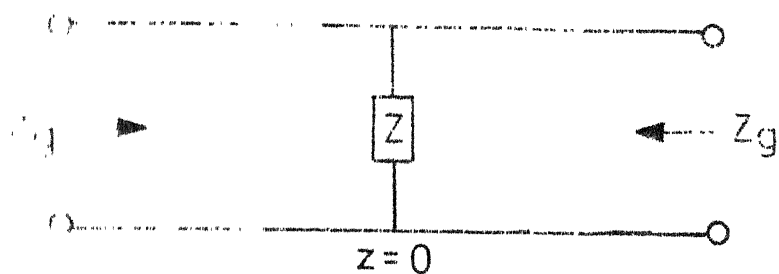


Fig. 4.4 Lumped-circuit equivalence

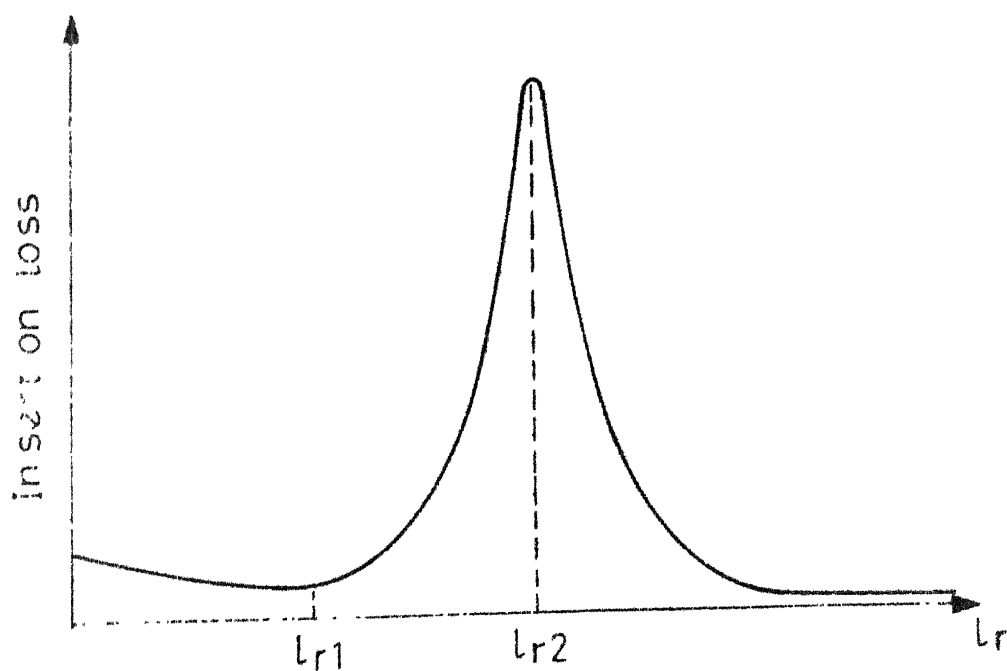


Fig. 4.7 Variation of insertion loss with the resonant length

The peak insertion loss is given by

$$IL_{\max} = 20 \log X \quad (4.1.17)$$

where,

$$X = \frac{\sqrt{[(Z_g + 2X_o^2 Z_g^2 G_a)^2 + (X_o Z_g^2 G_a)^2]}}{2X_o^2 Z_g^2 G_a} \quad (4.1.18)$$

At this juncture, it is worthwhile to make a comparison between the resonance condition given by eq. (4.1.16) and those given in Chapter 3. The values of resonant length calculated using eq. (3.1.56), those using the procedure outlined in subsection 3.5.1 (i.e. inclusion of the first higher-order mode in the calculation) and those calculated by eq. (4.1.46) are compared, for $r_p = 0.115$ mm, 0.435 mm, 0.635 mm and 0.800 mm, in Tables 4.1, 4.2, 4.3 and 4.4, respectively. The experimental values are also given. The following conclusions can be drawn from these tables:

- i) For $r_p = 0.115$ mm, eq. (3.1.56) is quite a good approximation of eq. (4.1.46). For higher values of r_p , however, the difference between the values given by these equations becomes larger.
- ii) The approach outlined in subsection 3.5.1 yields values that are on the higher side of those given by eq. (3.1.56).

Table 4.1: Comparison between resonance condition given by eq. (4.1.16) and those given in Chapter 3 ($r_p = 0.115 \text{ mm}$)

$a=22.86 \text{ mm}$, $b=10.16 \text{ mm}$, $D_2=10.00 \text{ mm}$, $D_1=4.00 \text{ mm}$,

$Z_0 = 55.00 \text{ ohms}$

Maximum uncertainty in the measurement of length = $\pm 0.10 \text{ mm}$

Frequency in GHz	Resonant length (in mm)			Experimental
	Theoretical		using eq.(4.1.16)	
	Using eq.(3.1.56)	Using procedure outlined in subsection 3.5.1		
8.00	9.1918138	9.3211797	9.1729944	9.20
8.50	8.5055587	8.6467741	8.4544353	8.50
9.00	7.8866967	8.0405968	7.8119451	7.90
19.50	7.3206272	7.4908025	7.2301398	7.30
10.00	6.7946093	6.9840761	6.6960248	6.80
10.50	6.2967136	6.5116618	6.1979732	6.20
11.00	5.8148061	6.0585316	5.7247242	5.70
11.50	5.3346031	5.6183808	5.2641683	5.20
12.00	4.8384864	5.1726022	4.8015304	4.70

Table 4.2: Comparison between resonance condition given by eq. (4.1.16) and those given in Chapter 3 ($r_p=0.435$ mm)

$a=22.86$ mm, $b=10.16$ mm, $D_2=10.00$ mm, $D_1=3.95$ mm, $Z_0=55.73$ ohms
Maximum uncertainty in the measurement of length = ± 0.05 mm

Frequency in GHz	Resonant length (in mm)		
	Theoretical		Experimental
	Using eq.(3.1.56)	Using procedure outlined in subsection 3.5.1	
8.00	9.0952087	9.3673745	9.53
8.50	8.3366880	8.6330554	8.71
9.00	7.6482022	7.9722631	7.95
9.50	7.0130893	7.3706248	7.25
10.00	6.4167736	6.8140180	6.62
10.50	5.8457020	6.2910201	6.01
11.00	5.2863731	5.7874946	5.49
11.50	4.7243893	5.2929211	4.92
12.00	4.1435806	4.7905491	4.38

Table 4.3: Comparison between resonance condition given by eq. (4.1.16) and those given in Chapter 3($r_p=0.635$ mm)
 $a=22.86$ mm, $b=10.16$ mm, $D_2=10.00$ mm, $D_1=3.95$ mm, $Z_0=55.73$ ohms
Maximum uncertainty in the measurement of length = ± 0.05 mm

Frequency in GHz	Resonant length (in mm)		
	Theoretical		Experimental
	Using eq.(3.1.56)	Using procedure outlined in subsection 3.5.1	
8.00	9.0480683	9.4033705	9.97
8.50	8.2540485	8.6412062	9.03
9.00	7.5313441	7.9565848	8.20
9.50	6.8625363	7.3311727	7.41
10.00	6.2325276	6.7508829	6.72
10.50	5.6275664	6.2050344	6.11
11.00	5.0344919	5.6805603	5.48
11.50	4.4402199	5.1634939	4.91
12.00	3.8316511	4.6380034	4.33

Table 4.4: Comparison between resonance condition given by eq. (4.1.16) and those given in Chapter 3 ($r_p = 0.800$ mm)

$a=22.86$ mm, $b=10.16$ mm, $D_2=10.00$ mm, $D_1=3.95$ mm, $Z_0=55.732$ Ohms
Maximum uncertainty in the measurement of lengths = ± 0.05 mm

Frequency in GHz	Resonant length (in mm)		
	Theoretical		Experimental
	Using eq.(3.1.56)	Using procedure outlined in subsection 3.5.1	
8.00	9.0105870	9.4382130	10.39
8.50	8.1882609	8.6539900	9.27
9.00	7.4383137	7.9492529	8.51
9.50	6.7428710	7.3055103	7.61
10.00	6.0866329	6.7086221	6.89
10.50	5.4560038	6.1453561	6.16
11.00	4.8385412	5.6033006	5.51
11.50	4.2227814	5.0709842	4.91
12.00	3.5986218	4.5308799	4.28

- iii) The difference between the values given by the approach of subsection 3.5.1 and those by eq. (4.1.16) changes sign at a frequency which depends on the radius of the post. For example, for $r_p = 0.800$ mm, the value of this frequency is somewhere between 10.50 and 11.00 GHz, whereas, for $r_p = 0.115$ mm, this frequency shifts to a value below 8.00 GHz.
- iv) Of all the theoretical values, those given by eq. (4.1.16) show the best agreement with the experimental results, although, for $r_p = 0.115$ mm, eq. (3.1.56) is also quite accurate.

Two typical comparisons between the loss characteristic calculated by using eq. (4.1.15) and the experimental values are shown in Figs. 4.5 and 4.6. The agreement between theory and experiment is better for $r_p = 0.115$ mm than for $r_p = 0.435$ mm. The theory, which tacitly includes the effects of all higher-order waveguide modes, does not predict the pass-band ripples that are actually observed. This substantiates the trend observed in subsection 3.5.2 of Chapter 3 that the excitation of higher-order waveguide modes in the vicinity of the post is not the cause of pass-band ripples. The inability of the various theories to predict the pass-band ripples seems to be due to the assumption of a constant G_a (or a constant R_a , as in Chapter 3) throughout

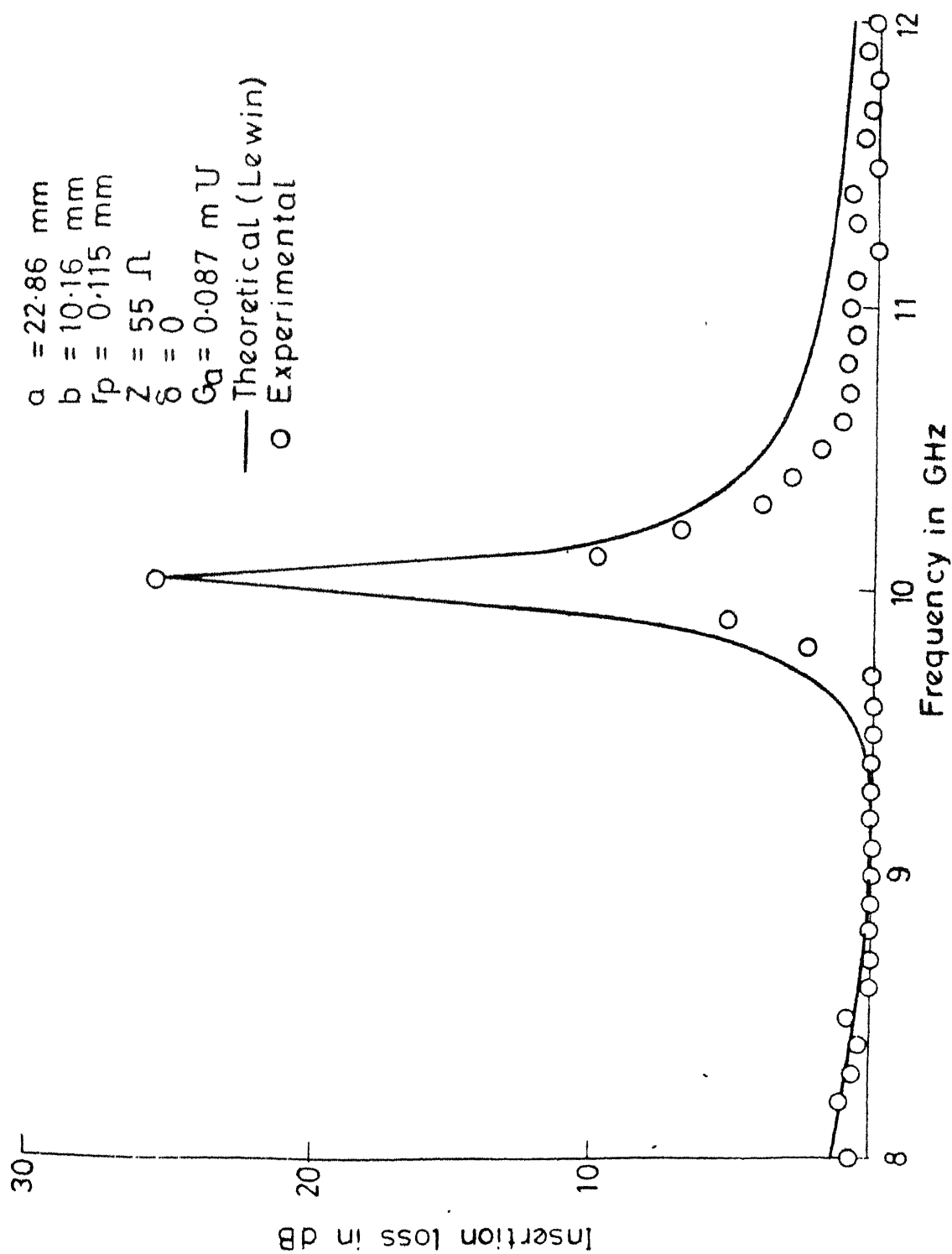


Fig. 4.5 Theoretical (Lewin) and experimental attenuation characteristic for $f_0 = 10 \text{ GHz}$ and $r_p = 0.115 \text{ mm}$

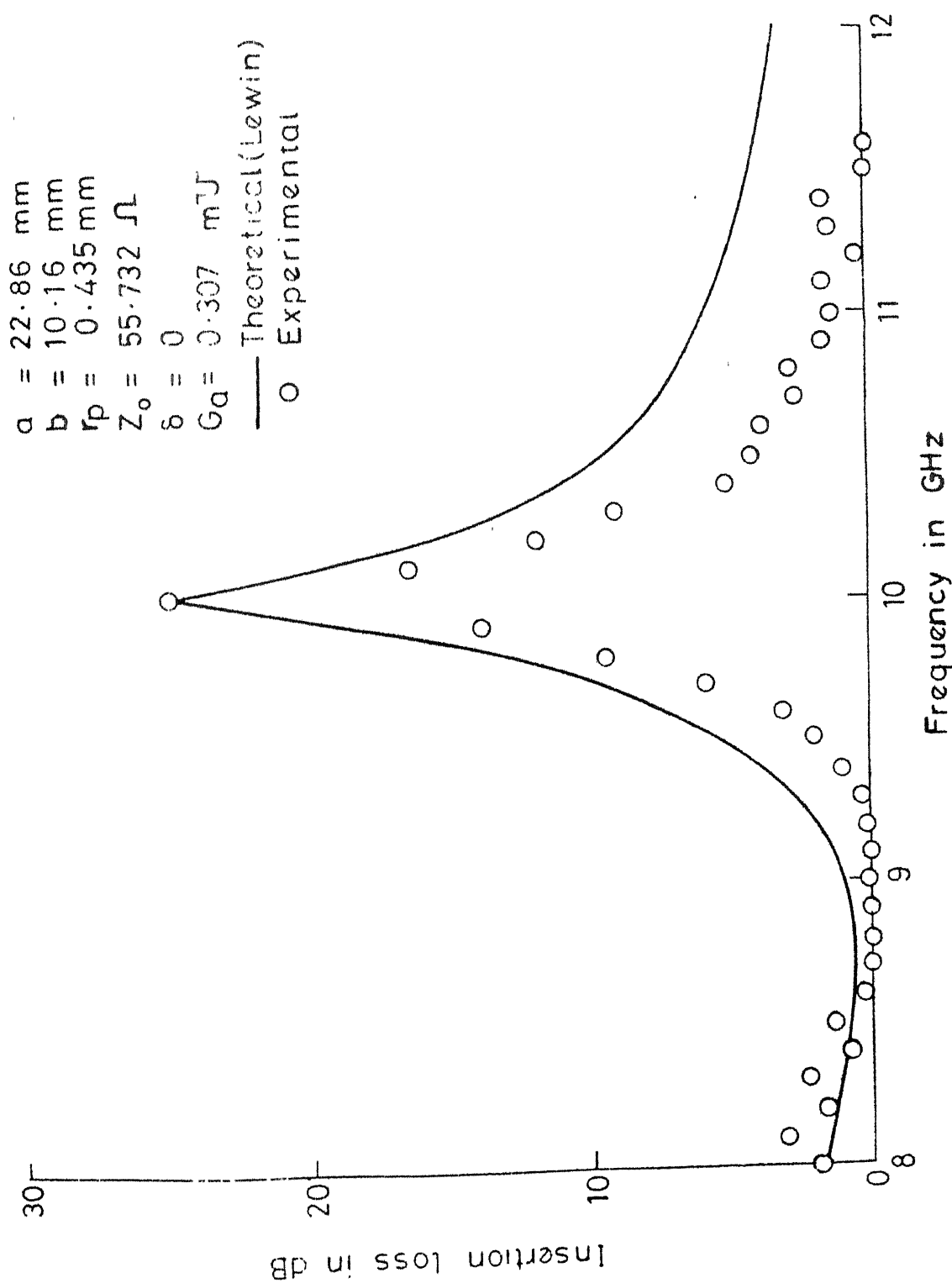


Fig. 4.6 Theoretical (Lewin) and experimental attenuation characteristic for $f_o = 10 \text{ GHz}$ and $r_p = 0.435 \text{ mm}$

the band. It may, however, be re-emphasised that a viable filtering application of the resonant contour will, in any case, require the use of an extremely thin (electrically) post for which the assumption of a constant loss parameter is reasonably accurate. Moreover, the theory is quite accurate in predicting the experimental values of resonant length (see Tables 4.1, 4.2, 4.3, and 4.4), which is natural because the resonance conditions can be expected to be independent of the system losses.

Before concluding this section, it is worth while to have an idea about the computer time required in the calculation of the resonant contour by means of the various theories developed so far. A typical comparison is given in Table 4.5. It is clear that the calculation based on the present formulation is much more time consuming than the ones based on the models presented in Chapter 3. This constitutes a major advantage of the formulations presented in Chapter 3 over the present formulation. The advantage of the present formulation, on the other hand, is the fact that all higher-order waveguide modes are easily accounted for, which thereby facilitates an accurate prediction of the resonant lengths, as seen in Tables 4.1 through 4.4.

Table 4.5

Comparison of CPU time⁺ required to calculate a full-band resonant contour by the various theoretical models.

$a=22.86$ mm, $b = 10.16$ mm, $Z_0 = 55.73$ ohms, $f_0 = 10$ GHz

Radius of the post, r_p (in mm)	CPU time (in seconds)		
	Using eq. (3.1.39)	Using eq. (3.5.30)	Using eq. (4.1.15)
0.115	0.53	0.59	101.59
0.435	0.53	0.58	31.01
0.635	0.52	0.59	10.02
0.800	0.51	0.59	20.60

⁺All values of the CPU time are given as observed on the DEC-1090 system. For computing the Bessel functions involved while using eq. (4.1.15), standard NAG sub-routines were used.

4.2 EXPERIMENTAL CHARACTERIZATION OF SINGLY-LOADED POSTS IN A RECTANGULAR WAVEGUIDE

As we have already seen, a singly-loaded metallic post in a rectangular waveguide can be represented by means of an impedance Z across the guide. The value of Z , as given by eq. (4.1.1), is a function of the load Z_1 and of the two post parameters, X_0 and $\Sigma(1/X_n)$. In a given situation, Z_1 will be known and the designer will be interested in knowing X_0 and $\Sigma(1/X_n)$.

The post parameters need to be calculated on a computer by using eqs. (4.1.2)-(4.1.11) as no method of experimental determination of these parameters is till date available. The aim of the present section is to exploit the Rectangular Waveguide-Tunable Coaxial Line Junction of Fig. 4.3a for the experimental evaluation of X_0 and $\Sigma(1/X_n)$. The formulation presented in Section 4.1 is used.

The typical variation of the insertion loss between the waveguide ports of the junction under consideration with the position of the movable short is shown qualitatively in Fig. 4.7. The loss will be minimum when

$$\frac{1}{X_k} = \sum_{n=1}^{\infty} \frac{1}{X_n} \quad (4.2.1)$$

and will be maximum when

$$\frac{1}{X_k} = \sum_{n=1}^{\infty} \frac{1}{X_n} - \frac{1}{X_0 Z_g} \quad (4.2.2)$$

At a given frequency f , let us say that $l_r = l_{r1}$ for minimum loss and $l_r = l_{r2}$ for maximum loss. Then, in view of eqs. (4.1.12), (4.2.1) and (4.2.2), one can write

$$X_0 = \frac{Z_o/Z_g}{\cot \beta l_{r1} - \cot \beta l_{r2}} \quad (4.2.3)$$

and,

$$\sum \frac{1}{X_n} = \frac{\cot \beta l_{r1}}{Z_o} \quad (4.2.4)$$

Thus, to measure X_0 and $\sum(1/X_n)$ at a given frequency, one has to measure l_{r1} and l_{r2} , and then use eqs. (4.2.3) and (4.2.4).

4.2.1 Measurement Errors:

The main source of error in the measurement is the accuracy with which l_{r1} and l_{r2} can be measured. If Δ is the maximum expected error in the measurement of lengths, the corresponding maximum expected errors in X_0 and $\sum(1/X_n)$ are given by

$$|\Delta X_0| = \frac{\beta Z_o}{Z_g} \frac{\operatorname{cosec}^2 \beta l_{r1} + \operatorname{cosec}^2 \beta l_{r2}}{(\cot \beta l_{r1} - \cot \beta l_{r2})^2} |\Delta| \quad (4.2.5)$$

$$\text{and } |\Delta(\sum \frac{1}{X_n})| = \frac{\beta \operatorname{cosec}^2 \beta l_{r1}}{Z_o} |\Delta| \quad (4.2.6)$$

The effects of varying f, r_p and Z_0 on the percentage errors in X_0 and $\Sigma(1/X_n)$ are depicted graphically in Figs. 4.8, 4.9 and 4.10, respectively. The following conclusions can be drawn from these figures:

- i) The error in $\Sigma(1/X_n)$ is not very sensitive to changes in frequency, whereas the error in X_0 increases monotonously with frequency.
- ii) The errors decrease with increasing diameter of the post. In comparison with the error in $\Sigma(1/X_n)$, the error in X_0 is much more sensitive to changes in the diameter of the post.
- iii) The errors can be minimised through using a coaxial line of the highest feasible characteristic impedance. It should, however, be kept in mind that the characteristic impedance of the coaxial line can not be made arbitrarily high because of practical reasons such as the propagation of higher-order modes in the coaxial line, the constraints on the physical size of the line, etc.
- iv) The error in X_0 is always much higher than that in $\Sigma(1/X_n)$.

4.2.2 Results and Discussion:

The method proposed above was applied, at X-band, to posts having $r_p = 0.435$ mm, 0.635 mm, and 0.800 mm. Keeping

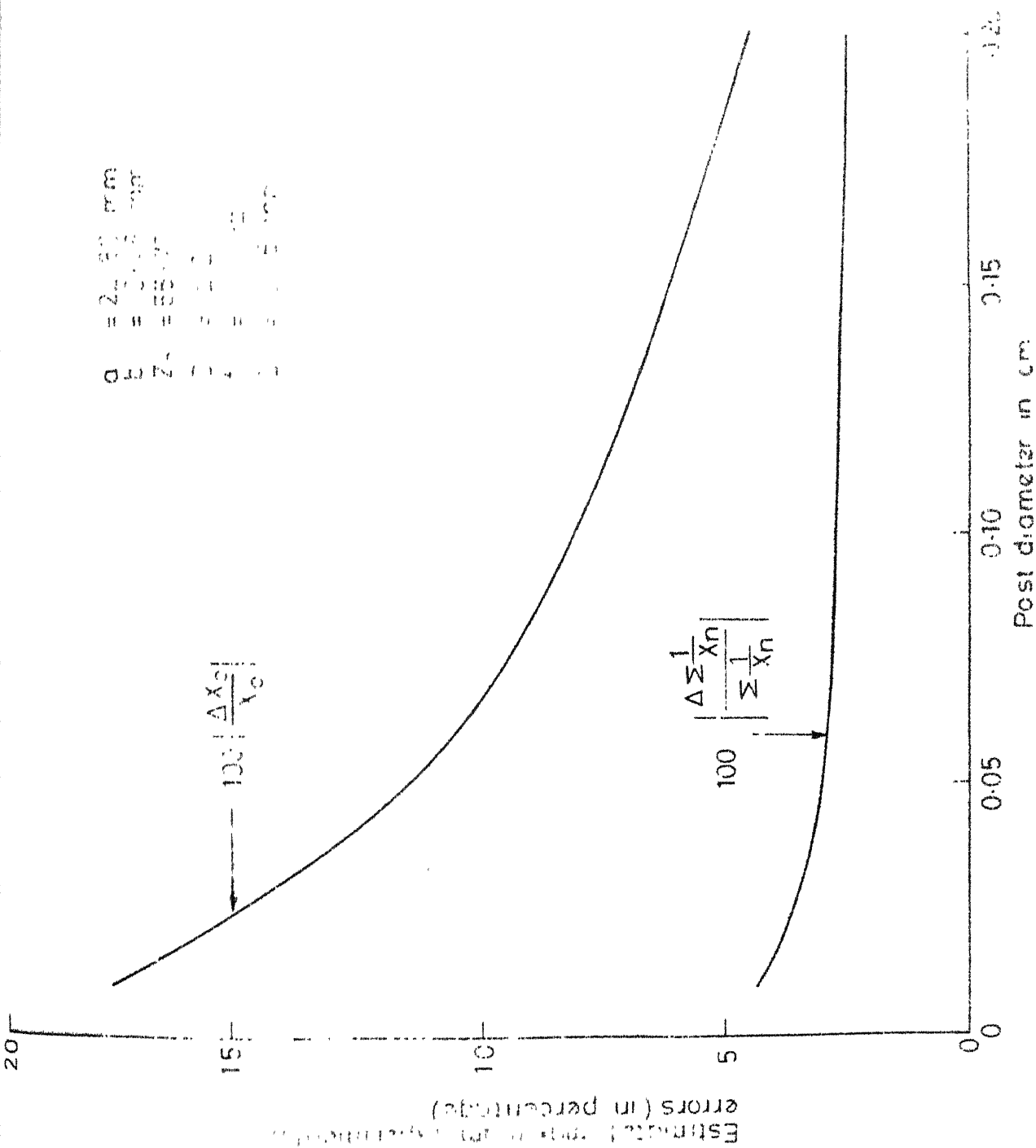


Fig.4.9 Variation of percentage errors with post diameter

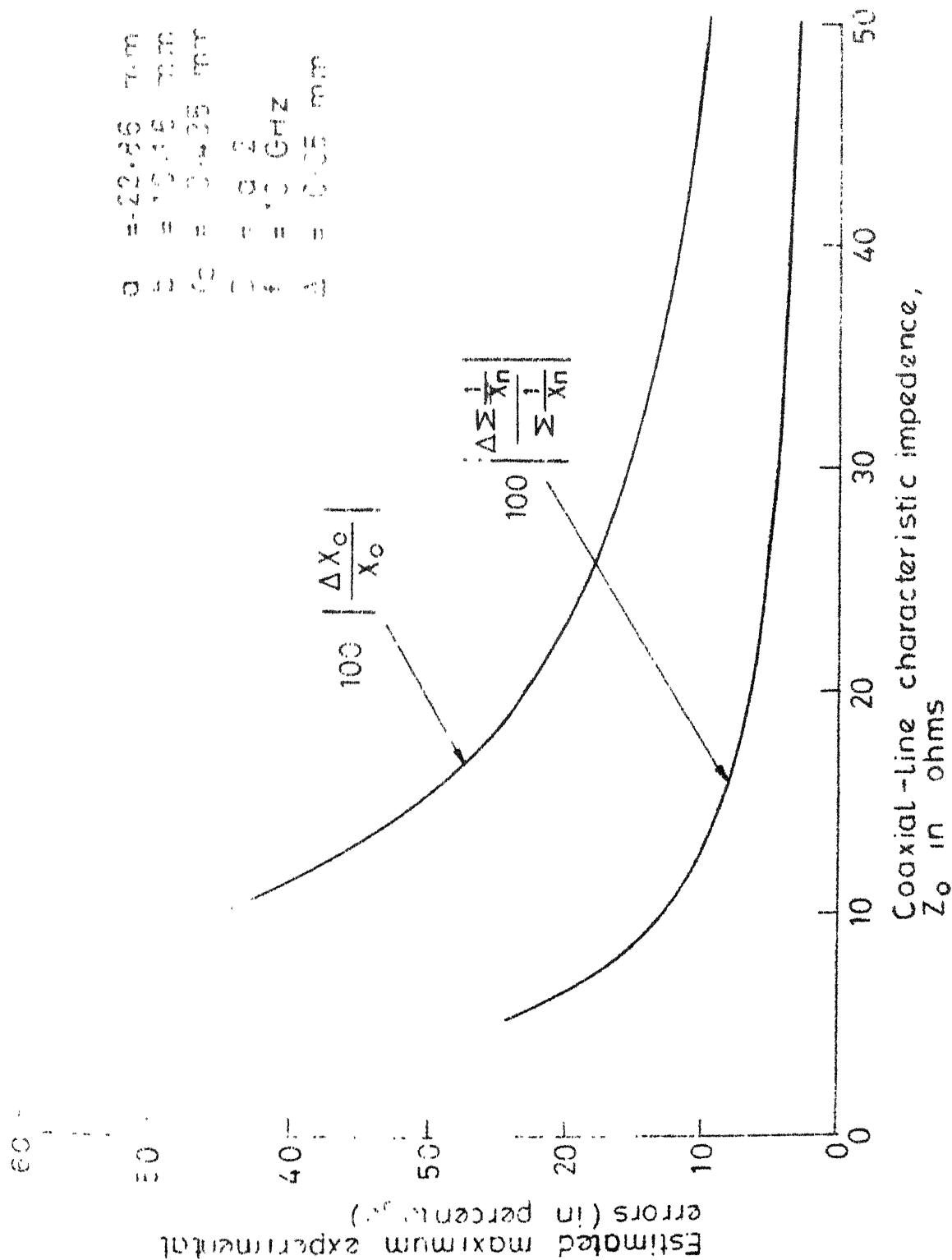


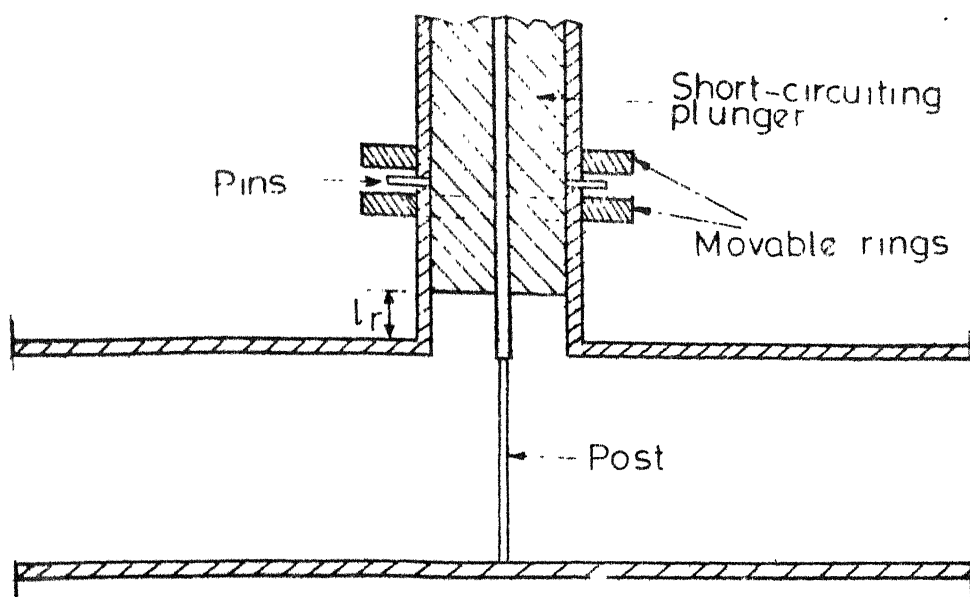
Fig. 4-10 Variation of percentage errors with the characteristic impedance of the coaxial-line

in view the conclusions drawn from Fig. 4.10, a coaxial line with internal diameter equal to 3.95 mm and external diameter equal to 10.00 mm (i.e. $Z_0 = 55.73$ ohms) was used. An accurate measurement of the resonant lengths was made possible by using the configuration shown in Fig. 4.11. In this configuration, the movement of the short-circuiting plunger is finely controlled by means of two rotatable rings between which the plunger is held in position with the help of two metallic pins. By employing a standard precision vernier, the maximum uncertainty in the measurement of lengths was limited to ± 0.05 mm.

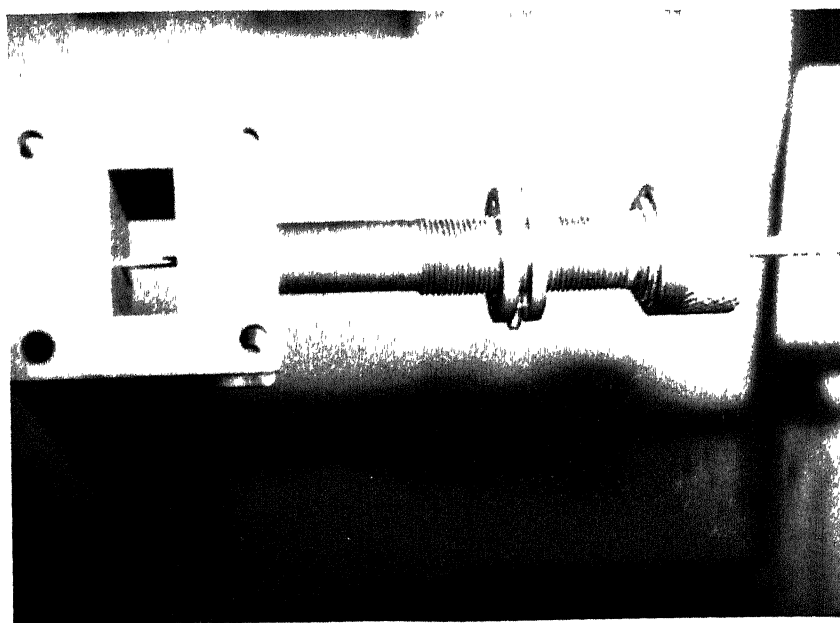
The experimentally measured values of l_{r1} and l_{r2} are given in Table 4.6. The theoretical and experimental values of X_0 and $\Sigma(1/X_n)$ are compared in Figs. 4.12 and 4.13, respectively. The agreement between theory and experiment is clearly very good.

4.3 EXPERIMENTAL CHARACTERIZATION OF DOUBLY-LOADED POSTS IN A RECTANGULAR WAVEGUIDE: A DISCUSSION

The configuration of the doubly-loaded post is shown in Fig. 4.14. The equivalent circuit of this configuration, as worked out by Lowin [13], is given in Fig. 4.15. The parameters X_0 and Z_g in the equivalent circuit are given by eqs. (4.1.2) and (4.1.6), respectively. The other parameters are



(a) Schematic diagram



(b) Photograph

Fig. 4.11 Configuration used for fine measurement of resonant lengths

Table 4.6: Experimental Values of l_{r1} and l_{r2}

$a = 22.86$ mm, $b = 10.16$ mm, $Z_o = 55.73$ ohms

Maximum expected error = ± 0.05 mm

Frequency in in GHz	Resonant lengths (in mm)					
	$r_p = 0.435$ mm		$r_p = 0.635$ mm		$r_p = 0.800$ mm	
	l_{r1}	l_{r2}	l_{r1}	l_{r2}	l_{r1}	l_{r2}
8.00	7.57	9.53	7.38	9.97	7.21	10.39
8.50	6.96	8.71	6.78	9.03	6.49	9.27
9.00	6.43	7.95	6.24	8.20	6.11	8.51
9.50	5.95	7.25	5.72	7.41	5.52	7.61
10.00	5.48	6.62	5.28	6.72	5.09	6.89
10.50	5.01	6.01	4.83	6.11	4.62	6.16
11.00	4.62	5.49	4.40	5.48	4.20	5.51
11.50	4.19	4.92	3.99	4.91	3.81	4.91
12.00	3.77	4.38	3.57	4.33	3.39	4.28

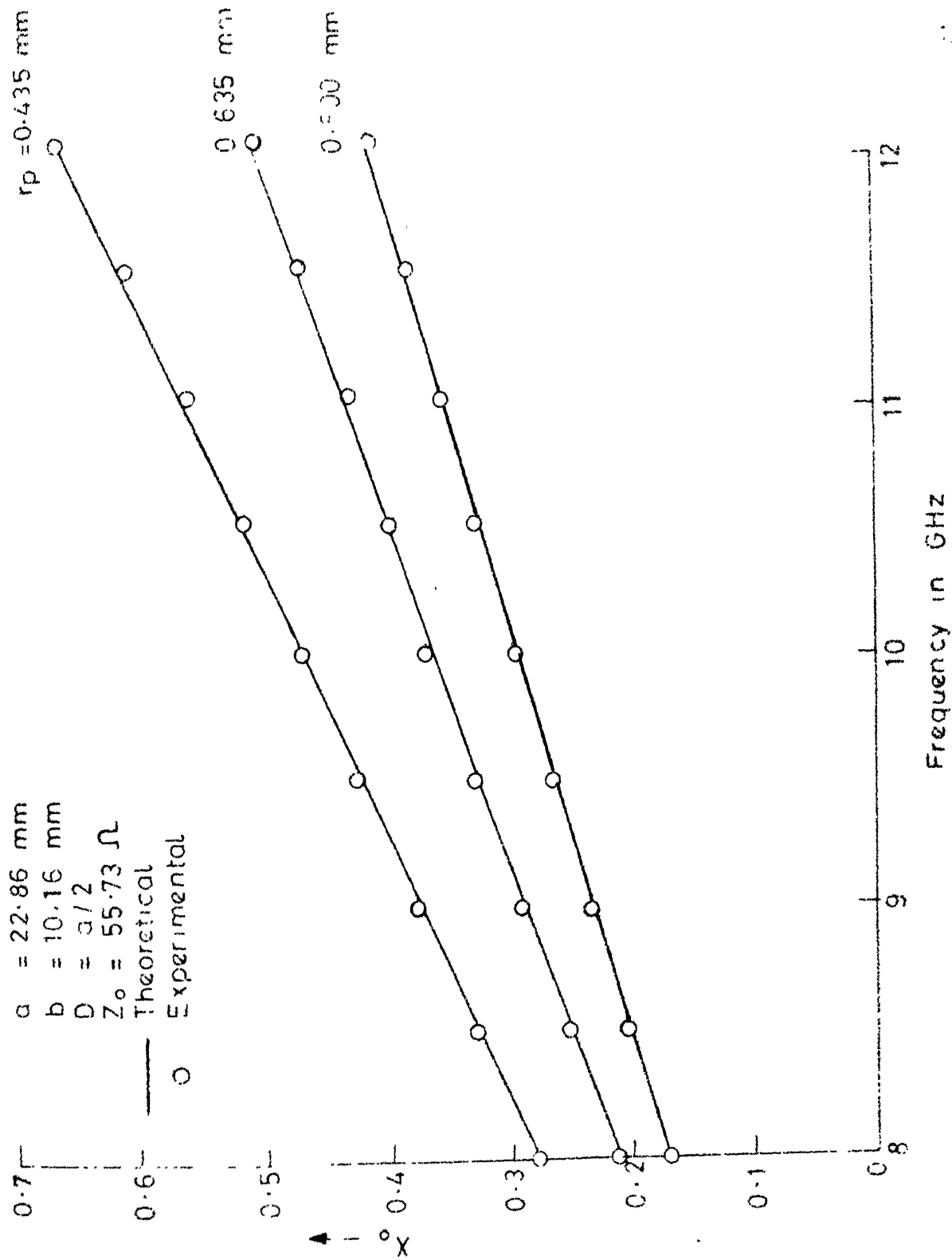


Fig. 4.12 Variation of X_0 with frequency (for $r_p = 0.435, 0.635$ and 0.800 mm)

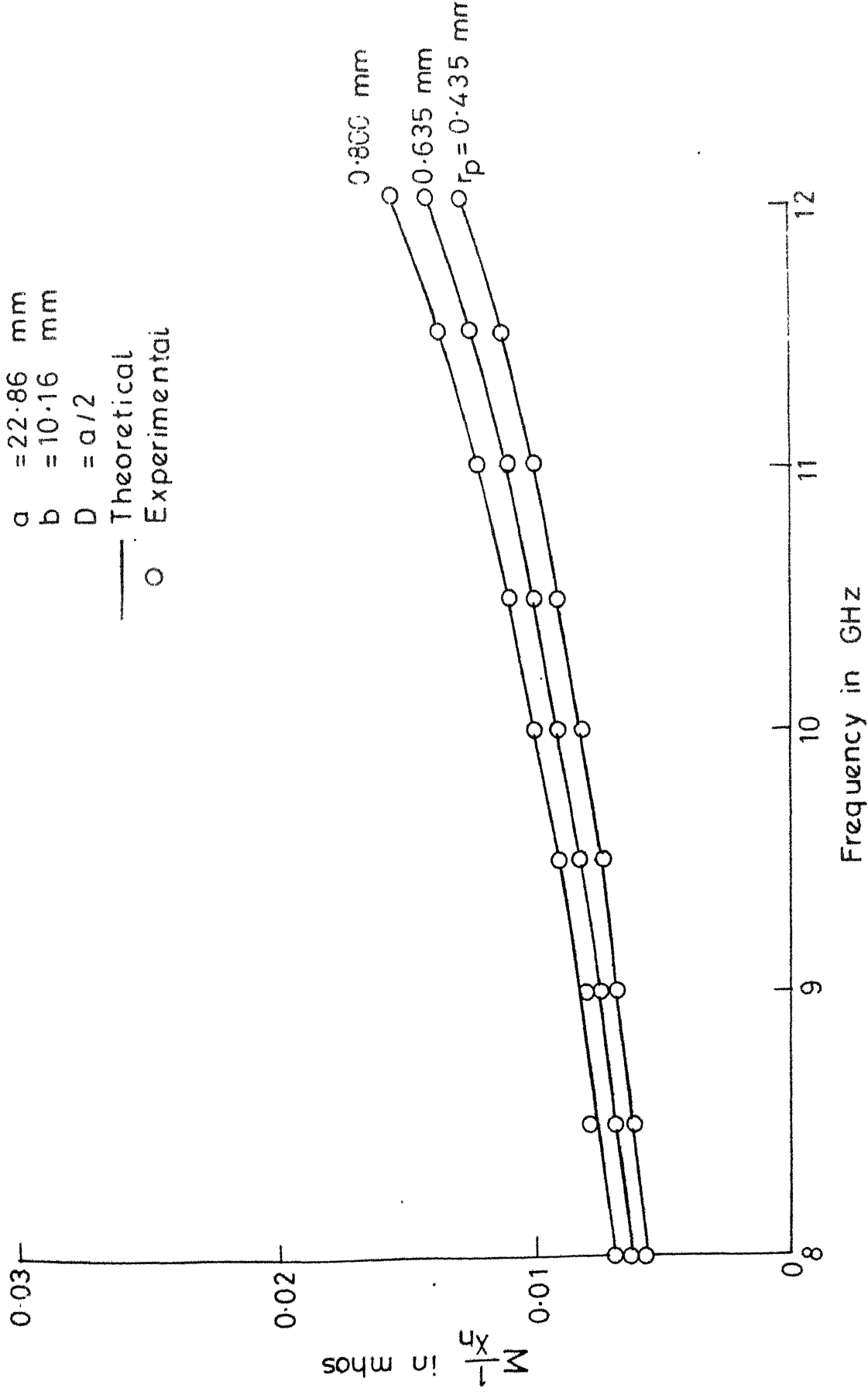


Fig. 4-13 Variation of $\Sigma \frac{1}{x_n}$ with frequency (for $r_p = 0.435 \text{ mm}$, 0.635 mm , and 0.800 mm)

$$N = \operatorname{cosec} \frac{\pi D}{a} \quad (4.3.1)$$

$$\frac{1}{X} = \sum_{n=1}^{\infty} \frac{1}{X_n} \quad (4.3.2)$$

and

$$\frac{1}{X'} = - \sum_{n=1}^{\infty} \frac{(-1)^n}{X_n} \quad (4.3.3)$$

The aim of the present section is to discuss theoretically the extension of the measurement technique of Section 4.2 to the doubly-loaded posts. As is evident from the equivalent circuit shown in Fig. 4.15, the complete characterization of a doubly-loaded post will need the measurement of X_0 , X and X' . The following subsections discuss, in brief, the various techniques that can be used to measure these parameters.

4.3.1 Use of Post Loaded at both Ends with Tunable Coaxial Lines:

For a centered post, $D=a/2$, and the equivalent circuit shown in Fig. 4.15 simplifies as illustrated in Fig. 4.16.

We can write

$$\frac{1}{Z_1'} = \frac{1}{Z_1} + \frac{1}{jX'} - \frac{1}{jX} \quad (4.3.4)$$

$$\frac{1}{Z_2'} = \frac{1}{Z_2} + \frac{1}{jX'} - \frac{1}{jX} \quad (4.3.5)$$

$$\text{and} \quad \frac{1}{Z_{eq}} = \frac{1}{jX'} + \frac{1}{Z_1' + Z_2'} \quad (4.3.6)$$

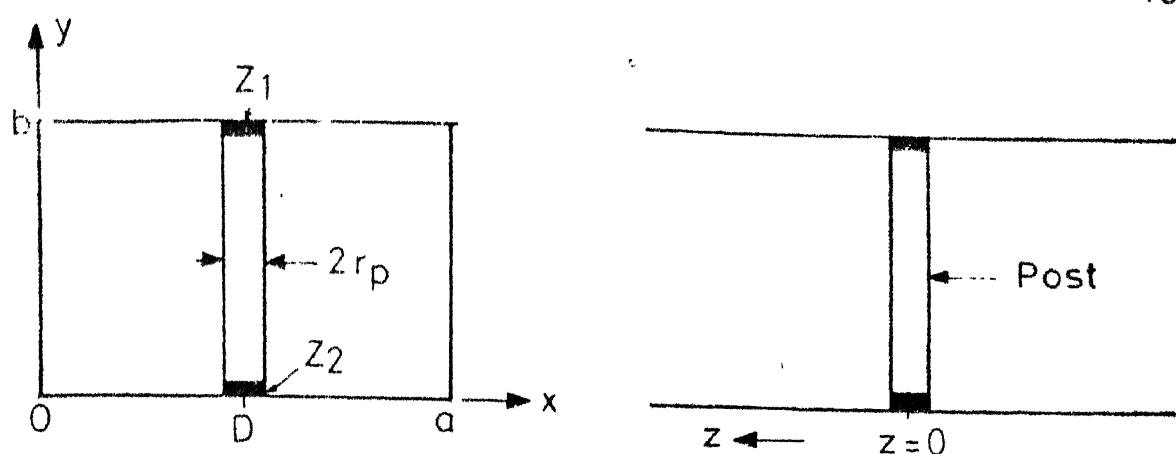


Fig. 4.14 Arrangement of a doubly-loaded metallic post in a rectangular waveguide

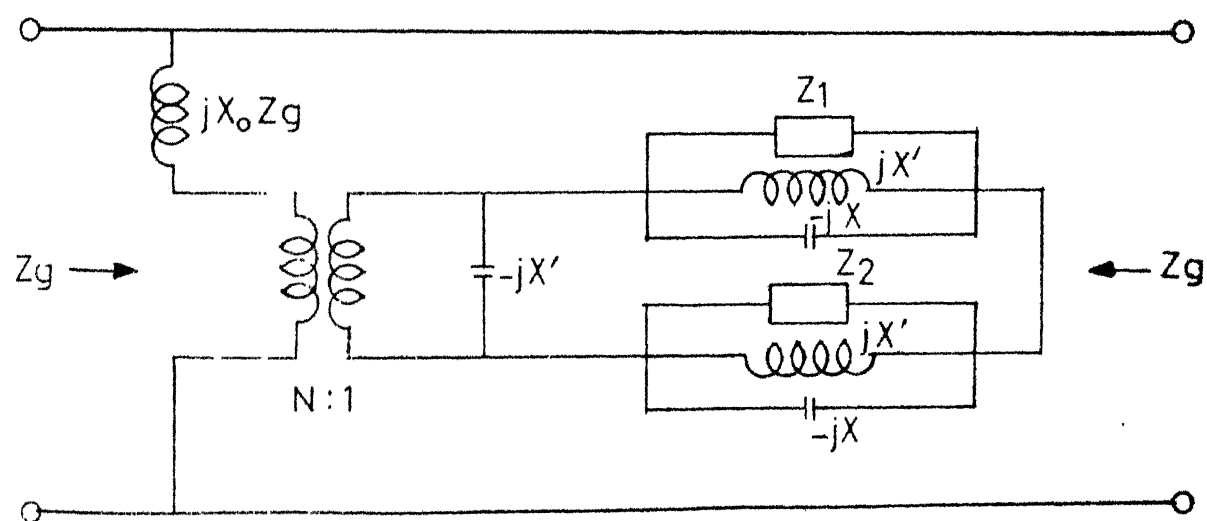


Fig. 4.15 Equivalent circuit of the doubly-loaded post

If we let the both ends of the post be terminated into tunable coaxial lines, we can write

$$Z_1 = jX_{k1} = jZ_0 \tan \beta l_{r1} \quad (4.3.7)$$

$$\text{and } Z_2 = jX_{k2} = jZ_0 \tan \beta l_{r2} \quad (4.3.8)$$

where l_{r1} and l_{r2} are the positions of the movable short in the first and second line, respectively, and where both the lines have been assumed to be of characteristic impedance Z_0 .

Substituting eqs. (4.3.7)-(4.3.8) in eqs. (4.3.4) - (4.3.6), we get,

$$Z_1' = \frac{jXX'X_{k1}}{XX' + XX_{k1} - X'X_{k1}} \quad (4.3.9)$$

$$Z_2' = \frac{jXX'X_{k2}}{XX' + XX_{k2} - X'X_{k2}} \quad (4.3.10)$$

$$Z_1' + Z_2' = jXX' \frac{XX'(X_{k1} + X_{k2}) + 2X_{k1}X_{k2}(X - X')}{X_{k1}X_{k2}(X - X')^2 + XX'(X - X')(X_{k1} + X_{k2}) + X^2X'^2} \quad (4.3.11)$$

and,

$$Z_{eq} = -jX'X \frac{XX'(X_{k1} + X_{k2}) + 2X_{k1}X_{k2}(X - X')}{XX'^2(X_{k1} + X_{k2}) + (X^2 - X'^2)X_{k1}X_{k2} - X^2X'^2} \quad (4.3.12)$$

Let us say that initially we put $X_{k2} = 0$, which essentially means converting the present system into the one employed in Section 4.2 for the measurement of X_0 and X . If the movable short in the other line assumes the position $l_{r1} = l_{r11}$ for maximum transmission and the position $l_{r1} = l_{r12}$ for minimum transmission, one can write

$$X = Z_0 \tan \beta l_{r11} \quad (4.3.13)$$

and

$$X_0 = \frac{Z_0/Z_q}{\cot \beta_{r11} - \cot \beta_{r12}} \quad (4.3.14)$$

which are same as eqs. (4.2.4) and (4.2.3) of Section 4.2.

To determine the remaining unknown parameter X' , one can now introduce a finite value of X_{k2} and measure X_{k1} for either maximum or minimum transmission between the waveguide ports. Let us assume that a value

$$X_{k2} = Z_0 \tan \beta l'_{r2} \quad (4.3.15)$$

is introduced and that this necessitates $l_{r1} = l'_{r11}$ for maximum transmission and $l_{r1} = l'_{r12}$ for minimum transmission. Then, since for maximum transmission Z_{eq} should have a vanishing denominator, one can write

$$Z_0 \tan \beta l'_{r11} + Z_0 \tan \beta l'_{r2} + \frac{X^2 - X'^2}{XX'^2} Z_0^2 \tan \beta l'_{r11} \tan \beta l'_{r2} = X \quad (4.3.16)$$

Using eq. (4.3.13) in eq. (4.3.16), one gets,

$$\left(\frac{X'}{Z_o}\right)^2 = \frac{1}{1 + \tan^2 \beta l_{r11} \cot \beta l'_{r11} \cot \beta l'_{r2} - \tan \beta l_{r11} (\cot \beta l'_{r11} + \cot \beta l'_{r2})} \quad (4.3.17)$$

which can be used to calculate X' , as all other parameters are known.

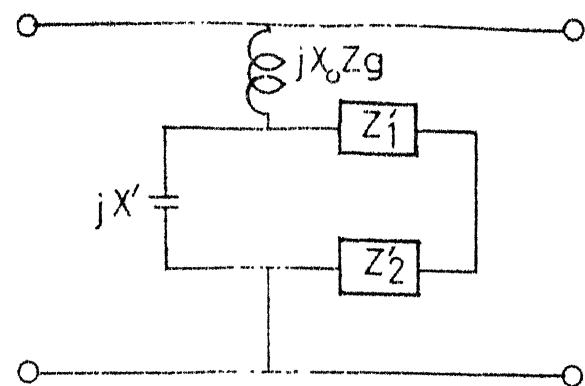
Similarly, for minimum transmission, we have

$$X_{k1} + X_{k2} + (X - X') \frac{X_o Z_g (X + X') - 2XX'}{XX'^2 (X_o Z_g - X)} X_{k1} X_{k2} = \frac{XX_o Z_g}{X_o Z_g - X} \quad (4.3.18)$$

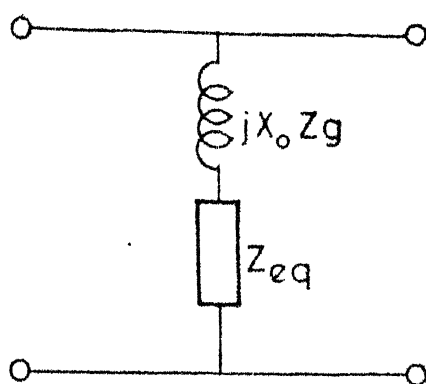
which leads to

$$Z_o \tan \beta l'_{r12} + Z_o \tan \beta l'_{r2} + (X - X') \frac{X_o Z_g (X + X') - 2XX'}{XX'^2 (X_o Z_g - X)} Z_o^2 \tan \beta l'_{r12} \\ \tan \beta l'_{r2} = \frac{XX_o Z_g}{X_o Z_g - X} \quad (4.3.19)$$

Substituting for X and X_o from eqs. (4.3.13) and (4.3.14) in eq. (4.3.19), an expression for X' as a function of Z_o , Z_g , l_{r11} , l_{r12} , l'_{r11} , l'_{r12} and l'_{r2} can easily be derived. This expression will be useful in determining X' from the value of l_{r1} which, for a fixed l_{r2} , minimises the transmission between the waveguide ports.



(a) Intermediate stage of simplification



(b) Final stage of simplification

Fig. 4-16 Simplified equivalent circuit for a centered post

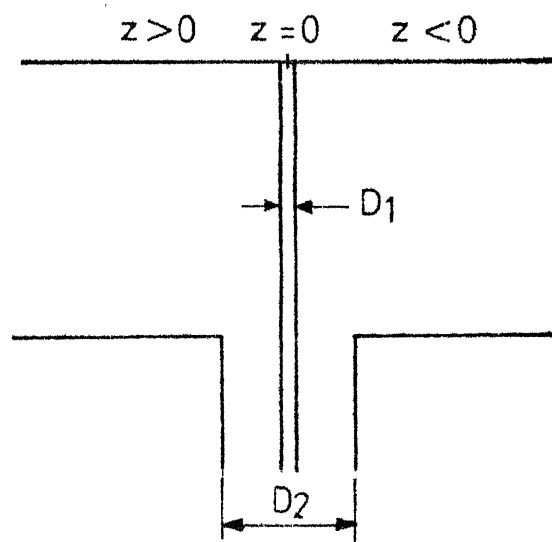
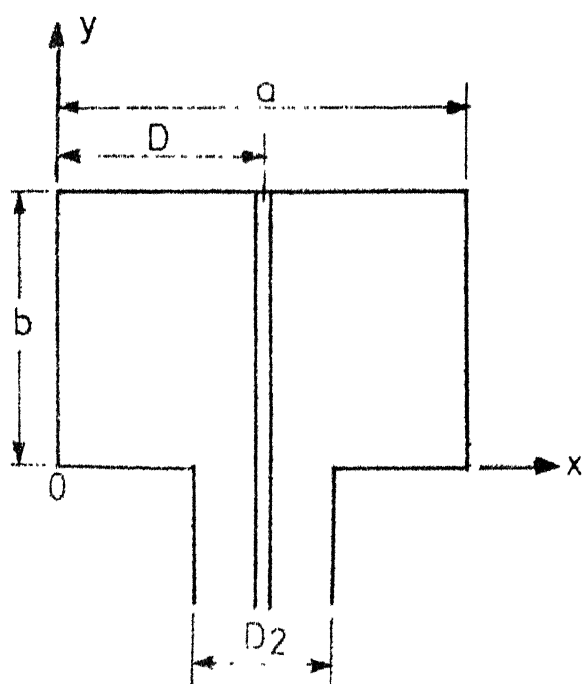


Fig. 4-17 Broad-wall coaxial-waveguide junction considered by Williamson

4.3.2 Use of Post Loaded at one end with the Tunable Coaxial Line and at the other end with a known Reactance:

The post loaded at one end with a tunable coaxial line and at the other end with a fixed known reactance (say, a small air-gap) provides an alternative useful mechanism for the measurement of X' , provided X_0 and X have already been measured by the method of Section 4.2. Let us say that

$$Z_1 = jX_k = jZ_0 \tan \beta l_r \quad (4.3.20)$$

$$\text{and } Z_2 = jX_a \quad (4.3.21)$$

where X_a is a fixed known reactance. In practice, X_a can be easily simulated by a small air-gap between the tip of the post and the waveguide wall. For a given length δ of the gap, the value of X_a can be calculated by using eq. (3.2.3).

With the values of Z_1 and Z_2 as given by eqs. (4.3.20) and (4.3.21), it can easily be shown that

$$Z_{eq} = -jXX' \frac{XX'(X_k - X_c) - 2X_c X_k (X - X')}{XX'^2(X_k - X_c) - X_c X_k (X^2 - X'^2) - X^2 X'^2} \quad (4.3.22)$$

Initially we set $X_a = 0$ and measure the values of l_r for maximum and minimum transmission between the waveguide ports. Say $l_r = l_{r1}$ for maximum transmission, and $l_r = l_{r2}$

for minimum transmission. Then, as usual, we can write

$$X = Z_0 \tan \beta l_{r1} \quad (4.3.23)$$

and

$$X_0 = \frac{Z_0/Z_g}{\cot \beta l_{r1} - \cot \beta l_{r2}} \quad (4.3.24)$$

from which X and X_0 can be computed. Then we can introduce a finite value of X_a and measure the value of l_r which gives maximum transmission. Let this value be l'_{r1} . Then, from eq. (4.3.22), one gets

$$\frac{Z_0 \tan \beta l'_{r1} - X_a}{X} = 1 + X_a Z_0 \tan \beta l'_{r1} \frac{X^2 - X'^2}{X^2 X'^2} \quad (4.3.25)$$

which, after using eq. (4.3.24), yields

$$\left(\frac{Z_0}{X'}\right)^2 = \frac{Z_0}{X_a} (\cot \beta l_{r1} - \cot \beta l'_{r1}) - 1 + \cot^2 \beta l_{r1} \quad (4.3.26)$$

Eq. (4.3.26) can be used to calculate X' , as all other parameters in this equation are known. Alternatively, one can measure the value (say l'_{r2}) of l_r for minimum transmission. The formula to be used for computing X' from a knowledge of Z_0 , Z_g , l_{r1} , l_{r2} and l'_{r2} can easily be derived, as in subsection 4.3.1.

4.4 EXPERIMENTAL DETERMINATION OF THE ADMITTANCE SEEN BY THE COAXIAL LINE IN A BROAD-WALL COAXIAL-WAVEGUIDE JUNCTION: A DISCUSSION

The Rectangular Waveguide - Tunable Coaxial Line Junction, which has been exploited in the preceding sections for the experimental characterization of waveguide mounts, can also be used for experimentally determining the equivalent-circuit parameters of the input admittance seen by the coaxial line in a broad-wall coaxial-waveguide junction. The typical coaxial-waveguide junction is shown in Fig. 4.17. Various dimensions and the coordinate axes are chosen as marked. Several attempts to analyse this junction have been made (see, e.g., [2]-[6], [9]-[10], [13], [59], [229]-[231]). Of all, the analysis reported by Williamson [231] is the most recent and the most rigorous one. Unlike all other analyses, Williamson's analysis also takes into account the effects of the dimensions of the coaxial aperture, and is thus capable of accurately predicting the complex value of the admittance seen by the coaxial line in such a junction.

Williamson has written the input admittance of the junction in terms of the integrals of the coaxial aperture fields at the junction plane and has adopted a magnetic current frill representation for the coaxial source. The effects of the waveguide walls have been considered by him through image theory.

The admittance seen by the coaxial line at the junction plane, as derived by Williamson [231], is given by

$$Y = \frac{1}{(R^2 Z_g / 2) + jXR^2} + jB \quad (4.4.1)$$

where Z_g is given by eq. (4.1.6) and

$$R = \frac{\frac{2}{\pi} \ln \frac{D_2}{D_1} J_0\left(\frac{\beta D_1}{2}\right) \sin \frac{\pi D}{a}}{J_0\left(\frac{\beta D_1}{2}\right) Y_0\left(\frac{\beta D_2}{2}\right) - J_0\left(\frac{\beta D_2}{2}\right) Y_0\left(\frac{\beta D_1}{2}\right)} \quad (4.4.2)$$

$$X = Z_g \frac{V(\beta^2 a^2 - \pi^2)}{4\pi} \operatorname{cosec}^2 \frac{\pi D}{a} \left[2 \sum_{m=2}^{\infty} \sin^2 \frac{m\pi D}{a} \right. \\ \left. \{ (m^2 - \beta^2 a^2 / \pi^2)^{-1/2} - 1/m \} - 2 \sin^2 \frac{\pi D}{a} + \ln\left(\frac{C_2 a}{\pi} \sin \frac{\pi D}{a}\right) \right. \\ \left. - \frac{\pi}{2} \frac{Y_0(0.5\beta D_1)}{J_0(0.5\beta D_1)} \right] \quad (4.4.3)$$

$$B = B_1 + B_2 \quad (4.4.4)$$

$$B_1 = - \frac{2\pi}{\eta \ln \frac{D_2}{D_1}} \cot \beta b \quad (4.4.5)$$

$$B_2 = \frac{2\pi}{\eta \beta b \ln^2 \frac{D_2}{D_1}} \left[2 \sum_{n=1}^{\infty} D_n + \frac{\pi}{2} \frac{J_0(0.5\beta D_2)}{J_0(0.5\beta D_1)} \right. \\ \left. \{ J_0(0.5\beta D_1) Y_0(0.5\beta D_2) - J_0(0.5\beta D_2) Y_0(0.5\beta D_1) \} \right] \quad (4.4.6)$$

and

$$C = 1.78107... \quad (4.4.7)$$

In eq. (4.4.6), D_n 's are defined by

$$\begin{aligned} D_n = & -\frac{\pi}{2} [Y_0(0.5\bar{q}_n\beta D_1)J_0(0.5\bar{q}_n\beta D_2) - Y_0(0.5\bar{q}_n\beta D_2)J_0(0.5\bar{q}_n\beta D_1)] \\ & \times \frac{1}{q_n^2} \left[\frac{J_0(0.5\bar{q}_n\beta D_2)}{J_0(0.5\bar{q}_n\beta D_1)} \right. \\ & \left. + j \frac{J_0(0.5\bar{q}_n\beta D_2)Y_0(0.5\bar{q}_n\beta D_1) - J_0(0.5\bar{q}_n\beta D_1)Y_0(0.5\bar{q}_n\beta D_2)}{J_0(0.5\bar{q}_n\beta D_1)S^*(0.5\bar{q}_n\beta D_1, \bar{q}_n\beta a, D/a)} \right] \\ & \text{for } \frac{n\pi}{\beta b} < 1 \quad (4.4.8a) \end{aligned}$$

$$\begin{aligned} = & [K_0(0.5q_n\beta D_1)I_0(0.5q_n\beta D_1) - K_0(0.5q_n\beta D_1)I_0(0.5q_n\beta D_2)] \\ & \times \frac{1}{q_n^2} \left[\frac{I_0(0.5q_n\beta D_2)}{I_0(0.5q_n\beta D_1)} \right. \\ & \left. - \frac{I_0(0.5q_n\beta D_2)K_0(0.5q_n\beta D_1) - I_0(0.5q_n\beta D_1)(K_0(0.5q_n\beta D_2))}{I_0(0.5q_n\beta D_1)S(0.5q_n\beta D_1, q_n\beta a, D/a)} \right] \\ & \text{for } \frac{n\pi}{\beta b} > 1 \quad (4.4.8b) \end{aligned}$$

$$\bar{q}_n = \sqrt{1 - \frac{n^2\pi^2}{\beta^2 b^2}} \quad (4.4.9a)$$

$$q_n = \sqrt{\frac{n^2\pi^2}{\beta^2 b^2} - 1} \quad (4.4.9b)$$

$$\begin{aligned}
S^*(0.5\beta D_1, \beta a, D/a) = & \frac{2j}{\pi} J_0(0.5\beta D_1) \left[\sum_{m=1}^{\infty} (1 - \cos \frac{2m\pi D}{a}) \right. \\
& \times \{ (m^2 - \beta^2 a^2 / \pi^2)^{-1/2} - 1/m \} + \ln(\frac{C\beta a}{\pi} \sin \frac{\pi D}{a}) \\
& \left. - jY_0(0.5\beta D_1) \right] \quad (4.4.10a)
\end{aligned}$$

and

$$\begin{aligned}
S(0.5qD_1, qa, D/a) = & K_0(0.5qD_1) + I_0(0.5qD_1) \left[\ln(\frac{Cqa}{\pi} \sin \frac{\pi D}{a}) \right. \\
& + \sum_{m=1}^{\infty} (1 - \cos \frac{2m\pi D}{a}) \{ (m^2 + q^2 a^2 / \pi^2)^{-1/2} - 1/m \} \left. \right] \quad (4.4.10b)
\end{aligned}$$

The input admittance Y can be represented, in view of eq. (4.4.1), by the equivalent circuit shown in Fig. 4.18. The equivalent circuit, as seen from the waveguide terminals, is given in Fig. 4.19. The reactance parameters X_B and X_A are given by

$$X_B = \frac{2\pi D_1^2 Z_g}{4a^2} (\beta^2 a^2 - \pi^2)^{1/2} \sin^2 \frac{\pi D}{a} \quad (4.4.11)$$

$$\text{and } X_A = X + X_B/2 \quad (4.4.12)$$

In eqs. (4.4.8) and (4.4.10), $J_0(x)$ and $Y_0(x)$ represent the Bessel functions of first and second kind, respectively, of order zero and having an argument x , whereas $I_0(x)$ and

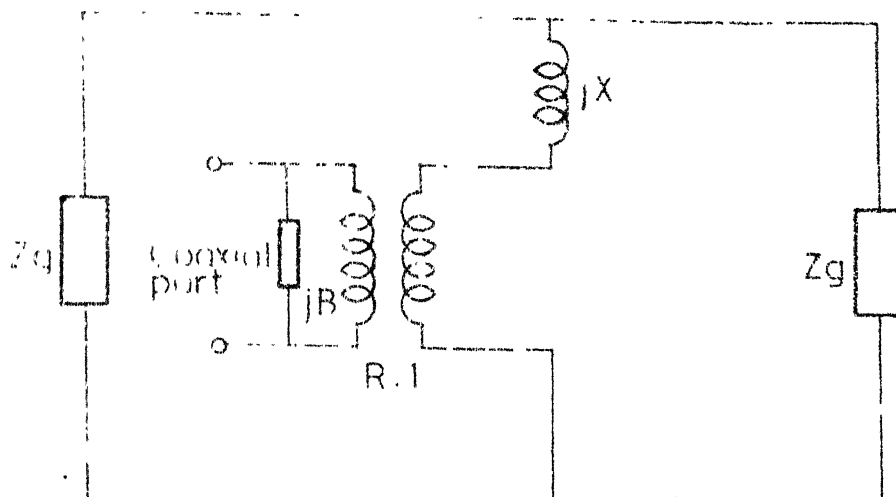


Fig. 4-18 Equivalence for the admittance seen at the coaxial port of the junction shown in Fig. 4-17

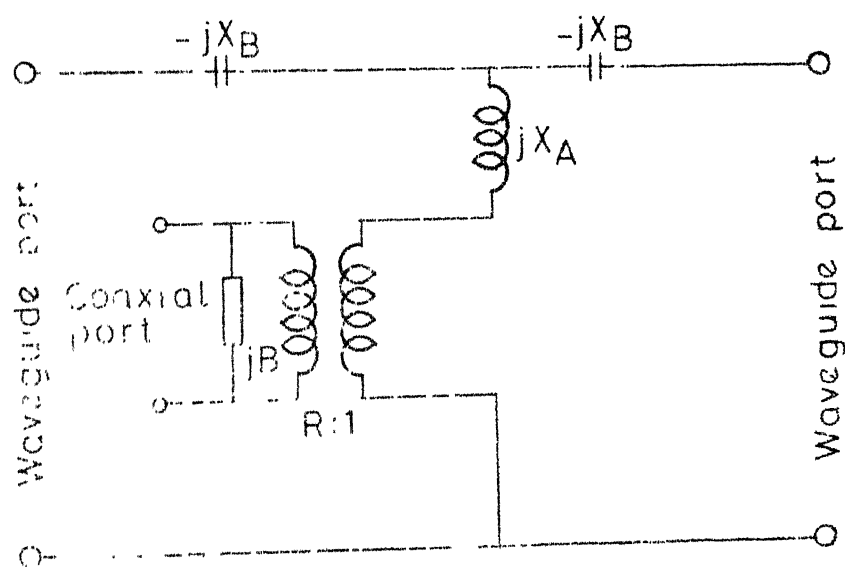


Fig. 4-19 Equivalent circuit of the junction shown in Fig. 4-17, looking from waveguide terminals

$K_0(x)$ represent the modified Bessel functions of first and second kind, respectively, of order zero and having an argument x .

The measurement of real and imaginary components of Y is generally done by using subminiature coaxial cables, as reported by several authors (see, e.g., [105], [122]-[123], [271]). In the following subsection, an alternative scheme which facilitates the measurement of X and B (see eq. (4.4.1)) is suggested and analysed.

4.4.1 Use of Tunable Coaxial Line to Determine X and B :

In Fig. 4.17, if the coaxial line is allowed to be terminated into a movable short, the equivalent circuit, as seen from the waveguide ports, of the resulting structure will be as shown in Fig. 4.20. It can be shown that

$$X_{eq} = X_A - \frac{1}{R^2(B - \frac{1}{X_k})} \quad (4.4.13)$$

The parameters X_A and B can be measured, as before, by noting the positions of the movable short for minimum and maximum loss between the waveguide ports. If $l_1 = l_{r1}$ for minimum loss and $l_r = l_{r2}$ for maximum loss, it is easy to see that

$$X_A = \frac{Z_0}{R^2(\cot\beta l_{r1} - \cot\beta l_{r2})} \quad (4.4.14)$$

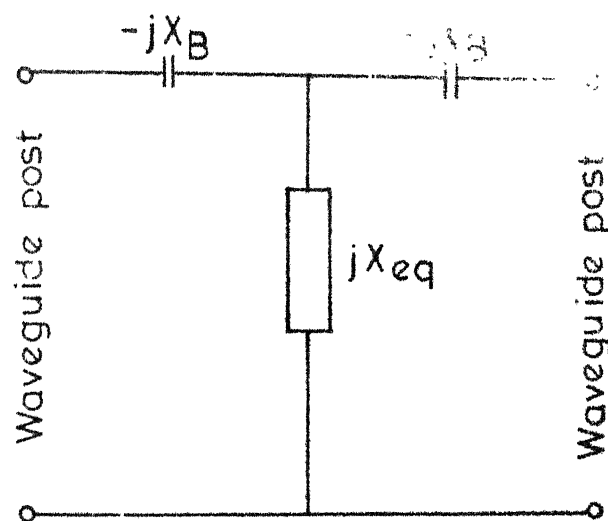


Fig. 4-20 Equivalent circuit of the Rectangular Waveguide - Tunable Coaxial line Junction by using Williamson's analysis

$$\text{and } B = \frac{\cot \beta l_{rl}}{Z_0} \quad (4.4.15)$$

where Z_0 is the characteristic impedance of the coaxial line and R will have to be calculated using eq. (4.4.2). The parameter X can be calculated from X_A by using eqs. (4.4.11) and (4.4.12).

4.5 CONCLUSIONS:

- i) The broad-wall junction of a rectangular waveguide and a tunable coaxial line, which was considered in Chapter 3 for its filtering applications, has been reconsidered. The emphasis now is on its application as a method of experimental evaluation of waveguide mounting structures. This is an aspect which has hitherto not been investigated.
- ii) Lewin's formulation for a singly-loaded metallic post in a rectangular waveguide has been extended to the configuration under consideration. The analysis reveals that the positions of the movable short for minimum and maximum transmission between the waveguide ports can be related to the parameters of the post through simple mathematical equations. Consequently, a novel new method of experimental evaluation of singly-loaded waveguide posts emerges.

- iii) The above mentioned method enjoys unique advantages like easy-to-implement configuration, simple working equations, no need of electrical measurements, etc. The error analysis shows that the errors due to uncertainty in the measurement of lengths can be minimised through using a coaxial line of highest feasible characteristic impedance.
- iv) The proposed method is applied to three different values of the post diameter. The agreement between theory and experiment is good.
- v) The extension of the method to characterize doubly-loaded posts is proposed and formulated.
- vi) It is shown that the proposed configuration can also be used for experimentally determining the admittance seen at the coaxial port in a broad wall coaxial-waveguide junction. It needs to be mentioned that the measurement of Y is generally difficult because the terminals of interest are not accessible, and special techniques such as use of subminiature coaxial cable are to be employed. The present method can serve as an alternate simpler method of measuring Y .

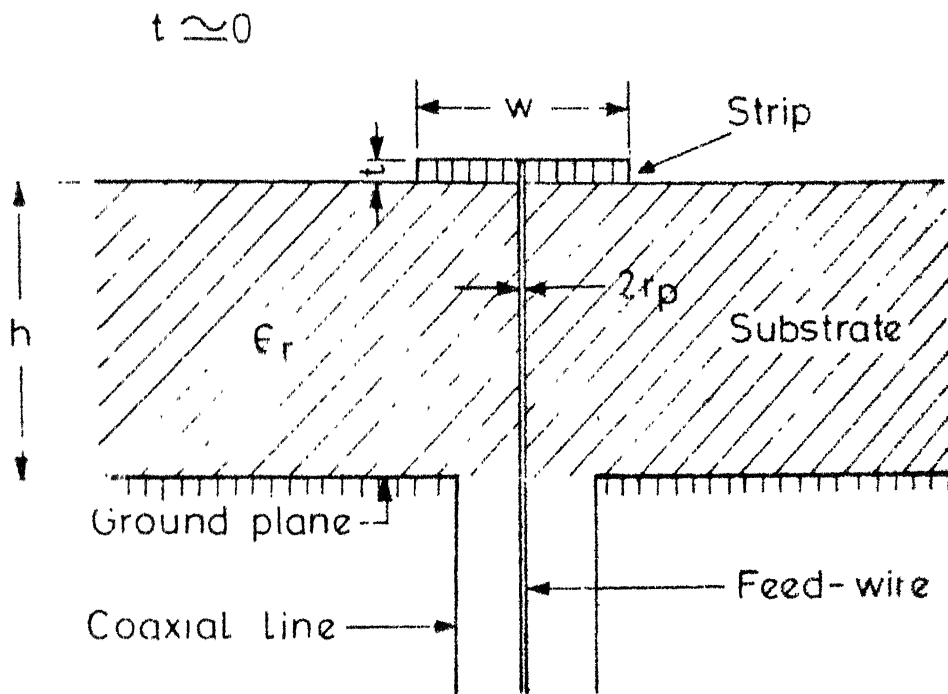
CHAPTER 5

INPUT IMPEDANCE SEEN BY THE COAXIAL LINE IN A BROAD-WALL COAXIAL-MICROSTRIP LAUNCHER

The use of coaxial probes to feed microstrips and striplines is quite well-established. The most commonly employed techniques consist in launching the electromagnetic energy from the edge of the line (see subsections 2.6.2 and 2.6.3 of Chapter 2). However, there are situations in which it is convenient to launch into the line from the broad-wall rather than from the edge. Such a configuration, called a broad-wall launcher, is shown, in its microstrip version, in Fig. 5.1. In this configuration, the coaxial line is mounted on the ground plane of the microstrip. The inner conductor of the coaxial line penetrates the substrate through a cylindrical hole to feed the strip.

The broad-wall launcher is particularly useful when small ground plane spacings are involved. The use of this launcher is generally not recommended at frequencies above S-band. This is so because at C- and X-bands the input VSWR becomes intolerably large (greater than 1.5) and/or tedious adjustments are required.

Although some discussion on the broad-wall coaxial-microstrip/stripline launchers is available in literature[160],



- h = height of substrate
- w = width of strip
- ϵ_r = dielectric constant of substrate
- t = thickness of strip (assumed to be zero)
- r_p = radius of the feed-wire

Fig.5.1 Broad-wall coaxial-microstrip launcher

directly usable results regarding the analysis/synthesis of such launchers seem to be lacking. The intent of this chapter is to report an investigation on the input impedance (say Z_i) seen by the coaxial line in such a launcher. Only the reactive part (say X_i) of Z_i has been studied. The basic configuration used in the study is similar to the one considered in Chapter 3, the essential difference being in the replacement of the waveguide by the microstrip line. The basic line of attack as regards the analysis of the proposed configuration is also same as that followed in Chapter 3. The planar waveguide dispersion model [189] of the microstrip is used to convert the proposed configuration into an equivalent planar waveguide configuration which is tenable to an easy analysis. The condition of resonance which the analysis yields is experimentally verified, for two different sets of parameter values. This resonance condition establishes, after proper interpretation, that the input reactance of the feed-wire can be written by treating the wire as a thin cylindrical antenna situated in an unbounded homogeneous dielectric-filled space.

The following section introduces the proposed configuration and outlines its analysis.

5.1 ANALYSIS OF THE PROPOSED CONFIGURATION

The proposed configuration is shown in Fig. 5.2. It consists of a tunable coaxial line which is mounted on the

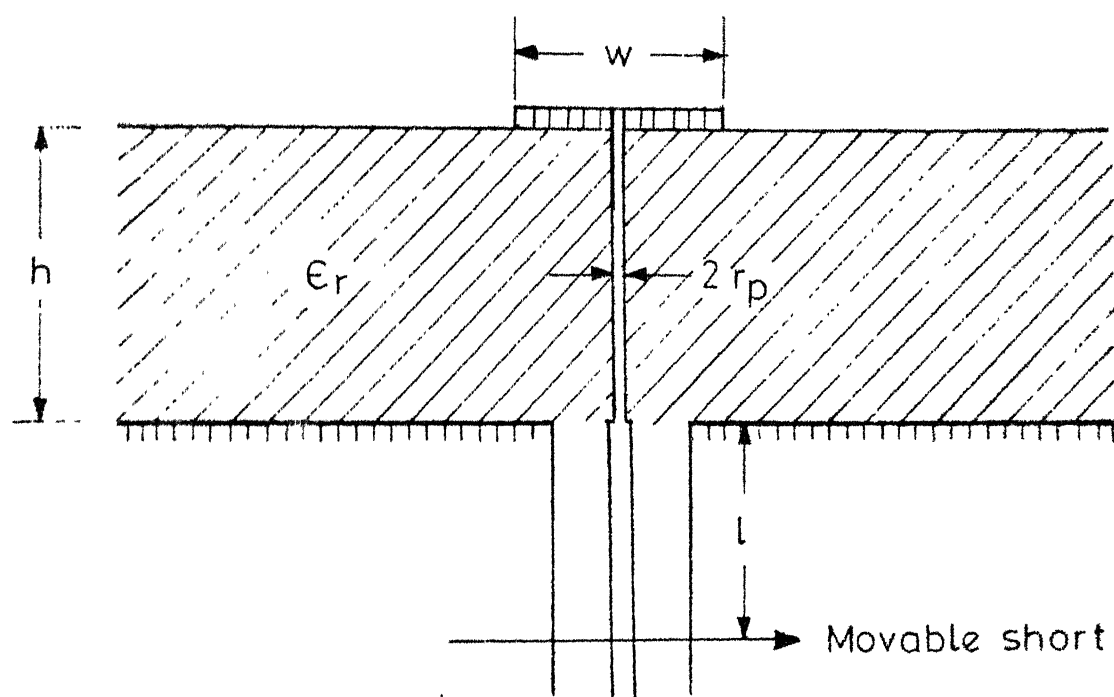


Fig 5.2 Proposed resonant structure

ground plane of the microstrip. The inner conductor of the coaxial line drives the feed-wire as shown. The electromagnetic analysis of the configuration can be conveniently handled by writing its planar waveguide equivalence, as shown in Fig. 5.3. In this equivalence, the microstrip is represented by a parallel plate waveguide of width w_e and of height h . The top and bottom plates of the waveguide are electrically conducting, and there are magnetic walls at the sides. The guide is assumed to be filled with a medium of dielectric constant ϵ_{re} . The frequency-dependent values of w_e and ϵ_{re} are given [166], [189] by

$$w_e(f) = w + \frac{w_e(o) - w}{1 + f/f_g} \quad (5.1.1)$$

and,

$$\frac{1}{\sqrt{\epsilon_{re}(f)}} = \frac{(1/\sqrt{\epsilon_r})(f/f_g)^2 + 1/\sqrt{\epsilon_{re}(o)}}{1 + (f/f_g)^2} \quad (5.1.2)$$

where f is the frequency of operation and

$$f_g = \frac{c}{2w\sqrt{\epsilon_r}} \quad (5.1.3)$$

The parameters $w_e(o)$ and $\epsilon_{re}(o)$ are the effective width and effective dielectric constant, respectively, as calculated from quasi-static analyses. Using Wheeler's latest results [163], one can write

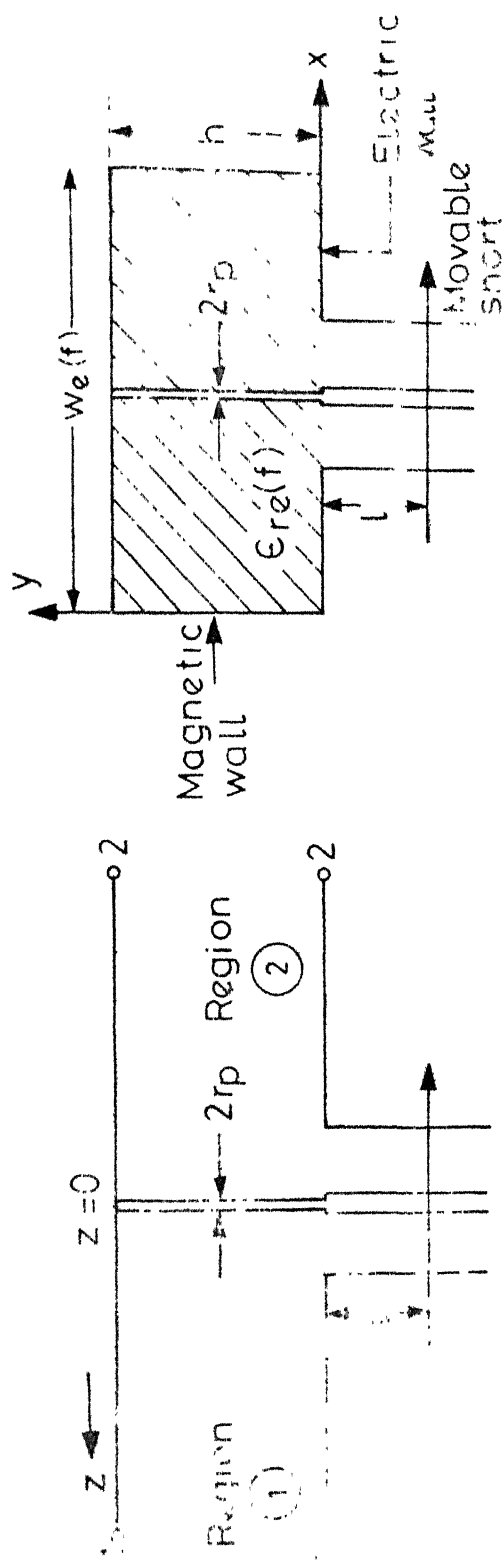


Fig.5.3 Planar waveguide equivalence of the proposed structure

$$\epsilon_{re}(o) = 1 - q + q\epsilon_r \quad (5.1.4)$$

where the filling fraction is

$$q = \frac{1}{2} \left[1 + \frac{1}{\sqrt{(1+10h/w)}} \right] \quad (5.1.5)$$

Also,

$$w_e(o) = \frac{120\pi h}{Z_{om} \sqrt{[\epsilon_{re}(o)]}} \quad (5.1.6)$$

where Z_{om} , the quasi-static impedance of the line, is given by

$$Z_{om} = \frac{42.4}{\sqrt{(\epsilon_r+1)}} \ln (1+F_2F_4) \quad (5.1.7)$$

where,

$$F_1 = \frac{14+8/\epsilon_r}{11} \quad (5.1.8a)$$

$$F_2 = \frac{4h}{w} \quad (5.1.8b)$$

$$F_3 = \frac{\pi^2}{2} (1+1/\epsilon_r) \quad (5.1.8c)$$

and

$$F_4 = F_1F_2 + \sqrt{(F_1^2F_2^2+F_3)} \quad (5.1.8d)$$

The frequency-dependent impedance of the microstrip line is given by

$$Z_{om}(f) = \frac{120\pi h}{w_e(f)\sqrt{[\epsilon_{re}(f)]}} \quad (5.1.9)$$

Now, keeping in view the field expressions derived in Appendix I and assuming a unity amplitude of the incident electric field, the total electric field in regions 1 and 2 can be written as

$$E_{y1} = e^{jkz} + \sum_{m=0}^{\infty} \sum_{n=0}^{\infty} R_{m,n} \cos \frac{m\pi x}{w_e} e^{-jk_{z_{m,n}} z} \quad (5.1.10a)$$

and

$$E_{y2} = \sum_{m=0}^{\infty} \sum_{n=0}^{\infty} T_{m,n} \cos \frac{m\pi x}{w_e} \cos \frac{n\pi y}{h} e^{jk_{z_{m,n}} z} \quad (5.1.10b)$$

where R's are the various reflection coefficients, and T's the various transmission coefficients. The z-direction propagation constant is given by

$$k_{z_{m,n}} = \sqrt{[k^2 - (m\pi/w_e)^2 - (n\pi/h)^2]} \quad (5.1.11)$$

and

$$k = \omega \sqrt{(\mu_0 \epsilon_0 \epsilon_{re})} \quad (5.1.12)$$

One can similarly construct the expressions for the magnetic field as

$$H_{x1} = \frac{1}{\omega\mu_0} \left[ke^{jkz} - \sum_{m=0}^{\infty} \sum_{n=0}^{\infty} k_{z_{m,n}} R_{m,n} \cos \frac{m\pi x}{w_e} \cos \frac{n\pi y}{h} e^{-jk_{z_{m,n}} z} \right] \quad (5.1.13a)$$

and

$$H_{x2} = \frac{1}{\omega\mu_o} \sum_{m=0}^{\infty} \sum_{n=0}^{\infty} k_{z_{m,n}} T_{m,n} \cos \frac{m\pi x}{w_e} \cos \frac{n\pi y}{h} e^{jk_{z_{m,n}} z} \quad (5.1.13b)$$

Simulating the E-plane probe by a y-directed filamental current $I(y)$ and applying boundary conditions similar to those given by eqs. (3.1.5) and (3.1.7), one gets

$$\begin{aligned} 1 + R_{o,o} &= T_{o,o} & \text{for } m=0, n=0 \\ R_{m,n} &= T_{m,n} & \text{for } m > 0, n > 0 \end{aligned} \quad (5.1.14)$$

and

$$R_{o,o} = \frac{1}{N_o} \int_0^h I(y) dy \quad (5.1.15)$$

where,

$$\begin{aligned} N_o &= - \frac{2kw_e h}{\omega\mu_o} \\ &= - \frac{w_e h \sqrt{\epsilon_{re}}}{60\pi} \end{aligned} \quad (5.1.16)$$

Now, in order to determine $I(y)$, we assume, as in Chapter 3, that the scalar potential and current along the length of the wire are representable by means of transmission-line equations, and apply suitable boundary conditions at $y=0, h$ to calculate the arbitrary constants involved.

Eq. (5.1.15) can then be used to calculate the fundamental (TEM) mode reflection coefficient. It turns out that

$$\tau = \frac{f_7 + jf_8}{\eta_1 + j\eta_2} \quad (5.1.17)$$

where,

$$f_5 = 2R_a(Z_{ow} \cosh kh - X_k \sinh kh) \quad (5.1.18a)$$

$$f_6 = 2Z_{ow}(Z_{ow} \sinh kh + X_k \cosh kh) \quad (5.1.18b)$$

$$f_7 = -2Z_{ow}X_k \sinh kh + kh f_6 \quad (5.1.18c)$$

$$f_8 = -4X_k R_a(1 - \cosh kh) + 2Z_{ow}R_a \sinh kh - kh f_5 \quad (5.1.18d)$$

and,

$$\eta_1 = -f_7 + k^2 Z_{ow} N_o f_5 \quad (5.1.19a)$$

$$\eta_2 = -f_8 + k^2 Z_{ow} N_o f_6 \quad (5.1.19b)$$

In eq. (5.1.17), the notation τ has been used, in place of $R_{o,o}$, for the fundamental-mode reflection coefficient. The fundamental-mode transmission coefficient is given by

$$T = 1 + \tau = k^2 Z_{ow} N_o \frac{f_5 + jf_6}{\eta_1 + j\eta_2} \quad (5.1.20)$$

In the preceding equations, R_a is the usual loss parameter (assumed to be lumped at $y=h$), X_k is the reactance of the tunable coaxial line (given by eq. (3.1.22) and Z_{ow}

is the characteristic impedance of the feed-wire. The expression for Z_{ow} will be presented in the next section.

5.2 RESULTS AND DISCUSSION

The configuration shown in Fig. 5.2 exhibits, like its waveguide counterpart, a tunable sharp transmission minimum which can be exploited for developing microstrip notch filters with large mechanical tunabilities. A more important use of this junction, however, is the exploitation of its resonance condition for modelling the reactance presented by the feed-wire to the coaxial line as illustrated below.

The variation of the insertion loss with the position of the movable short is of the type shown in Fig. 5.4. The loss is found to be minimum when $f_6 = 0$, i.e. when

$$Z_o \tan \beta l_r + Z_{ow} \tan kh = 0 \quad (5.2.1)$$

by virtue of which the near-resonance conditions can be modelled by means of the lumped equivalence shown in Fig. 5.5.

In order to verify the theory proposed above, a prototype with $Z_{om} = 50$ ohms, $h = 3.175$ mm, $\epsilon_r = 2.55$, $r_p = 0.41$ mm and $Z_o = 55$ ohms was fabricated. The photograph of the fabricated unit is shown in Fig. 5.6. The measurement setup employed is shown in Fig. 5.7.

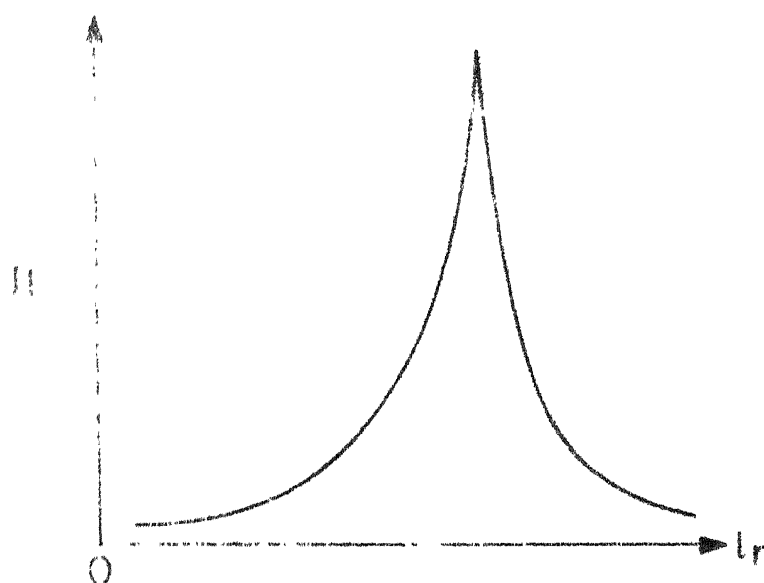


Fig. 5-4 Variation of insertion loss with the position of the movable short

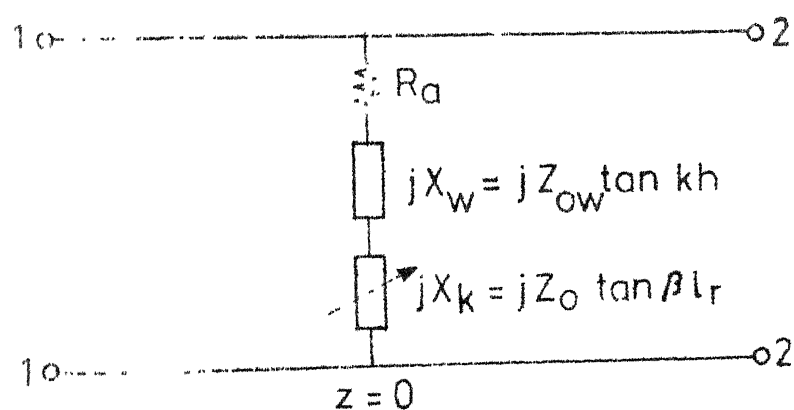


Fig. 5-5 Near-resonance equivalent circuit

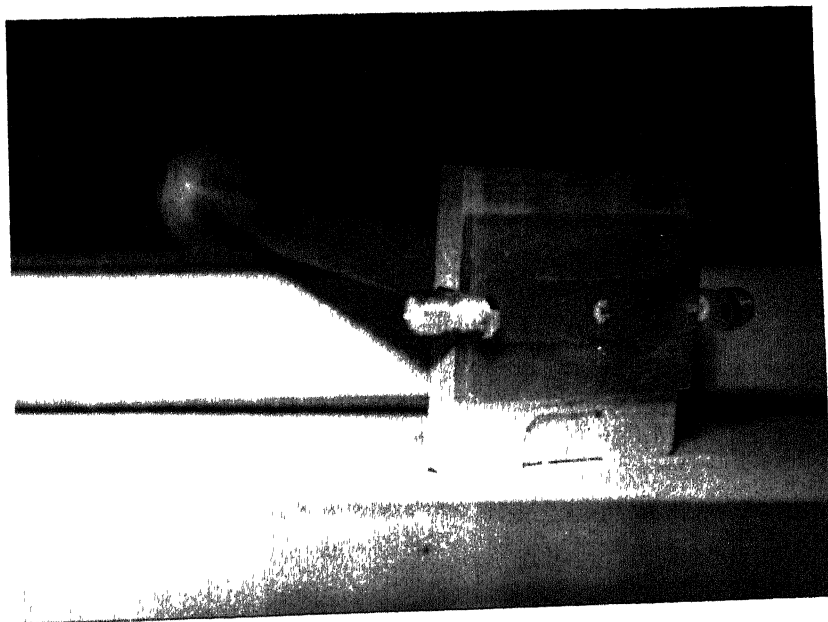


Fig. 5.6: Photograph showing one fabricated unit

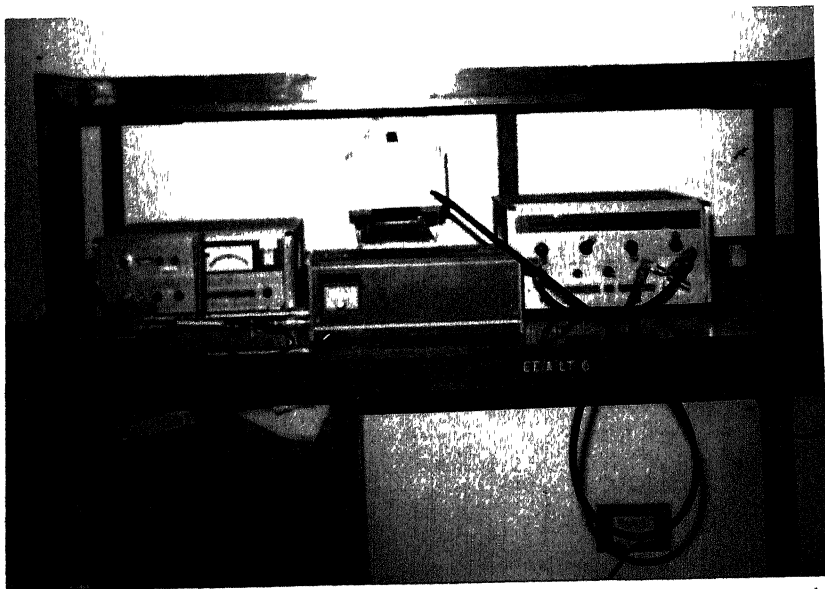


Fig. 5.7: Photograph showing the measurement setup for coaxial components.

The theoretical and experimental loss characteristics are compared, for $f_0 = 2, 3$ and 4 GHz, in Fig. 5.8. The discrepancies between theory and experiment can be attributed, as in Chapter 3, to the various simplifying assumptions made in the analysis, the assumption of a constant R_a throughout the band being probably the most crucial of all.

The theoretical and experimental values of the resonant length are compared, for nine different frequencies, in Table 5.1. For theoretical calculations, the following expression for Z_{ow} was used as this expression gave the best agreement between theoretical and experimental values of resonant length.

$$Z_{ow} = \frac{120}{\sqrt{[\epsilon_{re}(f)]}} \left[\ln \frac{h}{r_p} - 1 \right] \quad (5.2.2)$$

Another unit with $Z_{om} = 40$ ohms, $h = 3.175$ mm, $\epsilon_r = 2.55$, $r_p = 0.755$ mm and $Z_0 = 55$ ohms was fabricated. The 40-ohms line was terminated, on both sides, into standard 50-ohm lines through using tapered-line matching sections. The values of resonant length that were obtained are shown, alongwith the theoretical values, in Table 5.2.

The agreement between theoretical and experimental values of l_r , as manifest in Tables 5.1 and 5.2, is reasonably good, especially when one keeps in mind i) the empiricalness of the planar waveguide model employed for

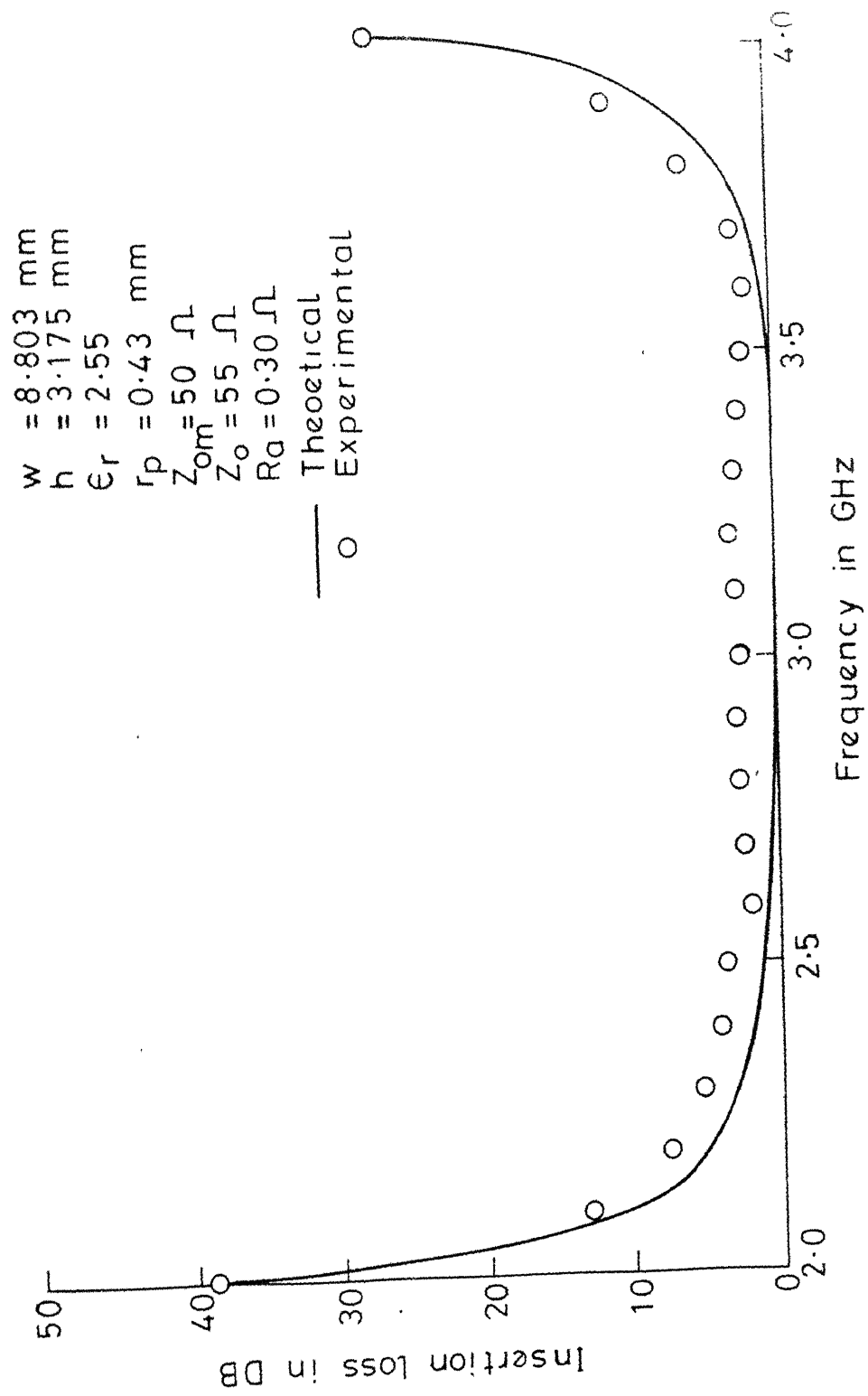
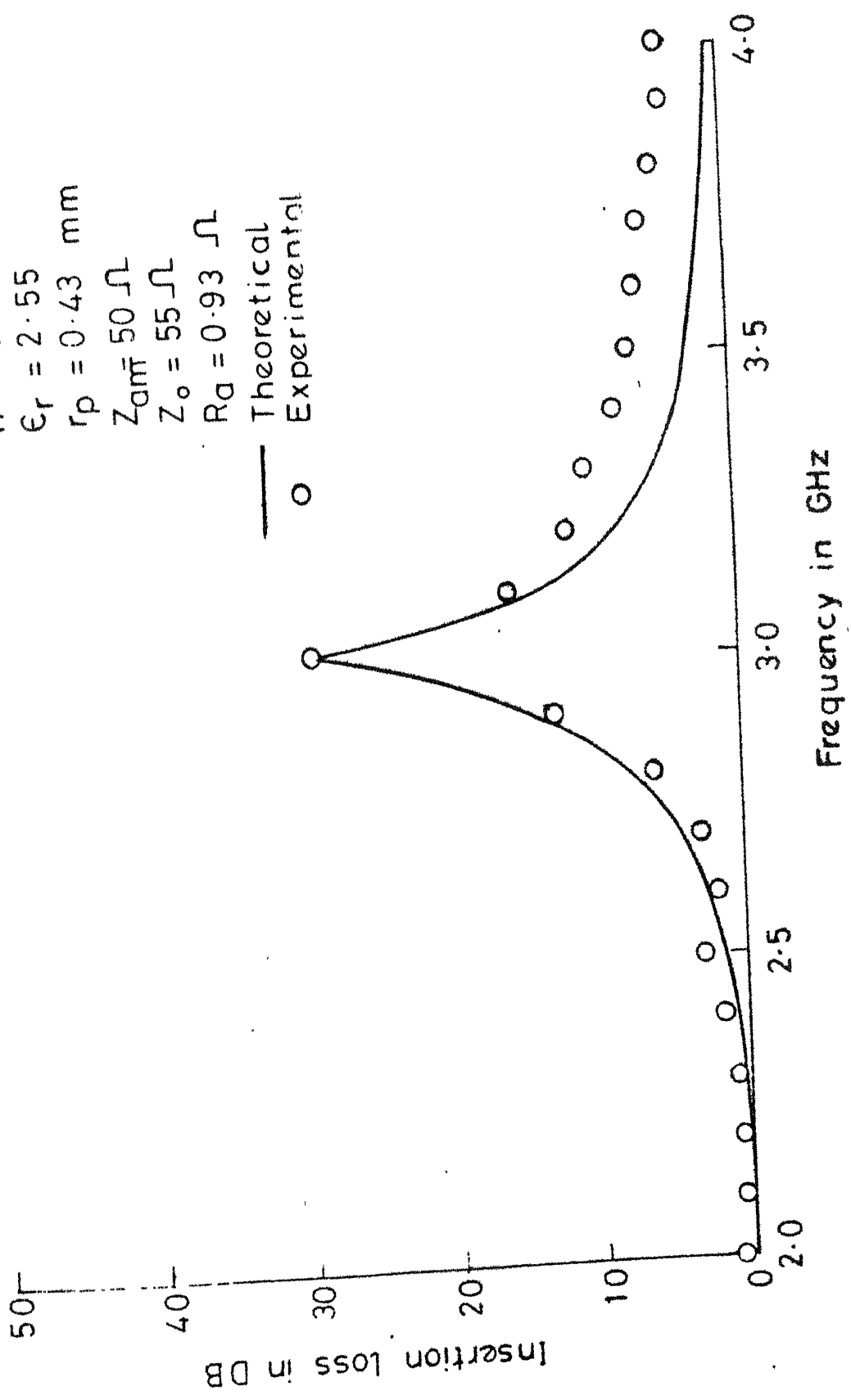


Fig.5-8a Attenuation characteristic of the proposed coaxial microstrip junction ($f_o = 2 \text{ GHz}$)



$w = 8.803 \text{ mm}$
 $h = 3.175 \text{ mm}$
 $\epsilon_r = 2.55$
 $r_p = 0.43 \text{ mm}$
 $Z_{am} = 50 \Omega$
 $Z_o = 55 \Omega$
 $R_d = 0.93 \Omega$

Fig. 5.8b Attenuation characteristic of the proposed coaxial- microstrip junction ($f_0 = 3 \text{ GHz}$)

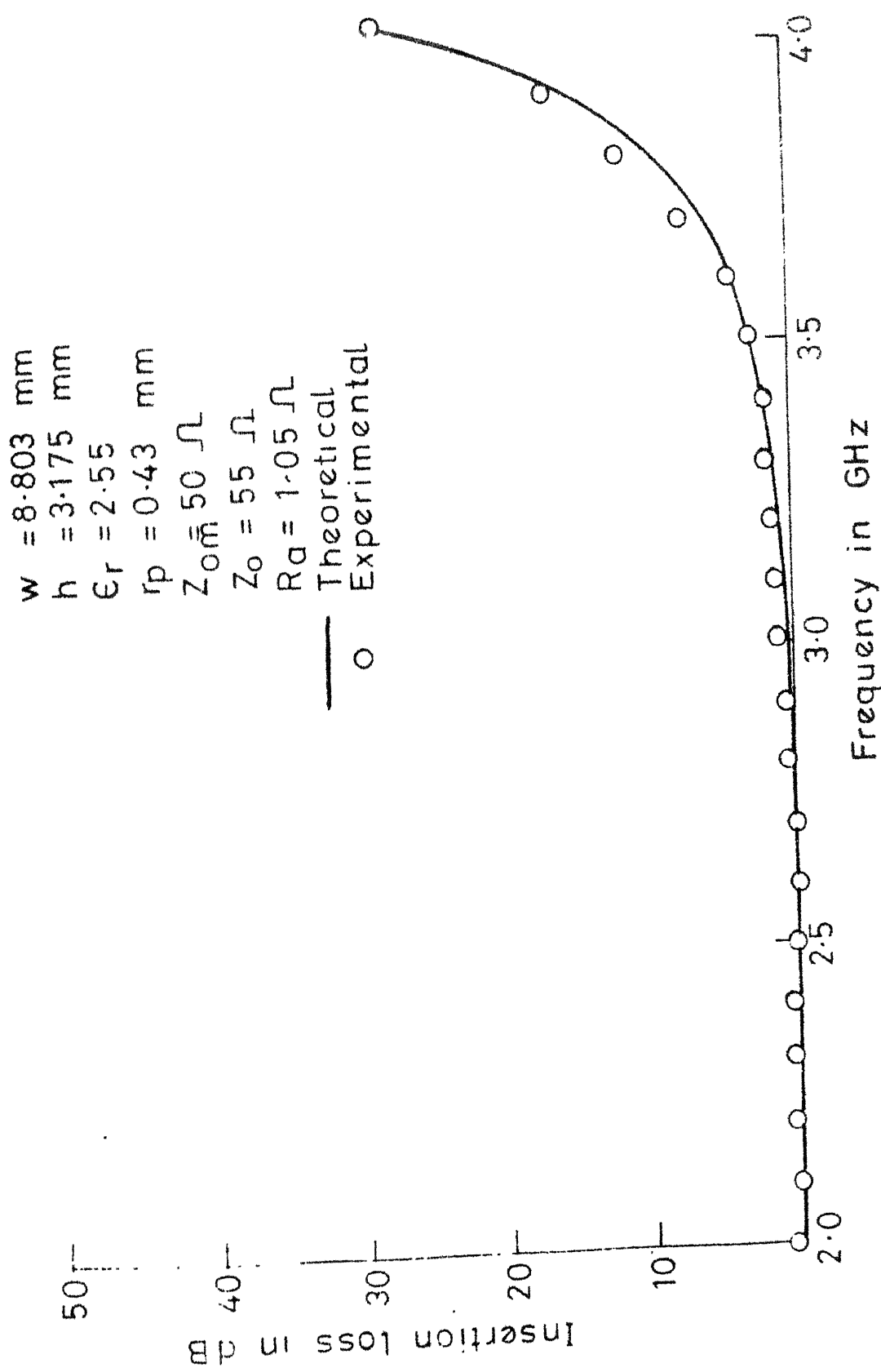


Fig. 5.8c Attenuation characteristic of the proposed coaxial-microstrip junction ($f_o = 4 \text{ GHz}$)

Table 5.1: Comparison between theoretical and experimental values of resonant length ($r_p=0.41$ mm, $Z_{om} = 50$ ohms)

$$w = 8.803 \text{ mm}, h = 3.175 \text{ mm}, \epsilon_r = 2.55,$$

$$D_2 = 10.00 \text{ mm}, D_1 = 4.00 \text{ mm}$$

Maximum uncertainty in the measurement of length = ± 0.10 mm

Frequency in GHz	Resonant length (in mm)		Percentage error
	Theoretical	Experimental	
2.00	67.87123	68.58	1.0442864
2.25	59.56971	60.40	1.3938124
2.50	52.93779	54.10	2.1954260
2.75	47.52069	46.74	1.6428423
3.00	43.01515	42.70	0.7326488
3.25	39.21114	38.90	0.7934989
3.50	35.95856	34.98	2.7213548
3.75	33.14730	31.78	4.1249212
4.00	30.69471	30.13	1.8742449

Table 5.2: Comparison between theoretical and experimental values of resonant length ($r_p=0.755$ mm, $Z_{om}=40$ ohms)
 $w=12.172$ mm, $h=3.175$ mm, $\epsilon_r = 2.55$,
 $D_2 = 10.00$ mm, $D_1 = 4.00$ mm
 Maximum uncertainty in the measurement of length = ± 0.10 mm

Frequency in GHz	Resonant length (in mm)		Percentage error
	Theoretical	Experimental	
2.00	71.95282	69.82	2.9641924
2.25	63.61315	62.89	1.1367933
2.50	56.93932	55.84	1.9306869
2.75	51.47676	48.40	5.9769885
3.00	46.92242	43.81	6.6331191
3.25	43.06649	39.74	7.7240797
3.50	39.75907	37.72	5.1285656
3.75	36.89027	34.04	7.7263463
4.00	34.37761	30.60	10.988577

the analysis and ii) the various other approximations made in the analysis. The resonance condition contained in eq. (5.2.1) can thus be taken to be valid within an error range of generally a few percent and at the worst around ten percent. The error involved is less for thinner wires, which can be expected.

One can now have a close look at eqs. (5.2.1) - (5.2.2) and Fig. 5.5. The equivalent circuit shown in Fig. 5.5 is constituted by two reactances, X_k and X_w . X_k is the reactance of the tunable coaxial line, and X_w is the reactance offered by the feed-wire to the coaxial line. One can write

$$X_w = Z_{ow} \tan kh \quad (5.2.3)$$

Now, eq. (5.2.2) is the well-known expression for the characteristic impedance of a thin cylindrical antenna (see, e.g., [280]-[282]) of length h and radius r_p and radiating in an unbounded space filled with a homogeneous medium of dielectric constant $\epsilon_{re}(f)$. On the other hand, eq. (5.2.3) is the equation for the input reactance of a short-circuited antenna of length h and having characteristic impedance equal to Z_{ow} . Thus the overall picture that emerges is that the feed-wire can be treated as a short-circuited thin cylindrical antenna situated in an infinite homogeneous dielectric-filled space, and X_i can be written as its input reactance.

5.3 CONCLUSIONS

i) The input reactance of the feed-wire in a broad-wall coaxial-microstrip launcher has been studied through making the wire part of a resonant structure involving a tunable coaxial line and studying the resonance condition of the resulting structure.

ii) It turns out that, for the purposes of writing its input reactance, the feed-wire can be treated as a short-circuited thin cylindrical antenna situated in an unbounded homogeneous dielectric-filled space. This result seems to be a natural outcome of representing the scalar potential and current on the wire by means of transmission-line equations. The experimental validity, at least to a first degree of approximation, of this result is demonstrated for two different sets of parameter values.

iii) The present study will help in filling, at least partially, the vacuum that currently exists regarding the results on the input impedance seen by the coaxial line in a broad-wall coaxial-microstrip launcher.

iv) The results of the study can easily be extended to the corresponding coaxial-stripline launcher.

CHAPTER 6

CHARACTERIZATION OF A MICROSTRIP LINE TRANSVERSELY LOADED WITH THIN CONDUCTING POST

As we have seen in Chapter 2, the transversely placed (both in E and H planes) discontinuities play a very important role in systems involving coaxial lines and waveguides. A tremendous amount of research has thus been, and is being, done on the characterization (both theoretical and experimental) of such discontinuity structures. Barring a few exceptions like the transverse slit considered by Hoefer [283], the characterization of microstrip/stripline discontinuities has, however, been largely limited to the discontinuities along the strip, i.e. steps, open-ends, gaps, etc. The transverse discontinuities in MIC's have not received much attention. The reason behind this trend is presumably the fact that an actual realisation of transverse discontinuities is a little more cumbersome in case of MIC's than in case of coaxial lines or waveguides. For instance, drilling of transverse hole(s) in the substrate is a pre-requisite for creating transverse discontinuities in MIC's, whereas there is no such requirement for coaxial lines and waveguides.

The intent of this chapter is to analyse the case of a microstrip line which is loaded in the transverse plane

with a metallic circular post. Only a thin post is considered. The planar waveguide dispersion model [189] of the microstrip is used for the analysis as, like in Chapter 5, this model suits the geometry of the problem involved. The analysis reveals that the post can be represented by means of an inductive reactance across the line. The mathematical expression for this reactance is derived. The experimental verification of the theory is done, for two different sets of parameter values, by forming a resonant structure involving the unknown post and a known discontinuity (gap or open-end, which can be characterized using available results) and noting the frequency of resonance. The theory and experiment tally within the attributable error range.

The following section presents the analysis of the proposed configuration using the planar waveguide model.

6.1 THEORETICAL ANALYSIS OF THE CONFIGURATION

The microstrip line loaded with a thin metallic E-plane post is shown in Fig. 6.1. The planar waveguide equivalence of the configuration is shown in Fig. 6.2. Various dimensions, parameters, and the coordinate axes are chosen as shown. The analysis of the 'equivalent' configuration shown in Fig. 6.2 can easily proceed along lines

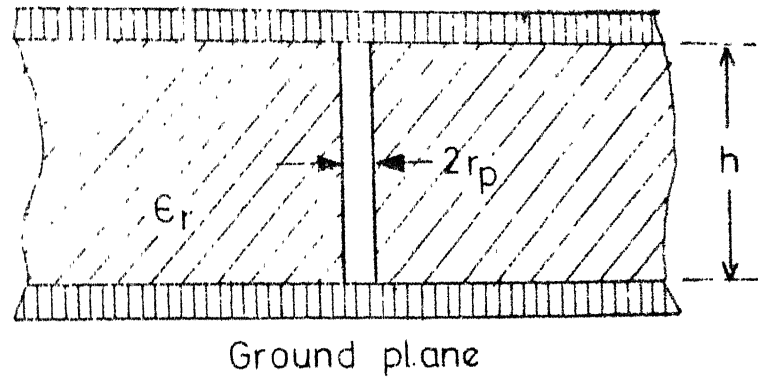


Fig.6-1 A microstrip line loaded with thin metallic post

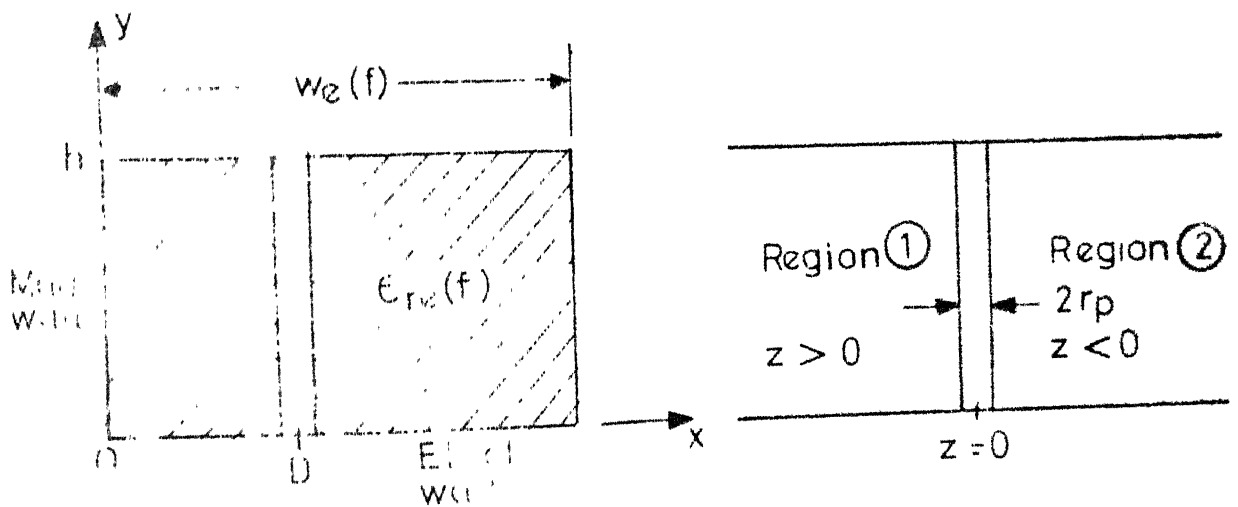


Fig.6-2 Planar waveguide equivalence of the configuration shown in Fig.6-1

similar to those followed by Lewin [13] in analysing a similar problem in 'ordinary' waveguide form.

Assuming that the radius r_p of the post is negligible as compared with the free-space wavelength λ , the post can be replaced by a y-directed filamental current $I(y)$ situated at $x = D$, $z = 0$. For all practical cases, the height h of the substrate is much lesser than λ . One can thus safely neglect all y-variations and, consequently, can replace $I(y)$ by a mere constant, say I .

Now, on either side of the plane $z = 0$, the fields can be expanded in terms of the planar waveguide modes⁺ with the electric field E_y continuous at $z = 0$, and the magnetic field also continuous except at $x = D$ where its discontinuity gives the current I . One can write

$$E_{y1} = \sum_{m=0}^{\infty} A_m \cos \frac{m\pi x}{w_e} e^{-\gamma'_m z} \quad (6.1.1a)$$

and

$$E_{y2} = \sum_{m=0}^{\infty} A_m \cos \frac{m\pi x}{w_e} e^{\gamma'_m z} \quad (6.1.1b)$$

Similarly

$$H_{x1} = \frac{j}{\omega\mu} \sum_{m=0}^{\infty} \gamma'_m A_m \cos \frac{m\pi x}{w_e} e^{-\gamma'_m z} \quad (6.1.2a)$$

⁺For details on modes in a planar waveguide, see the Appendix I.

and

$$H_{x2} = - \frac{j}{\omega\mu} \sum_{m=0}^{\infty} \gamma'_m A_m \cos \frac{m\pi x}{w_e} e^{\gamma'_m z} \quad (6.1.2b)$$

In eqs. (6.1.1) and (6.1.2) the propagation constant in z-direction is given by

$$\gamma'_m = \sqrt{(m^2 \pi^2 / w_e^2 - k^2)} \quad (6.1.3)$$

$$\gamma'_0 = jk \quad (6.1.4)$$

$$\text{and } k = \omega \sqrt{\mu \epsilon} \quad (6.1.5)$$

The discontinuity in H_x from $z > 0$ to $z < 0$ must equal $I \delta(x-D) \delta(z)$. This yields

$$A_m = -j \frac{\omega\mu \hat{\epsilon}_m}{2w_e \gamma'_m} I \cos \frac{m\pi D}{w_e} \quad (6.1.6)$$

Eq. (6.1.1) can then be re-written as

$$E_y = - \frac{j\omega\mu I}{2w_e} \sum_{m=0}^{\infty} \frac{\hat{\epsilon}_m}{\gamma'_m} \cos \frac{m\pi D}{w_e} \cos \frac{m\pi x}{w_e} e^{-\gamma'_m |z|} \quad (6.1.7)$$

An incident electric field of unity amplitude in the dominant (TEM) mode can be represented by

$$E_i = e^{jkz} \quad (6.1.8)$$

At the surface of the post, we can take, for example, $x = D + r_p$, $z = 0$. To get zero total tangential electric field, the strength of the equivalent current filament must therefore satisfy the equation

$$\frac{j\omega\mu I}{2w_e} \sum_{m=0}^{\infty} \left[\frac{\hat{E}_m}{\sqrt{\epsilon_m}} \cos \frac{m\pi D}{a} \cos \frac{m\pi(D+r_p)}{a} \right] = 1 \quad (6.1.9)$$

Any other points around the post could also be chosen to achieve cancellation, and all would have yielded an equation similar to eq. (6.1.9), differing by small terms dependent on r_p due to the slight variation of the incident and reflected fields around the post.

According to eq. (6.1.7), the dominant mode produced by the current filament is just the first term of the series, and in region 1 (i.e. when z is positive), this is the reflected component of the wave. Hence, the fundamental (TEM) mode reflection coefficient is related to the strength of the current filament by⁺

$$\tau = - \frac{\omega\mu}{2kw_e} I \quad (6.1.10)$$

The corresponding transmission coefficient is

$$T = 1 + \tau \quad (6.1.11)$$

⁺Compare eq. (6.1.10) with eq. (5.1.15) of Chapter 5.

so that the post can be represented by an impedance across the line.

Eliminating I between eqs. (6.1.9) and (6.1.10), and solving, one finally arrives at

$$\tau = - \frac{1}{1+2jX_0} \quad (6.1.12)$$

where the normalised post-reactance is given by

$$X_0 = \frac{k}{2} \sum_{m=1}^{\infty} \left[\frac{1}{\gamma'_m} \left(\cos \frac{m\pi r}{w_e} + \cos \frac{2m\pi D}{w_e} \right) \right] \quad (6.1.13)$$

and the approximation

$$2 \cos \frac{m\pi D}{w_e} \cos \frac{m\pi(D+r_p)}{w_e} \simeq \cos \frac{m\pi r}{w_e} + \cos \frac{2m\pi D}{w_e} \quad (6.1.14)$$

has been made use of.

Thus the post can be represented by a shunt equivalent circuit as shown in Fig. 6.3. The expression for X_0 , as given by eq. (6.1.13), can be further simplified as follows:

In each term of the series

$$S = \sum_{m=1}^{\infty} \frac{1}{\gamma'_m} \left(\cos \frac{m\pi r}{w_e} + \cos \frac{2m\pi D}{w_e} \right) \quad (6.1.15)$$

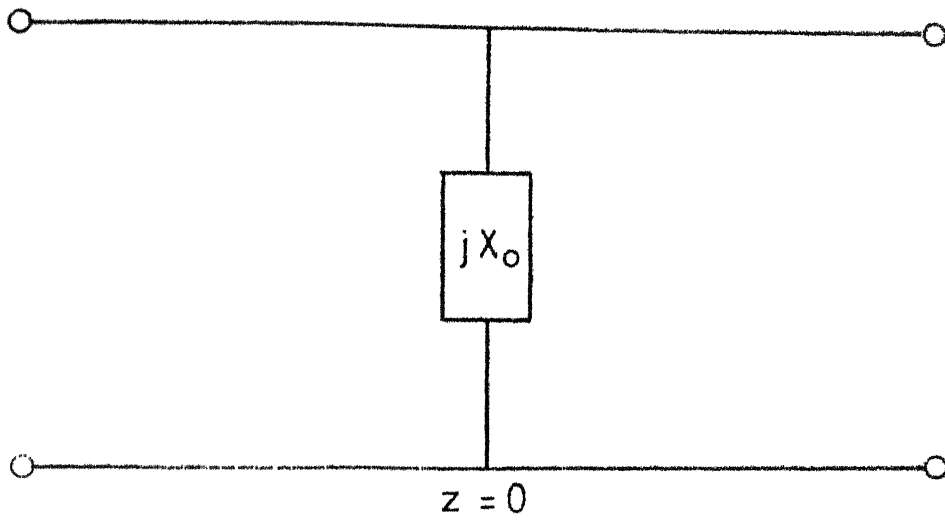


Fig.6.3 Lumped – circuit equivalence

if we add and subtract the term

$$\frac{w_e}{m\pi} \left(\cos \frac{m\pi r}{w_e} p + \cos \frac{2m\pi D}{w_e} \right)$$

the series becomes

$$S = \sum_{m=1}^{\infty} \left[\frac{w_e}{m\pi} \left(\cos \frac{m\pi r}{w_e} p + \cos \frac{2m\pi D}{w_e} \right) - \frac{w_e}{m\pi} \left(\cos \frac{m\pi r}{w_e} p \right. \right. \\ \left. \left. + \cos \frac{2m\pi D}{w_e} \right) + \frac{1}{m} \left(\cos \frac{m\pi r}{w_e} p + \cos \frac{2m\pi D}{w_e} \right) \right] \quad (6.1.16)$$

Using the well-known relation

$$\sum_{m=1}^{\infty} \frac{\cos px}{p} = -\ln \left| 2 \sin \frac{x}{2} \right| \quad (6.1.17)$$

the dominant part of S sums to

$$-\frac{w_e}{\pi} \ln \left(4 \sin \frac{\pi r}{2w_e} \sin \frac{\pi D}{w_e} \right)$$

Hence, eq. (6.1.13) yields

$$X_0 = \frac{w_e \sqrt{\epsilon_{re}}}{\lambda} \left[-\ln \left(4 \sin \frac{\pi r}{2w_e} \sin \frac{\pi D}{w_e} \right) + \sum_{m=1}^{\infty} \left(\cos \frac{m\pi r}{w_e} p \right. \right. \\ \left. \left. + \cos \frac{2m\pi D}{w_e} \right) \left\{ (m^2 - k^2 w_e^2 / \pi^2)^{-1/2} - 1/m \right\} \right] \quad (6.1.18)$$

which, as compared with eq. (6.1.13), will not diverge with increasing m , and can thus easily be summed up on a computer. Putting $r_p = 0$, eq. (6.1.18) simplifies to

$$X_o = \frac{w_e \sqrt{\epsilon_{re}}}{\lambda} \left[\ln \frac{w_e}{2\pi r_p} - \ln \sin \frac{\pi D}{w_e} + 2 \sum_{m=1}^{\infty} \cos^2 \frac{m\pi D}{w_e} \left\{ (m^2 - k^2 w_e^2 / \pi^2)^{-1/2} - 1/m \right\} \right] \quad (6.1.19)$$

For all practical purposes, eq. (6.1.19) can be used instead of eq. (6.1.18), without introducing a noticeable error.

For a centered post, $D = w_e/2$ and eq. (6.1.19) simplifies to

$$X_o = \frac{w_e \sqrt{\epsilon_{re}}}{\lambda} \left[\ln \frac{w_e}{2\pi r_p} + 2 \sum_{m=2,4,6,\dots}^{\infty} \left\{ (m^2 - w_e^2 k^2 / \pi^2)^{-1/2} - 1/m \right\} \right] \quad (6.1.20)$$

6.2 THEORETICAL RESULTS AND DISCUSSION

The variations of normalised and non-normalised values of the post reactance and of the corresponding inductance with respect to r_p/w , w/h and ϵ_r are shown in Figs. 6.4, 6.5 and 6.6, respectively. The following observations can be made:

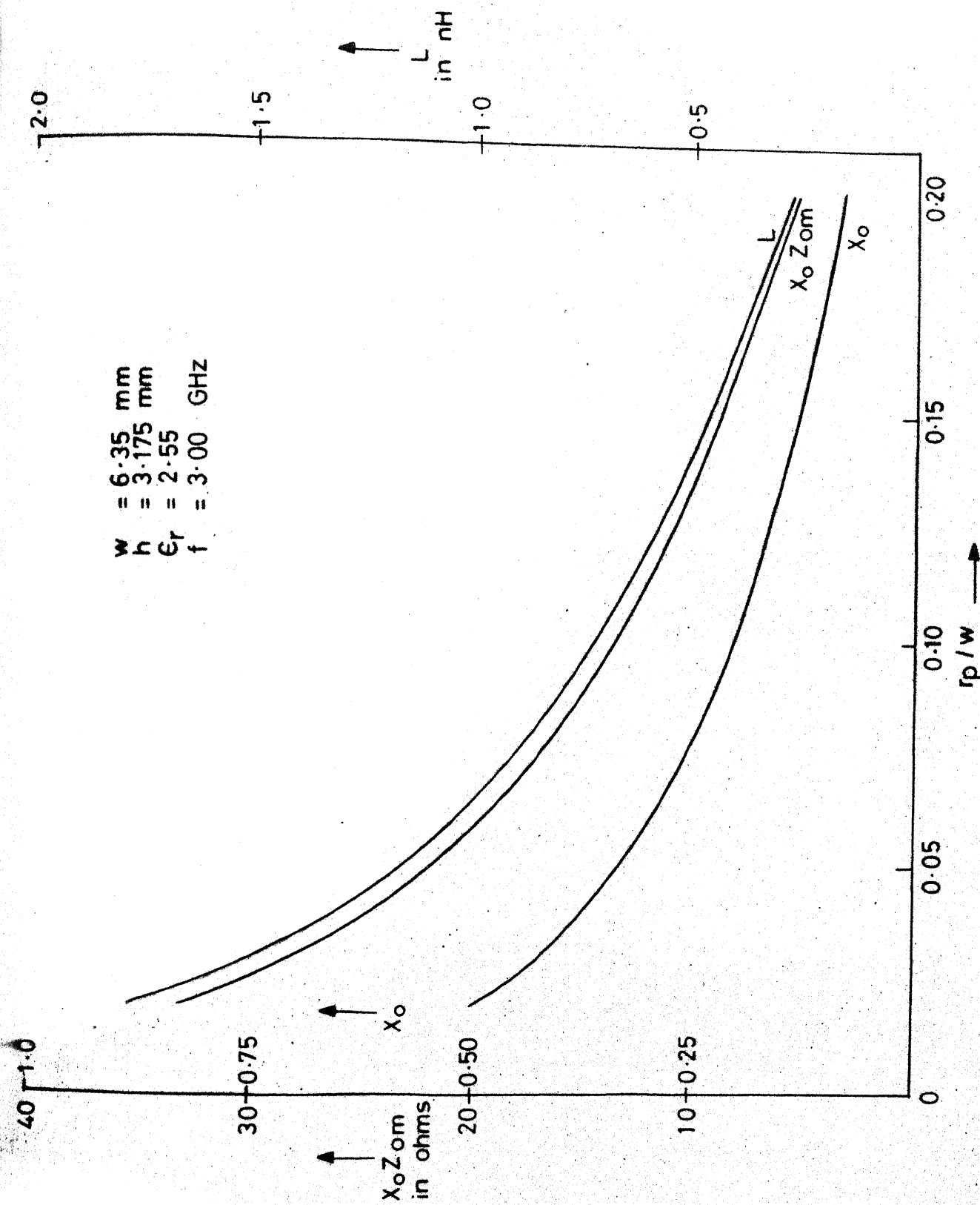


Fig. 6.4 Variation of post reactance and post inductance with r_p/w

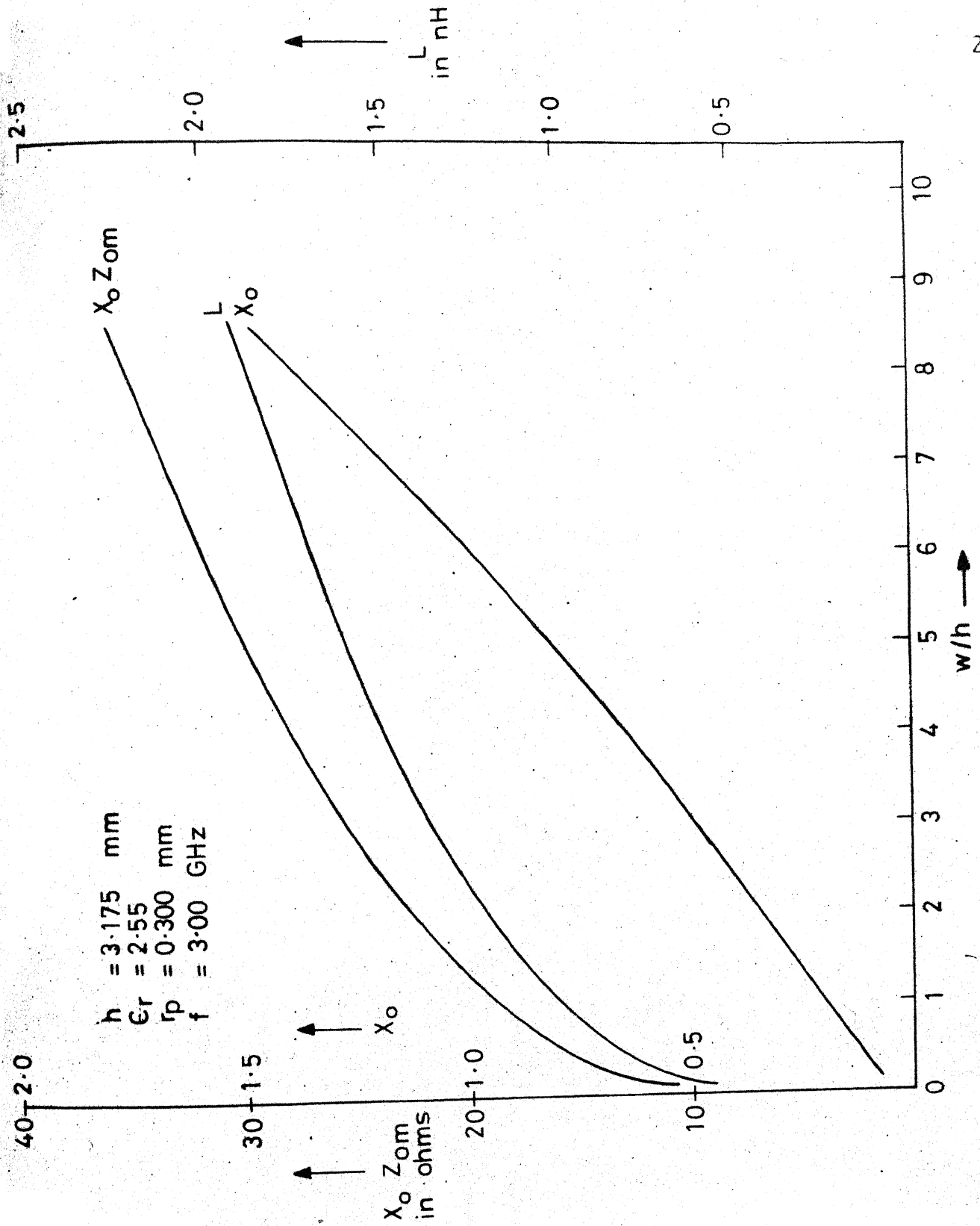
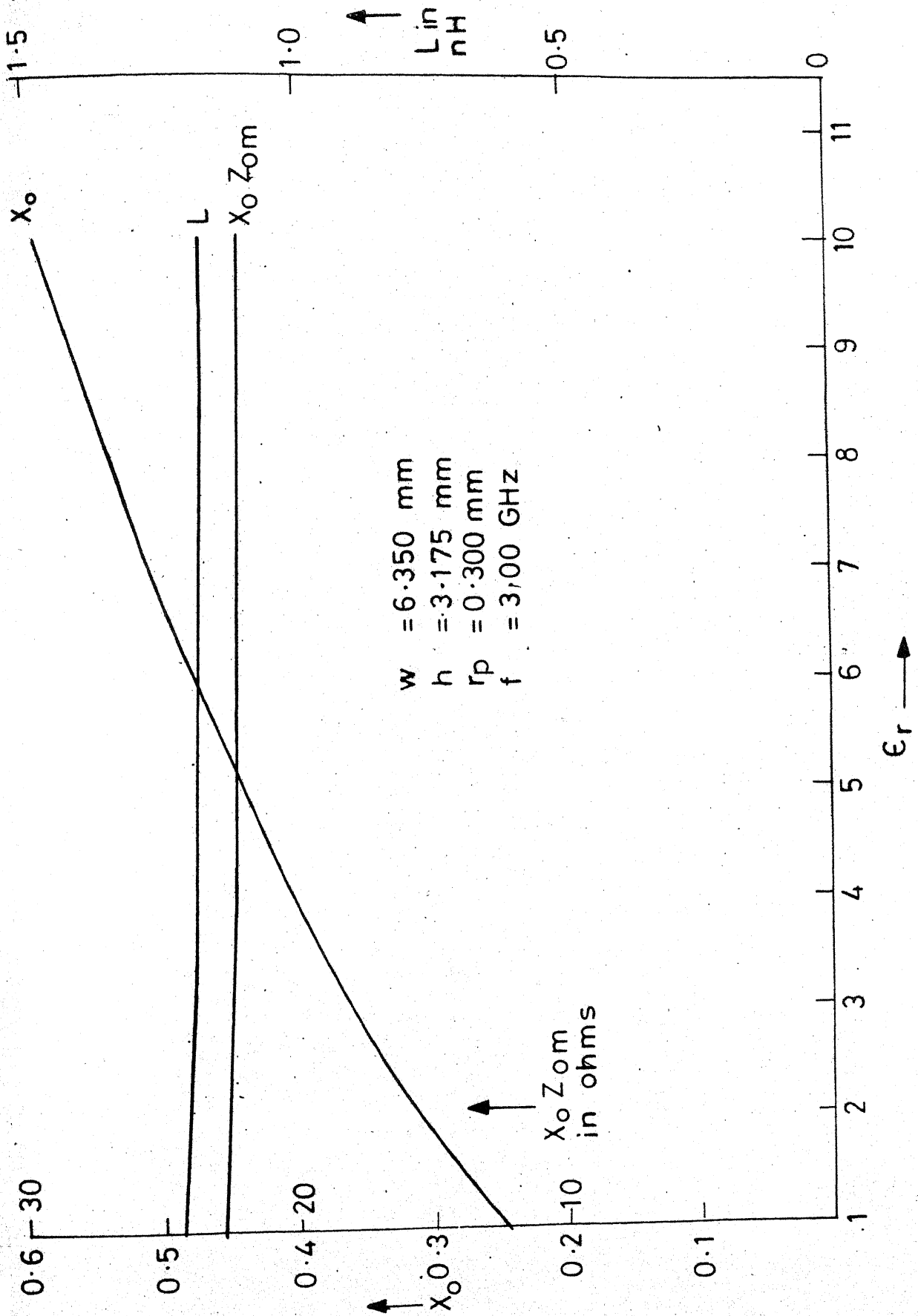


Fig. 6.5 Variation of post reactance and post inductance with w/h

Fig. 6.6 Variation of post reactance and post inductance with ϵ_r

- i) The values of X_o , $X_o Z_{om}$ and L decrease with increase in r_p/w ratio. This behavior is similar to the dependence of post reactance on r_p/a in the case of metallic rectangular waveguide (for results on post loaded rectangular waveguide, see, e.g. reference [5]).
- ii) The values of X_o , $X_o Z_{om}$ and L increase monotonously with increasing w/h ratio. The variation of X_o is approximately linear, whereas the variations of L and $X_o Z_{om}$ are considerably nonlinear.
- iii) The value of X_o increases monotonously with increasing ϵ_r . The values of $X_o Z_{om}$ and L , however, remain more or less constant, which can be expected because, as far as magnetic effects are concerned, the value of ϵ_r is immaterial. Whatever small variations are exhibited by $X_o Z_{om}$ and L can be attributed to the empiricalness of the planar waveguide model employed in the analysis.

6.3 EXPERIMENTAL RESULTS AND DISCUSSION

A direct measurement of the post inductance L through measuring transmission/reflection coefficient would be erroneous due to the uncertain behavior of the ~~coaxial~~-microstrip transitions. It was thus decided to measure L by making

the unknown post resonate with the capacitance of a gap which was deliberately introduced in the strip (see Fig. 6.7a). As is known, the gap can be represented by a Pi-equivalent circuit consisting of a series capacitance C_g and two parallel capacitances C_p (see subsection 2.4.2b of Chapter 2). Thus the configuration shown in Fig. 6.7a can be represented by means of the equivalent capacitance circuit shown in Fig. 6.7b. The equivalent capacitance is

$$C_{eq} = C_p + \frac{C_g C_p}{C_g + C_p} \quad (6.3.1)$$

where C_p and C_g are given by closed-form expressions given in Appendix II. The structure under consideration will thus show maximum transmission at a frequency f_o given by

$$f_o = \frac{1}{2\pi\sqrt{L C_{eq}}} \quad (6.3.2)$$

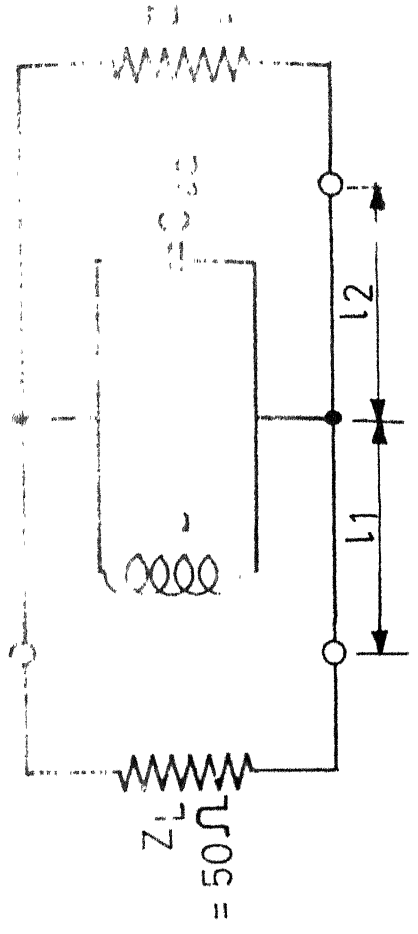
from which L can be calculated as C_{eq} is calculable through eq. (6.3.1) and eqs. (A.2.10)-(A.2.17) and f_o can be measured directly. In the case tested, the following parameter values were used:

$$w = 6.350 \text{ mm}$$

$$h = 3.175 \text{ mm}$$

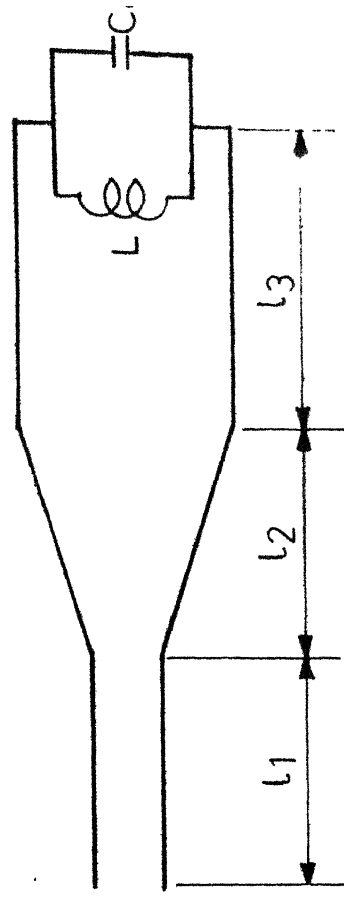
$$s = 3.175 \text{ mm}$$

$$\epsilon_r = 2.55$$

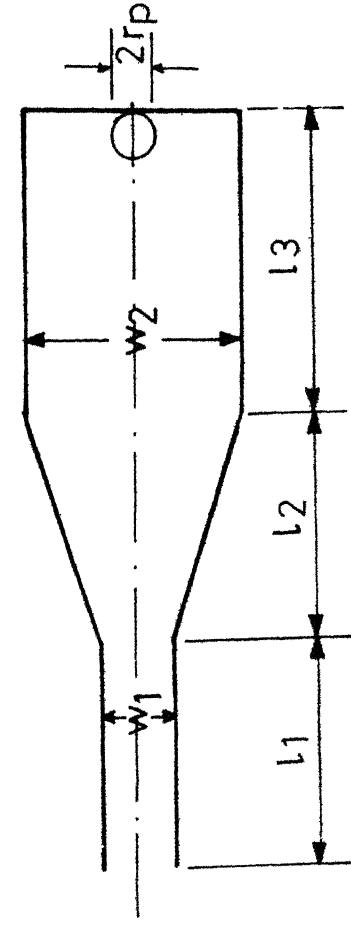


(b) Equivalent circuit

Fig. 6-7 Resonant structure involving a gap and the unknown post



(b) Equivalent circuit



(a) The structure

Fig. 6-8 Resonant structure involving an open-end and the unknown post

$$r_p = 0.406 \text{ mm}$$

$$\ell_1 = 9.00 \text{ mm}$$

$$\text{and } \ell_2 = 10.00 \text{ mm}$$

The maximum transmission was seen to occur at $f_o = 4.98 \text{ GHz}$ which leads to $L = 1.0297 \text{ nH}$. The theoretical value of L at 4.98 GHz is approximately 0.9819 nH . Thus the error involved is approximately 4.87 percent which can easily be attributed to the following factors:

- i) The error due to empirical relations (eqs. (A.2.10)-(A.2.17)) that were used for calculating the gap capacitances, C_p and C_g .
- ii) The planar waveguide model which has been used in the analysis is also a semi-empirical model, and some amount of error can easily be attributed to this factor.

Another configuration was fabricated in which the post was made to resonate with the capacitance C_{oc} produced by an open-end in the microstrip. The configuration is shown, alongwith its equivalent-circuit, in Fig. 6.8. The following values of the parameters were chosen:

$$w_1 = 8.803 \text{ mm}$$

$$w_2 = 17.947 \text{ mm}$$

$$\begin{aligned}
 h &= 3.175 \text{ mm} \\
 \epsilon_r &= 2.55 \\
 r_p &= 0.512 \text{ mm} \\
 \rho_1 &= 10.00 \text{ mm} \\
 \rho_2 &= 30.00 \text{ mm} \\
 \rho_3 &= 10.00 \text{ mm} \\
 Z_{0ml} &= 50 \text{ ohms} \\
 Z_{0m2} &= 30 \text{ ohms}
 \end{aligned}$$

The resonance between L and C_{oc} was experimentally seen to occur at 8.72 GHz. Using eq. (A.2.1) for C_{oc} , this leads to $L = 1.3255 \text{ nH}$, whereas use of eq. (A.2.4) yields $L = 1.7789 \text{ nH}$. The theoretical value of L at 8.72 GHz is 2.1808 nH approximately. The error involved is thus approximately 39.22 percent while using eq. (A.2.1), and approximately 18.43 percent if use of eq. (A.2.4) is made. The following observations can be made:

- i) The error with using eq. (A.2.4) is lesser than that using eq. (A.2.1). This can be expected because eq. (A.2.4) accounts for dispersion effects, whereas eq. (A.2.1) is just a quasi-static approximation.
- ii) Even eq. (A.2.4) accounts for dispersion effects in, at the best, a semi-empirical way. This factor should be kept in mind while analysing the rather large error involved.

- iii) The empiricalness involved by the planar waveguide model should also be kept in mind.
- iv) Since the frequency of resonance is much smaller in case of the configuration shown in Fig. 6.7 than in the configuration of Fig. 6.8, the configuration of Fig. 6.7 yields much more accurate results.

6.4 CONCLUSIONS

- i) The transversely placed discontinuities in MIC lines seem to have received little attention till now. In this chapter, the microstrip loaded with a thin metallic post has been considered.
- ii) The planar waveguide dispersion model of the microstrip has been used for analysis.
- iii) The experimental verification of the theory is done by making the post part of a resonant structure employing open-end/gap discontinuity, and noting the frequency of resonance. The agreement between theory and experiment is within the attributable range.
- iv) The proposed structure can be used to create parallel inductances in microstrip line,

the methods for doing which seem to be unexplored. The characterization of transversely placed post will also help in the design/analysis of many microstrip-slot line launchers (see Fig. 2.23) that use such posts.

- v) The work can easily be extended to the corresponding stripline case.

CHAPTER 7

CONCLUSIONS

7.1 GENERAL

This thesis has been aimed at analysing new types of discontinuity structures involving coaxial line, rectangular waveguide and microstrip line. Numerous practical applications of these new structures have emerged.

A review of the significant work done and the scope of further work follow.

7.2 REVIEW OF THE SIGNIFICANT WORK

Chapter 2 presents the basic principles and an overview of microwave transmission lines currently in use and their discontinuities. The various aspects are put in perspective by dividing the content into six main sections, namely i) coaxial discontinuities, ii) waveguide discontinuities, iii) microstrip discontinuities, iv) junctions of similar lines, v) junctions of dissimilar lines, and vi) methods of experimental characterization of discontinuities. A special emphasis is given on configurations (or aspects thereof) that are relevant to the work reported in this thesis.

Chapter 3 analyses the commonly known broadwall coaxial line - rectangular waveguide junction from the

viewpoint of its applicability to microwave filtering, an aspect which has hitherto not been looked into. It turns out that by terminating the far end of the coaxial line into a movable short-circuit, the configuration can be exploited as a new type of basic prototype for developing waveguide notch filters with large continuous mechanical tunability. Two types of cases are considered, namely i) short-circuited case where the tip of the probe terminates on the waveguide wall and ii) air-gap case where a small air-gap is allowed to exist between the probe tip and waveguide wall. Simple closed-form formulas for the insertion loss of single-stage prototypes are derived, under some suitable simplifying assumptions; the assumption of a constant loss parameter throughout the band and neglect of higher-order waveguide modes that are excited in the vicinity of the E-plane probe being the main ones. The theory, when compared with the experimental results, is seen to be valid mainly for extremely thin (electrically) probes. An extremely thin probe is also necessitated by another practical consideration, namely the pass-band ripples which are experimentally observed to come down to an acceptably low level with extremely thin probes. The theory presented is thus useful for all practical purposes. Detailed theoretical results describing the dependence of filtering parameters (i.e. Q 's, peak insertion loss and

skirt selectivities) on physical parameters (waveguide dimensions, probe radius and characteristic impedance of coaxial line) are presented graphically. These results will serve as a useful guideline to the designer interested in extracting the best possible performance out of the single-stage section, before going to multi-stage designs. Lastly, an attempt is made to incorporate the effects of higher-order waveguide modes in the analysis. It is seen that the amount of algebra involved increases tremendously with the inclusion of each new mode, thereby putting a practical limit to this kind of approach.

The junction considered in Chapter 3 is reconsidered in Chapter 4, with a viewpoint of its applicability to experimental characterization of waveguide mounting structures. Lewin's formulation [13] for a singly-loaded waveguide post is extended to the junction under consideration. The advantage of this formulation over the one presented in Chapter 3 is that all higher-order modes are automatically taken care of. This advantage is, however, partly offset by the larger CPU time required in computations using this formulation. The maxima and minima of the transmission coefficient between the waveguide ports are investigated. It is found that the positions of the movable short for minimum and maximum transmission can be correlated to the parameters of the post

through extremely simple working equations. Consequently, a new simple method of experimental characterization of singly-loaded waveguide posts emerges. The method enjoys unique advantages like ease of implementation, simple working equations, no need of electrical measurements, etc. The method is applied, at X-band, to three different posts and yields excellent results. The extensions of the method to doubly-loaded posts are worked out. The applicability of the method in measuring the input impedance seen at the coaxial port in a broadwall coaxial-waveguide junction is also demonstrated.

Chapter 5 analyses the microstrip counterpart of the junction considered in Chapters 3 and 4. The analysis is done using planar waveguide dispersion model [189] of the microstrip. The resonance condition thus derived is experimentally verified, for two different sets of parameter values. This resonance condition, when properly interpreted, establishes a very useful equivalence for the input reactance seen by the coaxial line in a broadwall coaxial-microstrip launcher namely that the reactance can be written by treating the feed-wire as a thin cylindrical antenna situated in an unbounded homogeneous dielectric-filled space. This result assumes a very special significance in view of the fact that till now virtually no results have been published

on the broadwall coaxial-microstrip launcher. The study reported in Chapter 5 makes a useful beginning in this direction and can be further elaborated.

Chapter 6 analyses the case of a microstrip line loaded in the transverse plane with a thin metallic post. The planar waveguide model [189] is again used. As expected, it turns out that the post offers an inductive reactance across the microstrip. The expression for this reactance is worked out. The theory is experimentally verified, for two different sets of parameter values, by making the post resonate with open-end/gap discontinuity (which can be characterized by available methods) and noting the frequency of resonance. The theory and experiment tally within the attributable error range. Theoretical results describing the dependence of reactance on physical parameters (i.e. aspect ratio of the microstrip, dielectric constant of the substrate and radius of the post) are presented graphically. It should be mentioned that the transverse discontinuities in MIC's, unlike their counterparts in coaxial lines and waveguides, have not received much attention till now. The characterization of a transversely placed metallic post in microstrip, which is the subject of study in Chapter 6, is virtually a totally new beginning and will find application in i) simulating parallel inductances in microstrip lines

and ii) characterization of some microstrip-slot line junctions where transversely placed metallic wires are involved. The results reported can easily be extended to the corresponding stripline case.

7.3 SCOPE FOR FURTHER WORK

Further work can be taken up in the following directions:

- i) Use of theory presented in Chapter 3 to evolve suitable synthesising procedures whereby a given set of specifications as regards notch filtering can be met (using more than one stage if necessary).
- ii) Experimental verification of methods suggested in Sections 4.3 and 4.4.
- iii) Extension of the method presented in Chapter 4 to more complicated mounting structures like centrally-placed gaps, dual gaps, multiple gaps, etc., using formulations given by Eisenhart and Khan [105], El-Sayed [110], Joshi and Cornick [115]-[116], [120] and Williamson [122].
- iv) Extension of the method presented in Chapter 4 to 'two-gap' coaxial-waveguide junctions, using the formulation recently given by Williamson [284].

- v) More detailed experimental verification of the model developed in Chapter 5 for the reactance seen by the coaxial line in a broadwall coaxial-microstrip launcher, with a view to determining the ranges of parameter values within which the model is acceptably accurate.
- vi) More detailed theoretical and experimental characterization of transversely-placed discontinuities in MIC lines.

APPENDIX I

MODES IN A PLANAR WAVEGUIDE

The planar waveguide equivalence of a microstrip line consists of a dielectric-filled rectangular waveguide whose top and bottom walls are electrically conducting and whose side walls are magnetically conducting. The configuration of the planar waveguide is shown in Fig. 2.11. Various dimensions and parameters and the coordinate axes have been chosen as shown.

The planar waveguide structure shown in Fig. 2.11 can support TEM, TE and TM modes. The field analysis of this waveguide for various modes follows.

TEM-mode: In this mode

$$E_z = 0 \quad (\text{A.1.1})$$

$$\text{and } H_z = 0 \quad (\text{A.1.2})$$

The Maxwell's equation $\nabla \times \vec{E} = -j\omega\mu_0 \vec{H}$ gives

$$H_x = \frac{1}{j\omega\mu_0} \frac{\partial E_y}{\partial z} \quad (\text{A.1.3})$$

$$\text{and } H_y = -\frac{1}{j\omega\mu_0} \frac{\partial E_x}{\partial z} \quad (\text{A.1.4})$$

The equation $\nabla \times \vec{H} = j\omega\epsilon_0\epsilon_r \vec{E}$ yields

$$E_x = -\frac{1}{j\omega\epsilon_0\epsilon_{re}} \frac{\partial H_y}{\partial z} \quad (\text{A.1.4})$$

$$\text{and } E_y = \frac{1}{j\omega \epsilon_0 \epsilon_{re}} \frac{\partial H_x}{\partial z} \quad (\text{A.1.6})$$

Suitable eliminations between eqns. (A.1.3)-(A.1.6) give the following equations in E_x and E_y :

$$\frac{\partial^2 E_x}{\partial z^2} + k^2 E_x = 0 \quad (\text{A.1.7a})$$

$$\text{and } \frac{\partial^2 E_y}{\partial z^2} + k^2 E_y = 0 \quad (\text{A.1.7b})$$

$$\text{where } k^2 = \omega^2 \mu_0 \epsilon_0 \epsilon_{re} \quad (\text{A.1.8})$$

It can similarly be shown that

$$\frac{\partial^2 H_x}{\partial z^2} + k^2 H_x = 0 \quad (\text{A.1.7c})$$

$$\text{and } \frac{\partial^2 H_y}{\partial z^2} + k^2 H_y = 0 \quad (\text{A.1.7d})$$

That is, all the non-zero field components E_x , E_y , H_x and H_y satisfy the homogeneous wave equation with respect to the z -coordinate. The z -dependence in all the field components is obviously of the type $\exp(\pm jkz)$.

Now, it is very easy to show from eqns. (A.1.3) - (A.1.6) that

$$\frac{\partial E_y}{\partial x} = \frac{\partial E_x}{\partial y} \quad (\text{A.1.9})$$

$$H_x = H_{xx}(x) e^{\pm jkz} \quad (\text{A.1.15c})$$

$$\text{and } H_y = H_{yy}(y) e^{\pm jkz} \quad (\text{A.1.15d})$$

The boundary conditions to be satisfied by the fields are

$$\begin{aligned} \text{(a) } E_x(y=0, h) &= 0 & 0 \leq x \leq w_e \\ & & -\infty \leq z \leq +\infty \end{aligned} \quad (\text{A.1.16})$$

and

$$\begin{aligned} \text{(b) } H_y(x=0, w_e) &= 0 & 0 \leq y \leq h \\ & & -\infty \leq z \leq +\infty \end{aligned} \quad (\text{A.1.17})$$

Since E_x is anyway independent of y , the boundary condition a) demands that

$$\begin{aligned} E_x &= 0 & 0 \leq x \leq w_e \\ & & 0 \leq y \leq h \\ & & -\infty \leq z \leq +\infty \end{aligned} \quad (\text{A.1.18})$$

Similarly the boundary condition b) demands that

$$\begin{aligned} H_y &= 0 & 0 \leq x \leq w_e \\ & & 0 \leq y \leq h \\ & & -\infty \leq z \leq +\infty \end{aligned} \quad (\text{A.1.19})$$

So the only non-vanishing field components are E_y and H_x . These field components are related through eq. (A.1.3). Thus

$$j\omega\mu_0 H_x = \pm jkE_y$$

or

$$\frac{E_y}{H_x} = \pm \frac{\omega\mu_0}{k} \quad (\text{A.1.20})$$

which means both E_{yy} and H_{xx} in eq. (A.1.15) must be constants. Thus finally

$$E_y = A e^{+jkz} + B e^{-jkz} \quad (\text{A.1.21})$$

and

$$H_x = \frac{k}{\omega\mu_0} [A e^{+jkz} - B e^{-jkz}] \quad (\text{A.1.22})$$

are the general solutions for the field components, where A and B are the two arbitrary constants involved.

TE-modes : Say $\vec{E} = \nabla \times (\psi_e \hat{i}_z)$ (A.1.23)

whereby $E_x = \frac{\partial \psi'_e}{\partial y}$ (A.1.24)

$$E_y = -\frac{\partial \psi'_e}{\partial x} \quad (\text{A.1.25})$$

$$H_x = -\frac{1}{j\omega\mu_0} \frac{\partial^2 \psi'_e}{\partial x \partial z} \quad (\text{A.1.26})$$

$$H_y = -\frac{1}{j\omega\mu_0} \frac{\partial^2 \psi'_e}{\partial y \partial z} \quad (\text{A.1.27})$$

and

$$H_z = \frac{1}{j\omega\mu_0} \left[\frac{\partial^2 \psi'_e}{\partial x^2} + \frac{\partial^2 \psi'_e}{\partial y^2} \right] \quad (\text{A.1.28})$$

It can easily be shown that the scalar function ψ_e satisfies the inhomogeneous wave equation

$$(\nabla^2 + k^2) \psi_e = 0 \quad (\text{A.1.29})$$

where

$$\nabla^2 \equiv \frac{\partial^2}{\partial x^2} + \frac{\partial^2}{\partial y^2} + \frac{\partial^2}{\partial z^2}$$

and k is defined by eq. (A.1.8).

Assuming a product solution

$$\psi'_e(x, y, z) = X(x) Y(y) Z(z) \quad (\text{A.1.30})$$

and substituting in eq. (A.1.29) as usual, we arrive at the general expression for ψ_e :

$$\begin{aligned} \psi'_e(x, y, z) = & (A \sin k_x x + B \cos k_x x) (C \sin k_y y + D \cos k_y y) \\ & (E e^{jk_z z} + F e^{-jk_z z}) \end{aligned} \quad (\text{A.1.31})$$

where A, B, C, D, E and F are the six arbitrary constant involved and

$$k^2 = k_x^2 + k_y^2 + k_z^2 \quad (\text{A.1.32})$$

The arbitrary constants can be evaluated using the following boundary conditions:

$$\begin{aligned} \text{a) } E_x(y=0, h) &= 0 & 0 \leq x \leq w_e \\ & & -\infty \leq z \leq \infty \end{aligned} \quad (\text{A.1.33})$$

$$\begin{aligned} \text{b) } H_y(x=0, w_e) &= 0 & 0 \leq y \leq h \\ & & -\infty \leq z \leq +\infty \end{aligned} \quad (\text{A.1.34})$$

$$\begin{aligned} \text{c) } H_z(x=0, w_e) &= 0 & 0 \leq x \leq w_e \\ & & 0 \leq y \leq h \end{aligned} \quad (\text{A.1.35})$$

The condition a) gives $C = 0$ (A.1.36)

$$k_y = \frac{n\pi}{h} \quad (\text{A.1.37})$$

and the condition b) gives $B = 0$ (A.1.38)

$$k_x = \frac{m\pi}{w_e} \quad (\text{A.1.39})$$

It can be shown that the condition c) is, in view of eqs. (A.1.36)-(A.1.39), is automatically satisfied. Thus,

$$\psi_{c_{m,n}} = A_{m,n} \sin \frac{m\pi x}{w_e} \cos \frac{n\pi y}{h} e^{\pm jk_{z_{m,n}} z} \quad (\text{A.1.40})$$

where $m = 1, 2, 3, \dots$

$n = 0, 1, 2, \dots$

and

$$k_{z_{m,n}}^2 = k^2 - \left(\frac{m\pi}{w_e}\right)^2 - \left(\frac{n\pi}{h}\right)^2 \quad (\text{A.1.41})$$

The expressions for the field components follows.

$$E_x = -\frac{n\pi A_{m,n}}{h} \sin \frac{m\pi x}{w_e} \sin \frac{n\pi y}{h} e^{\pm jk_{z_{m,n}} z} \quad (\text{A.1.42a})$$

$$E_y = -\frac{m\pi A_{m,n}}{w_e} \cos \frac{m\pi x}{w_e} \cos \frac{n\pi y}{h} e^{\pm jk_{z_{m,n}} z} \quad (\text{A.1.42b})$$

$$(\text{A.1.42c})$$

$$E_z = 0$$

$$H_x = \mp \frac{k_{z_{m,n}}}{\omega\mu_0} \frac{n\pi A_{m,n}}{h} \sin \frac{m\pi x}{w_e} \sin \frac{n\pi y}{h} e^{\pm jk_{z_{m,n}} z} \quad (\text{A.1.42e})$$

and

$$H_z = - \frac{\Lambda_{m,n}}{j\omega\mu_0} \left[\left(\frac{m\pi}{w_e} \right)^2 + \left(\frac{n\pi}{h} \right)^2 \right] \sin \frac{m\pi x}{w_e} \cos \frac{n\pi y}{h} e^{\pm jk_{z_{m,n}} z} \quad (\text{A.1.42f})$$

TM-modes: Assume $\vec{H} = \nabla \times (\psi_h \mathbf{i}_z)$ (A.1.43)

so that $H_x = \frac{\partial \psi_h}{\partial y}$ (A.1.44)

$$H_y = -\frac{\partial \psi_h}{\partial x} \quad (\text{A.1.45})$$

$$E_x = \frac{1}{j\omega \epsilon_0 \epsilon_{re}} \frac{\partial^2 \psi_h}{\partial x \partial z} \quad (\text{A.1.46})$$

$$E_y = \frac{1}{j\omega \epsilon_0 \epsilon_{re}} \frac{\partial^2 \psi_h}{\partial y \partial z} \quad (\text{A.1.47})$$

and

$$E_z = - \frac{1}{j\omega \epsilon_0 \epsilon_{re}} \left[\frac{\partial^2 \psi_h}{\partial x^2} + \frac{\partial^2 \psi_h}{\partial y^2} \right] \quad (\text{A.1.48})$$

ψ_h can be shown to satisfy

$$(\nabla^2 + k^2) \psi_h = 0 \quad (\text{A.1.49})$$

whose solution, consistent with the boundary conditions involved, is

$$\psi_{h_{m,n}} = A_{m,n} \cos \frac{m\pi x}{w_e} \sin \frac{n\pi y}{h} e^{\pm jk_{z_{m,n}} z} \quad (\text{A.1.50})$$

where $k_{z_{m,n}}$ is as given by eq. (A.1.41).

The field expressions follow:

$$H_x = \frac{n\pi A_{m,n}}{h} \cos \frac{m\pi x}{w_e} \cos \frac{n\pi y}{h} e^{\pm jk_{z_{m,n}} z} \quad (\text{A.1.51a})$$

$$H_y = - \frac{m\pi A_{m,n}}{w_e} \sin \frac{m\pi x}{w_e} \sin \frac{n\pi y}{h} e^{\pm jk_{z_{m,n}} z} \quad (\text{A.1.51b})$$

$$H_z = 0 \quad (\text{A.1.51c})$$

$$E_x = \pm \frac{k_{z_{m,n}}}{\omega \epsilon_o \epsilon_{re}} \frac{m\pi A_{m,n}}{w_e} \sin \frac{m\pi x}{w_e} \sin \frac{n\pi y}{h} e^{\pm jk_{z_{m,n}} z} \quad (\text{A.1.51d})$$

$$E_y = \pm \frac{k_{z_{m,n}}}{\omega \epsilon_o \epsilon_{re}} \frac{n\pi A_{m,n}}{h} \cos \frac{m\pi x}{w_e} \cos \frac{n\pi y}{h} e^{\pm jk_{z_{m,n}} z} \quad (\text{A.1.51e})$$

$$E_z = \frac{A_{m,n}}{j\omega \epsilon_o \epsilon_{re}} \left[\left(\frac{m\pi}{w_e} \right)^2 + \left(\frac{n\pi}{h} \right)^2 \right] \cos \frac{m\pi x}{w_e} \sin \frac{n\pi y}{h} e^{\pm jk_{z_{m,n}} z} \quad (\text{A.1.51f})$$

For practical cases, $h \ll \lambda$. This makes the propagation of any mode having $n > 0$ impossible at the conventional microwave frequencies, as can be seen from eq. (A.1.41). In other words, for $h \ll \lambda$, only $n=0$ mode has its operating band in the microwave region. However, as can be seen from eq. (A.1.51), $n=0$ makes all the field components zero. Thus, it can be concluded that for $h \ll \lambda$, no TM modes can exist on a planar waveguide.

APPENDIX II

EQUIVALENT-CIRCUIT PARAMETERS OF OPEN-END AND GAP DISCONTINUITIES IN A MICROSTRIP LINE

The open-end and gap discontinuities in a microstrip line are shown, alongwith their equivalent circuits, in Figs. 2.12 and 2.13, respectively. The various closed-form easy-to-use expressions for the parameters of equivalent circuits of these discontinuities follow.

OPEN-END: A very simple empirical formula for the capacitance C_{oc} of an open-ended microstrip was given by Silvester and Benedek [202] in 1972. This formula was obtained by Curve-fitting the numerical results that were computed by these authors using the method of line sources with charge reversal. The formula follows:

$$\frac{C_{oc}}{w} (\text{pF/m}) = \exp \left[\ln 10 \sum_{i=1}^5 C_i (\epsilon_r) \left(\log \frac{w}{h} \right)^{i-1} \right] \quad (\text{A.2.1})$$

where C_i 's are the numerical constants tabulated in reference [202] for $\epsilon_r = 1.0, 2.5, 4.2, 9.6, 16.0$ and 51.0 . For $\epsilon_r = 2.5$, the values of C_i are $1.295, -0.2817, 0.1367, -0.0133, -0.0267$ for $i=1,2,3,4,5$ respectively.

The equivalent line length Δl_{oc} can be obtained from C_{oc} by

$$\Delta Z_{oc} = \frac{C_{oc} Z_{om}}{\sqrt{\epsilon_{re}}} \quad (A.2.2)$$

An empirical expression for $\Delta l_{oc}/h$ was also reported by Gary and Bahl [207] in 1978. The expression follows:

$$\frac{\Delta l_{oc}}{h} = 0.412 \frac{(\epsilon_{re} + 0.300)(w/h + 0.264)}{(\epsilon_{re} - 0.258)(w/h + 0.800)} \quad (A.2.3)$$

Maximum relative error in this expression, as compared against eq. (A.2.1), is less than 4 percent for $w/h \geq 0.20$ and $2 \leq \epsilon_r \leq 50$.

The above mentioned expressions are obtained quasi-statically and do not take into account the effects of dispersion. A frequency-dependent expression for C_{oc} in case of a shielded microstrip has recently been given by Bedair and Sobhy [203]-[204]. For an unshielded microstrip, the formula given by these authors simplifies to

$$C_{oc} = \frac{C}{\beta_e} \arccot \left[\frac{0.882 + w/h}{0.220 + w/h} \cot(0.441 \beta_e h) \right] \quad (A.2.4)$$

$$\text{where } \beta_e = \frac{2\pi}{\lambda} \epsilon_r \quad (A.2.5)$$

and the capacitance per unit length of the microstrip is given by

$$C = \frac{\epsilon_r}{c 60\pi} \frac{K(k)}{K(k')} \quad (A.2.6)$$

$$\text{with } k = \tanh \left(\frac{\pi}{4} \frac{w}{h} \right) \quad (\text{A.2.7})$$

$$\text{and } k' = \sqrt{1-k^2} \quad (\text{A.2.8})$$

In eq. (A.2.5), $K(k)$ represents the complete elliptic integral of first kind having argument k . The following relations can be used to compute $K(k)/K(k')$:

$$\frac{K(k)}{K(k')} = \frac{1}{\pi} \ln \frac{2(1+\sqrt{k})}{1-\sqrt{k}}$$

$$\text{for } 0.707 \leq k < 1$$

$$= \frac{\pi}{\ln \frac{2(1+\sqrt{k'})}{1-\sqrt{k'}}}$$

$$\text{For } 0 \leq k \leq 0.707 \quad (\text{A.2.9})$$

A simplified quasi-static expression that approximates eq. (A.2.4) within 3 percent for $\beta_e h \leq 0.68$ is

$$C_{oc} = 0.441hC \frac{0.220+w/h}{0.882+w/h} \quad (\text{A.2.10})$$

GAP: Only quasi-static results seem to have been reported for a gap in microstrip. By curve-fitting the numerical results computed by Benedek and Silvester [205], Garg and Bahl [207] derived the following expressions for the equivalent-circuit parameters of a microstrip gap:

$$\frac{C_o}{w} \text{ (pF/m)} = \left(\frac{s}{w} \right)^{mo} \exp(k_o) \quad (\text{A.2.11})$$

$$\frac{C_e}{w} \text{ (pF/m)} = \left(\frac{s}{w}\right)^{m_e} \exp(k_e) \quad (\text{A.2.12})$$

where

$$\begin{aligned} m_o &= \frac{w}{h} (0.619 \log \frac{w}{h} - 0.3853) \\ k_o &= 4.26 - 1.453 \log \frac{w}{h} \\ &\text{for } 0.1 \leq s/w \leq 1.0 \end{aligned} \quad (\text{A.2.13})$$

$$\begin{aligned} m_e &= 0.4675 \\ k_e &= 2.043 \left(\frac{w}{h}\right)^{0.12} \\ &\text{for } 0.1 \leq s/w \leq 0.3 \end{aligned} \quad (\text{A.2.14a})$$

$$\begin{aligned} m_e &= \frac{1.565}{(w/h)^{0.16}} - 1 \\ k_e &= 1.97 - \frac{0.03}{w/h} \\ &\text{for } 0.3 \leq s/w \leq 1.0 \end{aligned} \quad (\text{A.2.14b})$$

These formulas are valid for the range $0.5 \leq w/h \leq 2.0$ and apply for $\epsilon_r = 9.6$ only. For any other value of ϵ_r in the range of $2.5 \leq \epsilon_r \leq 15.0$, the values of C_o and C_e can be calculated from

$$C_o(\epsilon_r) = C_o(9.6) (\epsilon_r/9.6)^{0.8} \quad (\text{A.2.15})$$

and

$$C_e(\epsilon_r) = C_e(9.6) (\epsilon_r/9.6)^{0.9} \quad (\text{A.2.16})$$

Once C_o and C_e are known, C_p and C_g can be found from

$$C_p = \frac{1}{2} C_e \quad (\text{A.2.17})$$

and

$$C_g = \frac{1}{2} (C_o - \frac{C_e}{2}) \quad (\text{A.2.18})$$

Equivalent line length may be calculated using

$$\Delta l_g = \frac{c C_p Z_{om}}{V \epsilon_{re}} \quad (\text{A.2.19})$$

The accuracy of the above expressions is within 7 percent, as compared against the numerical results [205], for the specified ranges of parameters values.

REFERENCES

- [1] L.G.H. Huxley, A Survey of the Principles and Practice of Waveguides , Cambridge: University Press, 1947.
- [2] G.L. Ragan, Microwave Transmission Circuits , New York: McGraw Hill, 1948.
- [3] C.G. Montgomery, R.H. Dicke and E.M. Purcell, Principles of Microwave Circuits , New York: McGraw Hill, 1948.
- [4] T. Moreno, Microwave Transmission Design Data , New York: Dover Publications, 1948.
- [5] N. Marcuvitz, 'Waveguide Handbook', New York: McGraw-Hill, 1951.
- [6] L. Lewin, Advanced Theory of Waveguides , London: Illiffe, 1951.
- [7] R.W.P. King, H.R. Mimno and A.H. Wing, Transmission Lines Antennas and Waveguides', New York: Dover Publications, 1965.
- [8] J. Schwinger and D.S. Saxon, Discontinuities in Waveguides . New York: Gordon and Breach, 1968.
- [9] R.E. Collin, Field Theory of Guided Waves , New York: McGraw-Hill, 1960.
- [10] R.F. Harrington, Time-Harmonic Electromagnetic Fields , New York: McGraw-Hill, 1961.
- [11] L. Young, Advances in Microwaves. vol. 2, New York: Academic Press, 1967.
- [12] R. Mittra and S.W. Lee, 'Analytical Techniques in the Theory of Guided Waves', New York: MacMillan, 1971.
- [13] L. Lewin, Theory of Waveguides . London: Newnes-Butterworths, 1975.
- [14] J.R. Whinnery and H.W. Jamieson, 'Equivalent circuits for discontinuities in transmission lines', Proc. IRE, vol. 32, pp. 98-114, February 1944.

- [15] J.R. Whinnery, H.W. Jamieson, and T.E. Robbins, 'Coaxial line discontinuities', Proc. IRE, vol. 32, pp. 695-709, November 1944.
- [16] P.I. Somlo, 'Calculating Coaxial transmission line step capacitance', IEEE Transact. on MTT, vol. 11, no. 9, p. 454, September 1963.
- [17] P.I. Somlo, 'The computation of coaxial line step capacitances', IEEE Transact. on MTT, vol. 15, no. 1, pp. 48-53, January 1967.
- [18] A. Giefing, 'Coaxial impedance inverter design', IEEE Transact. on MTT, vol. 21, no. 3, p. 135, March 1973.
- [19] A. Jurkus, 'Computation of step discontinuities in coaxial line', IEEE Transact. on MTT, vol. 20, no. 10, pp. 708-709, October 1972.
- [20] I. Sreenivasiah and D.C. Chang, 'A variational expression for the scattering matrix of a double-step discontinuity in a coaxial line and its application to a TEM cell', IEEE, Transact. on MTT, vol. 29, no. 1, pp. 40-47, January 1981.
- [21] H.J. Riblet, 'The exact dimensions of a family of rectangular coaxial lines with given impedance', IEEE Transact. on MTT, vol. 20, no. 8, pp. 538-541, August 1972. Also see Addendum: vol. MTT-22, pp. 473-474, April 1974.
- [22] H.J. Riblet, 'An accurate determination of the characteristic impedance of the coaxial system consisting of a square concentric with a circle', IEEE Transact. on MTT, vol. 23, no. 8, pp. 714-715, August 1975.
- [23] R. Terakado, 'The characteristic impedance of rectangular coaxial line with ratio 2:1 of outer-to-inner conductor side length', IEEE Transact. on MTT, vol. 24, no. 2, pp. 124-125, February 1976.
- [24] P.A.A. Laura and L.E. Luisoni, 'Approximate determination of the characteristic impedance of the coaxial system consisting of a regular polygon concentric with a circle', IEEE Transact. on MTT, vol. 25, no. 2, pp. 160-161, February 1977.

- [25] P.A.A. Laura and L.E. Luisoni, 'An application of conformal mapping to the determination of the characteristic impedance of a class of coaxial systems', IEEE Transact. on MTT, vol. 25, no. 2, pp. 162-163, February 1977.
- [26] C.M. Weil, 'The characteristic impedance of rectangular transmission lines with thin center conductor and air dielectric', IEEE Transact. on MTT, vol. 26, no. 4, pp. 238-242, April 1978.
- [27] J.C. Tippet and D.C. Chang, 'Characteristic impedance of a rectangular coaxial line with offset inner conductor', IEEE Transact. on MTT, vol. 26, no. 11, pp. 876-883, November 1978.
- [28] H.J. Riblet, 'The characteristic impedance of a family of rectangular coaxial structures with off-centered strip inner conductors', IEEE Transact. on MTT, vol. 27, no. 4, pp. 294-298, April 1979.
- [29] L. Gruner, 'Estimating rectangular coaxial cut-off', Microwave Journal, vol. 22, no. 4, pp. 88-92, April 1979.
- [30] K. Tsuruta and R. Terakado, 'Easy determination of the characteristic impedance of the coaxial system consisting of an inner regular polygon concentric with an outer circle', IEEE Transact. on MTT, vol. 28, no. 2, pp. 147-149, February 1980.
- [31] L. Gruner, 'Characteristics of crossed rectangular coaxial structures', IEEE Transact. on MTT, vol. 28, no. 6, pp. 622-627, June 1980.
- [32] H.J. Riblet, 'Upper limits on the error of an improved approximation for the characteristic impedance of rectangular coaxial line', IEEE Transact. on MTT, vol. 28, no. 6, pp. 666-667, June 1980.
- [33] H.J. Rib let, 'Two limiting values of the capacitance of symmetrical rectangular coaxial strip transmission line', IEEE Transact. on MTT, vol. 29, no. 7, pp. 661-666, July 1981.
- [34] W.Lin, 'A critical study of the coaxial transmission line utilizing conductors of both circular and square cross-sections', IEEE Transact. on MTT, vol. 30, no. 11, pp. 1981-1988, November 1982.

- [35] J.C. Beal, J. Jostak, S.F. Mahmoud, and V. Rawat, 'Continuous-access guided communication (CAGC) for ground transportation systems', Proc. IEEE, vol. 61, no.5, pp. 562-568, May 1973.
- [36] D.J.R. Martin, 'A general study of the leaky feeder principle', Radio Electron. Engr., vol. 45, pp. 205-214, 1975.
- [37] P. Delogne and M. Safak, 'Electromagnetic theory of the leaky coaxial cable', Radio Electron. Engr., vol. 45, pp. 233-240, 1975.
- [38] J.R. Wait, 'Electromagnetic theory of the loosely braided coaxial cable: Part I', IEEE Transact. on MTT, vol. 24, no. 9, pp. 547-554, September 1976.
- [39] J.R. Wait, 'Electromagnetic field analysis for a coaxial cable with periodic slots', IEEE Transact. on EMC, vol. 19, no. 1, pp. 7-13, February 1977.
- [40] R.S. Tomar, 'Analysis of leaky coaxial cable used in mine communication', M.Tech. thesis, Department of Elect. Engrg., Indian Institute of Technology, Kanpur, India, 1978.
- [41] R.S. Tomar and Alaknanda Paul, 'Surface transfer impedance of a loosely braided cable', IEEE/AP-s Int. Symp., 1979.
- [42] R.S. Tomar and Alaknanda Paul, 'Analysis of leaky coaxial cable used in mine communication', IEEE/AP-s Int. Symp., 1980.
- [43] D.A. Hill and J.R. Wait, 'Propagation along a coaxial cable with a helical shield', IEEE Transact. on MTT, vol. 28, no. 2, pp. 84-89, February 1980.
- [44] D.A. Hill and J.R. Wait, 'Electromagnetic theory of the loosely braided coaxial cable: Part II, Numerical results', IEEE Transact. on MTT, vol. 28, no. 4, pp. 326-331, April 1980.
- [45] P.P. Delogne and A.A. Laloux, 'Theory of the slotted coaxial cable', IEEE Transact. on MTT, vol. 28, no. 10, pp. 1102-1107, October 1980.

- [46] A.S.D.C. Fernandes, 'Slotted and loose braided cables: Brief conclusions of a comparative study', IEEE Transact. on MTT, vol. 29, no. 3, pp. 273-275, March 1981.
- [47] C.P. Womack, 'The use of exponential transmission lines in microwave components', IEEE Transact. on MTT, vol. 10, no. 2, pp. 124-132, March 1962.
- [48] N. Seshagiri, 'A nonuniform coaxial line with an isoperimetric sheath deformation', IEEE Transact. on MTT, vol. 11, no. 6, pp. 478-486, November 1963.
- [49] J.E. Cruz and R.L. Brooke, 'A variable characteristic impedance coaxial line', IEEE Transact. on MTT, vol. 13, no. 4, pp. 477-478, July 1965.
- [50] R.S. Mueller and F.J. Rosenbaum, 'Propagation in ferrite-filled coaxial transmission lines', IEEE Transact. on MTT, vol. 16, no. 10, pp. 835-842, October 1968.
- [51] M.M. Weiner, 'Conditions for approximating the limit - TEM mode by quasi-TEM mode in a ferrite-filled coaxial line', IEEE Transact. on MTT, vol. 21, no. 3, pp. 156-157, March 1973.
- [52] K. Kobayashi, Y. Nemoto and R. Sato, 'Kuroda's identity for mixed lumped and distributed circuits and their application to nonuniform transmission lines', IEEE Transact. on MTT, vol. 29, no. 2, pp. 81-86, February 1981.
- [53] K. Kobayashi, Y. Nemoto, and R. Sato, 'Equivalent representations of nonuniform transmission lines based on the extended Kuroda's identity', IEEE Transact. on MTT, vol. 30, no. 2, pp. 140-146, February 1982.
- [54] R.A. Sparks, 'A technique for obtaining d.c. isolation in coaxial cable RF transmission lines', IEEE Transact. on MTT, vol. 9, no. 4, p. 360, July 1961.
- [55] H.N. Dawirs, 'Equivalent circuit of a series gap in the center conductor of a coaxial transmission line', IEEE Transact. on MTT, vol. 17, no. 2, pp. 127-129, February 1969.
- [56] S. Sen and P.K. Saha, 'Equivalent circuit of a gap in the central conductor of a coaxial line', IEEE Transact. on MTT, vol. 30, no. 11, pp. 2026-2029, November 1982.

- [57] G. Goubau, 'Surface waves and their application to transmission line', J. Appl. Phys., vol. 21, no. 11, pp. 1119-1128, November 1950.
- [58] S.S. Attwood, 'Surface wave propagation over a coated plane conductor', J. Appl. Phys., vol. 22, no. pp. 504-509, April 1954.
- [59] R.E. Collin, Foundations for Microwave Engineering. New York: McGraw-Hill, 1966.
- [60] L. Young, Advances in Microwaves, vol. 1. New York: McGraw-Hill, 1966.
- [61] L. Young, Advances in Microwaves, vol. 4, New York: McGraw-Hill, 1969.
- [62] N.S. Kapany and J.J. Burke, Optical Waveguides. New York: Academic Press, 1972.
- [63] A.K. Ghatak and M.S. Sodha, Inhomogeneous Optical Waveguides. New York: Plenum Press, 1977.
- [64] R.M. Knox, 'Dielectric waveguide microwave integrated circuits - an overview', IEEE Transact. on MTT, vol. 24, no. 11, pp. 806-814, November 1976.
- [65] Special Issue on Open Guided Wave Structures, IEEE Transact. on MTT, vol. 29, no. 9, pp. 841-996, September 1981.
- [66] L.J. Chu, 'Electromagnetic waves in elliptic hollow pipes of metal', J. Appl. Phys., 9, 583 (1938).
- [67] G. Goubau, Electromagnetic Waveguides and Cavities. Oxford: Pergamon Press, 1961.
- [68] M. Chi and P.A. Laura, 'Approximate method of determining the cut-off frequencies of waveguides of arbitrary cross-section', IEEE Transact. on MTT, vol. 12, no. 2, pp. 248-249, March 1964.
- [69] R.A. Waldron, The Theory of Waveguides and Cavities. New York: Gordon and Breach, 1967.
- [70] J.G. Kretzschmar, 'Wave propagation in hollow conducting elliptical waveguides', IEEE Transact. on MTT, vol. 18, no. 9, pp. 547-554, September 1970.

- [71] J.G. Kretzschmar, 'Attenuation characteristics of hollow conducting elliptical waveguides', IEEE Transact. on MTT, vol. 20, no. 4, pp. 280-284, April 1972. Also see comments by G. Falciasecca et.al. , vol. MTT-21, no. 3, p. 154, March 1973.
- [72] P.A. Laura, 'The solution of Helmholtz equation in elliptical domain', IEEE Transact. on MTT, vol. 20, no. 4, p. 292, April 1972.
- [73] P. Lagasse and J.V. Bladel, 'Square and rectangular waveguides with rounded corners', vol. 20, no. 5, pp. 331-337, May 1972.
- [74] T. Larsen, 'On the relation between modes in rectangular, elliptical, and parabolic waveguides and a mode-classifying system', IEEE Transact. on MTT, vol. 20, no. 6, pp. 379-384, June 1972.
- [75] J. Davies, 'Review of methods for numerical solution of the hollow waveguide problem', Proc. IEEE, vol. 119, pp. 33-37, 1972.
- [76] A.M.B. Al-Sherbiny, 'Cut off wavelengths of ridged, circular, and elliptic guides', IEEE Transact. on MTT, vol. 21, no. 1, pp. 7-12, January 1973.
- [77] M.J. English, 'The circular waveguide step-discontinuity mode transducer', IEEE Transact. on MTT, vol. 21, no. 10, pp. 633-636, October 1973.
- [78] F.L. Luk, 'Tabulation of methods for the numerical solution of the hollow waveguide problem', IEEE Transact. on MTT, vol. 22, no. 3, pp. 322-329, March 1974.
- [79] P. Dely, 'Polar geometry waveguides by finite-element methods', IEEE Transact. on MTT, vol. 22, no. 3, pp. 202-209, March, 1974.
- [80] L. Lewin and A.M.B. Al-Hariri, 'The effect of cross-section curvature on attenuation in elliptic waveguides and a basic correction to previous formulas', IEEE Transact. on MTT, vol. 22, no. 5, pp. 504-509, May 1974.
- [81] M.H. Chen, G.N. Tsandoulas, and F.G. Willwerth, 'Modal characteristics of quadruple-ridged circular and square waveguides', IEEE Transact. on MTT, vol. 22, no. 8, pp. 301-304, August 1974.

- [82] T. Lugiura and H. Suga, 'The susceptance of an annular metallic strip in a circular waveguide with incident TE₀₁ mode', IEEE Transact. on MTT, vol. 27, no. 2, pp. 160-167, February 1979.
- [83] L. Lewin and T. Ruehle, 'Propagation in twisted square waveguide', IEEE Transact. on MTT, vol. 28, no. 1, pp. 44-48, January 1980.
- [84] P.A.A. Laura, K. Nagaya, and G.S. Sarmiento, 'Numerical experiments on the determination of cutoff frequencies of waveguides of arbitrary cross-section', IEEE Transact. on MTT, vol. 28, no. 6, pp. 568-572, June 1980.
- [85] A. Kisliuk, 'Dyadic Green's functions for cylindrical waveguides and cavities', IEEE Transact. on MTT, vol. 28, no. 8, pp. 894-898, August 1980.
- [86] J. Mazumdar, 'A method for the study of TE and TM modes in waveguides of very general cross-section', IEEE Transact. on MTT, vol. 28, no. 9, pp. 991-995, September 1980.
- [87] S.N. Rangarajan and J.E. Lewis, 'Dielectric loaded elliptical waveguides', IEEE Transact. on MTT, vol. 28, no. 10, pp. 1085-1089, October 1980.
- [88] D. Dasgupta and P.K. Saha, 'Eigen-value spectrum of rectangular waveguide with two symmetrically placed double ridges', IEEE Transact. on MTT, vol. 29, no. 1, pp. 47-51, January 1981.
- [89] F. Cap, 'Toroidal resonators and waveguides of arbitrary cross-section', IEEE Transact. on MTT, vol. 29, no. 10, pp. 1053-1059, October 1981.
- [90] T.E. Rozzi, 'Equivalent network for thick inductive irises', IEEE Transact. on MTT, vol. 20, no. 5, pp. 323-330, May 1972.
- [91] T.E. Rozzi, 'A series transformation for diaphragm type discontinuities in waveguide', IEEE Transact. on MTT, vol. 20, no. 11, pp. 770-771, November 1972.
- [92] L. Lewin and J.P. Montgomery, 'A quasi-dynamic method of solution of a class of waveguide discontinuity problems', IEEE Transact. on MTT, vol. 20, no. 12, pp. 849-852, December 1972.

- [93] T.E. Rozzi, 'The variational treatment of thick interacting inductive irises', IEEE Transact. on MTT, vol. 21, no. 2, pp. 82-83, February 1973.
- [94] T.E. Rozzi, 'Network analysis of strongly coupled transverse apertures in waveguides', Int. J. Circuit Theory Appl., vol. 1, pp. 161-173, June 1973.
- [95] R.J. Luebbers and B.A. Munk, 'Analysis of thick rectangular waveguide windows with finite conductivity', IEEE Transact. on MTT, vol. 21, no. 7, pp. 461-468, July 1973.
- [96] T.E. Rozzi and J.F.G. Mecklenbrauker, 'Wide-band network modeling of interactive inductive irises and steps', IEEE Transact. on MTT, vol. 23, no. 2, pp. 235-245, February 1975.
- [97] T.E. Rozzi, 'A new approach to network modeling of capacitive irises and steps in waveguide', Int. J. Circuit Theory Appl., vol. 3, pp. 339-354, December 1975.
- [98] A.S. Havarro, T.E. Rozzi, and Y.T. Lo, 'Propagation in a rectangular waveguide periodically loaded with resonant irises', IEEE Transact. on MTT, vol. 28, no. 8, pp. 857-865, August 1980.
- [99] K. Chang and P.J. Khan, 'Analysis of a narrow capacitive strip in waveguide', IEEE Transact. on MTT, vol. 22, no. 5, pp. 536-541, May 1974.
- [100] K. Chang and P.J. Khan, 'Coupling between narrow transverse inductive strips in waveguide', IEEE Transact. on MTT, vol. 24, no. 2, pp. 101-105, February 1976.
- [101] K. Chang and P.J. Khan, 'Equivalent circuit of a narrow axial strip in waveguide', IEEE Transact. on MTT, vol. 24, no. 9, pp. 611-615, September 1976.
- [102] W.J. Getsinger, 'The packaged and mounted diode as a microwave circuit', IEEE Transact. on MTT, vol. 14, no. 2, pp. 58-69, February 1966.
- [103] W.J. Getsinger, 'Mounted diode equivalent circuits', IEEE Transact. on MTT, vol. 15, no. 11, pp. 650-651, November 1967.

- [104] B.D. Van Iperen, 'Impedance relations in a diode waveguide mount', IEEE Transact. on MTT, vol. 16, no. 11, pp. 961-963, November 1968.
- [105] R.L. Eisenhart and P.J. Khan, 'Theoretical and experimental analysis of a waveguide mounting structure', IEEE Transact. on MTT, vol. 19, no. 8, pp. 706-719, August 1971.
- [106] R.J. Gutmann and K.E. Mortenson, 'An ordered array of terminated metallic posts as an embedding network for lumped microwave devices', IEEE Transact. on MTT, vol. 20, no. 3, pp. 215-223, March 1972.
- [107] J.F. White, 'Simplified theory for post coupling gunn diodes to waveguide', IEEE Transact. on MTT, vol. 20, no. 6, pp. 372-378, June 1972.
- [108] J.P. Jethwa and R.L. Gunshor, 'An analytical equivalent circuit representation for waveguide-mounted gunn oscillators', IEEE Transact. on MTT, vol. 20, no. 9, pp. 565-572, September 1972. Also see comments by Singh, D.N., vol. MTT-21, p. 569, August 1973.
- [109] J.A. Bradshaw, 'Scattering from a round metal post and gap', IEEE Transact. on MTT, vol. 21, no. 5, pp. 313-322, May 1973.
- [110] O.L. El-Sayed, 'Impedance characterization of a two - post mounting structure for variator tuned gunn-oscillators', IEEE, Transact. on MTT, vol. 22, no. 8, pp. 769-776, August 1974.
- [111] R.L. Eisenhart, 'Comments on a two-gap waveguide mount', International Microwave Symposium, June 1976.
- [112] J.S. Joshi and J.A.F. Cornick, 'Analysis of a waveguide mounting configuration for electronically tuned transferred-electron-device oscillators and its circuit application', IEEE Transact. on MTT, vol. 24, no. 9, pp. 573-584, September 1976.
- [113] R.L. Eisenhart, 'Discussion of a 2-gap waveguide mount', IEEE Transact. on MTT, vol. 24, no. 12, pp. 987-990, December 1976.
- [114] O.L. El-Sayed, 'General analysis of parallel two-post mounting structures in waveguide', IEEE Transact. on MTT, vol. 25, no. 1, pp. 24-33, January 1977.

- [115] J.S. Joshi and J.A.F. Cornick, 'Analysis of waveguide post configurations: Part I - Gap immittance matrices', IEEE Transact. on MTT, vol. 25, no. 3, pp. 169-173, March 1977.
- [116] J.S. Joshi and J.A.F. Cornick, 'Analysis of waveguide post configurations: Part II - Dual-gap cases', IEEE Transact. on MTT, vol. 25, no. 3, pp. 173-181, March 1977.
- [117] S. Mizushina, N. Kuwabara, and H. Kondoh, 'Theoretical analysis of a ridged-waveguide mounting structure', IEEE Transact. on MTT, vol. 25, no. 12, pp. 1131-1134, December 1977.
- [118] V.M. Pandharipande and B.N. Das, 'Equivalent network of a variable-height post in a rectangular waveguide', Proc. IEE, vol. 124, no. 12, pp. 1160-1162, December 1977.
- [119] T.A. Abele, 'Inductive post arrays in rectangular waveguide', Bell Syst. Tech. J., vol. 57, no. 3, pp. 577-594, March 1978.
- [120] J.S. Joshi and J.A.F. Cornick, 'Analysis of waveguide post configurations: Part III - Influence of general waveguide terminations', IEEE Transact. on MTT, vol. 26, no. 4, pp. 319-320, April 1978.
- [121] G.E. Hagstrom and E.L. Kolberg, 'Measurements of embedding impedance of millimeter-wave diode mounts', IEEE Transact. on MTT, vol. 28, no. 8, pp. 899-904, August 1980.
- [122] A.C. Williamson, 'Analysis and modelling of a single-post waveguide mounting structure', Proc. IEE, Pt. H, MOA, vol. 129, no. 5, pp. 271-277, October 1982.
- [123] A.J. Hicks and P.J. Khan, 'Improved waveguide diode mount circuit model using post equivalence factor analysis', IEEE Transact. on MTT, vol. 30, no. 11, pp. 1914-1920, November 1982.
- [124] E.D. Nielson, 'Scattering by a cylindrical post of complex permittivity in a waveguide', IEEE Transact. on MTT, vol. 17, no. 3, pp. 148-153, March 1969.

- [125] R. Hirota and K. Suzuki, 'Field distribution in a magnetoplasma-loaded waveguide at room temperature', IEEE Transact. on MTT, vol. 18, no. 4, pp. 188-195, April 1970.
- [126] N. Okamoto, I. Nishioka, and Y. Nakanishi, 'Scattering by a ferrimagnetic circular cylinder in a rectangular waveguide', IEEE Transact. on MTT, vol. 19, no. 6, pp. 521-527, June 1971. Also see Correction, vol. MTT-20, no. 11, pp. 782-783, November 1972, and comments by P. Bhartia, vol. MTT-22, no. 11, p. 975, November 1974.
- [127] T. Yoshida, M. Umeno, and S. Miki, 'Propagation characteristics of a rectangular waveguide containing a cylindrical rod of magnetized ferrite', IEEE Transact. on MTT, vol. 20, no. 11, pp. 739-743, November 1972.
- [128] F.J. Vernues and D.M. Bolle, 'The ferrite-loaded waveguide discontinuity problem', IEEE Transact. on MTT, vol. 22, no. 12, pp. 1187-1193, December 1974.
- [129] J.J.L. Wang, 'Analysis of a three-dimensional arbitrarily shaped dielectric or biological body inside a rectangular waveguide', IEEE Transact. on MTT, vol. 26, no. 7, pp. 457-462, July 1978.
- [130] N. Okamoto, 'Computer-aided design of H-plane waveguide junctions with full-height ferrites of arbitrary shape', IEEE Transact. on MTT, vol. 27, no. 4, pp. 315-321, April 1979.
- [131] E.G. Royer and R. Mittra, 'The diffraction of electromagnetic waves by dielectric steps in waveguides', IEEE Transact. on MTT, vol. 20, no. 4, pp. 273-279, April 1972.
- [132] J.P. Montgomery and L. Lewin, 'Note on an E-plane waveguide step with simultaneous change of media', IEEE Transact. on MTT, vol. 20, no. 11, pp. 763-764, November 1972.
- [133] T. Ruchle and L. Lewin, 'The E-plane step-diaphragm junction discontinuity', IEEE Transact. on MTT, vol. 27, no. 2, pp. 158-160, February 1979.

- [134] H. Patzelt and F. Arndt, 'Double-plane steps in rectangular waveguides and their application for transformers, irises and filters', IEEE Transact. on MTT, vol. 30, no. 5, pp. 771-776, May 1982.
- [135] A. Safavi-Naini and R.H. MacPhie, 'Scattering of rectangular-to-rectangular waveguide junctions', IEEE Transact. on MTT, vol. 30, no. 11, pp. 2060-2063, November 1982.
- [136] S.D. Malviya and V.P. Singh, 'Transmission lines loaded at regular intervals', IEEE Transact. on MTT, vol. 27, no. 10, pp. 854-859, October 1979.
- [137] J. Perini, 'Periodically loaded transmission lines', IEEE Transact. on MTT, vol. 28, no. 9, pp. 1029-1031, September 1980.
- [138] J.J. Campbell and A.H. Jones, 'Symmetrically truncated right-angle corners in parallel-plate and rectangular waveguides', IEEE Transact. on MTT, vol. 16, no. 8, pp. 517-529, August 1968.
- [139] A. Bahar, 'Fields in waveguide bends expressed in terms of coupled local annular waveguide modes', IEEE Transact. on MTT, vol. 17, no. 4, pp. 210-217, April 1969.
- [140] A. Bahar and G. Govindrajan, 'Rectangular and annular modal analyses of multimode waveguide bends', IEEE Transact. on MTT, vol. 21, no. 12, pp. 819-824, December 1973.
- [141] G. Govindrajan and A. Bahar, 'Waveguide bend spurious mode program', IEEE Transact. on MTT, vol. 25, no. 8, p. 713, August 1977.
- [142] M.F. Iskander and M.A.K. Hamid, 'Iterative solutions of waveguide discontinuity problems', IEEE Transact. on MTT, vol. 25, no. 9, pp. 763-768, September 1977.
- [143] S.C. Kashyap, 'A simple 180° waveguide bend', Int. J. Electronics, vol. 46, no. 1, pp. 103-105, 1979.
- [144] F.C. Deronde, 'A simple full-band matched 180° E-plane waveguide bend', IEEE Transact. on MTT vol. 28, no. 4, pp. 432-433, April 1980.
- [145] P.I. Somlo, 'Conductive contacting spheres on the center of the broad-wall of rectangular waveguides', Electron. Letters, vol. 8, no. 20, pp. 507-508, 5th October 1972.

- [146] J.H. Hinken, 'Conducting spheres in rectangular waveguides', IEEE Transact. on MTT, vol. 28, no. 7, pp. 711-714, July 1980.
- [147] Y. Konishi, K. Uenakada, N. Yazawa, N. Hoshino and T. Takahashi, 'Simplified 12-GHz low noise converter with mounted planar circuits in waveguide', IEEE Transact. on MTT, vol. 22, no. 4, pp. 451-454, April 1974.
- [148] Y. Konishi and K. Uenakada, 'The Design of a bandpass filter with inductive strip-planar circuit mounted in waveguide', IEEE Transact. on MTT, vol. 22, no. 10, pp. 869-873, October 1974.
- [149] Y. Konishi, 'Planar circuit mounted in waveguide used as a down converter', IEEE Transact. on MTT, vol. 26, no. 10, pp. 716-719, October 1978.
- [150] Y. Konishi and H. Matsumura, 'Short end effect of ridge guide with planar circuit mounted in a waveguide', IEEE Transact. on MTT, vol. 27, no. 2, pp. 168-170, February 1979.
- [151] Y. Utsumi, 'Analysis of image recovery down converter made by planar circuit mounted in a waveguide', IEEE Transact. on MTT, vol. 30, no. 6, pp. 858-868, June 1982.
- [152] K. Gruner, 'Method of synthesizing nonuniform waveguides', IEEE Transact. on MTT, vol. 22, no. 3, pp. 317-322, March 1974.
- [153] E.A. Ohm, 'A low-loss branching filter for broad widely spaced bandwidths', IEEE Transact. on MTT, vol. 22, no. 10, pp. 891-894, October 1974.
- [154] A. Konrad, 'Higher-order triangular finite elements for electromagnetic waves in anisotropic media', IEEE Transact. on MTT, vol. 25, No. 5, pp. 353-360, May 1977.
- [155] A.K. Mallick and G.S. Sanyal, 'Electromagnetic wave propagation in a rectangular waveguide with sinusoidally varying width', IEEE Transact. on MTT, vol. 26, no. 4, pp. 243-249, April 1978.
- [156] A. Chakraborty and G.S. Sanyal, 'Transmission matrix of a linear double taper in rectangular waveguides', IEEE Transact. on MTT, vol. 28, no. 6, pp. 577-579, June 1980.

- [157] I.V. Lindell, 'Variational methods for nonstandard eigenvalue problems in waveguide and resonator analysis', IEEE Transact. on MTT, vol. 30, no. 8, pp. 1194-1204, August 1982.
- [158] S.B. Cohn, 'Problems in strip transmission lines', IEEE Transact. on MTT, vol. 3, no. 2, pp. 119-126, March 1955.
- [159] IEEE Transact. on MTT, vol. 3, no. 2, March 1955 issue.
- [160] H. Howe, Stripline Circuit Design. Dedham: Artech House, 1974.
- [161] H.A. Wheeler, 'Transmission-line properties of parallel wide strips by conformal-mapping approximation', IEEE Transact. on MTT, vol. 12, no. 5, pp. 280-289, May 1964.
- [162] H.A. Wheeler, 'Transmission-line properties of parallel strips separated by a dielectric sheet', IEEE Transact. on MTT, vol. 13, no. 3, pp. 172-185, March 1965.
- [163] H.A. Wheeler, 'Transmission-line properties of a strip on a dielectric sheet on a plane', IEEE Transact. on MTT, vol. 25, no. 8, pp. 631-647, August 1977.
- [164] S.B. Cohn, 'Slotline on a dielectric substrate', IEEE Transact. on MTT, vol. 17, no. 10, pp. 768-778, October 1969.
- [165] K.C. Gupta and A. Singh, Microwave Integrated Circuits. New Delhi: Wiley Eastern, 1974.
- [166] K.C. Gupta, R. Garg and I.J. Bahl, Microstrip Lines and Slot Lines. Dedham: Artech House, 1979.
- [167] R. Garg and K.C. Gupta, 'Expressions for wavelength and impedance of a slotline', IEEE Transact. on MTT, vol. 24, no. 8, pp. 532, August 1976.
- [168] T. Kitazawa, Y. Hayashi, and M. Suzuki, 'Analysis of the dispersion characteristic of slot line with thick metal coating', IEEE Transact. on MTT, vol. 28, no. 4, pp. 387-392, April 1980.

- [169] R.N. Simons and R.K. Arora, 'Coupled slot line field components', IEEE Transact. on MTT, vol. 30, no. 7, pp. 1094-1099, July 1982.
- [170] C.P. Wen, 'Coplanar waveguide: A surface transmission line suitable for non-reciprocal gyromagnetic device applications', IEEE Transact. on MTT, vol. 17, no. 12, pp. 1087-1090, December 1969.
- [171] M.E. Davis, E.W. Williams, and A.C. Celestini, 'Finite-boundary corrections to the coplanar waveguide analysis', IEEE Transact. on MTT, vol. 21, no. 9, pp. 594-596, September 1973.
- [172] J.B. Knorr and K.D. Kuchler, 'Analysis of coupled slots and coplanar strips on dielectric substrate', IEEE Transact. on MTT, vol. 23, no. 7, pp. 541-548, July 1975.
- [173] T. Kitazawa and Y. Hayashi, 'Quasi-static characteristics of coplanar waveguide on a sapphire substrate with its optical axis inclined', IEEE Transact. on MTT, vol. 30, no. 6, pp. 920-922, June 1982.
- [174] M.V. Schneider, 'Microstrip lines for microwave integrated circuits', Bell Syst. Tech. J., vol. 48, no. 5, pp. 1421-1444, May 1969.
- [175] H.E. Stinehelfer, 'An accurate calculation of uniform microstrip transmission lines', IEEE Transact. on ED, vol. 13, no. 7, pp. 501, July 1968.
- [176] P. Silvester, 'TEM wave properties of microstrip transmission lines', Proc. IEE, vol. 115, no. 1, pp. 43-48, January 1968.
- [177] A. Farrar and A.T. Adams, 'Characteristic impedance of microstrip by method of moments', IEEE Transact. on MTT, vol. 18, no. 1, pp. 65-66, January 1970.
- [178] A. Farrar and A.T. Adams, 'Computation of lumped microstrip capacities by matrix methods - Rectangular sections and end effect', IEEE Transact. on MTT, vol. 19, no. 5, pp. 495-497, May 1971. Also see correction, vol. MTT-20, no. 4, p. 294, April 1972.
- [179] P. Silvester and P. Bnedek, 'Electrostatics of the microstrip-revisited', IEEE Transact. on MTT, vol. 20, no. 11, pp. 756-758, November 1972.

- [180] E. Yamashita and R. Mittra, 'Variational method for the analysis of microstrip lines', IEEE Transact. on MTT, vol. 16, no. 4, pp. 251-256, April 1968.
- [181] E. Yamashita, 'Variational method for the analysis of microstrip-like transmission lines', IEEE Transact. on MTT, vol. 16, no. 8, pp. 529-535, August 1968.
- [182] T. Itoh and R. Mittra, 'A method for computing edge capacitance of finite and semi-infinite microstrip lines', IEEE Transact. on MTT, vol. 20, no. 12, pp. 847-849, December 1972.
- [183] B. Bhat and S.K. Koul, 'Unified approach to solve a class of strip and microstrip-like transmission lines', IEEE Transact. on MTT, vol. 30, no. 5, pp. 679-686, May 1982. Also see correction, vol. MTT-30, no. 11, p. 2067, November 1982.
- [184] R. Mittra and T. Itoh, 'Analysis of microstrip transmission lines', in *Advances in Microwaves*, vol. 8, New York: Academic Press, 1974.
- [185] O.P. Jain, 'Coupled mode model of dispersion in microstrip', Electronics Letters, vol. 7, pp. 405-407, 1971.
- [186] M.V. Schneider, 'Microstrip dispersion', Proc. IEEE, vol. 60, no. 1, pp. 144-146, January 1972.
- [187] H.J. Getsinger, 'Microstrip dispersion model', IEEE Transact. on MTT, vol. 21, no. 1, pp. 34-39, January 1973.
- [188] H.J. Carlin, 'A simplified circuit model for microstrip', IEEE Transact. on MTT, vol. 21, no. 9, pp. 589-591, September 1973.
- [189] G. Kompa and R. Mehran, 'Planar waveguide model for calculating microstrip components', Electronics Letters, vol. 11, no. 19, pp. 459-460, 18th September, 1975.
- [190] T.C. Edwards and R.R. Owens, '2-18 GHz dispersion measurements on 10-100 ohm microstrip lines on sapphire', IEEE Transact. on MTT, vol. 24, no. 8, pp. 506-513, August 1976.

- [191] E. Yamashita, K. Atsuki, and T. Ueda, 'An approximate dispersion formula of microstrip lines for computer - aided design of microwave integrated circuits', IEEE Transact. on MTT, vol. 27, no. 12, pp. 1036-1038, December 1979.
- [192] E. Yamashita, K. Atsuki, and T. Hirahata, 'Microstrip dispersion in a wide-frequency range', IEEE Transact. on MTT, vol. 29, no. 6, pp. 610-611, June 1981.
- [193] R. Mittra and T. Itoh, 'A new technique for the analysis of the dispersion characteristics of microstrip lines', IEEE Transact. on MTT, vol. 19, no. 1, pp. 47-56, January 1971.
- [194] E.F. Kuester and D.C. Chang, 'Theory of dispersion in microstrip of arbitrary width', IEEE Transact. on MTT, vol. 28, no. 3, pp. 259-265, March 1980.
- [195] D.G. Corr and J.B. Davies, 'Computer analysis of the fundamental and higher order modes in single and coupled microstrip', IEEE Transact. on MTT, vol. 20, no. 10, pp. 669-678, October 1972.
- [196] T. Itoh and R. Mittra, 'Spectral-domain approach for calculating dispersion characteristics of microstrip lines', IEEE Transact. on MTT, vol. 21, no. 7, pp. 496-499, July 1973.
- [197] J.B. Knorr and A. Tufekcioglu, 'Spectral-domain calculation of microstrip characteristic impedance', IEEE Transact. on MTT, vol. 23, no. 9, pp. 725-728, September 1975.
- [198] E.F. Kuester and D.C. Chang, 'An appraisal of methods for computation of the dispersion characteristics of open microstrip', IEEE Transact. on MTT, vol. 27, no. 7, pp. 691-694, July 1979.
- [199] A. Farrar and A.T. Adams, 'Matrix methods for microstrip three-dimensional problems', IEEE Transact. on MTT, vol. 20, no. 8, pp. 497-504, August 1972.
- [200] M. Macda, 'An analysis of gap in microstrip transmission lines', IEEE Transact. on MTT, vol. 20, no. 6, pp. 390-396, June 1972.

- [201] T. Itoh, R. Mittra, and R.D. Ward, 'A method for computing edge capacitance of finite and semi-finite microstrip line', IEEE Transact. on MTT, vol. 20, no. 10, pp. 847-849, December 1972.
- [202] P. Silvester and P. Benedek, 'Equivalent capacitances of microstrip open circuits', IEEE Transact. on MTT, vol. 20, no. 8, pp. 511-516, August 1972.
- [203] S.S. Bedair and M.I. Sobhy, 'Accurate formulae for the computer-aided-design of shielded microstrip circuits', Proc. IEE, Pt. H, MOA, vol. 127, no. 6, pp. 305-308, December 1980.
- [204] S.S. Bedair and M.I. Sobhy, 'Open-end discontinuity in shielded microstrip circuits', IEEE Transact. on MTT, vol. 29, no. 10, pp. 1107-1107, October 1981.
- [205] P. Benedek and P. Silvester, 'Equivalent capacitances of microstrip gaps and steps', IEEE Transact. on MTT, vol. 20, no. 11, pp. 729-733, November 1972.
- [206] Y. Rahmat-Samii, T. Itoh, and R. Mittra, 'A spectral domain analysis for solving microstrip discontinuity problems', IEEE Transact. on MTT, vol. 22, no. 4, pp. 372-378, April 1974.
- [207] R. Garg and I.J. Bahl, 'Microstrip discontinuities', Int. J. Electronics, vol. 45, no. 1, pp. 31-87, July 1978.
- [208] R. Horton, 'Equivalent representation of an abrupt impedance step in microstrip line', IEEE Transact. on MTT, vol. 21, no. 8, pp. 562-564, August 1973.
- [209] R.E. Neidert and G.T. O'Reilly, 'Very large impedance steps in microstrip', IEEE Transact. on MTT, vol. 22, no. 8, pp. 808-810, August 1974.
- [210] A. Gopinath, A.F. Thomson, and I.M. Stephenson, 'Equivalent circuit parameters of microstrip step change in width and cross junctions', IEEE Transact. on MTT, vol. 24, no. 3, pp. 142-144, March 1976.
- [211] G. Kompa, 'S-matrix computation of microstrip discontinuities with a planar waveguide model', Arch. Elek. Ubertragung, vol. 30, no. 2, pp. 58-64, February 1976.

- [212] P. Anders and F. Arndt, 'Microstrip discontinuity capacitances and inductances for double steps, mitered bends with arbitrary angle, and asymmetric right-angle bends', IEEE Transact. on MTT, vol. 28, no. 11, pp. 1213-1217, November 1980.
- [213] R. Horton, 'The electrical characterization of a right - angled bend in microstrip line', IEEE Transact. on MTT, vol. 21, no. 6, pp. 427-429, June 1973.
- [214] R. Mehran, 'The frequency-dependent scattering matrix of microstrip, right-angle bends, T-junctions and crossings', Arch. Elek. Ubertragung, vol. 29, no. 11, pp. 454-460, November 1975.
- [215] R. Mehran, 'Frequency-dependent equivalent circuits for microstrip right-angle bends, T-junctions and crossings', Arch. Elek. Ubertragung, vol. 30, no. 2, pp. 80-82, February 1976.
- [216] R. Mehran, 'Calculation of microstrip bends and Y-junctions with arbitrary angle', IEEE Transact. on MTT, vol. 26, no. 6, pp. 400-405, June 1978.
- [217] J. Helszajn, Passive and Active Microwave circuits. New York: John Wiley, 1978.
- [218] S.Y. Liao, Microwave Devices and Circuits. New Jersey: Prentice Hall, 1980.
- [219] B.M. Neale and A. Gopinath, 'Microstrip discontinuity inductances', IEEE Transact. on MTT, vol. 26, no. 10, pp. 827-831, October 1978.
- [220] A. Gopinath and C. Gupta, 'Capacitance parameters of discontinuities in microstriplines', IEEE Transact. on MTT, vol. 26, no. 10, pp. 831-836, October 1978.
- [221] G.L. Mystem, 'Analysis and synthesis of broad-band symmetric power dividing trees', IEEE Transact. on MTT, vol. 28, no. 11, pp. 1182-1187, November 1980.
- [222] N.G. Alexopoulos and S.A. Maas, 'Characteristics of microstrip directional couplers on anisotropic substrates', IEEE Transact. on MTT, vol. 30, no. 8, pp. 1267-1270, August 1982.

- [223] E.D. Sharp, 'An exact calculation for a T-junction of rectangular waveguides having arbitrary cross sections', IEEE Transact. on MTT, vol. 15, no. 2, pp. 109-116, February 1967.
- [224] R. Safavi-Naini and R.H. MacPhie, 'On solving waveguide junction scattering problems by the conservation of complex power technique', IEEE Transact. on MTT, vol. 29, no. 4, pp. 337-343, April 1981.
- [225] M. Razaz and J.B. Davies, 'Capacitance of the abrupt transition from coaxial-to-circular waveguide', IEEE Transact. on MTT, vol. 27, no. 6, pp. 564-569, June 1979.
- [226] M.D. Deshpande and B.N. Das, 'Input impedance of coaxial line to circular waveguide feed', IEEE Transact. on MTT, vol. 25, no. 11, pp. 954-957, November 1977. See correction, vol. MTT-26, no. 4, p. 315, April 1978. Also see comments by P.K. Bondyopadhyay, vol. MTT-27, no. 3, pp. 284-285, March 1979. Also see correction to comments by P.K. Bondyopadhyay, vol. MTT-27, no. 6, p. 621, June 1979.
- [227] M.D. Deshpande and B.N. Das, 'Analysis of an end launcher for a circular cylindrical waveguide', IEEE Transact. on MTT, vol. 26, no. 9, pp. 672-675, September 1978. See correction, vol. MTT-28, no. 1, p. 55, January 1980. Also see comments by P.K. Bondyopadhyay, vol. MTT-27, no. 6, p. 621, June 1979.
- [228] M.D. Deshpande and B.N. Das, 'Analysis of an end launcher for an X-band rectangular waveguide', IEEE Transact. on MTT, vol. 27, no. 8, pp. 731-735, August 1979.
- [229] M.M. Braly, 'Rectangular waveguide-to-coax line transitions: 1968', IEEE Transact. on MTT, vol. 17, no. 3, p. 170, March 1969.
- [230] R.L. Eisenhart, P.T. Greiling, L.K. Roberts, and R.S. Robertson, 'A useful equivalence for a coaxial-waveguide junction', IEEE Transact. on MTT, vol. 26, no. 3, pp. 172-174, March 1978.
- [231] A.G. Williamson, 'Analysis and modelling of a coaxial-line/rectangular-waveguide junction', Proc. IEE, pt. H, MOA, vol. 129, no. 5, pp. 262-270.

- [232] A. G. Chapman and C.S. Aitchison, 'A broad-band model for a coaxial-to-stripline transition' IEEE Transact. on MTT, vol. 28, no. 2, pp. 130-136, February 1980.
- [233] J. S. Wight, O.P. Jain, W.J. Chudobiak, and V. Makios, 'Equivalent circuits of microstrip impedance discontinuities and launchers', IEEE Transact. on MTT, vol. 22, no. 1, pp. 48-52, January 1974.
- [234] E. H. England, 'A coaxial to microstrip transition', IEEE Transact. on MTT, vol. 24, no. 1, pp. 47-48, January 1976.
- [235] M. L. Majewski, R.W. Rose, and J.R. Scatt, 'Modelling and characterization of microstrip-to-coaxial transitions', IEEE Transact. on MTT, vol. 29, no. 8, pp. 799-805, August 1981.
- [236] J.R. Souza and E.C. Talboys, 'S-parameter characterization of coaxial to microstrip transition', proc. IEEE, Pt. H, MOA, vol. 129, no. 1, pp. 37-40, February 1982.
- [237] M.V. Schneider, 'Microwave and millimeter wave hybrid integrated circuits for radio systems', Bell System Tech. Journal, 48, 1969, pp. 1703-1726,
- [238] R.H. Knerr, 'A new type of waveguide-to-stripline transition', IEEE Transact. on MTT, vol. 16, no. 3, pp. 192-194, March 1968.
- [239] E.L. Ginzton, Microwave Measurements. New York: McGraw-Hill, 1957.
- [240] S.F. Adam, Microwave Theory and Applications. Englewood Cliffs: Prentice-Hall, 1969.
- [241] T.L. Laverghetta, Microwave Measurements and Techniques. Dedham: Artech House, 1976.
- [242] S.F. Adam, 'A new precision automatic microwave measurement system', IEEE Transact. on Inst. and Meas., vol. 17, no. 4, pp. 308-313, December 1968.
- [243] R.A. Hackborn, 'An automatic network analyzer system', Microwave Journal, vol. 11, No. 5, pp. 45-52, May 1968.

- [244] J.G. Evans, 'Measuring frequency characteristics of linear two-port networks automatically', Bell System Technical Journal, vol. 48, no. 5, p. 1335, May-June 1969.
- [245] D.H. Olson and F.J. Rosenbaum, 'MICTPT- A minicomputer general-purpose microwave two-port analysis program', IEEE Transact. on MTT, vol. 22, no. 3, pp. 340-342, March 1974.
- [246] S. Rehnmark, 'On the calibration process of automatic network analyzer systems', IEEE Transact. on MTT, vol. 22, no. 3, pp. 457-458, April 1974.
- [247] W.J. Geldart, 'Improved impedance measuring accuracy with computer-operated transmission measuring sets', IEEE Transact. on Inst. and Meas., vol. 24, no. 4, pp. 327-331, December 1975.
- [248] G.F. Engen, 'Advances in microwave measurement sciences', Proc. IEEE, vol. 66, no. 4, pp. 374-384, April 1978.
- [249] S.F. Adam, 'Automatic microwave network measurements', Proc. IEEE, vol. 66, no. 4, pp. 384-391,
- [250] T. Mukaihata and R.D. Johnstone, 'Implementation and use of small automated-test systems', Proc. IEEE, vol. 66, no. 4, pp. 403-413,
- [251] J.R. Andrews, 'Automatic network measurements in the time domain', Proc. IEEE, vol. 66, no. 4, pp. 414-423, April 1978.
- [252] B. Ulriksson, 'A time domain reflectometer using a semi-automatic network analyzer and the fast-fourier transform', IEEE Transact. on MTT, vol. 29, no. 2, pp. 172-174, February 1981.
- [253] G.F. Engen, 'The six-port reflectometer: An alternative network analyzer', IEEE Transact. on MTT, vol. 25, no. 12, pp. 1075-1080, December 1977.
- [254] G.F. Engen, 'An improved circuit for implementing the six-port technique of microwave measurements', IEEE Transact. on MTT, vol. 25, no. 12, pp. 1080-1083, December 1977.

- [255] C.A. Hoer, 'A network analyzer incorporating two six-port reflectometers', IEEE Transact. on MTT, vol. 25, no. 12, pp. 1070-1074, December 1977.
- [256] M.P. Weidman, 'A semiautomated six-port for measuring millimeter-wave power and complex reflection coefficient', IEEE Transact. on MTT, vol. 25, no. 12, pp. 1083-1085, December 1977.
- [257] H.M. Cronson and L. Susman, 'A six-port automatic network analyzer', IEEE Transact. on MTT, vol. 25, no. 12, pp. 1086-1091, December 1977.
- [258] H.M. Cronson and L. Susman, 'A dual six-port automatic network analyzer', IEEE Transact. on MTT, vol. 29, no. 4, pp. 373-378, April 1981.
- [259] J.A. Galwas, 'Measurement of reflection coefficient by means of slotted line and homodyne detection system', IEEE Transact. on Inst. and Meas., vol. 24, no. 3, pp. 215-229, September 1975.
- [260] D. Kuffez, 'Numerical determination of two-port parameters from measured undunrestricted data', IEEE Transact. on Inst. and Meas., vol. 24, no. 1, pp. 4-11, March 1975.
- [261] D. Woods, 'Multiport-network analysis by matrix renormalisation employing voltage-wave S-parameters with complex normalisation', Proc. IEEE, vol. 124, no. 3, pp. 198-204, March 1977.
- [262] D. Woods, 'Reappraisal of computer-corrected network analyser design and calibration', Proc. IEE, vol. 124, no. 3, pp. 205-211, March 1977.
- [263] D. Woods, 'Multiport network analysis by matrix renormalisation', Proc. IEE, vol. 124, no. 9, pp. 749-753, September 1977.
- [264] J. Holszajn, 'Measurement of symmetrical waveguide discontinuities using the eigenvalue approach', Proc. IEEE, Pt. H, vol. 127, no. 2, pp. 74-81, April 1980.
- [265] A. Boulouard, 'Delay-line based techniques for micro-wave and millimeter-wave transmission/reflection test sets', IEEE Transact. on MTT, vol. 30, no. 8, pp. 1174-1183, August 1982.

- [266] V. Rizzoli and A. Lipparini, 'A resonance method for the broad-band characterization of general two-port microstrip discontinuities', IEEE Transact. on MTT, vol. 29, no. 7, pp. 655-660, July 1981.
- [267] P.C. Sharma and K.C. Gupta, 'A generalized method for de-embedding of multiport networks', IEEE Transact. on Inst. and Meas., vol. 30, no. 4, pp. 305-307, December 1981. Also see correction: vol. IM-31, no. 2, p. 145, June 1982.
- [268] R.A. Speciale, 'Multiport network analyzers: Meeting the design need', Microwave System News, vol. 10, June 1980.
- [269] J.C. Tippet and R.A. Speciale, 'A rigorous technique for measuring the scattering matrix of a multiport device with a 2-port network analyzer', IEEE Transact. on MTT, vol. 30, no. 5, pp. 661-666, May 1982.
- [270] D. Woods, 'Multiport network analysis by matrix renormalisation: Extension to 5- and 6-ports', Proc. IEE, vol. 125, no. 11, p. 1217, November 1978.
- [271] N.R. Shetty and B.V. Rao, 'An experimental method for the determination of circuit admittance as seen at the Gunn diode terminals and hence time averaged admittance of an oscillating Gunn diode in a X-band post mounted waveguide cavity G.E.O.', in Proceedings, International Symposium on Microwaves and Communication, Indian Institute of Technology, Kharagpur, India, December 1981.
- [272] B. Bianco, M. Parodi, and S. Ridella, 'Launcher and microstrip characterization', IEEE Transact. on Inst. and Meas., vol. 25, no. 4, pp. 320-323, December 1976.
- [273] K. Chang and R.L. Ebert, 'W-band power combiner design', IEEE Transact. on MTT, vol. 28, no. 4, pp. 295-305, April 1980.
- [274] C. Das Gupta, 'Microwave measurement of a complex dielectric constant over a wide range of values by means of a waveguide resonator method', IEEE Transact. on MTT, vol. 22, no. 4, pp. 365-372, April 1974.
- [275] S.A. Schelkunoff and M.T. Friis, Antennas: Theory and Practice. New York: John Wiley, 1952, p. 232.

- [276] G.L. Matthaei, L. Young, and E.M.T. Jones, *Microwave Filters, Impedance-Matching Networks, and Coupling Structures*. New York: McGraw-Hill, 1964.
- [277] G.L. Matthaei, 'Magnetically-tunable band-stop filters', *IEEE Transact. on MTT*, vol. 13, No. 2, pp. 203-212, March, 1965.
- [278] J. Helszajn. *Principles of Microwave Ferrite Engineering*. New York: John Wiley, 1969.
- [279] R.F. Bauer and P. Penfield, 'De-embedding and Unterminating', *IEEE Transact. on MTT*, vol. 22, no. 3, pp. 282-288, March, 1974.
- [280] E.C. Jordan and K.G. Balmain, *Electromagnetic Waves and Radiating Systems*. New Delhi: Prentice Hall, 1971, p.387.
- [281] G. Markov, *Antennas*. Moscow: Progress Publishers, 1965, p. 52.
- [282] H. Jasik, *Antenna Engineering Handbook*. New York: McGraw-Hill, 1961, p. 3.2.
- [283] W.J.R. Hoefer, 'Equivalent series inductivity of a narrow transverse slit in microstrip', *IEEE Transact. on MTT*, vol. 25, no. 10, October 1977, pp. 822-825.
- [284] A.G. Williamson, 'Analysis and modeling of 'two-gap' coaxial line rectangular waveguide junctions', *IEEE Transact. on MTT*, vol. 31, no. 3, pp. 295-302, March 1983.